# DYNAMICAL COMPLEXITY OF LARGE-SCALE NEUROCOGNITIVE NETWORKS IN HEALTHY AND PATHOLOGICAL BRAIN STATES.

Thomas H. Alderson (BSc, MSc)

FACULTY OF COMPUTING, ENGINEERING, AND THE BUILT ENVIRONMENT

ULSTER UNIVERSITY

Thesis is submitted for the degree of Doctor of Philosophy

2019

I confirm that the word count of this thesis is less than 100,000

# Abstract

Contemporary theories suggest that the brain operates in a metastable regime of dynamics in which the tendencies for local areas to integrate and segregate is simultaneously realised. Current theoretical and empirical observations suggest that this behaviour occurs spontaneously through the interaction of local dynamics with underling anatomical connectivity. The metastable regime likely confers important behavioural qualities through the flexible coupling and uncoupling of distributed cortical regions into context-dependent neurocognitive networks. Thus, one of the principle goals of neuroscience, to understand how structure and dynamics interact to generate cognition, may be realised by leveraging the metastable regime of dynamics to link across the interrelated domains of structure, function, and cognition. Accordingly, the proposed approach, grounded in dynamical systems theory, neuroimaging, and theoretical computer modelling, aims to explore how: (1) complex metastable neural dynamics are modulated by cognitive state; (2) structural connectivity confers cognitive flexibility on a fixed network topology through metastable neural dynamics; (3) structural disconnection impacts metastable neural dynamics and how this relates to cognitive performance.

The thesis presents findings from three studies. The first uses the theoretical framework of metastable coordination dynamics to explore how cognition arises from the dynamic assembly of local areas into neurocognitive networks. Previous work has suggested that the probability of transitioning between network states is maximised when subjects are not explicitly engaged in a task. Contrary to expectations, metastability between networks was higher during task engagement than during periods of 'cognitive rest'. Task-based reasoning was characterised by dynamic stability in sensory regions and dynamic flexibility in regions devoted to cognitive control. Critically, this dynamic flexibility appeared to confer superior problem solving ability in tests of fluid intelligence.

The second study leverages an example of incipient neurodegeneration, mild cognitive impairment (MCI), to test the essential proposition that

cognitive deficits are linked to structural disconnection in the brain's large-scale network architecture. Accordingly, this study examines the structural connectivity between thalamus and key regions of the cortex implicated in 'cognitive rest': the default mode network (DMN). Abnormal structural connectivity and altered patterns of causation were identified in this 'thalamo-DMN' loop and, crucially, these deficits were linked to memory recall. Taken together, these findings provide new insight into the causal pathways underlying DMN dysfunction in MCI and Alzheimer's disease (AD) and provides preliminary evidence that AD represents a failure of circulating information consistent with its status as a 'disconnection syndrome'.

The third and final study uses a joint theoretical and empirical approach to examine how dynamics and cognitive ability are shaped by the macroscopic connectivity of the brain. Accordingly, this study investigates the asymptotic decline of neural metastability in an example of structural disconnection, AD, and its prodrome, MCI. Whole-brain computer modelling mechanistically linked reduced metastability to anatomical disconnection. Moreover, metastability was linked to features of the brain's structural topology. Crucially, empirical estimates of metastability were linked to global cognitive performance. Taken together, these findings suggest a critical linkage between metastability, cognition, and network topology in the damaged or diseased brain.

Overall, these three studies provide insight into the dynamic principles by which cognitive architecture is organised and suggest that the metastable regime of dynamics offers considerable potential as a theoretical and conceptual framework for linking structure, function, and cognition in the human brain.

# Contents

# List of Figures

# Acknowledgements

*"Science, my boy, is made up of mistakes, but they are mistakes which it is useful to make, because they lead little by little to the truth."*

—Jules Vern

As any dedicated reader knows someone else has already said it best. So if you can't top it, start strong and use a quote. I am indebted to those anonymous geniuses of the past whose *"mistakes"* made this contribution possible and to my supervisors and family for their continued guidance and support.

# 1 Preliminaries

## 1.1 Introduction

The classical view of systems neuroscience is that individual regions of the brain are specialised for particular functions. This is supported by a wealth of empirical lesion and neuroimaging studies linking localised neural activity with specific behavioural and cognitive events. Recently, there has been a transition from the classical viewpoint. Rather than trying to carve up the brain into a taxonomy of mental functions, an alternative approach is to ask how a given anatomical substrate can support a number of different cognitive functions (Poldrack, 2012; Poldrack and Farah, 2015). New techniques have revealed intrinsic connectivity networks (ICNs; Fig. 1.1) that reflect underlying patterns of anatomical connectivity. The activity of these networks is contingent on intrinsic fluctuations and current behavioural context, and is dynamically reconfigured over time (Sadaghiani and Kleinschmidt, 2013). Thus, any investigation of brain networks must consider not only the structural anatomy which constrains and supports functional interactions (van den Heuvel et al., 2009) but also the dynamic changes in functional interactions (Cohen, 2018). An outstanding challenge, therefore, is to incorporate these neural dynamics into a coherent

framework that combines insights from structure, function, and cognition.

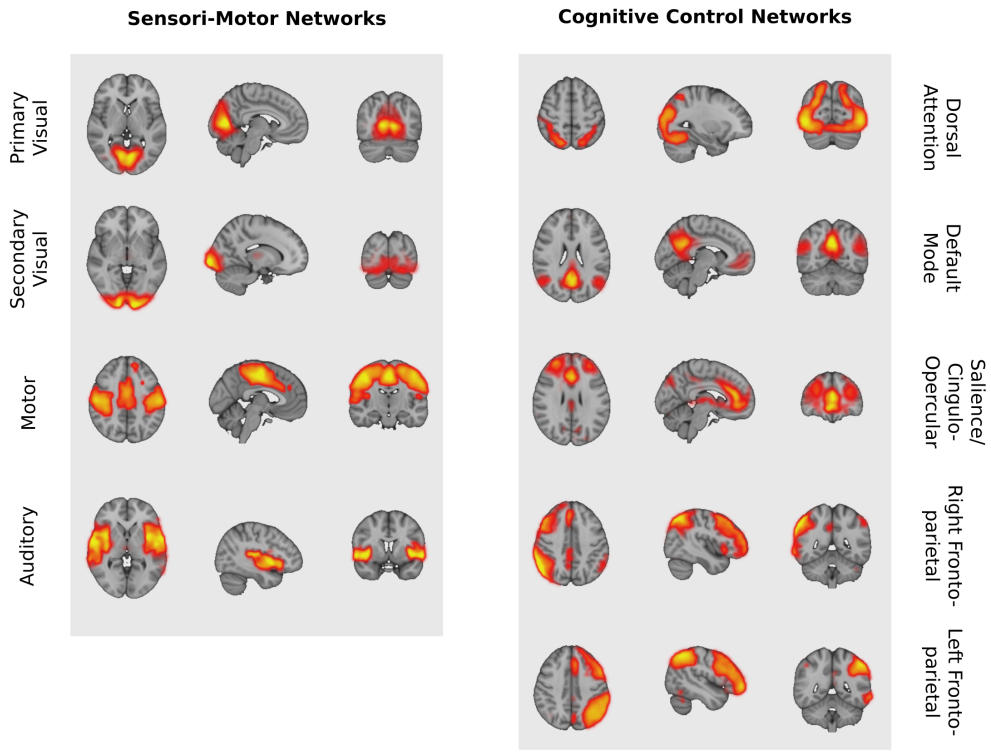


Figure 1.1: Intrinsic connectivity networks represent a fundamental organisational principle of functional brain architecture. The term 'intrinsic connectivity networks' expands upon the notion of 'resting state networks' to include the set of large-scale functionally connected brain regions that emerge in resting state or task-based data (Laird et al., 2011). Shown are nine intrinsic connectivity networks of the brain commonly identified in fMRI data when subjects are at 'cognitive rest'. Viewed up through the patients body, hence left and right are reversed. (Smith et al., 2009).

Today, the most common methods for observing neural activity include electroencephalography (EEG), magnetoencephalography (MEG), positron emission tomography (PET), and functional magnetic resonance imaging (fMRI). These approaches are augmented by animal studies in which single unit recordings monitor the electro-physiological response of individual neurons. Each type is sensitive to and hence concerned with different levels of functional organisation. Given the proliferation of techniques for observing

brain activity, it is perhaps unsurprising that methods of observing brain connectivity are as equally varied (Horwitz, 2003; Lee et al., 2003; Jirsa and McIntosh, 2007). Brain connectivity falls into three main categories: structural, functional and effective connectivity. Structural connectivity refers to the physical substrate by which cortical regions are connected (Hagmann et al., 2010; Behrens and Sporns, 2012; Cammoun et al., 2012; Craddock et al., 2013; Sporns, 2013*c*). On a shorter timescale (seconds to minutes) their physical pattern can be thought of as the physical 'wiring diagram' of the brain. On a longer timescale (days to weeks) the physical linkages may be thought of as more plastic and reflect the accumulation of experience acquired through learning and development. Functional connectivity refers to the statistical dependence between the time series of two regions and is typically estimated through correlation (Friston, 1994, 2011). It refers to the 'dynamic interactions' that take place between network elements on the anatomical substrate. In contrast to structural connectivity, functional connectivity dynamically evolves over a variety of temporal scales (from the millisecond to the minute and beyond), and is modulated via external task exigencies, incoming sensory stimuli, and internal state (e.g. arousal/fatigue)(Hutchison, Womelsdorf, Allen, Bandettini, Calhoun, Corbetta, Della Penna, Duyn, Glover, Gonzalez-Castillo, Handwerker, Keilholz, Kiviniemi, Leopold, de Pasquale, Sporns, Walter and Chang, 2013; Gonzalez-Castillo and Bandettini, 2017; Cohen, 2018). Unlike effective connectivity, functional connectivity makes no explicit reference to causality amongst neural components whereas effective connectivity explicitly describes the causal relationships between pairwise regions (Stephan and Friston, 2007, 2010; Valdes-Sosa et al., 2011; Friston et al., 2012). Like functional connectivity these can be modulated on a rapid timescale. A parsimonious approach to mapping effective connectivity is to leverage the knowledge that cause must precede effect. In this way, directed (or probabilistic causal) interactions can be extracted from time series data without recourse to complex dynamics or any assumptions regarding an underlying structural model (Friston, 2003; Friston et al., 2017). One of the most widely adopted methods – Granger causality (GC) – estimates the amount

of information gained about the future state of a variable by including past states of another (Granger, 1969). GC has been widely applied to neuroscientific data including fMRI time series (Goebel et al., 2003; Roebroeck et al., 2005; Bressler et al., 2008). Another approach, dynamic causal modelling (DCM), seeks to clarify directed connectivity between regions by identifying the most likely model to have produced the empirically observed data (Friston, 2003).

On their own, none of these methods is sufficient to explain how networks of neural elements coordinate their activity over space and time. Some proponents may claim that once the wiring between elements has been fully determined, say at the microscopic level, the inner workings of the brain will become self-evident. Such views may be overly optimistic, as knowledge of wiring alone cannot account for the brain's spontaneous patterns of endogenous activity or temporally patterned task-dependent responses. Nor can it explain how a multiplicity of functional states arise from static connectivity. Thus, this thesis examines how complex spatiotemporal brain activity emerges from the interplay between wiring *and* local dynamics (Rubinov et al., 2009). The present thesis addresses a core goal of neuroscience, to understand how structural anatomy shapes and constrains spontaneous patterns of dynamic functional connectivity in the brain (Damoiseaux and Greicius, 2009).

The emergence of time-varying functional networks from static anatomical connectivity demands a formal computational approach to neural information processing that resolves the dialectic between structure and function (Park and Friston, 2013). Dynamical systems theory may provide a conceptual bridge to unite these interrelated levels of description (Breakspear, 2017). Theoretical and empirical data suggest that flexible cognition and behaviour are enabled by neural activity operating in a metastable regime of dynamics in which individual regions express their intrinsic dynamics but also coordinate globally (Kelso, 1995; Kelso and Tognoli, 2007; Tognoli and Kelso, 2014*b*).

Metastability is closely related to the concept of 'chaotic itinerancy' (Kaneko and Tsuda, 2003) or the itinerant/roaming trajectory of a high di-

mensional system through a series of ordered states. Here, low-dimensional motion in dynamically unstable 'attractor ruins' gives way to high-dimensional chaotic transitions. Chaotic dynamics is observed in physical systems that operate far from equilibrium, are globally coupled, and/or engage in turbulent flow. Examples of chaotic systems include chaotic fluids and atmospheric dynamics, electrochemical oscillators and lasers. Chaotic behaviour has also been observed in EEG brain recordings (Freeman, 1987) and artificial neural networks (Sompolinsky et al., 1988).

The concept of metastability is important, as it furnishes a dynamical explanation for understanding how large-scale regions of cortex coordinate their activity in space and time to support cognition (Bressler, 1995; Bressler and Kelso, 2001, 2016; Bressler and Tognoli, 2006; Bressler and Mcintosh, 2007; Bressler and Menon, 2010). These large-scale coordinative dynamics are likely shaped by underlying anatomy (Hellyer et al., 2014, 2015; Váša et al., 2015; Deco et al., 2017), however, it is unclear how metastable neural dynamics relate to cognition, or how they are constrained by the brain's structural topology — issues that the present thesis directly addresses. Furthermore, although dynamical descriptions attribute considerable importance to the brain's structural connectivity (Shanahan, 2010, 2012; Wildie and Shanahan, 2012), it is unclear how metastable neural dynamics is affected by pathological disease processes resulting in structural disconnection (Seeley et al., 2009). Accordingly, this thesis explores these dynamical accounts using tools from neuroimaging and computational modelling. Critical linkages between structure, function, and cognition are examined in the healthy human brain and, in an example of structural disconnection, namely, Alzheimer's disease (AD) and its prodromal state, mild cognitive impairment (MCI). The approach here is motivated by the understanding that AD represents the most common and economically burdensome forms of dementia, and one for which treatment options are presently unavailable (Kumar et al., 2015; Masters et al., 2015; Wang et al., 2017). Although links between structural disconnection (Villain et al., 2008; Radanovic et al., 2013; Sachdev et al., 2013; Amlien and Fjell, 2014; Caso et al., 2016), functional connectivity (Brier et al., 2014; Li et al., 2015; Bad-

hwar et al., 2017), and cognition have been found in many studies of AD, to date, these observations are predominantly correlative, and no satisfactory mechanism is available to link these interrelated levels of description. An important issue, therefore, is to understand how spontaneous neural activity, expressed in terms of functional network interactions, and constrained by the structural anatomy, relates to behaviour and cognition.

A promising approach is to consider the brain as a complex dynamical system and use computational modelling to provide insight (Rabinovich et al., 2006; Deco et al., 2008; Breakspear, 2017). These computational models provide detailed descriptions of how local activity interacts with macroscopic patterns of structural connectivity to produce dynamic changes in behaviour over time (Deco et al., 2008, 2009; Deco and Corbetta, 2011; Deco and Jirsa, 2012; Deco et al., 2012; Deco, Ponce-Alvarez, Mantini, Romani, Hagmann and Corbetta, 2013; Deco and Kringelbach, 2014; Cabral et al., 2011, 2014, 2017; Kringelbach et al., 2015; Ponce-Alvarez et al., 2015). Models of this type have been used to understand the brain's spontaneous patterns of activity, and to clarify the relationship between functional and structural connectivity (Honey and Kötter, 2007; Honey and Sporns, 2008; Honey et al., 2009, 2010). Several models have incorporated the graph of connectivity – the anatomical/structural connectome – defined by tractography, to specify the coupling strength between nodes that represent individual cortical regions (Hagmann et al., 2007, 2008; Bullmore and Sporns, 2009; Hagmann et al., 2010; Sporns, 2010, 2011*b*; Behrens and Sporns, 2012; Sporns, 2012, 2013*a*). These 'mean-field' models – based on the ensemble activity of large populations of neurons – have captured features of spontaneous neural activity with impressive accuracy (Messé et al., 2014), and in the field of movement, task-specific patterns of neural activity (Kelso et al., 2013). Increasingly, these computational techniques have been applied to neurological and psychiatric disorders to model the affect of structural disconnection on resting state functional connectivity (Jirsa et al., 2010; Cabral, Hugues, Kringelbach and Deco, 2012; Cabral, Kringelbach and Deco, 2012; Cabral et al., 2013; Hellyer et al., 2015; Váša et al., 2015; Demirtaş et al., 2017).

In light of the foregoing, this thesis leverages a dynamical account of the brain – metastable neural dynamics – to link across the three domains of analysis: structure, function, and cognition. Metastable neural dynamics has considerable potential for providing both a conceptual and computational framework for mechanistically linking structure to function (Hellyer et al., 2014, 2015; Váša et al., 2015; Deco et al., 2017). The discovery of how structural aspects of network connectivity in the brain inform and interact with function and cognition, can be expected to further advance our understanding of the brain's self-organising behaviour (Kelso, 1995). Metastable neural dynamics has a strong intuitive association with aspects of cognition relying on flexibility, exploration, and integration of information, and may play a central role in supporting higher order cognition (Kelso, 2008; Kringelbach et al., 2015; Deco and Kringelbach, 2016; Balaguer-Ballester et al., 2018). The proposed approach also provides a theoretical foundation for the development of clinically relevant biomarkers linked to cognitive dysfunction (Kaiser, 2013; Gomez-Ramirez and Wu, 2014; Jacobs et al., 2013; Jack et al., 2013; Acosta-Cabronero et al., 2012).

## 1.2 Rationale and research problem

A principal goal of neuroscience – to infer causality from a dual knowledge of circuitry and local neural dynamics – is unrealised. Although links between structural disconnection, altered functional connectivity, and cognitive impairment have been revealed in many studies of the brain including schizophrenia (van den Heuvel et al., 2010; Fornito et al., 2012; van den Heuvel et al., 2013; van den Heuvel and Fornito, 2014), traumatic brain injury (Mac Donald, Dikranian, Song, Bayly, Holtzman and Brody, 2007; Mac Donald, Dikranian, Bayly, Holtzman and Brody, 2007; Kinnunen et al., 2010; Bonnelle et al., 2011, 2012), and AD, these accounts are primarily descriptive and mechanisms to link these interrelated levels of description are lacking. An important challenge, therefore, is to situate these correlative accounts of structure, function, and cognition in a causal context. Whole-brain computer modelling and dynamic systems theory may offer a

theoretical and conceptual framework to mechanistically link function and structure. The central tenet is that patterns of components and their structural connections captured by the connectome place specific constraints on complex brain dynamics, and therefore shape the operation and processes of human cognition (Menon, 2011; Sporns, 2014; Fornito et al., 2015). The network approach to cognition moves us closer to resolving the long standing antagonism of localisationist and distributionalist accounts of brain function (McIntosh, 2000). This approach is especially important for examining how patterns of spontaneous neural activity are generated and how they relate to underlying structural connectivity, and cognition (Honey and Kötter, 2007; Honey et al., 2009, 2010).

## Research aims

In light of these observations, the principal aim of this thesis is to use insights from dynamical systems theory in conjunction with tools from neuroimaging, computational modelling, and network theory to examine the impact of (1) task-induced changes in cognitive state and (2) structural disconnection on a complex measure of metastable neural dynamics in which the complementary tendencies toward integration and segregation in the brain are simultaneously realised (Kelso, 1995, 2012; Kelso and Tognoli, 2007; Tognoli and Kelso, 2009, 2014*a*,*b*). Thus, this thesis aims to explore:

- the modulation of complex metastable neural dynamics under different conditions of task.
- how structural connectivity confers cognitive flexibility on a fixed network topology through metastable neural dynamics.
- how structural disconnection impacts metastable neural dynamics and how this relates to cognitive performance.

The concept and phenomena of metastability is important as it provides a dynamical explanation of how large-scale networks coordinate their activity in space and time to support cognition (Kelso, 1992; Bressler, 1995, 2002; Bressler and Kelso, 2001, 2016; Bressler and Tognoli, 2006; Bressler

and Mcintosh, 2007; Bressler and Menon, 2010). Accordingly, this thesis uses structural and functional MRI data recordings of healthy controls (HCs), and patients with AD and its prodromal state, MCI, to investigate the relationship between structural disconnection, metastable neural dynamics, and cognition in the human brain. The proposed approach aims to provide new insights into the nature of structure and function both in the normal and the damaged or diseased brain.

## Research objectives

To achieve the aims outlined above the core objectives of the thesis are:

- To test the proposition that metastability is related to cognitive function by examining neural dynamics across several types of behaviour.
  - To determine how the metastability of the brain's large-scale network organisation facilitates individual cognitive performance.
- To interrogate an example of incipient neurodegeneration, MCI, for structural and functional changes linked to large-scale network organisation.
  - To investigate how structural and functional changes in the brain's large-scale network connectivity is linked to cognitive performance.
- To construct and validate a computational model based on the macroscopic structural connectivity of the brain and use it to simulate the intrinsic neural dynamics observed when subjects are at 'cognitive rest'.
- To mechanistically link structural disconnection and metastable neural dynamics in MCI and AD using computational modelling informed by anatomical connectivity.
  - To examine how pathological network damage in the model is constrained by the topological organisation of the connectome.
  - To investigate the relationship between simulated neural metastability and the topological organisation of the anatomical connec-

tome.

- To evaluate healthy neural dynamics for metastability and to compare them to the metastability of neural dynamics obtained in subjects with MCI and AD.
  - To investigate how changes in empirical metastability translate to changes in general cognition as pathophysiology unfolds.

## 1.3 Thesis outline

Chapter 2 provides an overview of the methods. This includes the general principles of MRI, the non-invasive mapping of structure and function of the human brain, and the use of graph theory to describe network topology.

Chapter 3 explores the proposal that cognition emerges from large-scale systems of distributed and interconnected neuronal populations that operate and interact according to dynamic principles. Substantive evidence is presented that complex dynamics self-organised on the brain's anatomical backbone may best be understood in the language of dynamical systems theory. Special emphasis is placed on dynamic descriptions of the brain in which the spontaneous transition between network configurations is expressed most accurately as a sequence of transients between metastable states. Finally, theoretical and empirical evidence is provided that AD represents a 'disconnection syndrome'.

Chapter 4 introduces the theoretical framework of metastable coordination dynamics to investigate how the interactions of large-scale brain networks support cognition. Motivated by the observation that the probability of network switching is maximised when subjects are cognitively 'at rest', this chapter tests the fundamental proposition that metastable neural dynamics is higher at rest than during periods of heightened cognitive activity.

Chapter 5 tests the essential hypothesis that structural disconnection of large-scale network organisation is relevant to cognition by interrogating an example of incipient neurodegeneration, MCI, for structural and functional

disconnection between thalamus and regions of the brain associated with elevated activity during 'cognitive rest', the default mode network (DMN).

Chapter 6 explores the relationship between white matter and neural dynamics by developing and validating a theoretical computer model of the cerebral cortex based on the large-scale pattern of macroscopic structural connectivity between regions. This work provides a proof-of-principle that a relatively simple network of coupled Kuramoto phase oscillators is capable of capturing key properties of spontaneous neural dynamics when coupled according to anatomical principles. This chapter also integrates several strands of research, relating structural disconnection, neural dynamics, and cognition to explore how general cognitive ability is shaped by the underlying anatomical connectivity in an example of neurodegenerative disease, AD, and its precursor, MCI. Moreover, this chapter draws upon the aforementioned computer model to mechanistically link structural disconnection and metastable neural dynamics. Finally, by exploiting tools derived from graph theory, metastable neural dynamics is shown to be related to key features of the anatomical connectome.

# 2 Methodology

## 2.1 Introduction

This chapter outlines general principles of MRI necessary for non-invasively mapping the structure and function of the human brain. Special emphasis is placed on techniques relevant to the findings presented in subsequent chapters.

## 2.2 Integral principles of magnetic resonance imaging

MRI is a technique that exploits the properties of hydrogen atoms inside a strong magnetic field to produce images of biological tissue (Huettel, 2009; Savoy, 2001). MRI was discovered in 1947 simultaneously by two scientists, Felix Bloch (Bloch et al., 1946; Bloch, 1951, 1953) and Edward Mills Purcell (Purcell et al., 1946; Purcell, 1953) at the Massachusetts Institute of Technology. Bloch and Purcell received the Nobel prize for Physics in 1952 in recognition for their work, but it would not be until 1977 that the first clinical images were obtained (Bullmore, 2012). The nature of MRI as an evolving technology means its history is still being written (Blamire, 2012;

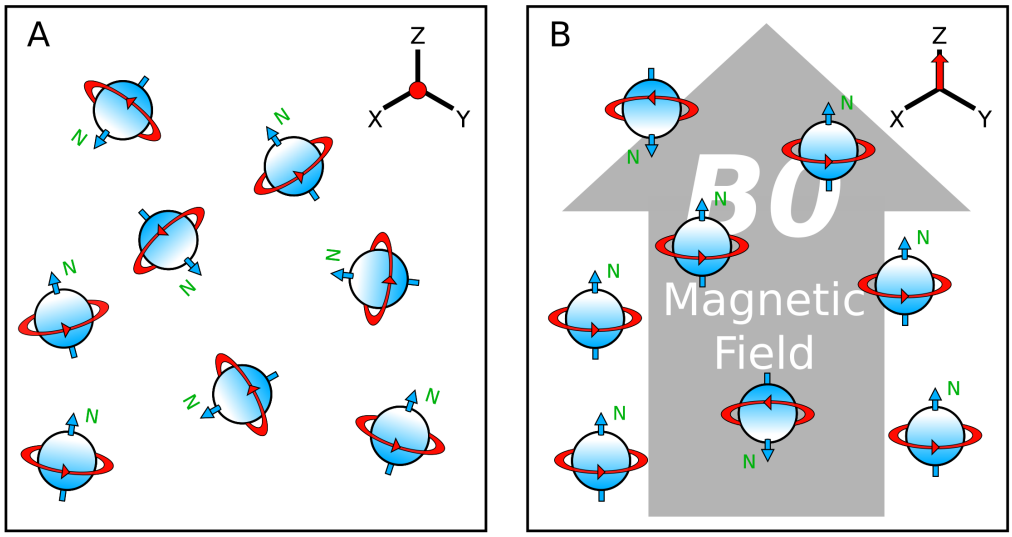


Figure 2.1: Magnetisation of hydrogen protons in relation to a strong magnetic field A) Hydrogen protons randomly align in the absence of a magnetic field B) Hydrogen protons align in either a parallel or anti-parallel position along the axis of the B0 magnetic field in the bore of an MRI scanner to produce a net vector of magnetisation in the z-axis. The net moment generated by the field of protons is shown in three dimensions in the top right.

Kwong, 2012; Turner, 2012; Uurbil, 2012). MRI differs from imaging such as plane film radiography and computerised tomography scanning as it uses magnetic fields and radio frequencies rather than ionising radiation. The majority of MRI systems in clinical practice produce an extremely strong magnetic field approximately 50,000 times that of the earth's magnetic field (0.00003 Tesla), in principle, sufficient to pick up a car.

Hydrogen protons spin or 'precess' about their axis much like miniature spinning tops (Fig. 2.1). The rate of this precession is known as the 'Larmor frequency'. Spin induces a small magnetic charge or polarity called the magnetic moment. These magnetic moments are randomly aligned in biological tissue, hence, the net moment is very small. However, when hydrogen protons are placed inside a strong magnetic field (such as in the bore of an MRI machine) these magnetic moments spontaneously align along the principle direction of the primary magnetic field (called the B0

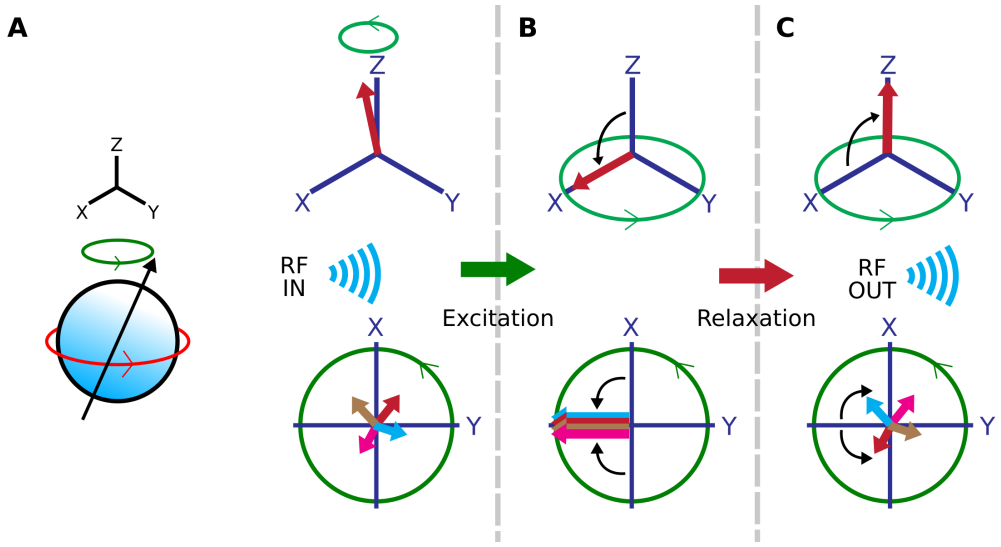


Figure 2.2: Radio frequency excitation and relaxation of hydrogen protons. A) Each hydrogen proton precesses around the net magnetisation vector of the B0 field at a rate known as the Larmor frequency (green). B) Application of radio frequency energy causes the net magnetic moment to 'flip' 90 degrees into the x-y plane and the angle of precession of each individual moment to become aligned. C) Hydrogen protons subsequently release radio frequency energy as the net magnetic moment becomes realigned with the principle axis of the B0 field and protons return to precessing out of phase.

field). Protons favour a thermodynamically stable configuration, hence, a greater proportion of the hydrogen protons align in the low energy state (parallel to the primary magnetic field), than align in the high energy state (antiparallel to the primary magnetic field). [1]

Hydrogen protons within a magnetic field continue to precess about their axis but change their conformation when bombarded with radio frequency (RF) energy. If the energy is at the Lamour frequency, the proton's rotational pole is flipped into the high energy state in a process known as 'excitation' (Fig. 2.2). If sufficient numbers of protons are excited the net magnetisation flips 90 degrees into the x-y plane, perpendicular to the axis

[1] Although this discussion is not presented in textbooks and papers, in reality, the wave function does not mandate that protons protons exist exclusively in either the 'spin up' or 'spin down' state but in a linear combination of the two.

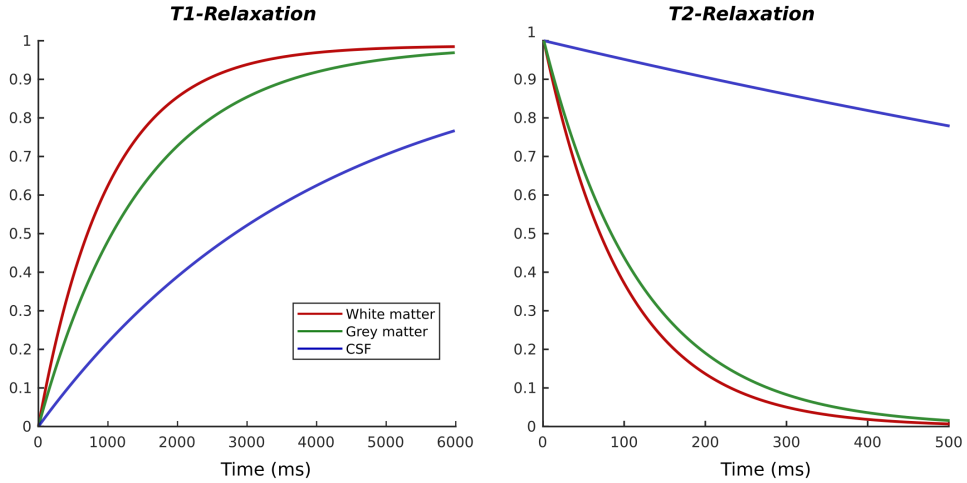


Figure 2.3: T1 and T2 relaxation rates for different tissue classes. T1 and T2 relaxation rates are dependent on the size and motion of the molecule on which the hydrogen nucleus resides. Additional factors cause T2 relaxation to proceed at a faster rate than T1 relaxation.

of the primary magnetic field. At the same time, a second phenomenon occurs whereby excited protons align their angle of precession and rotate in phase. Following the RF pulse, excited protons return to the thermodynamically stable low energy state in a process known as 'relaxation'. During this time protons release RF energy as a result of two independent processes: the return of the net magnetic moment to the principle longitudinal z axis (T1 relaxation) and the de-phasing of proton spins in the transverse x-y plane (T2 relaxation).

T1 and T2 refer to the time constants for the regrowth of longitudinal magnetisation and the de-phasing of transverse magnetisation respectively. T1 and T2 relaxation rates are therefore inverses of each other when plotted over time (Fig. 2.3). T2 relaxation always precedes at a faster rate than T1 relaxation. In general, T1 and T2 relaxation curves are determined by the size and motion of the molecule on which the hydrogen proton resides. In most organs T1 values are 5-10x longer than T2 values, pure liquids (water/CSF) have very long T1 and T2 values, and dense solids (proteins/tendons) have very short T2 values. In practice, inhomogene-

ity in the primary magnetic field causes protons undergoing T2 relaxation to de-phase faster still. This rapid relaxation imposes constraints on applying gradients and acquiring a signal. As a consequence, more sophisticated sequences of excitation such as 'spin echo' and 'gradient echo' have have been developed (Norris, 2012). The combination of T2 relaxation and field inhomogeneity is termed T2*. T2* effects are particularly sensitive to the presence of oxygenated and de-oxygenated haemoglobin making it favourable for studying brain activity (where oxygen consumption due to increased metabolic demand is a factor). T2* sensitive images therefore form the basis of fMRI. Gradient coils located in the bore of the scanner alter the precession frequencies between slices enabling slice selection and localisation along the x, y, and z axes (and is the source of the loud noises often audible within the scanner).

Many fMRI studies acquire data from the entire brain using 30 or more different slices with an MRI technique known as multi-shot echo planar imaging (EPI). Activity in adjacent brain regions is captured at different time points, thus, 'slice timing correction' is applied to make it appear as if the whole volume was acquired at the same time point. So-called single-shot EPI circumvents this step and ameliorates motion artefacts by capturing whole-brain T2* sensitive images at high speed after a single RF excitation pulse (~3 secs).

## Contrasts

Two key acquisition parameters can be manipulated to provide a suitable contrast for distinguishing tissue types or examining pathology: repetition time (TR), the length of time between repeats of the excitation pulse, and echo time (TE), the length of time between between the excitation pulse and the acquisition of signal. Different tissue contrasts are achieved in the acquired image by modulating TR and TE to capture different phases of the T1 and T2 relaxation curves . A short TE and TR results in an image contrast unrelated to the T2 relaxation. Known as T1-weighted structural images, these provide high contrast between grey matter, white matter, and

CSF compartments . When TE and TR are relatively extended, T1 relaxation effects are minimised meaning the contrast is primarily determined by T2 relaxation. Certain MR sequences using 'gradient echos' are further sensitive to T2* relaxation. These T2*-weighted images form the basis of fMRI using the BOLD technique.

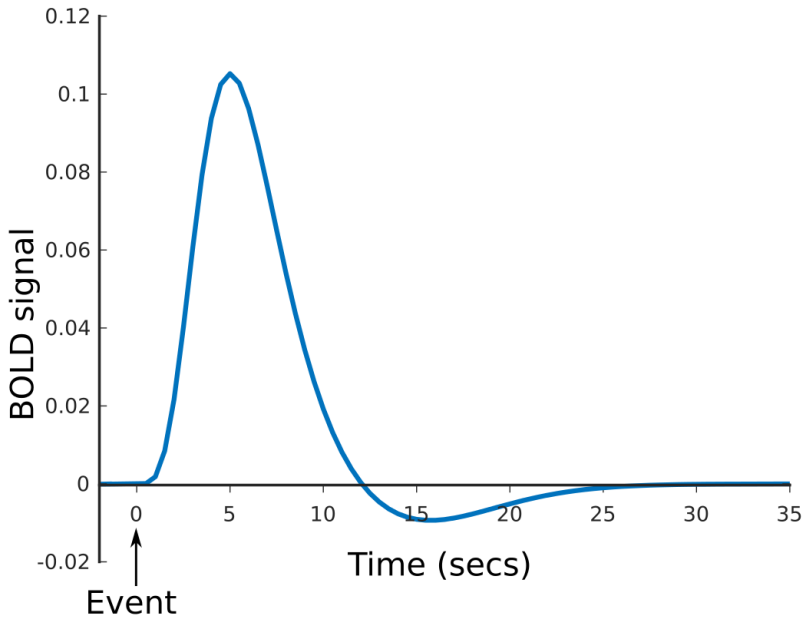


Figure 2.4: Canonical haemodynamic response. A neural event at time zero is accompanied by a rapid increase in BOLD signal over the course of ~5 seconds as local blood flow increases to satisfy a transient increase in metabolic demand. BOLD signal then rapidly decreases, followed by a short undershoot as blood flow returns to baseline over the course of ~20 seconds.

## Blood oxygen level dependent signal

Sites of elevated neural activity are associated with heightened metabolism of glucose and oxygen and an increase in cerebral blood flow to meet the demand. Known as the canonical haemodynamic response function (HRF), blood flow peaks around 5 seconds after the onset of local neural activity

followed by a short undershoot (van Zijl et al., 2012) as blood flow returns to its baseline level (Fig. 2.4). T2* imaging exploits the paramagnetic properties of oxygenated and de-oxygenated haemoglobin to measure blood flow in the brain. High metabolic demand alters the proportion of oxygenated to de-oxygenated haemoglobin in active regions of the brain. These changes are detected as local homogeneities within the primary magnetic field and referred to as the BOLD signal (Ogawa, 2012). The neural basis of fMRI BOLD signal is a matter of continued debate (Fox, 2012).

## Analysis of fMRI data

A typical neuroimaging session involves collecting a high-resolution T1-weighted structural image of the brain and several lower resolution T2*-weighted functional images. A number of different pre-processing techniques have been introduced to facilitate comparison of functional data across individuals and correct for motion and imaging artefacts. These steps typically include: (1) discarding the initial volumes of the image to remove 'off-scale' magnetisation effects that have yet to reach steady state; (2) removing skull and other non-brain tissue from the T1-weighted anatomical image to minimise issues with alignment; (3) tissue segmentation of the high resolution T1-weighted image; (4) alignment of individual functional volumes to a common template (co-registration) to minimise motion artefacts; (5) projecting the functional data to a common reference template to compare across subjects(normalisation); and (6) temporal and spatial filtering of functional data to improve the signal to noise ratio.

Tissue segmentation refers to separating grey matter, white matter, and cerebrospinal fluid on the basis of their distinctive intensities in the T1-weighted structural image (Huettel and Song, 2014). These 'regions of interest' may be used to extract the mean BOLD signal from a set of voxels. Problems arise when single voxels contain more than one tissue type leading to so-called 'partial volume effects'. Tissue segmentation algorithms from different vendors therefore take into account tissue probabilities (e.g. SPM)(Ashburner, 2012) and the geometric structure of the brain's grey-

white matter interface (e.g. Freesurfer)(Fischl, 2012).

A major challenge in neuroimaging is to correct the distortions introduced between successive time frames by the movement of the subject's head in the bore of the scanner (Power et al., 2014, 2015). The consequences of movement include: (1) a given voxel may contain signal from two types of tissue or lose signal at the edge of the volume; (2) the uniformity of the magnetic field which has been calibrated or 'shimmed' for one particular head position may be altered; and (3) images acquired one slice at a time may report incorrect patterns of excitation (Huettel and Song, 2014). If not accounted for, these distortions can lead to spurious correlations and faulty inferences regarding the nature of the brain's functional activity and connectivity (Power et al., 2012).

Motion correction or 'realignment' of successive frames to a standard reference image (usually the first volume or an average volume) ensures that the anatomical location of individual brain regions are consistent over the duration of the entire run (Huettel and Song, 2014). A typical workflow uses affine or rigid-body transformations to superimpose one volume upon the other. This process results in three rotational and three translational time courses capturing the brain's 3D motion within the scanner.

Although minor misalignments can be corrected and subjects with excessive movement removed from the analysis, a further source of error remains (Huettel and Song, 2014). Head movement following the RF pulse can lead to faulty assumptions regarding the spin history of localised slices and the introduction of small but significant levels of artefactual signal. Methods of removing this signal are an ongoing area of research and debate within the neuroimaging community (Power et al., 2014, 2015). Global signal regression and the anticorrelations it introduces are particularly controversial (Fox et al., 2009). Any effects of motion not corrected by realignment are 'regressed out' by including the motion related parameters estimated during the realignment procedure as 'nuisance regressors'. More elaborate approaches also include temporal derivatives of the motion parameters, squared time series, and temporal shifts in the data. The inclusion of additional motion related nuisance regressors to account for variance must

be balanced with the loss in degrees of freedom. It is currently unclear when genuine neuronal activity is also starting to be removed (Huettel and Song, 2014).

Co-registration refers to the spatial alignment of a sequence of image volumes (Huettel and Song, 2014). It most often refers to the alignment of functional and structural data from the same subject. Normalisation refers to the co-registration of a subject's anatomical image to a standard reference template to allow comparison between the brains of different subjects (Huettel and Song, 2014). Currently, the most common templates are proposed by the Montreal Neurological Institute (MNI). The current standard template, ICBM152, represents the average T1-weighted structural images of 152 individuals (Grabner et al., 2006). Typically, the subject's average functional image is co-registered to their structural image through an affine transformation. A nonlinear transformation is then used to 'warp' the anatomical image to a standard reference template. The resulting transformation rule is applied to co-register the functional image from the first step into the standard space of the reference template (Huettel and Song, 2014).

Measurements made by MRI are often contaminated by physiological noise (Huettel and Song, 2014). Low frequency components such as vascular and metabolic fluctuations are easily removed via temporal filtering. High frequency confounds related to breathing (~0.3 Hz) or heartbeat (~1.0 Hz) are less easily removed. Standard MRI under-samples these higher frequencies and consistent with the Nyquist theorem aliases them into lower frequency components. Breathing and cardiac rate occur at low frequencies, impacting the cerebral blood flow (and hence the BOLD response) through carbon dioxide vasodilation and blood pressure, respectively. Addressing these confounds is especially difficult given that neural signal and physiological noise may be coupled temporally (Huettel and Song, 2014). In resting state, these physiological fluctuations can occur in the frequencies of interest (<0.1Hz), potentially introducing spurious correlations between regions (Snyder and Raichle, 2012). Physiological noise regression is the standard approach to removing these confounds from the raw signal. As in

the case of correction motion, time series of physiological noise are entered into the general linear model (GLM; see below) as nuisance regressors (Poline and Brett, 2012). The signal of interest can then be separated from the nuisance regressors and recovered in the residuals. By removing the structured, non-random parts of the residuals, physiological noise regression renders the data more normally distributed or 'white'. This satisfies an important requirement of the GLM, that the error terms be identically and normally distributed. Ideally, physiological data related to heart beat and respiration are acquired in parallel with the scan, however in practice, this approach is rarely taken. Since the signal of interest should be located in the grey matter, the most common approach to modelling physiological noise is to extract mean time series from the white matter or ventricles and use these as nuisance regressors in the GLM (Huettel and Song, 2014). More recently, data-driven approaches such as independent component analysis (ICA; see below) have been used to isolate and remove noisy components from genuine signal of interest (Beckmann and Smith, 2004).

Temporal filtering refers to improving the signal to noise ratio by attenuating frequencies that are not of interest (Huettel and Song, 2014). These include very low frequency trends (<0.01Hz) such as 'scanner drift' (where the mean of the data drifts up or down gradually over the course of the session), coil interference (caused by heating of the gradient coils), and slow vascular/metabolic oscillations (Huettel and Song, 2014). This also includes higher frequency physiological components such as heartbeat ( ~0.3Hz) or breathing (~0.1Hz). Frequencies of interest can be isolated by using an appropriate Fourier filter. High pass filters attenuate low frequencies whereas low pass filters attenuate high frequencies. Since resting state studies are mainly interested in low frequency components, most of the data is bandpass filtered between 0.01-0.1 Hz. Low pass filtering may impose autocorrelation (or sample dependence) on the signal thereby violating the temporal independence assumption used for statistical testing (Huettel and Song, 2014). Thus, while the majority of studies routinely perform high pass filtering, the use of low pass filtering is more controversial (although still prevalent).

Standard fMRI preprocessing uses spatial smoothing to tackle anatomical variability not accounted for by normalisation and to boost the signal to noise ratio (Huettel and Song, 2014). Studies show that most spatial noise is Gaussian, independent from voxel to voxel, and centred around zero. Averaging intensity across several voxels therefore tends to average noise to zero and boost the signal of interest to a non-zero value (Desmond and Glover, 2002). Most functional data is spatially smoothed using a Gaussian kernel with full-width half maximum approximately the same diameter as activated voxels (5-8 mm).

## Analysis using the general linear model

The GLM, part of a family of statistical techniques known as linear regression, is the most widely used approach for analysing task-based fMRI. Linear regression finds the 'line of best fit' between a predicator or explanatory variable (on the x axis) and a scalar or dependent variable (on the y axis). For example, plotting the level of illumination on the x axis and the mean BOLD signal in the visual cortex on the y axis would yield a positive linear relationship between the two variables (i.e. a positive slope). Linear regression uses the method of least squares to calculates the line of best fit and a single number (the slope of the line) to indicate how much the dependent variable should increase if the predictor variable were to increase by one unit (all other things being held constant). The model assumes that errors are random, independent, and conform to a Gaussian distribution of mean zero. The line of best fit is the one in which the sum of the squared errors between the data points and the line are minimised. Linear regression produces separate equations equal to the number of data points. These are expressed with matrix algebra as:

$$Y = XB + e$$

where Y is the measured fMRI BOLD signal from a single voxel, X are the experimental design variables, B is the weighting factor (the slope), and e is some random error. X, Y, and e are column vectors and B is a scalar.

In the GLM (as opposed to standard linear regression), Y and e remain as single column vectors but X takes on additional columns. Typically, the experimental design variables are assigned their own column each representing a specific factors (or regressor) thought to influence the outcome of the experiment. By convention, the first column represents an idealised prediction of the haemodynamic response function in voxels activated by the task or stimulus. So-called 'nuisance regressors', designed to account for known sources of variance in the raw signal are placed in subsequent columns. These data are often experimentally determined by measuring head motion or physiological noise during the scan. The number of elements in B (the slope or strength of the relationship) corresponds to the number of columns in the experimental design matrix X therefore B is now a column vector.

A voxel that is activated by the experimental design is associated with a positive slope B as the raw fMRI signal Y correlates with the idealised haemodynamic response in X (the task blocks). In contrast, an unresponsive voxel is not associated with a positive slope B as its resting state 'noise' is not correlated with the task. The same logic applies to every other voxel of the brain. A formal test of statistical significance separates voxels which are activated by the experiential design from voxels which are not. The first step involves specifying the null hypothesis that no net BOLD response is observed in a voxel during the experimental task as compared to rest. In reality, we hope that there is a response so we can reject the null hypothesis and find a statistically significant activation (depending upon the aims of the investigation). When we say something is 'statistically significant' we usually mean that the probability (or p value) of a Type I error (a false positive) is below a certain threshold. The probability of getting a false positive by random chance and rejecting the null hypothesis (when in fact we should not) is traditionally set to less than or equal to 5% ($p < 0.05$). The GLM provides a measure for B (the slope) and its standard deviation (which depends on the sum of the mean square errors and the size of the design matrix) from which a test statistic is calculated T = B/SD. The statistic T follows a student's t-distribution (similar to a standard normal

distribution) from which p value percentiles can be determined for every voxel. P values below the 5% threshold are interpreted as significant 'activations' due to task. However, the lack of reproducibility in scientific studies has prompted recommendations to alter the default p-value threshold for statistical significance from 0.05 to 0.005 for claims of new discoveries.

## Data driven functional connectivity analysis

A significant limitation of the GLM is the need to define *a priori* psychological regressors to examine neural activity. Thus, the GLM is unsuitable for analysing resting state data which lacks an explicit experimental task. Also, since every voxel in the brain (>500,000) is considered an independent t test, mass univariate testing presents a multiple comparison correction problem. ICA is a data-driven computational technique designed to overcome these limitations by decomposing a 4D data set (a set of functional volumes) into a set of independent spatial functional connectivity maps (ICNs) together with their associated time courses. The benefit of this approach is that no explicit knowledge of the experimental setup or time course is required (Beckmann et al., 2005, 2009). ICA of fMRI datasets is usually performed by dedicated software e.g. MELODIC, which is part of the FSL software library (Smith et al., 2004; Woolrich et al., 2009).

A major shorting coming of the ICA approach is that it separates components blindly. It also makes no assumptions regarding BOLD signal change or task properties, nor can standard statistical tests be used to determine the significance of particular components. An important challenge in ICA is to match components to cognitive processes evoked by specific experimental tasks (and their corresponding haemodynamics). Several recent approaches have combined data-driven ICA with hypothesis-driven statistics to address this issue (McKeown, 2000). Another challenge lies in combining data from across subjects. Since the pattern of components extracted by ICA is unique to each dataset, each subjects data will yield a different set of components. While it is possible for the ICA algorithm to generate a single set of components across subjects, differences in functional

organisation at the subject-level will not be retained. Recently, quantitative approaches have been developed to improve inferences from group-level data. Dual regression ICA is robust to inter-subject variability in the spatial properties of networks and provides a quantitative assessment of how well each voxel matches onto each network for individual subjects (Huettel and Song, 2014).

## 2.3 Integral principles of diffusion tensor imaging

The random (or Brownian) motion of water molecules is expressed in terms of the diffusion coefficient (D) (Kingsley, 2006). In principle, a perfectly homogeneous fluid is isotropic – its diffusion coefficient is equal in all directions. In reality, diffusion is constrained by the boundaries of its container, thus, the diffusion coefficient is not equal in every direction but anisotropic. Diffusion tensor imaging (DTI) is a method for quantifying the relative proportion of diffusion in each direction (Le Bihan et al., 2001; Le Bihan, 2011). When performed on an MRI image, this technique enables estimation of the predominant direction of diffusion in a voxel and the major white matter fibre bundles of the brain to be reconstructed via a process known as tractography (Hermundstad et al., 2013).

As well as T1 and T2 relaxation, diffusion weighted images are also sensitive to the direction of water molecules along a specific vector. As in traditional MRI, diffusion weighted images rely on an excitatory RF pulse to induce hydrogen protons to precess in phase, however, this is followed by an additional pair of strong (b ~1000) opposing magnetic gradients. The so-called 'b-value' is expressed in units of time/area. Typical b-values available on modern MRI scanners range from 0 to about 4000 s/mm$^2$. The first gradient induces protons to spin at different rates depending on their location within the gradient. Protons in the strongest part of the gradient spin faster than protons in the weakest part of the gradient. The second gradient, designed to cancel the effect of the first gradient, is applied in the

opposite direction. Successful re-phasing of protons only occurs if water molecules are static in relation to the axis of the gradient i.e. there has been no diffusion (equivalent to a standard diffusion-free T2 weighted image). If however, protons move during the de-phasing and re-phasing cycles, the re-phasing field will incorrectly re-phase protons leading to less energy being released and signal dropout (as compared to a standard diffusion-free T2 weighted image).

In diffusion weighted imaging, the b-value refers to the strength and timing of the diffusion gradients. The optimal choice of b-value is not clearly defined and depends on several factors such as field strength, number of signals averaged, anatomical features, and anticipated pathology. Standard diffusion weighted imaging always begins by obtaining a baseline b-zero (b ~0) image (not to be confused with the primary magnetic field B0) while the diffusion-sensitive gradients are turned off. Thereafter, source images sensitized to diffusion in different directions are generated by applying the high b-value gradients (b ~1000). At a minimum, three sets of source images are produced that correspond to the x, y, and z axes of the laboratory reference frame. More modern schemes acquire source images in at least 20 or more different directions. Source and b-zero images are not viewed separately but combined into a single image known as the 'apparent diffusion coefficient' map.

Diffusion is described by a matrix called the diffusion tensor which expresses the diffusion rates in each combination of direction (Fig. 2.5). After simplification, six unique directions remain, where the diagonal elements (Dxx, Dyy, Dzz) represent diffusion coefficients along the three principal axes and the off diagonal elements (Dxy, Dyz, Dxz) represent the correlated motion between each pair of principal axes. For perfect isotropic diffusion, the diagonal elements are equal and the off diagonal elements are zero. For anisotropic diffusion, the diagonal elements are unequal and the off diagonal elements are non-zero. Convention dictates that individual tensor elements are calculated in relation to the laboratory (x, y, z) reference frame where the z axis aligns with the primary magnetic field and the patients body (toes to head). The laboratory reference frame is subsequently converted into a

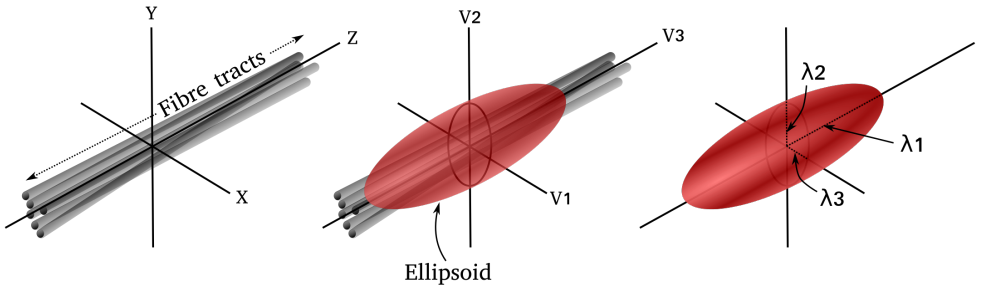


Figure 2.5: The diffusion tensor model. Diffusion of water molecules is modelled in each voxel using the diffusion weighted signal along each of the principal diffusion gradients, fitted to an ellipsoid. The ellipsoid is described using six parameters, V1-3 (or eigenvectors), which specify the angle of diffusion in each direction and $\lambda$1-3 (or eigenvalues) , which correspond to the mean signal in each of the principal directions.

more convenient coordinate system where the principle axes align with the anatomical structure itself. This reference frame, based on the 'diffusion ellipsoid', is fully determined by six parameters: the three dimensions of the ellipsoid, the eigenvalues, and the three vectors representing the orientation of the fibres, the eigenvectors. The eigenvalues express the deviation of a particle's position with respect a reference position over time (and are proportional to mean squared displacement). By convention, eigenvalues are labelled in descending magnitude ( $\lambda 1 > \lambda 2 > \lambda 3$ ). The fitted ellipsoid is specified in 3D space by multiplying each eigenvector with its corresponding eigenvalue.

The eigenvectors and eigenvalues are used to calculate metrics describing the shape and quantity of diffusion within individual voxels. The average of the three eigenvalues represents the overall magnitude of diffusion within a voxel and is referred to as the mean diffusivity (MD). The ratio of eigenvalues may be used to quantify the direction of diffusion. Axial diffusivity (AD), defined as the largest eigenvalue, and radial diffusivity (RD), defined as the average of the two smaller eigenvalues, are interpreted as diffusivity parallel to and perpendicular to the direction of the fibre tract respectively. Fractional anisotropy (FA) – the most widely used measure of diffusivity

– ranges from zero to one and reflects the amount of diffusion asymmetry within a voxel (Basser and Pierpaoli, 1996, 1998; Basser et al., 2000). FA of zero corresponds to perfect isotropic diffusion (a spherical diffusion ellipsoid characterised by equal eigenvalues) whereas FA approaching one corresponds to a progressively elongated diffusion ellipsoid (characterised by unequal eigenvalues). Accordingly, the 'FA map' is a greyscale image where brighter areas reflect more anisotropic diffusion.

## Tractography

Tractography refers to the process of reconstructing the brain's anatomical fibre pathways by plotting the direction of the primary eigenvector from an initial 'seed point' through a series of contiguous voxels until some termination criteria is achieved. These artificial fibre tracts are known as 'streamlines'. Although several thousand microscopic axons may be contained within a single voxel, they are primarily organised into coherent fibre bundles at the macroscopic scale thereby allowing their predominant orientation to be estimated. There are two types of tractography algorithm: deterministic and probabilistic. Deterministic algorithms estimate the most likely fibre orientation and therefore fail in voxels without a predominant direction of diffusion. This situation primarily occurs in regions where fibres cross, kiss, or branch (Jbabdi et al., 2010). Probabilistic tractography overcomes this limitation by using a deterministic algorithm to generate thousands of streamlines at slightly different orientations. The set of all these connections is then used to generate an overall probability distribution map for the spatial extent of the fibre. Since the direction in each voxel is not determined by the largest eigenvector but by the probability function, the streamline will follow either of the appropriate fibre directions in regions of crossing fibres (Behrens et al., 2003). DTI and fibre tracking algorithms have proven valuable for comparing groups of subjects but their application to clinical diagnosis of individuals is controversial (Jones and Cercignani, 2010; Jones et al., 2013). Considerable variation in regional FA exists between subjects as a function of age, gender, location, and MRI technique

(Jones and Cercignani, 2010; Jones et al., 2013). Moreover, tractography algorithms are vendor specific and differ in detail (Soares et al., 2013). Results are also strongly dependent on factors such as the size, orientation, and position of initial seed points, and the criteria used to terminate tracks (Schirner et al., 2015). One of the primary goals of tractography is to generate a graph of whole brain connectivity – a so-called 'connectome' – where regions are nodes and linkages are edges (Sporns, 2011*c*). The purpose is twofold: (1) to inform the coupling strength between nodes in whole-brain computer models (Bassett et al., 2018, 2017) and (2) to enable different features of the network's topology to be objectively quantified. The emerging overlap between dynamical systems theory and network science offers considerable potential as a framework for understanding the structural and functional basis of cognition (Sporns, 2011*c*, 2014; Petersen and Sporns, 2015). The latter aim is dependent on tools derived from graph theory.

## Graph theory

The essential proposition of graph theory is that nodes can represent particular entities and edges their interactions (Sporns, 2011*c*; Fornito et al., 2016). The construction of a graph proceeds along a prescribed series of steps (Kaiser, 2011). First, network nodes are defined, typically these are cortical regions identified through one or more neurobiological properties such as architecture, function, connectivity, or topography. These regions are typically derived by specifying an objective parcellation of cerebral tissue into non-overlapping areas based on either structural, functional or multi-modal data (Evans et al., 2012; de Reus and van den Heuvel, 2013). Often, these regions are compiled into an atlas for general use (Van Essen et al., 2017). These are often used by specialised software such as Freesurfer (Fischl, 2012) to guide tissue segmentation (Destrieux et al., 2010). The next step is to estimate some measure of association between the pairwise nodes. In principle, this includes any definition, be it structural, functional, or effective.

A graph is simply a mathematical representation of a real world net-

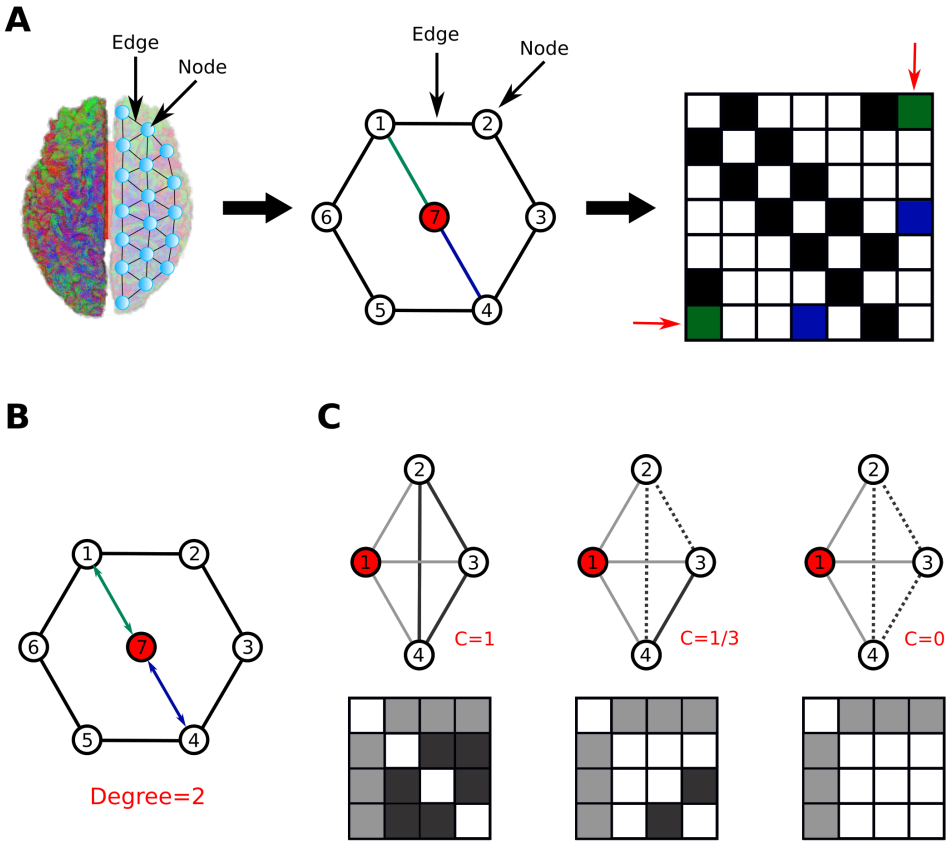


Figure 2.6: Graph theoretical representation of brain network connectivity. A) Structural connectivity is represented as a graph where each node corresponds to a region of the brain and the weight of each edge is defined by estimating the strength of empirical connectivity between a pair of regions (left). An example network composed of seven nodes arranged in topological space (centre) and corresponding weighted graph or 'connectome' (right). B) The degree of a node is determined by counting the number of connections made between it and all other nodes in the network. Here, node seven (in red) has a degree of two reflecting its connections to nodes one and four. C) More sophisticated graph theoretical measures are also available. One example, the local clustering coefficient, is a measure of the degree to which nodes cluster together. It quantifies how close a node's neighbours are to being a fully connected graph or clique.

work, or more generally, any system where network components interact over time. Graph theory is the mathematical study of these networks. The principle goal of constructing a 'connectome' is to represent brain networks as graphs where regions correspond to nodes and edges to interactions (Fig. 2.6)(Sporns, 2013*a*). It is the basic formalism of representing brain networks as graphs which permits a quantitative analysis of brain network connectivity to be performed. Measures of topological connectivity within the graph can then be defined using the mathematical tools of network science (Lowe et al., 2016; Bassett and Sporns, 2017). Graph theory is one of the most active branches of mathematics with applications in many fields. Its scope stems from its ability to represent any network regardless of its underlying physical instantiation as a series of nodes and edges. The most elementary representation of a graph is referred to as the 'adjacency' or 'connectivity matrix'. The connectivity matrix defines the topological relationships between network elements by representing nodes as rows/columns and representing edges as binary or weighted entries. Nodes can be linked directly or indirectly through a series of intermediary edges and nodes. Ordered sequences of unique edges and intermediate nodes are called 'paths'. A path between two nodes implies that one node can be reached from the other by traversing a series of edges. The 'distance' is the length of the shortest path linking two nodes where length does not refer to spatial distance but topological distance. An edge between two nodes indicates direct communication. Paths of various length demonstrate the many indirect routes a signal can traverse between two nodes. Many analyses focus on the shortest path length as these pertain to effective communication. Real-world systems like the brain engage in dynamics across multiple temporal and spatial scales where components and interactions are not well-defined. With this in mind, the choice of nodes and edges (components and interactions) must be carefully justified as they will have an impact on the computation and interpretation of the data. The present thesis leverages structural data obtained from HCs and subjects with MCI and AD to capture large-scale connectivity between cortical regions.

An important organising principle by which healthy brain networks

are arranged is the idea of 'small-worldness' (Bassett and Bullmore, 2006, 2017). The topology of small-world networks is characterised by high clustering within groups of nodes but sparse interconnectivity between clusters (Watts and Strogatz, 1998). Thus, small-worldness refers to the phenomena whereby functional modules are connected by a small number of long range pathways, ensuring a low overall path length between any two nodes. Small-worldness appears to be a ubiquitous property of nervous systems across multiple scales (Stam, 2004; Achard et al., 2006; Sporns and Honey, 2006; Sporns, 2006; He et al., 2007; Gallos et al., 2012; Hilgetag and Goulas, 2015). Small-worldness allows clusters to maintain their individual functionality yet also communicate using a minimal number of steps thereby minimising wiring cost (Bullmore and Sporns, 2012) and supporting the emergence of network hubs (Hagmann et al., 2007, 2008; Iturria-Medina et al., 2007, 2008; van den Heuvel and Sporns, 2013).

The 'rich-club' phenomena is a related concept whereby well-connected network hubs tend to link to one another rather than to hubs which are less well connected. Network hubs of the cerebral cortex aggregate into a single high performance backbone known as the rich-club network (van den Heuvel and Sporns, 2011; Collin et al., 2014; Harriger et al., 2012; van den Heuvel et al., 2012; Pedersen and Omidvarnia, 2016; Senden et al., 2014, 2017). Thus, hubs of the brain do not operate independently but as a single collective. This attribute of network organisation has important consequences in neurodegenerative disorders where pathology is linked to network structural change (Daianu et al., 2013, 2015; van den Heuvel and Sporns, 2013; Griffa and Van den Heuvel, 2018).

## 2.4 Summary and conclusion

Human functional neuroimaging as we know it today can trace its roots back more than a century but it would not be until the late 20th century that these tools would become widely available (Raichle, 2009). Some, such as PET, were limited in their spatial and temporal resolution by the decay properties of a radioactive isotope injected into the bloodstream. Others,

such as EEG, which measured electrophysiological recordings through the scalp, were able to detect rapid fluctuations in neural activity but were unable to pinpoint their exact source. Thus, fMRI, which offered spatial resolution on the order of millimetres and temporal resolution on the order of seconds, rapidly emerged as the dominant modality for mapping brain activity (Rosen and Savoy, 2012). The subsequent explosion of studies linking particular brain regions to behavioural states (Bandettini, 2012; Bullmore, 2012) led some commentators to suggest that fMRI represented the 'new phrenology' (Diener, 2010). Thus, in recent years, there has been a shift in the neuroimaging community, away from so-called 'blobology' (functional specialisation/segregation), toward a more holistic approach based on 'connectology' (functional integration)(Hasson and Honey, 2012; Poldrack, 2012; Smith, 2012).

The development of fMRI was accompanied by innovations in describing the brain's structural connectivity. The diffusion tensor model permitted, for the first time, the complex fibre tracts in the human brain to be comprehensively mapped and recorded in a graph of connectivity called the connectome (Sporns, 2010, 2012, 2013*a*,*c*). Conceptualising the brain in this way has significantly contributed to our understanding of how functional brain states emerge from their underlying structural substrate. Firstly, it has permitted the structural topology of the brain to be studied using tools of network science and graph theory (Sporns, 2011*a*; Fornito et al., 2016; Bassett and Sporns, 2017)). Secondly, it has stimulated the development of whole-brain computer models based on anatomically plausible connectivity (Cabral et al., 2017). The following section is devoted to exploring and contextualising this literature.

# 3 Background

## 3.1 Introduction

This chapter surveys the current state-of-the-art in relation to the aims and objectives of the thesis. The background material is divided into three main parts:

- Firstly, the importance of the brain's functional architecture or ICNs are discussed in relation to behaviour and cognition. Next, the activity of the ICNs are placed within a dynamic context by appealing to the concept of the 'neurocognitive network'.
- The second part presents theoretical and empirical evidence that the brain's derives this behaviour from its identity as complex dynamical system poised near criticality. Evidence is presented that the dynamics underlying these phenomena is most accurately described by a series of transitions between weakly or pseudo-stable attractor states rather than as convergence to a fixed-point attractor. These dynamics, which confer several features of benefit to information processing, are subsequently explored. The closing section uses findings from theoretical computer modelling to examine how this spontaneous behaviour emerges in the brain.

- The third part frames brain disorders as failures of circulating information or so-called 'disconnection syndromes'. To motivate this argument, the role of network topology in supporting synchronisation between neural assemblies is presented. This is followed by theoretical and empirical examples of structural disconnection in which neural synchrony is altered by lesions to the brain's structural connectivity. Finally, evidence that AD represents a disconnection syndrome is provided. Taken together, these findings suggests that functional and cognitive deficits associated with AD, stem, in part, from altered network topology.

## 3.2 Intrinsic connectivity networks

MRI was first introduced into clinical practice in the 1980s but it was not until the 1990s that it saw widespread adoption. At that time, brain regions activated by task were identified through a subtractive approach – the activity of the brain prior to stimulus presentation was subtracted from the activity of the brain in the post stimulus presentation (Ogawa et al., 1990). For instance, finding the areas of the brain associated with reading comprehension would involve scanning subjects while they were presented with a word ('Flood') and while they were presented with a non-word ('Floob'). If you were to then infer that the resulting difference in brain pattern were those regions involved in reading comprehension you have made two key assumptions: (1) that these changes do not reflect task difficulty and (2) that these changes do not reflect differential recruitment of areas between tasks. Recently, these assumptions have been challenged (Friston et al., 1996) and alternative strategies for mapping cognitive neural architecture have been proposed (Friston, 1994). Today, experimental designs typically employ the GLM to identify activated regions (Poline and Brett, 2012). This approach attempts to explain the variation in BOLD time course using a linear combination of explanatory variables (the physiological or psychological regressors of interest).

Defining the brain purely in terms of its neural inputs and outputs

yields a framework where cognition is a reflexive mode of brain function. Any pre-existing endogenous activity not directly related to external stimulation is regarded as noise that must be surmounted by meaningful activation. Accordingly, much of neuroscience has been concerned with the stimulus-driven or task-related paradigm in the presence of well-defined environmental stimuli and much less consideration has been given to the brain as a spontaneously active system with rich spatio-temporal dynamics in the absence of input (Cabral et al., 2014; Deco and Corbetta, 2011; Vogels et al., 2005; Raichle, 2010, 2015). The recurrent neural architecture of the brain is such that connections cannot be definitively associated with inputs or outputs. Thus, any model of the brain that presupposes predominately feed forward processing in a serial hierarchy is missing an important feature of the brain's physiology. Even in primary sensory regions most synapses received by pyramidal neurons are from other cortical neurons, with only a small percentage (5-20%) attributable to sensory input (Douglas et al., 1995; Douglas and Martin, 2004). Large-scale areas of the brain further removed from sensory input are interconnected through mono- and polysynaptic pathways. Re-entrant processing makes an important contribution to the shaping of coordinated global brain activity in the service of coherent behavioural responses and in the emergence of spontaneous neural dynamics. These dynamics are more accurately described as a series of transitions between a set of pseudo-stable attractor states rather than as convergence to a stable fixed-point attractor (Kelso, 1995).

An alternative to the task-based activation paradigm is the resting state protocol in which BOLD time series data are acquired over a period of several minutes when subjects are awake, with eyes open, and not explicitly engaged in task (Binder, 2012; Biswal, 2012; Lowe, 2012). Despite the unconstrained nature of the approach, the brains of subjects at 'cognitive rest' demonstrate characteristic spatio-temporal patterns of spontaneous functional connectivity between regions that are highly conserved between individuals (Fox et al., 2005; Fox and Raichle, 2007; van den Heuvel et al., 2009) and self-consistent with the definition of a module i.e. regions comprising a single network are strongly linked to each other but weakly linked

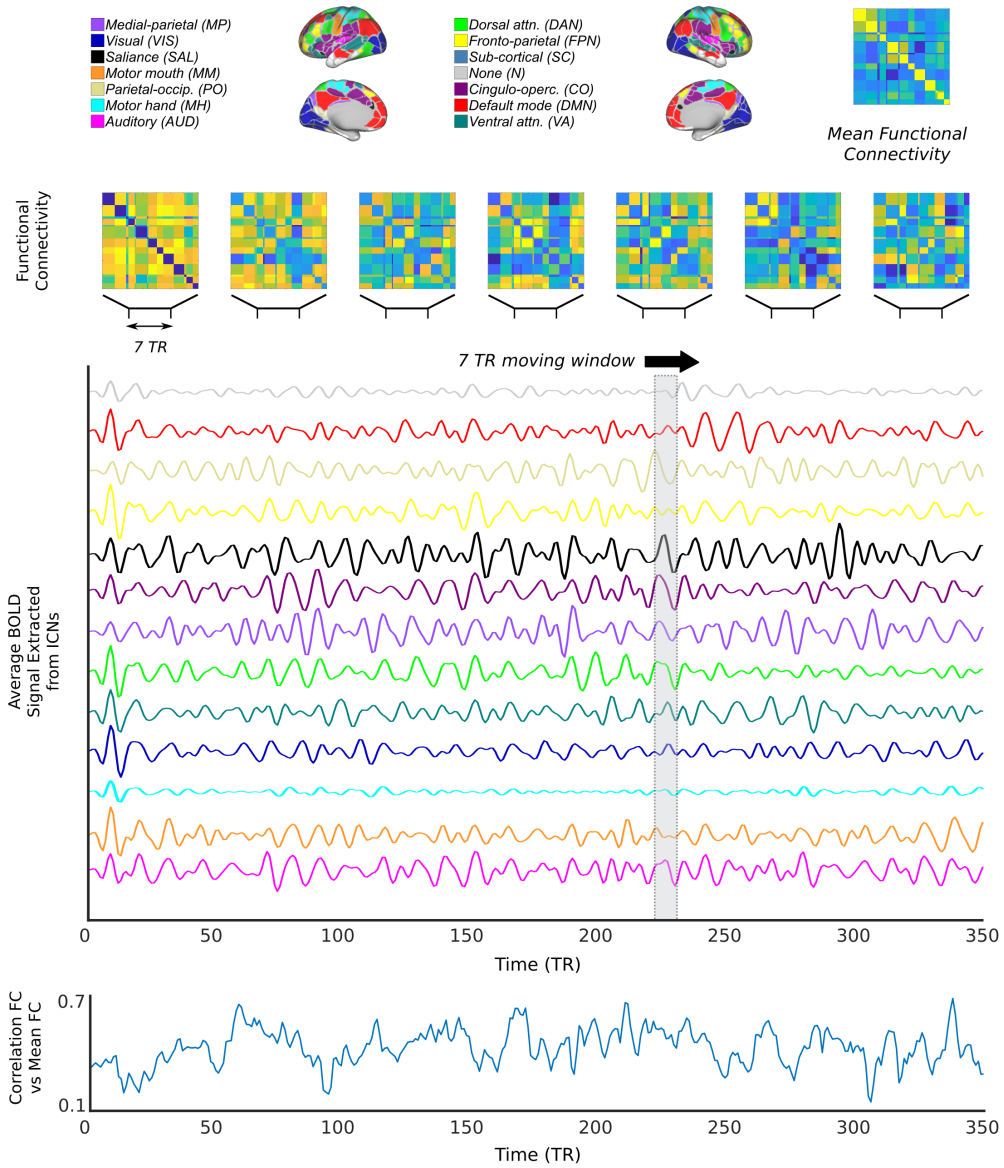


Figure 3.1: Functional connectivity between intrinsic connectivity networks obtained dynamically reconfigures over time. Resting state BOLD time series of intrinsic connectivity networks obtained in a single healthy subject at 'cognitive rest' (centre). Dynamic changes in functional connectivity estimated using a sliding window (top) compared to static or 'grand average' functional connectivity calculated over the entire time course (bottom).

to regions in other networks (Raichle, 2011). These modules, alternately referred to as intrinsic connectivity or resting state networks, are dynamically reconfigured over time as a function of internal fluctuations and behavioural context (Fig. 3.1). Studies of this type have shown that the neural correlates of cognition are not limited to task-based activations but also occur in the brain endogenously.

Subjects at 'quiet rest' show elevated metabolism in an interconnected and anatomically defined set of brain regions (Raichle et al., 2001; Greicius et al., 2003; Buckner et al., 2008) known as the DMN. This so-called 'task-negative' network was originally thought to be deactivated during goal-oriented processing (Fox et al., 2005), but it is now known to support elements of experience directly related to task performance (Spreng, 2012; Sormaz et al., 2018) and spontaneous cognition such as mind wandering or daydreaming (Mason et al., 2007; Kucyi et al., 2017). The DMN has been shown to be negatively correlated with other brain networks related to attention. Several other 'task-positive' networks present during rest are involved in mediating attention, cognitive control, detecting salience, motor output, and sensory processing (Damoiseaux et al., 2006; Wojtuń et al., 2010). Patterns of resting state activity derive their utility from several factors including consistency between individuals (Damoiseaux et al., 2006), test-retest reliability (Damoiseaux et al., 2006), stability over time (Shehzad et al., 2009) and over changes in brain state (Boly et al., 2008), reliable developmental trajectory (Fair et al., 2009), heritability (Glahn et al., 2010), and distinct pattern of alteration in disease (Bassett and Bullmore, 2009; Zhang et al., 2010). The unconstrained nature of the resting state has proven remarkably useful in studies of healthy brain function and in subject populations such as the very young or the elderly where compliance may be an issue.

Although the ICNs of the brain were initially discovered using seed-based approaches (Fox et al., 2005) where the mean time course from one set of voxels is correlated with the time course contained in every other voxel, more recent data-driven techniques have converged on a consistent set of around nine canonical ICNs from which spontaneous and task-evoked brain

dynamics are constructed (De Luca et al., 2006). The leading method, independent component analysis (ICA), decomposes resting state BOLD signal into temporally and spatially distinct patterns of covariation (Kiviniemi et al., 2003; Van De Ven et al., 2004; Beckmann, 2012). Although the spatial and temporal resolution of these networks is largely contingent on data acquisition parameters (e.g. voxel dimension, run duration, etc.) and choice of post processing pipeline (e.g. motion control strategies, etc.), recent studies mapping the functional architecture of the human brain have largely reported consistent findings (Doucet et al., 2011; Power et al., 2011; Yeo et al., 2011; Gordon et al., 2016). The robust nature of the brain's functional architecture at rest permits direct comparison of functional and structural connectivity. Several studies provide comparisons of whole-brain structure and function in the same cohort of healthy individuals (Hagmann et al., 2008; Honey et al., 2009, 2010; Skudlarski et al., 2008). These studies share a core message: structural connections, when present, are highly predictive of the strength of functional connections, however, less frequently, strong functional connections may also exist in the absence of direct structural links through indirect polysynaptic pathways (Goñi et al., 2014; Hermundstad et al., 2013).

Metabolic imaging studies have shown that only a small percentage of the brain's energy budget is allocated to processing momentary task demands; the vast majority is devoted to maintaining intrinsic activity (Raichle and Mintun, 2006; Zhang and Raichle, 2010). From this perspective, variation in sensory responses may best be understood as the interaction of an input with an intrinsic neural context generated by the brain's endogenous dynamics, modulated by attention, arousal, and experience (Fox et al., 2005). This perspective has gained considerable empirical support from a meta-analytic study comparing a large number of brain activation maps obtained during cognitive tasks to ICNs extracted using standard pattern extraction techniques (Smith et al., 2009). More direct evidence comes from comparing patterns of functional connectivity in the brain's large-scale functional architecture at rest and during task performance (Cole, Bassett, Power, Braver and Petersen, 2014; Schultz and Cole,

2016). Studies such as these demonstrate that large-scale functional networks deployed during task-orientated processing are spontaneously active when subjects are at rest. The ongoing rehearsal of functional activity may be required for maintaining the brain's cognitive architecture and for anticipating future stimuli by replaying previous experiences (Schacter et al., 2007).

The intrinsic activity of the brain appears to account for at least some of the behavioural variability observed in the context of a task. For example, much of the trial-to-trial variability of BOLD response in the left and right motor cortices, which are typically correlated at rest, is accounted for by persistent ongoing activity (Fox et al., 2006). Moreover, these spontaneous fluctuations in BOLD response also correlate with motor output (Fox and Raichle, 2007). Ongoing activity may bias the detection of preferred stimuli in regions dedicated to specialised sensory processing (Hesselmann, Kell and Kleinschmidt, 2008; Hesselmann, Kell, Eger and Kleinschmidt, 2008). These correlated fluctuations in ongoing activity and behaviour are often located in large-scale networks associated with higher order cognitive operations such as attentional control (Boly et al., 2007; Sadaghiani et al., 2009; Coste et al., 2011). The emerging picture is one in which ICNs support internal processes relevant to cognition by expressing themselves in different combinations on a relatively static set of structural connections (Fig. 3.1) (Sadaghiani and Kleinschmidt, 2013). These large-scale systems of distributed and interconnected neuronal populations appear to operate and interact according to dynamic principles. Bressler and Kelso (2001) proposed the neurocognitive network as a resolution to the antagonism between two opposing viewpoints: the first, localisation, which holds that complex cognitive functions are localised to specific regions of the brain, and the second, globalism, which posits they are distributed and arise through global coordination. The principle of the neurocognitive network is informed by a modern conception of cognitive function resulting from the dynamic interactions of distributed nodes in a complex network (Bressler and Tognoli, 2006; Bressler and Kelso, 2016).

## Neurocognitive networks

Instead of trying to frame cognition as a strictly localised phenomena, whereby serial processing occurs over precisely defined connectivity, the network approach characterises mental operations by their dynamic patterns of intrinsic or evoked activity. In this view, functions do not reside in discrete brain areas but are the product of network interactions which are rapidly reconfigured to provide dynamic changes in neural context (McIntosh, 1999, 2000, 2004, 2007; Bressler and Mcintosh, 2007). Thus, a given brain region can adopt more than one functional role depending on the pattern of network interactions in which it is embedded. Cognition is therefore distributed over a set of network connections and the large-scale ICNs of the brain are considered to be an essential substrate for supporting the emergence of real-time cognitive function (Bressler, 1995, 2002; Bressler and Menon, 2010; Shanahan, 2006; Mesulam, 2009).

Neurocognitive networks are defined as large-scale systems of distributed and interconnected neural populations in the central nervous system organised to perform cognitive functions (Bressler and Kelso, 2001). Cognition is expressed in real-time by the coordinated activity of distributed cortical areas whose states of mutual coordination are adjusted dynamically over time (Bressler and Tognoli, 2006; Bressler and Kelso, 2016). The neurocognitive network is a critical concept for linking the activity of the brain's large-scale ICNs with higher-level cognition and behaviour. This approach considers the anatomical organisation of the cerebral cortex to be of prime importance in shaping the activity of the brain's cognitive operations. There are many reasons to believe that the cortical region and not the neuron is the operational effector of neurocognitive function. Neurons are typically ineffective at triggering responses in the areas to which they project (Braitenberg and Schuz, 1991), whereas the joint action of local neural assemblies is sufficient to drive a response in a target area (Bush and Sejnowski, 1994). The circumscribed neuronal assembly is an anatomically distinct circuit composed of one to two hundred neurons arranged perpendicular to the cortical surface (Mountcastle, 1997). Around 50-80 of these minicolumns are aggre-

gated into higher level structures – the macrocolumns – that are organised to support basic cognitive operations. Several macrocolumns are bound together through short range interconnectivity into the local area cortical circuit, the fundamental computational unit of neurocognitive function (Mountcastle, 1997). In light of these observations, coupled with the understanding that the brain's long range fibre pathways are organised at the macroscopic scale, the neurocognitive network approach takes the large-scale cortical region as the relevant unit of analysis. The anatomical connectivity of the cerebral cortex provides the basis for an enormous space of possible network configurations (Bressler and Tognoli, 2006). The functional expression of a given cognitive operation requires the co-activation of a specific combination of interconnected local area networks. Members of a subset act in concert as a neurocognitive network with each member providing its own specialised contribution. The multifunctional character of nodes is evidenced by their participation in different network configurations where the relative phase between regional oscillators is seen as an important collective variable for characterising the dynamics of brain and behaviour (Kelso, 1995). Coordination of neurocognitive networks arises from a dynamic regime that balances counteracting tendencies toward integration and segregation (Bressler and Tognoli, 2006; Bressler and Kelso, 2001, 2016). The brain derives this behaviour from its identity as a complex system operating in the metastable regime of its coordination (Kelso, 2012; Kelso and Tognoli, 2007; Kelso, 2009; Tognoli and Kelso, 2014*b*).

## 3.3 The brain as a complex dynamical system

Complexity is often defined as systems in which the whole is greater than the sum of its parts, such that, given the properties of the parts and the principles by which they interact, it is difficult or impossible to infer the collective behaviour of the whole system (Laughlin and Pines, 2013). Complex systems contain many components that take part in structured interactions

to produce 'emergent' phenomena that cannot be reduced to the properties of their components. The highly interconnected, hierarchical, and dynamic character of complex systems poses a serious theoretical and experimental challenges; one that is not met by the reductionist approach. The limited success of reductionist approaches in complex biological networks speaks to the need for a new framework based on the principles of dynamical systems theory. A better understanding of complexity can provide insight into how the structure and function of the brain is organised (Koch and Laurent, 1999).

Complex systems are organised such that they display structure and behaviour half way between order and disorder (Tononi et al., 1998). When order and disorder coexist, complexity is high; when either is high, complexity is low. If all the components of a neural system were to be uncoupled the system would become highly disordered as all the parts would act independently. Conversely, a highly ordered neural system instigated by strong coupling would override any specialised functionality at the local level through global network synchronisation. Clearly, the operation and structure of the brain is not confined to either of these extremes but instead represents a mixture of order and disorder (Friston, 2009*a*). An important feature of large-scale system dynamics therefore, is the coexistence of opposing tendencies toward functional integration and segregation (Kelso, 1995, 2012; Kelso and Tognoli, 2007; Kelso, 2009; Tognoli and Kelso, 2014*b*). Integration and segregation represent fundamental organising principles of the cerebral cortex across all domains of cognition (Tononi et al., 1994; Friston, 2009*b*; Sporns, 2013*b*; Deco et al., 2015). This dichotomy arises from the need to balance locally encapsulated regional processing with coordinated global activity (Sporns et al., 2000).

Anatomical and functional segregation is a multiscale phenomenon that ranges from specialised neurons to neuronal assemblies and cortical regions. An example of segregation is found in the visual cortex where anatomically and functionally distinct regions respond to specific features e.g. orientation, spatial frequency, or colour (Van Essen et al., 1992). Segregation implies that neural responses are statistically independent from one another

and therefore represent specialised information. Structural connectivity also supports functional segregation by linking together populations of neurons with similar response properties. As cognitive functions increase in complexity and sophistication, more functional integration is required to recruit the necessary neural resources. The need to integrate specialised and distributed information recruited from multiple sources is exemplified by the 'binding together' of object attributes into a single coherent visual image (Zeki, 1993). It is thought that neural architectures achieve functional integration through two principles: convergence and phase synchrony. Convergence of hierarchically arranged neural inputs yield increasingly specialised brain regions capable of responding to high-level features of the environment (Quiroga et al., 2005). At the level of large-scale neural networks, some regions bind together multiple signals from unimodal areas to create multimodal representations (Mesulam, 1998; Damasio, 1989). Functional integration can also be achieved through network dynamics that include phase locking or synchronisation between neuronal populations (Fries, 2005, 2009). This mechanism is dependent on reciprocal connections between local area networks to link segregated populations. The 'binding' of perceptual information that occurs through stimulus-dependent neural synchrony, particularly in the gamma band (~20-80 Hz), is thought to underlie the unitary nature of consciousness (Gray and Singer, 1989). These principles are consistent with the essential proposition of the communication by coherence hypothesis (Fries, 2015): synchronisation facilitates neural processing by enabling the detection of coincident spikes in areas that receive convergent signals. Spontaneous or evoked changes in synchronisation can therefore implement rapid changes in functional and effective connectivity while the anatomical substrate remains fixed.

Dynamics evolving on complex networks depend critically on two factors: (1) the response characteristics of individual components i.e. their local dynamics and (2) the overall network structure. Thus, differing network topologies are associated with different complex dynamics. Some topologies create networks of stable attractors, others global synchronisation, still others produce dynamic transients, metastable states, and criticality. In a

series of computational studies, Olaf Sporns used evolutionary algorithms to analyse the link between structural topology and neural dynamics (Sporns, 2000; Sporns et al., 2000; Sporns and Tononi, 2001). Networks were optimised for high entropy, integration, and complexity. However, only networks evolved for high complexity showed patterns of network topology associated with small-world networks comparable to empirical brain networks. This included the presence of many reciprocal connections between nodes, and a modular architecture interlinked by hubs. Increased complexity was also accompanied by the emergence of short path length and high clustering. Moreover, structural re-organisation of large-scale connectivity (by random rewiring) has been found to reduce small-world attributes and the correlations between functional clusters (Honey and Kötter, 2007).

The spontaneous fluctuations of the brain tend to exhibit 'heavy-tail' or 'scale-free/invariant' power-law distributions in structural or functional parameters. Simply put, the shape of the distribution (either spatial or temporal) does not change if you zoom in or out. Distributions of cortical potentials are scale invariant across multiple frequencies and demonstrate transient long range correlations (Linkenkaer-Hansen et al., 2001; Freeman, 2003; Gong et al., 2003; Stam, 2004). Several authors have attributed the power-law phenomena to the existence of a self-organised critical state (Bak et al., 1987). This theory suggests that complex dynamic behaviour emerges spontaneously in spatially extended mediums resulting from a system's self-organising character. Spatially patterned complex systems tend to exhibit scale-invariant fractal properties and scale-free distributions in dynamic events. The regime is referred to as 'self-organised criticality' to reflect its spontaneous development through a balance of robust interactions and sensitivity to perturbations. Self-organised systems are able to self-tune themselves to the critical state without relying on external assistance. The classic example is the sand pile: add more grains and the slope grows, once it reaches a critical value an avalanche occurs to restore the 'critical angle of repose'. The distribution of avalanche sizes reflects a power law. In this regime, the system is said to exhibit 'critical' behaviour. Critical states occur in physical systems when they evolve from an ordered

into a disordered state and approach the 'edge of chaos' (Langton, 1990; Kauffman, 1993). Features shared by systems exhibiting self-organised criticality include scale-free distributions of dynamic events (the avalanches), the presence of phase transitions taking the system from an ordered to a disordered state, and spontaneous development toward criticality without the need to fine-tune system parameters. The diversity of systems in which criticality occurs raises the possibility that brain dynamics are also self-organised (Chialvo and Bak, 1999; Bak and Chialvo, 2001).

The first empirical evidence for self-organised criticality in the brain came from a study examining spontaneous patterns of neuronal activity in slices of rat cortex (Beggs and Plenz, 2003). These corresponded to sequences of spikes or 'neuronal avalanches' whose size distribution reflected power-law scaling. Beggs and Plenz (2003) found that slice preparations operated at or near a critical regime where spikes neither died out nor showed unbounded growth. Spike patterns tended to repeat over time suggesting that they form a stable storage medium or functional repertoire of network states (Plenz and Thiagarajan, 2007).

Criticality is associated with several features which are beneficial to information processing including maximal information transfer (Beggs and Plenz, 2003), a maximum number of metastable state (Haldeman and Beggs, 2005), and optimal sensitivity and dynamic range in response to perturbations (Kinouchi and Copelli, 2006). Some network architectures appear to actively promote critical dynamics. For example, an association between avalanche dynamics and small-world network attributes has been found (Pajevic and Plenz, 2009). More recently, ICN organisation has been shown to emerge at criticality from models incorporating the human connectome (Haimovici et al., 2013; Ódor, 2016). Additional evidence that brain dynamics operate in a critical regime come from EEG, MEG, and fMRI recordings of empirical resting state activity (Poil et al., 2008; Kitzbichler et al., 2009; Fraiman et al., 2009). Phenomena such as these represent a qualitatively different form of computation in which system dynamics evolve from one state to the next without becoming locked into rigid or repetitive behaviour. These neural transients are the subject of the following section.

## Neural transients

The brain's neuronal activity is expressed at several temporal scales, from fast synaptic processes at the millisecond resolution to dynamics that persist over seconds or minutes through the influence of synaptic plasticity. Neuronal activity and behaviour are associated with variability from a variety of sources. Some of these sources, such as the stochastic opening and closing of ion channels in the cell membrane (Faisal et al., 2008) are considered noise - they are generated from random microscopic processes and do not form part of a meaningful signal. However, substantial neuronal variability is not connected to noise at the molecular and cellular level but arises through the deterministic activity of the brain as a weakly coupled dynamical system. This activity emerges as a behaviourally relevant neural signal that is expressed in the variability of cognitive and behavioural states. Activity such as this is most accurately described as a sequence of transients between metastable states rather than as convergence to a fixed-point attractor (Kelso and Tognoli, 2007; Kelso, 2012; Tognoli and Kelso, 2014*b*, 2009).

Metastable dynamics unfold on a complex manifold with several regions that slow or entrap trajectories in the system dynamics to produce quasi-stable temporal behaviour (Fig. 3.2). Transients result from the successive visits to the 'ghosts' or 'remnants' of former fixed point attractors that are neither fully stable nor fully unstable. The manifold can be visualised as a landscape with several shallow indentations or 'wells' where an object moving along the surface is temporarily 'trapped' before jumping out again. The wells represent a succession of metastable states that constitute the system's functional repertoire. Unlike traditional fixed-point attractors, no energy or noise is required to transition to the next metastable state. Computer models with these dynamics are characterised by high system entropy, modular architectures and sparse extrinsic connectivity corresponding to small-world architecture (Friston, 1997; Shanahan, 2010).

A central question is how to mathematically represent and describe the evolution of cognitive information in time. Metastability and heteroclinic

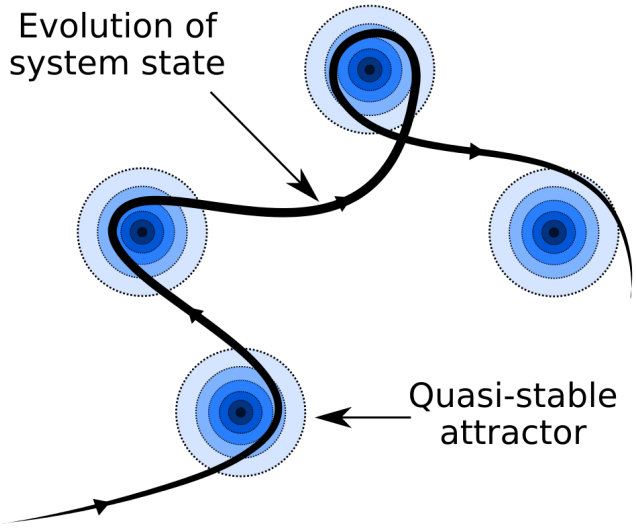


Figure 3.2: Schematic illustration of the time evolution of a system state in phase space (black line) through a series of metastable states (blue circles). The system's attractor manifold has several 'pockets' or 'wells' that entrap the system's trajectory for a time before the intrinsic dynamics of the system (or a perturbation) result in a transition to the next weakly stable state (Rabinovich et al., 2006).

channels provide a mechanism for the sequential coding of discrete cognitive information. Rabinovich et al. (2006) proposed the stable heteroclinic channel as a mathematical model to describe robust cognitive information flows based on sequential dynamics. A metastable state is characterised as a domain in state space in which the system's trajectory demonstrates relatively large dwell times and slow evolution that is separated from other metastable states by a fast transient regime (Rabinovich, Huerta and Laurent, 2008; Rabinovich, Huerta, Varona and Afraimovich, 2008). These slow dynamics may be constant states, oscillatory states, or even chaotic attractors (Tsuda, 2001). Metastable states are characterised as quasi-stationary combining an attractive input channel with a repulsive output channel. One example is the hyperbolic saddle, several of which may be connected via their stable and unstable manifolds to form a heteroclinic orbit (Guckenheimer and

Holmes, 1988). If the saddles are dispersive with one-dimensional unstable manifolds a heteroclinic orbit may become a stable heteroclinic sequence (Afraimovich et al., 2004; Rabinovich, Huerta, Varona and Afraimovich, 2008) or heteroclinic network (Ashwin and Postlethwaite, 2013). Example sequences include the solution of the generalised Lotka-Volterra model for the population of species, the instability occurring at the onset of convection in a Rayleigh-Benard experiment in the presence of rotation, and the Lorenz chaotic attractor. Recently, heteroclinic orbits between metastable states have been observed in biological systems including the insect olfactory bulb (Mazor and Laurent, 2005), in bird songs (Yildiz and Kiebel, 2011), in resting state (Van De Ville et al., 2010) and cognitive (Musso et al., 2010) electro-physiological activity measured at the scalp, in schizophrenia (Tomescu et al., 2014), and in the transition from unconsciousness to wakefulness (Hudson et al., 2014). Heteroclinic orbits are hypothesised to represent a neural coding scheme known as chaotic itinerancy (Ito et al., 2007; Bersini and Sener, 2002). Here, a closed-loop trajectory travels through high-dimensional state space of neural activity directing the cortex through a sequence of quasi-attractors.

Metastable and transient dynamics arise when so-called saddle points are arranged into a chain to form a network with a dynamic manifold (Afraimovich et al., 2004; Rabinovich, Huerta and Laurent, 2008). Trajectories spontaneously transition between nearby saddle points in state space via 'stable heteroclinic channels' thereby defining a robust and reliable sequence of cognitive/neural states following a stimulus evoked response – a possible model for sequential decision making (Hutt and beim Graben, 2017). Neural dynamics based on the transition between pseudo-stable attractor states represent an alternative to more classical models of neural computation based on fixed point attractors (Rabinovich, Huerta, Varona and Afraimovich, 2008). One example, 'liquid state computing' eschews the traditional attractor network (which computes in sequences of discrete states) and instead relies on transient state dynamics to implement real-time computing (Maass et al., 2002). These and other models of transient state dynamics offer an account of self-sustained computations in the brain

(Gros, 2009).

Metastability and multistability represent distinct dynamical regimes (Kelso, 2012). Multistability is the property of having multiple stable equilibrium points or attractors in the state space of the dynamical system where the stability of a state depends on how quickly the system returns to a state following a perturbation. Fluctuations in the nervous system destabilise self-sustaining patterns resulting in a switch from one attractor state to another (Braun and Mattia, 2010). Recently, biophysical modelling has revealed multistability and scale-invariant fluctuations in resting state cortical activity as a result of noisy input into thalamic neurons (Freyer et al., 2011). Crucially, analysis of resting state EEG data using surrogate data suggests that cortical activity operates in a regime of multistability (Valdes et al., 1999; Freyer et al., 2009). These and similar findings have yielded a consensus that is considerably more qualified than initial reports of simple chaos in neurophysiological data (Grassberger and Procaccia, 1983; Wolf et al., 1985). Although terms such as multistability, metastability, itinerant chaos, and criticality are often used interchangeably, these phenomenon arise from independent mechanisms and display characteristic ensemble statistics. Care should be taken to quantify the statistics of large-scale brain interactions so as to distinguish these underlying mechanisms. The development of resampling algorithms capable of generating surrogate data of the same length and possessing the same linear properties as the original data but with nonlinear structure removed represent an important step in this direction (Theiler et al., 1992; Prichard and Theiler, 1994). Only those data which differ significantly from this null distribution may be said to exhibit nonlinear properties.

Whole-brain models are frequently used to investigate observed empirical dynamics by providing candidate mechanisms. Models based on chaotic attractors invoke a form of metastability referred to as chaotic itinerancy (Honey and Kötter, 2007). Here, long periods of high synchrony are punctuated by bursts of desynchronisation. Metastability can also arise in large-scale models with limit cycle attractors due to the frustration caused by transmission delays (Deco et al., 2009). Another scenario is related

to 'ghost attractors' in state space which permit the system to wander through a landscape of remnant attractors (Deco and Jirsa, 2012). In the present thesis, the Kuramoto model of coupled phase oscillators is used to investigate the complex dynamics arising from the structural connectome (Kuramoto, 1984). Each node is assigned its own intrinsic operational frequency. The network dynamics of the system is then defined by the weak delayed coupling (or phase lag) between pairwise oscillators representing cortical regions. The overall dynamic stability of the system is estimated by calculating a well-defined order parameter (Shanahan, 2010). The Kuramoto order parameter captures the overall phase of a group of oscillators to quantify how 'phase-locked' they are at a given moment in time. The variation in this order parameter has been proposed as a measure of a system's metastability whilst the mean of the phase-locking across time is equivalent to a measure of the system's overall synchrony. Metastability is high in a system that visits a range of different states over time whereas both highly ordered and highly disordered states are associated with low metastability and high and low synchrony, respectively.

Scott Kelso developed the theoretical framework of Coordination Dynamics to explain the self-organising properties of brain and behaviour (Kelso, 1995). Coordination dynamics seeks to understand how patterns of coordinated behaviour arise, persist, and adapt over time using the concepts of synergetics (Haken, 1996) and the methods and tools of dynamical systems theory. Coordination dynamics describes a system's collective behaviour by capturing the temporal ordering between interacting components. It is the relative coordination between neural components that drives spatially extended patterns of neural activity. These time varying interrelationships of coordinated local areas give rise to metastability in the brain (Kelso, 1995; Bressler and Tognoli, 2006). The phenomenon of metastability is important as it furnishes a dynamical explanation for how large-scale networks of the brain coordinate their activity in space and time and support cognition (Bressler and Kelso, 2001, 2016). The metastable regime of neural dynamics reconciles two competing tendencies: the tendency for local brain regions to act independently and the tendency for local regions

to express their synergistic behaviour and coordinate globally (Kelso and Tognoli, 2007; Kelso, 2012; Tognoli and Kelso, 2014*b*, 2009). These patterns of coordinated activity fluctuate on a rapid time scale (within hundreds of milliseconds) (Bressler et al., 1993). Exogenous input is not required to engage in this behaviour as rapid transitions between metastable states occur spontaneously as a result of the system's internal network dynamics. In the functional architecture of the brain, each metastable state is equivalent to a set of couplings between different brain regions that expresses a functional network. Metastable dynamics are such that a large repertoire of functional networks can be visited in rapid succession without requiring noise to transition to the next state. These rapid transitions in functional connectivity have been observed in electrophysiological recordings of task-oriented and spontaneous neuronal behaviour and are thought to reflect the momentary flow of states that contribute to the unity of mind, body, and brain (Kelso, 1995; Kelso and Haken, 1995). Coordination dynamics places special emphasis on the metastable mode of brain operation and the relative phase relationships between local areas to account for cognition (Bressler and Kelso, 2001, 2016). It is the coordination dynamics of neurocognitive networks that determines the configuration of local areas that become dynamically linked in the execution of a particular cognitive operation, and how these patterns of dynamic connectivity evolve over time (Bressler and Tognoli, 2006). These dynamics are likely exploited by nervous systems to confer behavioural flexibility in the face of an unpredictable environment. This, and other advantages are discussed in the following section.

## The benefits of dynamic diversity

The preceding section paints a picture of neural dynamics rather different from that of classical modes of computation. Traditional computation emphasises serial processing hierarchies, noise free transmission of signal, limited spontaneous behaviour, reliable encoding of information, stable attractor dynamics and discrete well-defined states. Whilst application of these models has been successful in narrowly defined domains characterised

by an absence of conflicting requirements, models employing features of real brain dynamics including spontaneous transients, coordinated dynamics, and criticality are underdeveloped (Cabral et al., 2017). These phenomena, from neural avalanches to large-scale power-law distributions of synchrony and coherence are consistent with a complex dynamic system operating at or near criticality. Theoretical studies indicate that the critical regime confers fundamental computational advantages such as the transmission and storage of information. At the critical point, systems can preserve or transmit information regarding a stimulus or perturbation over an extended period of time whereas subcritical or supercritical dynamics exhibit a more compressed repertoire of responses (Kinouchi and Copelli, 2006). In principle, both of these regimes are beneficial under different circumstances. Criticality may have arisen as a response to an environment in which randomness and regularity (chaos and order) are primal constituents of reality. This regime likely reflects an optimal working point for the extraction and generation of new information (Kelso, 1994).

The itinerant motion of metastable trajectories and the linkages in state space of quasi-stable attractors likely derive from the pattern of macroscopic structural connectivity in the brain. Structural connections may constrain the system's trajectory and its response to exogenous input. It has been suggested that dimensionality reduction in the system's accessible state space is achieved through clustered or modular architecture. Thus small-world network attributes give rise to a landscape of attractor ruins (or saddle points) linked by channels that permit the system to transition from one metastable state to another via the shortest path. Hub regions may facilitate the transition from high to low dimensional states by guiding the system's trajectory between channels. The power-law scaling phenomena of nervous systems is also found at the level of human behaviour. Features such as scaling, coordination, and dimension reduction are a pervasive feature of behavioural activity such as movement, locomotion, and speech, as well as, higher order cognitive faculties (Kello et al., 2007, 2008). Metastability is thought to reveal the origin of cognition through the organisation of spatio-temporal patterns of brain, body, and environment (Kelso, 1995).

Such theories bridge the conceptual divide between a fixed anatomical structure and cognitive flexibility. Converging lines of inquiry suggest that the theoretical framework of metastable coordination dynamics (and the observable phenomenon of relative coordination of local areas), finely tuned to criticality, exhibit a subtle blend of integration and segregation from which the complexity of brain and behaviour arise. Theoretical computer modelling suggests that metastability is an intrinsic feature of the brain's dynamics when at rest. The following section explores the role of theoretical computer modelling in understanding how these spontaneous patterns of behaviour arise in the brain.

## Modelling spontaneous neural dynamics

Endogenous functional activity is organised into ICNs which largely overlap with the structure of the brain (Hagmann et al., 2008; Honey et al., 2009, 2010; Skudlarski et al., 2008). Computational modelling is a powerful technique for clarifying the relationship between this functional architecture and its structural foundations (Cabral et al., 2014, 2017). Recent advances in non-invasive neuroimaging technology have enabled the brain's physical 'wiring diagram' to be captured and represented as a graph (Sporns, 2010). Incorporating this map of connectivity into whole-brain computer models has allowed the creation of simulated neural time series which can be processed using the same pipeline as empirical data sets, ameliorating the confounding variables associated with measuring empirical brain activity e.g. physiological noise, movement or imaging artefacts, and issues with co-registration. A number of studies have used computational modelling to compare the simulated functional connectivity produced from the structural linkages of the brain with the empirical functional connectivity recorded using fMRI (Honey and Kötter, 2007; Honey et al., 2009). The message from these studies is clear: although the correspondence is not perfect, theoretical computer models based on anatomical connectivity capture much of the functional connectivity observed at rest (Messé et al., 2014). Accordingly, computational connectomics provides a tool for clarifying the structural

and functional basis of neuropsychiatric disorders (Deco and Kringelbach, 2014).

Even though the spiking mechanism of single neurons was discovered and described with mathematical precision over 50 years ago (Hodgkin and Huxley, 1990), there is, as yet, no broadly accepted mathematical theory describing the collective behaviour of neuronal populations (Breakspear, 2017). This lack of consensus is reflected in a zoo of 'mean-field' neural models describing the ensemble activity of cell populations. Recently, a concerted effort has been made to incorporate these models into a common mathematical framework (Sanz-Leon et al., 2015). The derivation of mean-field models is founded on two key assumptions: (1) that at large spatial scales the activity of individual neurons is irrelevant and (2) that the state of neurons across the ensemble are uncorrelated. The central limit theorem states the sum of uncorrelated random processes converges to a Gaussian probability distribution. Given this 'diffusion approximation', the activity of a patch of neurons can be described by the mean and variance of its firing rate. The mean firing rate reflects the response of the population to its afferent input while the variance reflects the dispersion of all stochastic effects. The equation which describes this linear, normally distributed ensemble can be derived from a simple integrate and fire neuron model where the diffusion approximation holds (Omurtag et al., 2000; Fourcaud and Brunel, 2002). This Fokker-Plank equation describes the collective response of a neuronal population to its inputs. The firing rate essentially encodes the most likely population-level representation of the input by summing all the individual responses. The Fokker-Plank equations also captures the precision by which the ensemble response is represented i.e. the dynamics of the population variance. When coherence is strong a reasonable assumption is that the variance is sufficiently close to the mean that it can be discarded. This reduces the dimensions to one and permits local populations of interacting excitatory and inhibitory neurons in different cortical layers to be modelled (Lopes da Silva et al., 1974; Jansen and Rit, 1995). These so-called 'neural mass models' come in a variety of forms. One class assumes that the coherence between neurons is sufficiently

strong that the dynamics of the whole assembly resembles that of a single neuron. Neural mass models of this type often consist of a conductance-based spiking excitatory pool connected to a passive local inhibitory pool which can exhibit steady state, periodic, and chaotic oscillations (Larter et al., 1999; Breakspear et al., 2003). The all-or-nothing firing of individual neurons is replaced by a sigmoid-shaped activation function that maps the average membrane potential to mean firing rate. A second class of neural mass is derived by carefully observing the response of a neural population to changes in its driving input (Freeman, 1979; Wilson and Cowan, 1972). Hybrid methods combining theoretical treatments of population dynamics with empirical synaptic and input response functions also exist (Stefanescu and Jirsa, 2011).

Mean-field models have been developed at a range of spatial and temporal scales that include models of connectivity between groups of neuronal subtypes coupled through excitatory (NMDA, AMPA) and inhibitory (GABA) synapses and mean-field approximations of neuronal populations which can be simulated at reduced computational cost (Deco et al., 2008, 2009, 2011; Deco and Jirsa, 2012; Deco et al., 2012; Deco, Ponce-Alvarez, Mantini, Romani, Hagmann and Corbetta, 2013; Deco, McIntosh, Shen, Hutchison, Menon, Everling, Hagmann and Jirsa, 2014). Typically, these models explore a range of different parameters including intrinsic noise and transmission delay to estimate an optimal fit between simulated and empirical time series. A key finding across these models, is that despite operating at different levels of description, they are all validated by their overlap with resting state activity in a dynamical regime poised between order and disorder.

Recent whole-brain models of primate cortex incorporating empirical neuroanatomical data have made significant progress in clarifying the nature of the structure-function dyad. Honey and Kötter (2007) examined the relationship between structural and functional connectivity in a model of macaque cortex. Their model used neuronal tract tracing data obtained from the CoCoMac database to reconstruct the brain's interregional fibre pathways. Local dynamics capable of chaotic behaviour were installed at

each node to simulate spontaneous neural activity (Breakspear et al., 2003). Millisecond resolution neural time series were transformed into synthetic BOLD signal using a nonlinear model of the brain's haemodynamic response (Friston, 2003). Simple cross correlations of BOLD time series yielded the functional connectivity between regions. In agreement with experimental findings, BOLD time series showed transient periods of synchronisation between different brain regions. On longer time scales, structural and functional data were largely in agreement. As human structural brain connectivity became available through diffusion MRI (Hagmann et al., 2008). The model was extended to include the entire human cerebral cortex (Honey et al., 2009). As before, the model strongly suggested a key link between patterns of functional connectivity in the resting state and the physical wiring between regions. Ghosh et al. (2008*a*,*b*) also examined endogenous activity in the cerebral cortex. Structural connectivity derived from the macaque monkey was incorporated into a neural mass model based on the dynamic equations of FitzHugh-Nagumo (FitzHugh, 1961; Nagumo et al., 1962). The model included conduction delays estimated from the distance between connected node pairs. The correlation structure of the model's functional connectivity was found to be in agreement with empirical estimates using resting state fMRI. Conduction delay and physiological noise were necessary elements for generating the structured patterns of spatiotemporal activity observed in the brain at rest. A subsequent model of spontaneous neural activity by Deco et al. (2009) adopted an approach similar to that of Honey and Kötter (2007). Deco et al. (2009) also incorporated transmission delay and noise into a model with connectivity informed by the macaque cortex. However, unlike Honey and Kötter (2007) local population dynamics based on the equations of Wilson and Cowan (Wilson and Cowan, 1972; Cowan et al., 2016) were tuned to stay below the oscillatory threshold unless perturbed by noise. Deco et al. (2009) observed patterns of anticorrelated activity that resembled the functional clustering reported by Honey (2007). The emergence of anticorrelations between clusters was contingent on an optimal level of noise suggesting the presence of 'stochastic resonance'. More recently, Cabral et al. (2011) employed a network

of coupled Kuramoto phase oscillators to investigate resting state neural dynamics in a large-scale simulation of the human cortex. As before, coupling between nodes was informed using empirical estimates of the brain's structural connectivity. For a given parameter regime, the behaviour of the network was characterised by a state of partial synchronisation in which subsets of nodes spontaneously coalesced into distinct clusters that resembled the ICNs of the brain. Taken together, these studies suggest that although structural wiring is largely predictive of functional connectivity, strong correlations also exist between regions lacking direct anatomical connectivity. Also, whilst anatomical connectivity can be considered largely static over the duration of the scan, functional connectivity changes dynamically (in the order of seconds or minutes) even when subjects are at rest (Hutchison, Womelsdorf, Allen, Bandettini, Calhoun, Corbetta, Della Penna, Duyn, Glover, Gonzalez-Castillo, Handwerker, Keilholz, Kiviniemi, Leopold, de Pasquale, Sporns, Walter and Chang, 2013; Hutchison, Womelsdorf, Gati, Everling and Menon, 2013; Allen et al., 2014; Handwerker et al., 2012; Zalesky et al., 2014; Smith, 2012). In this regard, understanding the organisation of resting state architecture is not only contingent on accurately estimating the structural anatomy of the brain, but also on evaluating the time-varying dynamic interactions of local areas that enable complex behaviour to arise over shorter time-scales.

The development of macroscopic whole-brain computer models provides an optimal framework for investigating the dynamic features that permit complex functional interactions to emerge from the structural connectome. Changes in dynamic functional connectivity have been linked to the structural topology of the anatomical connectome as well as various aspects of cognition and behaviour. Thus, theoretical models linking network dynamics and macroscopic structural connectivity are essential tools for bridging the conceptual gap between structure, function, and cognition in the human brain. In this regard, computational modelling provides insight into aspects of neuronal interactions and connectivity that engender the complexity of brain dynamics which would otherwise be unattainable. Moreover, computational modelling may be used in conjunction with tools from dynamic

systems theory to quantitatively analyse dynamics over and above the standard measures of functional connectivity. Two measures of complex brain dynamics are of particular interest: synchrony and metastability (Shanahan, 2010). Metastability resolves the antagonism between the brain's well-known tendency to permit regions to express their intrinsic behaviour (segregation) and to coordinate as global synergies (integration). Theoretical accounts stipulate that increases in metastability may enable more dynamic interactions between brain regions, whereas decreases in metastability may attend more persistent, stable states of brain activity (Hellyer et al., 2014).

In summary, models of spontaneous neural activity bolster the theory that resting state functional architecture emerges from the interplay of local neural dynamics and the brain's large-scale anatomical structure. It also suggests that this relationship is dependent upon the time frame and spatial resolution considered. The correspondence of structure and function is especially robust in functional network acquired at low frequencies using resting state fMRI and over a period of several minutes. In general, models such as these demonstrate how spontaneous neural activity emerges from an anatomical substrate that is approximately stationary over longer time scales. Moreover, they show how the collective dynamics of a large-scale neural system is capable of generating a rich set of spatio-temporal patterns. These findings reinforce the idea that endogenous activity is not a time-invariant pattern of interregional couplings but a series of spontaneous network transitions where functional connections are rapidly reconfigured. Spontaneous fluctuations in endogenous activity gives rise to sequences of network configurations that likely inform the flow of cognition by providing a repository of functional patterns. Task-dependent alterations in synchrony have been observed in a wide variety of human and animal experiments. Local field potential (LFP) recordings from primates with chronic or semi-chronic microelectrodes in the cerebral cortex have tracked the evolution of task processing at the millisecond-scale during a visual discrimination task (Bressler et al., 1993). Patterns of dynamic coupling changed within hundreds of milliseconds as a function of momentary motor and sensory processing demands. A task-dependent network of causal inter-

actions was subsequently revealed between recording sites (Brovelli et al., 2004). Models based on connectomic data are critical for establishing a mechanical linkage between the multiplicity of functional states that emerge from the static connections of the anatomical connectome and the emergent process of cognition. To date, modelling work has successfully captured key aspects of spontaneous network activity at rest but has yet to address the metastable dynamics evoked by active cognition. Whole-brain simulations have the potential to provide novel insight into so-called 'disconnection syndromes' where the underlying structural topology has been altered by pathological processes. Accordingly, the remainder of this chapter is devoted to exploring theoretical and empirical findings that link structural disconnection to altered patterns of functional connectivity, behaviour, and cognition.

## 3.4 Brain network disease

Norbert Wiener's 1948 treatise on control and communication – Cybernetics – framed mental illness as a disorder of 'circulating information' (Wiener, 1948). This influential view of mental illness traces the cause of neurological and psychiatric disturbances to altered flows or system dynamics in the brain. Many types of brain dysfunction can be conceptualised as a network disease (Rubinov and Bullmore, 2013; Bassett and Bullmore, 2009; Fornito et al., 2012). Pathological processes lead to the loss of neurons and their synapses through rapid mechanisms of action such as acute injury or stroke, or through more gradual processes such as neurodegeneration. As in other types of complex system, the complex network of the brain shows characteristic patterns of dysfunction related to robustness and vulnerability. Each type of disease demonstrates characteristic patterns of network failure that can be quantitatively assessed using the tools of graph theory (Stam and van Straaten, 2012). Effects are often nonlocal travelling to apparently unaffected regions in a process known as 'action at a distance' or diaschisis. In general, the modularity of biological networks associated with the small-world phenomenon serves to contain the spread of damaging and disruptive

effects of perturbations (Douw et al., 2010; He et al., 2009). Dynamically, these perturbations may be equivalent to changing the parameters of the coordination dynamic. The complex network approach has the potential to contribute to a deeper understanding and more effective treatment of brain injury and disease by revealing how different architectural features of complex networks demonstrate selective vulnerability. The following section is devoted to understanding how the spread of activity and thus the appearance of synchrony and coherence are shaped by the brain's heterogeneous, multi-scale structural connectivity.

## Synchrony in the brain

Synchronous oscillations are thought to enable higher-level cognitive operations via the flexible binding of distributed neuronal populations into large-scale neurocognitive networks. Accordingly, the role of network topology in neuronal synchronisation has been explored in some detail. Several studies have examined the capacity of networks to become fully synchronised; a behaviour typically associated with uniformly connected, homogeneous or noise free oscillators. Networks with a regular lattice or modular architecture are generally resistant to global synchronisation, however, the addition of randomised long range connections – as in the small-world architecture – generally facilitates synchronisation (Watts and Strogatz, 1998). Greater synchronisability of small-world networks appears to be independent of the type of dynamics employed (Masuda and Aihara, 2004; Netoff, 2004) and is attributed to reduced path length and increased efficiency. Fully randomised networks are easily synchronised but at a greater wiring cost (Buzsáki et al., 2004).

More realistic scenarios occur when networks display broader degree distributions, they have variation or symmetry breaking in their intrinsic parameters (such as frequency or coupling strength), or they experience noise and operate in a weakly coupled regime. In this case, more complex patterns of synchronisation emerge that include partial states of coherence among subsets of network nodes that change over time (Cabral et al., 2011).

Zhou et al. (2006) found that heterogeneous networks with nonidentical oscillators form a 'dynamic core' of synchronised high degree hubs (Gómez-Gardeñes et al., 2007*a*,*b*). The same phenomena have been observed between highly connected nodes in the brain's rich club architecture (Schmidt et al., 2015). Morgan and Soltesz (2008) showed that pathological processes in the dentate gyrus may create well-connected hubs leading to abnormally high levels of global synchronisation (i.e. epileptic discharges).

The synchronisation of large-scale network topologies derived from mammalian cerebral cortex have also been studied. Synchronisation behaviour of the cat connectivity matrix conforms to structurally defined modules and regions of inter-modular functional linkage to the brain's structural hubs (Hilgetag and Kaiser, 2004; Zhou and Kurths, 2006; Zhou et al., 2007). Computer modelling supports the idea that complex dynamics and a greater diversity of functional motifs emerge when connectivity is small-world, hierarchical, and fractal in its attributes (Sporns and Honey, 2006). The diversity of dynamic processes are not only shaped by network topology but also from activity-dependent plasticity and structural alterations at the level of dendrites and synapses. Dynamic diversity of a given network topology is therefore likely accompanied by a concomitant alteration in the pattern and diversity of synaptic contacts (Papadopoulos et al., 2017).

Just as the structural connections between network elements underpin the emergence of healthy synchronisation dynamics, it is the structural disconnection between network elements through injury, neurodegenerative disease, or aberrant developmental process that results in the altered synchrony associated with neurological disorder. Some conditions, such as traumatic brain injury, autism, schizophrenia, Parkinson's disease and AD, demonstrate an association between structural disconnection and altered neural synchrony sufficient to justify the title of 'disconnection syndrome' (Catani and Ffytche, 2005). Empirical and theoretical lesion studies suggest that the effects of structural disconnection are not solely realised as abnormal local information processing but encompass a wider spectrum of dysfunction that includes global system dynamics. Accordingly, the following section reviews evidence that structural lesions result in abnormal

functional couplings between brain regions.

## Brain lesions

Brain lesions are defined as perturbations of the structural substrate supporting physiological behaviour. The use of lesioning to infer the functional properties of principal brain regions has long been a mainstay of the neurosciences. Broca (1861) provided one of the earliest accounts of the link between localised brain function and specific mental faculties noting that patients with lesions in particular regions of cortex showed similar deficits in speech. Later, Carl Wernicke (1876) developed a rudimentary network model of higher cognitive function to show that speech depended on the integrity of cortico-cortical pathways as well as cortical grey matter. More recently, Norman Geschwind formulated the theory of disconnection syndromes that contributed to cognitive deficits arising from damage of association pathways (Geschwind, 1965; Miller, 2010). Recent innovations in neuroimaging technology has allowed disturbances in brain network connectivity to be mapped non-invasively (Catani, 2006). Modern approaches support the idea that the severity of neurological impairment is linked to both a lesion's local effects and on the wider pattern of damaged connectivity (Catani and Mesulam, 2008). Discerning the mechanistic origin of cognitive and behavioural effects associated with lesioning is often non-trivial. Effects of lesions include damage to the structural connectivity, which in turn, impact subsequent time varying properties of functional connectivity. Despite the complex interplay of structure and function, lesions of specific regions are often associated with particular cognitive and behavioural disturbances (likely because the cognitive functions are themselves distributed) (Damasio, 1989; Mesulam, 2000). Some effects are the direct result of structural deficits while other effects involve disrupted dynamic interactions between additional non-lesioned areas.

Several theoretical studies have examined the effects of lesions by deleting nodes and edges and characterising the resulting change in function. Achard et al. (2006) showed the targeted deletion of hubs impacts large-

scale functional networks in the human brain. Honey and Sporns (2008) studied the impact of lesions on the structure-function relationship by incorporating local dynamics in a model of macaque cortex (Breakspear et al., 2003). The lesioning of highly central and highly connected hub nodes, especially connector hubs linking two modules, produced the largest nonlocal effects. Subsequent studies extended this model to the human cortex. These included an analysis of endogenous resting state functional connectivity (Honey et al., 2009) and an examination of the functional impact of structural lesions on intrinsic activity (Alstott et al., 2009). Again, the centrality of nodes largely predicted the functional impact. In general, these modelling studies suggest that the functional impact of lesions can be predicted by understanding the topological embedding of nodes in the brain's overall network architecture. A crucial next phase in our understanding is to employ a lesioning process informed by clinical data and to link these simulated structural and functional changes to cognitive ability. Thus, a core objective of the present thesis is to perform a joint computational and empirical study of AD.

## Network damage in Alzheimer's disease

AD is the most common form of dementia accounting for around 60-70% of dementia cases worldwide (Alzheimer's Disease International, 2008; Burns and Iliffe, 2009). Early clinical symptoms are primarily related to short-term memory loss whereas more advanced stages are characterised by mood swings, problems with language, disorientation, loss of motivation, deterioration of self care, and behavioural issues (Goedert and Spillantini, 2006). As the disease progresses, patients retreat from family and society, bodily functions are gradually lost, and ultimately death occurs through secondary complications (Hurtado-Puerto et al., 2018). Most patients with AD die from aspiration pneumonia; difficulties with motor coordination mean that food often goes down the windpipe instead of the oesophagus causing damage or infection in the lungs (Kalia, 2003). Typically, life expectancy following diagnosis is three to nine years (Todd et al., 2013). Funding is low

in proportion to its economic and social impact (Brookmeyer et al., 2007). In developed nations AD is one of the most financially costly diseases, yet, for every ten pounds spent on health and social care for dementia, just eight pence is spent on research into the condition (Landeiro et al., 2018).

AD entails progressive neuronal degeneration and synaptic death due to the accumulation of intra-and inter-cellular neuritic plaques and neurofibrillary tangles (Perl, 2010; Mattson, 2004). The time course and topographic arrangement of protein shows regional specificity linked to the underlying anatomical connectivity (Buckner et al., 2005, 2008). Early stages of AD are characterised by atrophy of the medial temporal lobe, a region of the brain linked to memory formation that includes the hippocampus (Pennanen et al., 2004; Zhou et al., 2008; Chen, Zhang and Li, 2015; Zarei et al., 2013). The disruption of structural and functional organisation in patients with AD has led to the condition being described as a 'disconnection syndrome' (Delbeuck et al., 2003). The most consistent observation in the brains of subjects with early AD is reduced metabolic activity in a key component of the DMN, the posterior cingulate (Minoshima et al., 1997). Not only is metabolism in specific regions disrupted but so too is the pattern of functional interactions in the brain's large-scale dynamic structure. Resting state fMRI consistently shows abnormal patterns of functional connectivity in regions of the DMN that include the posterior cingulate and hippocampus (Greicius et al., 2004). Loss of functional connectivity in the DMN has also been found in subjects with MCI at risk of developing AD (Sorg et al., 2007). These findings suggest that disrupted DMN activity may provide a reliable biomarker for tracking the course of the disease (Greicius et al., 2004).

Buckner et al. (2005) revealed that several markers of neuropathology including amyloid concentration, atrophy, and metabolism, shared similar spatial profiles on the cortical surface of AD patients. Crucially, these regions corresponded to core regions of the DMN. More recently, amyloid deposition and abnormal functional connectivity were also found in the DMN of cognitively normal older adults (Hedden et al., 2009). This finding suggests that some feature of DMN operation or structure is actively encour-

aging the accumulation of plaque. Tellingly, the most vulnerable regions including precuneus and posterior cingulate cortex, have also been identified as the most topologically central nodes in studies of the brain's structural network (Hagmann et al., 2008). Buckner et al. (2009) later extended his analysis to include functional networks recorded during resting state fMRI. Cortical hubs correlated with amyloid deposition suggesting that highly central and well-connected regions are more susceptible to pathology, possibly due to their higher than baseline levels of metabolic activity. It is worth mentioning that since cortical hubs are a stable property of the brain's functional architecture, found at rest and during task-orientated processing, any changes to the brain's endogenous activity should be reflected in task-orientated processing.

Pathology appears to originate in medial temporal lobe memory structures before being transmitted via a prion-like process to posterior portions of DMN. Cognitive and behavioural effects associated with AD appear to result from a targeted attack of cortical hubs located in the DMN as a result of the deposition of neuritic plaques and the development of neurofibrillary tangles in association with the brain's anatomical fibre pathways. These factors result in a pattern of network failure characterised by reduced small-world attributes, including longer path length and reduced clustering (Stam, Jones, Nolte, Breakspear and Scheltens, 2007).

The first study to characterise functional brain networks using EEG data showed disease related increases in path length in the beta band frequency of AD subjects indicating a less efficient network structure (Stam, Nolte and Daffertshofer, 2007). Path length was negatively correlated with mini mental state examination (MMSE) test score – a widely used test of cognitive function that includes tests of orientation, attention, memory, language, and visual-spatial skills – thereby demonstrating a link between a graph theoretic measure of whole-brain functional network topology and a clinical measure of cognitive ability. Disorganised functional brain networks have also been found in resting state fMRI data using wavelet analysis (Supekar et al., 2008). In the low frequency interval 0.01-0.05Hz AD subjects showed significantly decreased global clustering in functional networks.

Both studies show disorganisation of the brain's small world architecture in AD although one showed reduced path length and the other reduced clustering. More recently, MEG recordings in AD subjects have confirmed the loss of small world attributes in AD subjects compared to HCs by estimating the phase lag index, a measure of synchrony (Stam et al., 2009). Functional networks in the lower alpha (8-10Hz) frequency band also showed a combination of decreased path length and clustering. Modelling suggested that this change corresponded to the loss of high degree hubs. Decreased synchronisation in high frequency bands or 'EEG slowing' reported in patients with AD (Berendse et al., 2000) appears at odds with hypersynchronisation reported in patients with MCI (López et al., 2014). Transient increases in synchronisation may arise from compensatory homoeostatic responses or an inhibitory deficit caused by the loss of GABAergic synapses. Taken together, these findings suggest that integration and segregation, enabled by the organisation of brain anatomy according to a small-world architecture, is disrupted in AD, leading to a more random network structure (Stam, Jones, Nolte, Breakspear and Scheltens, 2007).

## 3.5 Summary and conclusion

The brains of subjects at 'quiet rest' display circumscribed patterns of neural neural activity or 'resting state networks', that largely overlap with task-based activations. The term ICNs expands upon this definition to reflect their involvement in aspects of voluntary behaviour associated with motor control, sensory processing, mediating attention, cognitive control, and detecting salience. The regions comprising these networks are constantly being reconfigured over time in response to internal fluctuations and current behavioural context. Cognition, therefore, appears to arise from the interactions of large-scale networks that operate and interact according to dynamic principles. The flexibility of cognitive function is proposed to arise from the binding of disparate cortical regions into coherent coordinative structures known as neurocognitive networks. The concept of the neurocognitive network was proposed as an antidote to the apparent antag-

onism between local processing and global coordination of cortical regions. The brain appears to derive this behaviour from its identity as a complex dynamical system operating in the vicinity of a critical regime. Dynamics such as these are most accurately captured by a series of transitions between pseudo-stable regions of phase space rather than as convergence to a fixed-point attractor. This type of dynamic diversity is associated with superior information processing capabilities. Recently, whole-brain computer models based on structural connectivity have successfully reproduced key features of spontaneous neural activity observed in empirical data. These studies suggest that computer models incorporating anatomical connectivity represent an optimal framework for exploring how dynamic features such as metastability emerge from the static connections of the brain. Previous findings suggest that synchronous oscillations facilitate cognition by binding distributed neuronal assemblies into large-scale networks and that these oscillations are shaped and constrained by the brain's network connectivity. Accordingly, several neurological disorders exhibiting abnormal synchronisation are linked to altered structural connectivity. In AD, the prion-like spread of pathology appears to be constrained by the topology of the network resulting in a targeted attack of network hubs, altered functional connectivity, and degraded cognition.

The foregoing review highlights the ongoing challenge of establishing the causal pathways linking structure, dynamics, and cognition in the human brain. Although dynamical accounts attribute considerable importance to the brain's structural connectivity in shaping spontaneous neural activity, several interesting open questions remain. For example, how are endogenous metastable dynamics modulated by task performance, moreover, how is flexible cognition implemented on a set of static structural connections? Critical insight into the contribution of the anatomical connectome in shaping and constraining the neural dynamics of cognition may be gained by examining clinical conditions in which the network topology has been altered. Recent advances in neuroimaging technology have stimulated the development of anatomically plausible whole-brain computer models. These tools, alongside developments in dynamical systems and network theory,

afford the opportunity to address one of the principal goals of neuroscience: to understand how structure and dynamics gives rise to cognition. The following chapter investigates how neural dynamics are modulated by cognitive state, and closing the loop, how cognitive abilities are informed by metastable coordination.

# 4 Metastable neural dynamics underlies cognitive performance across multiple behavioural paradigms

## 4.1 Overview

This chapter invokes the principle of metastable coordination dynamics to explore how the interactions of large-scale cortical networks support cognition. To this end, it compares the coordinative interactions between the brain's large-scale ICNs at rest and during the performance of several tasks in a large cohort of healthy individuals (N=890). Although metastability between resting state networks increased during task performance, cognitive ability was more closely linked to spontaneous activity. The principle findings of this chapter are as follows: (1) task-based reasoning is characterised by a network structure in which metastability reflects the functional divisions of cortex into low metastability sensory networks and high metastability association areas; (2) subjects whose networks transitioned efficiently between rest and task-based configurations exhibited greater dynamic stability in primary sensory regions and greater dynamic flexibility in systems of cognitive control; (3) dynamic flexibility conferred superior problem solving in novel situations (i.e. fluid intelligence) but was less relevant in tasks recruiting previously acquired knowledge and experience (i.e. crystallised intelligence). Taken together, these findings support the con-

tention that metastable neural dynamics support cognitive flexibility via the dynamic construction of task-relevant neurocognitive networks. The chapter is structured as follows: introduction, methods, results, discussion, and conclusion.

## 4.2 Introduction

The brains of subjects at 'cognitive rest' display circumscribed patterns of neural activity or resting state networks (Fox et al., 2005; Fox and Raichle, 2007) that broadly overlap with task-based activations (Smith and Nichols, 2009; Cole, Bassett, Power, Braver and Petersen, 2014). Somehow these large-scale networks of the brain rearrange themselves on a fixed anatomical structure to support internal processes relevant to cognition (Lewis et al., 2009; Sadaghiani and Kleinschmidt, 2013; Braun et al., 2015; Spadone et al., 2015; Cohen, 2018). One proposal is that neuronal assemblies are dynamically bound into coherent coordinative structures known as neurocognitive networks (Bressler and Kelso, 2001, 2016). The concept of the neurocognitive network represents an important compromise between two antagonistic viewpoints: the first, localisation, which holds that complex cognitive functions are localised to specific regions of the brain, the second, globalism, which posits that complex functions are distributed and arise through global coordination (McIntosh, 1999, 2000, 2004, 2007; Bressler and Mcintosh, 2007). From the neurocognitive network perspective, the brain's tendencies toward integration and segregation are simultaneously realised. Local areas are permitted to express their intrinsic functionality yet also couple together and coordinate globally. Cognition, in this context, is the real-time expression of distributed local areas whose states of mutual coordination are adjusted dynamically over time (Bressler and Tognoli, 2006). An important challenge is to understand how these local areas become dynamically linked in the execution of particular cognitive operations, and equally, how these patterns of dynamic connectivity evolve over time (Cabral et al., 2017; Gonzalez-Castillo and Bandettini, 2017).

The coordination of neurocognitive networks appears to arise from a

dynamic regime that balances counteracting tendencies toward integration and segregation (Tononi et al., 1998; Shanahan, 2010; Sporns, 2013*b*; Tognoli and Kelso, 2014*b*). Empirical and theoretical accounts indicate that the brain derives this behaviour from its identity as a complex dynamical system operating in the metastable regime of its coordination dynamics (Kelso and Haken, 1995; Kelso, 2012; Kelso and Tognoli, 2007; Tognoli and Kelso, 2009, 2014*a*). The concept of metastability represents an important theoretical solution to the requirement that local areas operate independently yet also combine and behave synergistically (Kelso and Tognoli, 2007; Kelso, 2012; Tognoli and Kelso, 2014*a*). Metastability is important too as an observable phenomenon, furnishing a dynamical explanation for how large-scale brain regions coordinate their activity in space and time to support cortical function (Bressler and Kelso, 2001, 2016; Jirsa and McIntosh, 2007; Kelso, 2008; Tognoli and Kelso, 2009). In the language of dynamical system theory, metastability refers to a coupled or collective oscillatory activity which falls outside its equilibrium state for dwell times that depend on distance from equilibrium. A concrete example of a metastable dynamical system is the 'winnerless competition' (Rabinovich et al., 2006; Rabinovich, Huerta, Varona and Afraimovich, 2008), however, metastable phenomena may emerge from a variety of underlying mechanisms (where certain conditions are satisfied) and it is in this broader sense that we use the term (Friston, 1997; Deco and Jirsa, 2012; Kringelbach et al., 2015; Stratton and Wiles, 2015; Deco and Kringelbach, 2016; Balaguer-Ballester et al., 2018).

The overall dynamic stability of a system may be estimated by calculating a well-defined collective variable or order parameter (Kuramoto, 1984; Shanahan, 2010; Cabral et al., 2011; Wildie and Shanahan, 2012). The Kuramoto order parameter captures the average phase of a group of oscillators to quantify how 'phase-locked' they are at a given moment in time. Accordingly, the variation in this order parameter has been proposed as a measure of a system's metastability and the mean of the phase-locking across time as a measure of the system's overall synchrony. Metastability is high in a system that visits a range of different states over time whereas both highly ordered and highly disordered states are characterised by low

metastability, and high and low phase synchrony, respectively. The concept of phase synchronisation was originally introduced in physics to study the behaviour of weakly coupled oscillators (Rosenblum et al., 1996). The original motivation was to compare the temporal structure of two time series by ignoring information related to amplitude (Varela et al., 2001). Signal processing techniques such as the Hilbert transform make it possible to separate a time series into its amplitude and phase by converting the real signal into its complex analytic version (Boashash, 1992). However, unlike correlation-based sliding-window analysis, which mandates an arbitrary choice of window length, the phase synchronisation approach provides time-resolved functional connectivity at the same resolution as the input narrowband fMRI signal (Glerean et al., 2012). Moreover, unlike correlation, which is a linear measure of association between variables, phase synchronisation is a measure of statistical dependence that is sensitive to both linear and nonlinear relationships (Pereda et al., 2005). Recently, the phase synchronisation approach has successfully identified changes in the time-varying properties of brain connectivity associated with several neural disorders (Hellyer et al., 2015; Córdova-Palomera et al., 2017; Demirtaş et al., 2017; Alderson et al., 2018; Lee et al., 2018).

Theoretical accounts stipulate that metastability at rest corresponds to an optimal exploration of the dynamical repertoire inherent in the static structural linkages of the anatomy where the probability of network switching is maximal (Cabral et al., 2011; Ponce-Alvarez et al., 2015; Deco et al., 2017). A critical next step in our understanding is to evaluate not only the degree of metastability arising spontaneously from the brain's intrinsic network dynamics but also the degree of metastability engendered by the attendant demands of a task (Rabinovich, Huerta, Varona and Afraimovich, 2008). Here, we invoke the theoretical framework of metastable coordination dynamics to explain how resting state networks are dynamically linked into task-dependent neurocognitive networks. Given that patterns of brain activity appear to be more stable during cognitive operations requiring sustained attention (Chen, Zhang and Li, 2015; Elton and Gao, 2015; Hutchison and Morton, 2015; Cohen, 2018), we anticipated reduced metastability

between task-relevant neural networks as a function of task performance.

In light of the foregoing, we tested the hypothesis that coupling between the brain's large-scale networks is more metastable at rest than during the execution of an explicit task. We compared the metastability of fMRI BOLD signal in resting and task-evoked functional MRI data in a large cohort of healthy individuals (N=566) from the Human Connectome Project (Van Essen et al., 2013). Changes in metastability were sought among 13 resting state networks encompassing hundreds of regions and every major brain system (Gordon et al., 2016). Finally, a link between the metastability of individual network connections and task performance was sought across several cognitive domains.

Overall, we found that–contrary to expectations–the metastability of couplings between large-scale networks was actively enhanced by task performance, principally in regions known to be devoted to cognitive control. Moreover, the efficiency of the transformation between rest and task-driven states was promoted by a network structure characterised by dynamic flexibility in cognitive control networks and dynamic stability in sensory regions. Crucially, subjects with resting state architectures similar or 'preconfigured' to a task-orientated configuration demonstrated superior cognitive ability. Curiously, task-induced increases in metastability did not account for variations in cognitive performance. Rather, cognitive ability was linked to the metastability of the brain's intrinsic network dynamics. Overall, high intrinsic metastability of cognitive control networks was linked to novel problem solving (or fluid intelligence) but was less relevant in tasks dependent upon previous knowledge and experience (or crystallised intelligence).

## 4.3 Methods

### Participants

Data were obtained through the Washington University-Minnesota Consortium Human Connectome Project (HCP) (Van Essen et al., 2013). Sub-

jects were recruited from Washington University and surrounding area. The present paper used 566 subjects from the 1200 healthy young adult release (aged 22-35; see https://www.humanconnectome.org/data). All participants were screened for a history of neurological and psychiatric conditions and use of psychotropic drugs, as well as for physical conditions or bodily implants. Diagnosis with a mental health disorder and structural abnormalities (as revealed by fMRI) were also exclusion criteria. All participants supplied informed consent in accordance with the HCP research ethics board. The subset of subjects comprising monozygotic and dizygotic twin pairs were excluded from the present study. All subjects attained at a minimum a high school degree.

## MRI parameters

In all parts of the HCP, participants were scanned on the same equipment using the same protocol (Smith et al., 2013). Whole-brain echoplanar scans were acquired with a 32 channel head coil on a modified 3T Siemens Skyra with TR = 720 ms, TE = 33.1 ms, flip angle = 52º, BW = 2290 Hz/Px, in-plane FOV = 208×180 mm, 72 slices, 2.0 mm isotropic voxels, with a multi-band acceleration factor of 8. Rest (eyes open with fixation) and task-based fMRI data were collected over two sessions. Each session consisted of two rest imaging sessions of approximately 15 minutes each, followed by task-based acquisitions of varying length. The present study used only the first resting state run. Except for the run duration, task-based data were acquired using the same EPI pulse sequence parameters as rest. Seven tasks totalling one hour were acquired. Three tasks were collected in one session and four tasks another. The seven tasks (and their run times in mins) were as follows: emotion perception (4:32), relational reasoning (5:52), language processing (7:54), working memory (10:02), gambling/reward learning (6:24), social cognition (theory of mind; 6:54), and motor responses (7:08) (Barch et al., 2013). High-resolution 3D T1-weighted structural images were also acquired with the following parameters: TR = 2400 ms, TE = 2.14 ms, TI = 1000 ms, flip angle = 8º, BW = 210 Hz/Px, FOV =

224×224, and 0.7 mm isotropic voxels.

## Task protocols

Task-evoked fMRI data were downloaded to examine the changes in metastable interactions between large-scale cortical networks during attentionally demanding cognition. In total there were seven in-scanner tasks designed to engage a variety of cortical and subcortical networks related to emotion perception, relational reasoning, language processing, working memory, gambling/reward learning, social cognition (theory of mind), and motor responses. These included:

- *Emotion perception*: participants were presented with blocks of trials asking them to decide which of two faces presented on the bottom of the screen matched the face at the top of the screen, or which of two shapes presented at the bottom of the screen matched the shape at the top of the screen. The faces had either an angry or fearful expression (Hariri et al., 2002).
- *Relational reasoning*: participants were presented with 2 pairs of objects, with one pair at the top of the screen and the other pair at the bottom of the screen. Subjects were first asked to decide if the top pair of objects differed in shape or differed in texture and then to decide whether the bottom pair of objects also differed along the same dimension (Smith et al., 2007).
- *Language processing*: the task comprised a story and math component. The story blocks presented participants with brief auditory stories (5-9 sentences) adapted from Aesop's fables, followed by a 2-alternative forced-choice question that asked participants about the topic of the story. The math task also presented trials auditorily and required subjects to complete addition and subtraction problems (Binder et al., 2011).
- *2-back working memory*: task participants were presented with blocks of trials that consisted of pictures of places, tools, faces and body

parts (non-mutilated, non-nude). The task consisted of indicating when the current stimulus matched the one from 2 steps earlier.

- *Gambling/reward learning*: participants were asked to guess the number on a mystery card in order to win or lose money. Participants were told that potential card numbers ranged from 1-9 and that the mystery card number was more than or less than 5 (Delgado et al., 2000).
- *Social cognition (theory of mind)*: participants were presented with short video clips (20 seconds) of objects (squares, circles, triangles) that either interacted in some way, or moved randomly on the screen. After each video clip, participants were asked to judge whether a mental interaction had occurred; did the shapes appear to take into account each other's thoughts and feelings? (Wheatley et al., 2007; Castelli et al., 2013).
- *Motor responses*: participants were presented with visual cues that asked them to either tap their left or right fingers, squeeze their left or right toes, or move their tongue (Buckner et al., 2011; Yeo et al., 2011).

## Task fMRI behavioural data

Task performance was evaluated using behavioural accuracy and reaction time data. Only those tasks which showed normally distributed behavioural accuracy scores were utilised for subsequent analysis. As confirmed by a Kolmogorov-Smirnov test ($p<0.05$) three of the seven tasks satisfied this criteria including relational reasoning (M=0.76, SD=0.12), language processing (M=0.88, SD=0.71), and working memory (M=0.83, SD=0.10). Of the other four tasks, the gambling task accuracies were no better than chance (participants were asked to guess if a mystery card was higher or lower than five). The emotion (M=0.97, SD=0.03) and social (M=0.96, SD=0.12) task accuracies were perfect or near perfect for most subjects and hence showed a strong ceiling effect. Finally, the motor task accuracy scores were not recorded (subjects were asked to move tongue, hands, or

feet). All seven tasks showed normally distributed reaction time data, as confirmed by a one-sample Kolmogorov-Smirnov test ($p<0.05$).

## Cognitive measures

Cognitive performance was also evaluated using test scores obtained outside the scanner. These included two complementary factors of general intelligence: fluid and crystallised intelligence, the former linked to novel problem solving and the latter to previously acquired knowledge and experience (Jensen and Cattell, 2006). Executive function/inhibitory control was also investigated due to its strong association with tonic (Sadaghiani and D'Esposito, 2015) and phasic (Cole et al., 2012, 2013) aspects of attention. The HCP provides a comprehensive and well-validated battery of cognitive measures based on tools and methods developed by the NIH Toolbox for Assessment of Neurological and Behavioural Function (Gershon et al., 2013). Relevant cognitive measures were downloaded from the Connectome Database (https://db.humanconnectome.org)(Hodge et al., 2015). These included fluid intelligence (Penn Progressive Matrices; PMAT), crystallised intelligence (NIH Toolbox Picture Vocabulary Test and NIH Toolbox Oral Reading Recognition Test), and executive function/inhibitory control (NIH Toolbox Flanker Inhibitory Control and Attention Test). All three cognitive measures were consistent with a normal distribution as confirmed by a one-sample Kolmogorov-Smirnov test ($p<0.05$).

## fMRI pre-processing

All pre-processing was conducted using custom scripts developed in MATLAB 2017a (The MathWorks, Inc., Natick, Massachusetts, United States). Motion between successive frames was estimated using framewise displacement (FD) and root mean square change in BOLD signal (DVARS) (Power et al., 2012, 2014, 2015; Burgess et al., 2016). FD was calculated from the derivatives of the six rigid-body realignment parameters estimated during standard volume realignment. If more than 20% of a subject's resting state frames exceeded FD $>$ 0.5 mm or DVARS $>$ 5%, they were excluded from

further analysis. Based on this criteria, 566 out of 890 subjects were retained for further analysis. We used a minimally pre-processed version of the data that included spatial normalization to a standard template, motion correction, slice timing correction, intensity normalization, and surface and parcel constrained smoothing of 2 mm full width at half maximum (Glasser et al., 2013). The data corresponded to the standard 'grayordinate' space consisting of left and right cortical surface meshes and a set of subcortical volume parcels which have greater spatial correspondence across subjects than volumetrically aligned data (Glasser et al., 2016). To facilitate comparison between rest and task-based conditions both sets of data were identically processed. T1 weighted images aligned with the standard functional image were segmented into 3D volume masks with Freesurfer (Fischl et al., 2002; Fischl, Van Der Kouwe, Destrieux, Halgren, Ségonne, Salat, Busa, Seidman, Goldstein, Kennedy, Caviness, Makris, Rosen and Dale, 2004). Average signals were extracted from the voxels corresponding to the ventricles and white matter anatomy. Variables of no interest were removed from the time series by linear regression. These included six linear head motion parameters, mean ventricle and white matter signals, and corresponding derivatives. Since each task comprised two runs (one from each session) both runs were concatenated into a single time series. The individual signals were demeaned and normalised by z-scoring the data. To pre-empt the possibility that variation in synchrony (our definition of metastability) was being driven by alternating blocks of task and fixation, task blocks were concatenated. Since artificially concatenating a series of disjoint task blocks resulted in a discontiguous time series, the analysis was also performed with cue and fixation blocks included. Overall, retaining cue and fixation blocks did not alter the pattern of metastability between large-scale networks (only the statistical significance). The present analysis pertains to the case where cue and fixation blocks are removed. To ensure that any observed differences were due to dynamics rather than bias associated with signal length, the same number of contiguous frames from task and rest were utilised; the resting state scan was truncated to match the length of the task run (after cue and fixation blocks were removed). To

obtain meaningful signal phases and avoid introducing artefactual correlations, the empirical BOLD signal was bandpassed filtered (Glerean et al., 2012). Since low frequency components of the fMRI signal (0–0.15 Hz) are attributable to task-related activity whereas functional associations between high frequency components (0.2–0.4 Hz) are not (Sun et al., 2004), a temporal bandpass filter (0.06–0.125 Hz) was applied to the data (Shine, Bissett, Bell, Koyejo, Balsters, Gorgolewski, Moodie and Poldrack, 2016). The frequency range 0.06–0.125 Hz is thought to be especially sensitive to dynamic changes in task-related functional brain architecture (Bassett et al., 2011, 2013, 2015; Glerean et al., 2012).

## Brain parcellation

Mean time series were extracted from regions of interest defined by the Gordon atlas (Gordon et al., 2016). The separation of regions into functionally discrete time courses is especially suitable for interrogating dynamic fluctuations in synchrony between large-scale networks. The Gordon atlas assigns regions to one of 12 large-scale networks corresponding to abrupt transitions in resting state functional connectivity. These include dorsal attention, ventral attention, fronto-parietal, cingulo-opercular, salience, default mode, medial parietal, parietal-occipital, visual, motor mouth, motor hand, and auditory networks. Regions outside these domains are labelled as 'none'. The atlas was downloaded from the Brain Analysis Library of Spatial Maps and Atlases database (https://balsa.wustl.edu) (Van Essen et al., 2017). Whole-brain coverage consisted of 333 cortical regions (161 and 162 regions from left and right hemispheres respectively), and one subcortical volume corresponding to the thalamus. The thalamus, which exhibits domain-general engagement across multiple cognitive functions, also plays a critical role in integrating information across functional brain networks (Hwang et al., 2017).

## Calculating resting state network metastability

The first step in quantifying phase synchronisation of two or more time series is determining their instantaneous phases. The most common method is based on the analytic signal approach (Gabor, 1947). The advantage of the analytic signal is that by ignoring information related to amplitude additional properties of the time series become accessible. From a continuous signal $x(t)$ the analytic signal $x_a(t)$ is defined as,

$$x_a(t) = x(t) + iH[x(t)]$$

where $H$ is the Hilbert transform and $i = \sqrt{-1}$ . If Bedrosian's theorem (Bedrosian, 1962) is respected then the analytic signal of a time series can be rewritten as,

$$x_a(t) = a(t)e^{i\phi(t)}$$

where $a(t)$ is the instantaneous envelope and $\phi(t)$ the instantaneous phase. The Bedrosian theorem makes a clear prediction – the narrower the bandwidth of the signal of interest, the better the Hilbert transform is able to generate an analytic signal with meaningful envelope and phase. For this reason, bandpass filtering of empirical BOLD signal is essential prior to performing the transform. In accordance with the foregoing, the 334 narrowband mean BOLD time series were transformed into complex phase representation via a Hilbert transform. The first and last ten time points were removed to minimise border effects inherent to the transform (Ponce-Alvarez et al., 2015; Córdova-Palomera et al., 2017). The 'instantaneous' collective behaviour of a group of phase oscillators may be described in terms of their mean phase coherence or synchrony. A measure of phase coherence–the Kuramoto order parameter (Strogatz, 2000; Acebrón et al., 2005) was estimated for: (1) the set of regions comprising a single resting state network; and (2) to evaluate interactions, the set of regions comprising two resting state networks as:

$$R_{RSN}(t) = \frac{1}{N}\sum_{k=1}^{N} e^{i\theta_k(t)}$$

where $k = 1,...,N$ is region number and $\theta_k(t)$ is the instantaneous phase of oscillator $k$ at time $t$. Global metastability considers the interactions of all resting state networks simultaneously and is therefore considered a summary measure of large-scale network flexibility. Global metastability was estimated using all 334 cortical and subcortical time series. Under complete independence, all phases are uniformly distributed and $R_{RSN}$ approaches zero. Conversely, if all phases are equally distributed, $R_{RSN}$ approaches one and full synchrony. The maintenance of a particular communication channel through coherence implies a persistent phase relationship. The number or repertoire of such channels therefore corresponds to the variability of these phase relationships. Accordingly, metastability was defined as the standard deviation of $R_{RSN}$ (Kringelbach et al., 2015; Deco and Kringelbach, 2016) and synchrony as the mean of $R_{RSN}$. Metastability is calculated as the standard deviation of the mean coherence between a set of phase oscillators. In this case, groups of phase oscillators become transiently synchronised through the weak coupling of the structural connectome. However, frustration caused by phase lag between regions (approximately equivalent to transmission delay) prevents full synchronisation from occurring.

## Assessing changes in empirical resting state network metastability during tasks

Given that, (1) the current formulation of metastability permits calculation between a group of regions; and (2) interconnected subnetworks convey more behaviourally relevant information than functional connections observed between pairs of regions observed in isolation, we advocate for a method that exploits the clustering structure of connectivity alterations between functionally related networks. For this reason, we applied the network-based statistic (NBS) to estimates of empirical metastability obtained from fMRI data at the network rather than regional level (Alderson

et al., 2018). For each subject, we estimated an 'interaction matrix' reflecting the metastable interactions of the 13 resting state networks (and thalamus) defined by the Gordon atlas. The same procedure was applied to compute an equivalent interaction matrix based on synchrony. The NBS is a non-parametric statistical test designed to deal with the multiple comparisons problem by identifying the largest connected sub-component (either increases or decreases) in topological space while controlling the family wise error rate (FWER). To date, several studies have used the method to identify pairwise regional connections that are associated with either an experimental effect or between-group difference in functional connectivity (Zalesky et al., 2010). Here, we use the NBS to identify topological clusters of altered metastability (or synchrony) between empirical resting state networks under different conditions of task relative to rest. Mass univariate testing was performed at every connection in the graph to provide a single test statistic that captured the evidence in favour of the null hypothesis: that there was no statistically significant difference in the means of resting state and task-based metastability. The test statistic was subsequently thresholded at an arbitrary value with the set of supra-threshold connections forming a candidate set of connections for which the null hypothesis was tested. Topological clusters were identified between the set of supra-threshold connections for which a single connected path existed. The null hypothesis, therefore, was accepted or rejected at the level of the entire connected graph rather than at the level of an individual network connection. The above steps were repeated in order to construct an empirical null distribution of the largest connected component sizes. Finally, FWE-corrected p-values, corresponding to the proportion of permutations for which the largest component was of the same size or greater, were computed for each component using permutation testing.

## Classification of task and rest data

The interaction matrices corresponding to the seven different tasks (plus rest) were classified using a modified convolutional neural network (CNN)

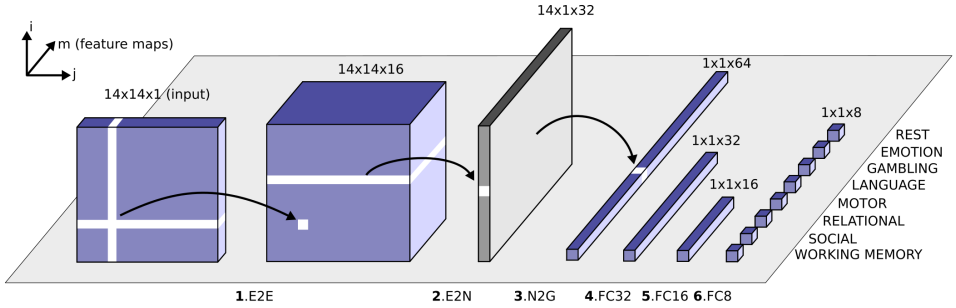


Figure 4.1: Schematic overview of the modified convolutional neural network architecture used to classify the eight different network configurations (seven tasks and one resting state); Kawahara et al., 2017). Each block represents the input/output of a numbered filter layer. The third dimension (m) represents the result of convolving the input with m different filters (feature maps). First, an interaction matrix composed of the interactions of 14 networks (based on synchrony or metastability) is entered as input. This is convolved with an edge-to-edge (1. E2E) filter which weights the edges associated with adjacent brain networks in topological space. The output from this layer is then convolved with an edge-to-node (2. E2N) filter which assigns each network a weighted sum of its edges. Next, a node-to-graph (3. N2G) layer outputs a single response based on all the weighted nodes. Finally, the number of features is reduced to eight output classifications through a series of fully connected (4/5/6. FC) layers.

architecture (Fig. 4.1). BrainNetCNN is the first deep learning framework designed specifically to leverage the topological relationships between nodes in brain network data, outperforming a fully connected neural network with the same number of parameters (Kawahara et al., 2017). The architecture of BrainNetCNN is motivated by the understanding that local neighbourhoods in connectome data are different from those found in traditional datasets informed by images. Patterns are not shift-invariant (as is a face in a photograph) and the features captured by the local neighbourhood (e.g. a 3×3 convolutional filter) are not necessarily interpretable when the ordering of nodes is arbitrary. To reduce the number of parameters we included only a single edge-to-edge layer (Meszlényi et al., 2017). The input to the CNN is the set of 14×14 interaction matrices that capture the metastability/synchrony between the 13 resting state networks (plus

the thalamus) defined by the Gordon atlas. The network classifies the data into one of the seven tasks or the subject's resting state (random classification accuracy is 12.5%). The model was evaluated using k-fold cross validation where . This value of has been shown to yield test error rate estimates that suffer neither from excessively high bias nor from very high variance (Kuhn and Johnson, 2013). The original dataset was partitioned randomly into training (60%), validation (20%), and testing sets (20%). That is, 340 subjects were assigned for training the model, 113 subjects were assigned for tuning the model's hyperparameters, and a further 113 were withheld for validating the performance of the trained model. In the case of metastability, each of the 566 subjects was associated with 8 interaction matrices (7 task-based interaction matrices and one resting state interaction matrix). The same was true in the case of synchrony. Performance was evaluated using classification accuracy i.e. the proportion of correctly identified instances. The above procedure was repeated twice, once for the interaction matrices capturing metastability and again using the interaction matrices based on synchrony. The CNN was implemented in Python using the Pytorch framework (Paszke et al., 2017). Rectified linear units (RELUs) (Nair and Hinton, 2010) were used as activation functions between layers and the probability of each class was calculated at the output layer using the soft max function Bridle (1990). The network was trained using the Adam optimiser (Kingma and Ba, 2015) with mini-batch size of 128, a learning rate of 0.001, and momentum of 0.9. Drop-out regularisation of 0.6 was applied between layers to prevent over-fitting (Wager et al., 2013; Srivastava et al., 2014). The model minimised a cost function associated with the cross-entropy loss. Hyperparameters used in the optimisation stage included momentum and drop-out regularisation.

## Defining update/reconfiguration efficiency

The ability to switch from a resting state network architecture into a task-based configuration was designated as update efficiency (Schultz and Cole, 2016). Highly similar rest and task-based network configurations are com-

mensurate with high update efficiency, as few changes are required to transition between the two whilst highly dissimilar resting state and task-based architectures are linked to low update efficiency, reflecting the many changes that are required to make the switch. Update efficiencies were calculated for all 566 subjects by vectorising the upper triangular half and diagonal of the rest and task-general interaction matrices and calculating their Pearson's correlation coefficient.

## 4.4 Results

### Higher global metastability during task than rest

The metastability of fMRI BOLD signal was examined during the resting state and during the execution of several cognitively demanding tasks. One-way ANOVA identified a statistically significant difference between groups ($F(7,4520) = 37.32$, $p < 0.01$). Subsequent Tukey post hoc test revealed significantly higher global metastability during the seven tasks as compared to resting state ($M = 0.112$, $SD = 0.019$). These included emotion perception ($M = 0.132$, $SD = 0.031$), relational reasoning ($M = 0.133$, $SD = 0.030$), language processing ($M = 0.134$, $SD = 0.027$), working memory ($M = 0.135$, $SD = 0.027$), gambling/reward learning ($M = 0.136$, $SD = 0.029$), social cognition ($M = 0.141$, $SD = 0.029$), and motor responses ($M = 0.143$, $SD = 0.030$).

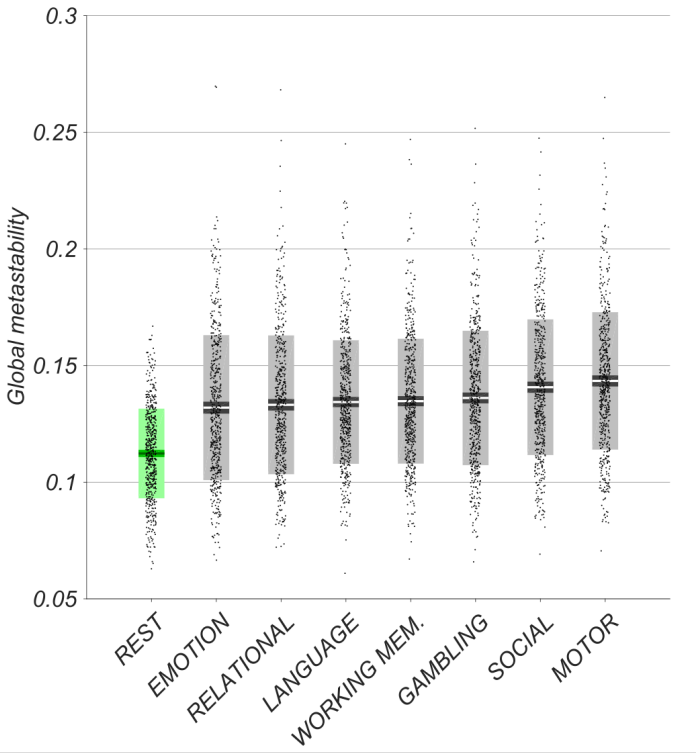


Figure 4.2: Empirical global metastability of fMRI BOLD signal in the resting state (in green) and during several cognitively demanding tasks (in grey). Bars display mean, 95% CI, and one standard deviation with individual subjects indicated. Tasks arranged in ascending order of mean metastability. One-way ANOVA revealed significantly higher metastability during task execution relative to resting state ($p < 0.01$).

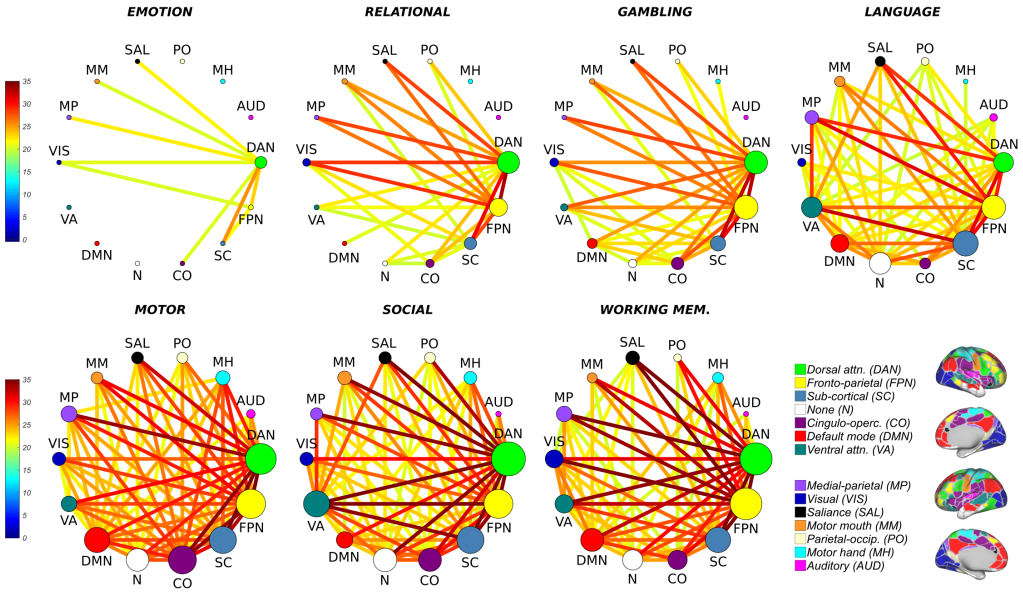


Figure 4.3: Statistically significant ($p < 0.01$; corrected) increases in BOLD signal metastability between empirical resting state networks during task as compared to resting state. Circular graphs show largest connected subgraph of increased metastability identified by the network-based statistic at a fixed threshold (16). Nodes are scaled to reflect the relative importance of their interactions (the sum of their effect sizes). Overall, the connectivity of the dorsal attention (green) and fronto-parietal networks (yellow) were the most metastable.

## Task related increases in metastability between resting state networks

The fMRI BOLD signal of individual network connections was subsequently examined for changes in metastability (task versus rest) using the NBS. In total, 566 resting state interaction matrices (one per subject) were compared to 566 task-based interaction matrices within each of the seven behavioural domains. The null hypothesis, that there was no difference in metastability between rest and task, could then be rejected at the level of individual network connections.

Consistent with the role of resting state networks in mediating behaviour, the NBS identified statistically significant ($p < 0.01$; corrected) increases in metastability between several large-scale networks during task engagement relative to the more unconstrained resting state. Figure 3 shows the largest connected sub-graph of increased metastability detected by the NBS at a fixed threshold for all seven tasks where each node is scaled to reflect its relative importance within the sub-graph (the sum of its effect sizes). Cortical regions associated with top-down attentional/cognitive control (including fronto-parietal and dorsal attention networks) were the most active across the seven tasks along with thalamo-cortical interactions thought to support integrative roles in cognition ranging from memory and learning to flexible adaptation (Alcaraz et al., 2018; Wolff and Vann, 2019).

## Increases in metastability were more widespread than equivalent increases in synchrony

Edges associated with each sub-graph (metastability and synchrony) were summed to reveal the total number of network connections recruited by each task (Fig. 4.4). Increases in metastability encompassed a greater number of systems than equivalent increases in synchrony (in all but emotion and motor tasks). In both cases, the NBS received an identical threshold.

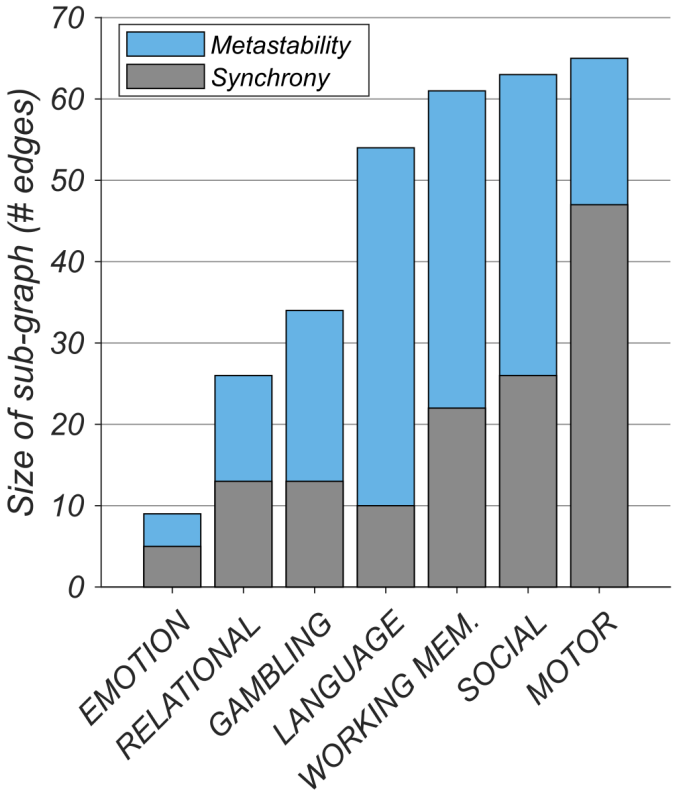


Figure 4.4: Increases in metastability (blue) were associated with a greater number of network connections than equivalent increases in synchrony (grey). Figure shows size of sub-graph identified by the network-based statistic (see Fig. 4.3) rank ordered by metastability.

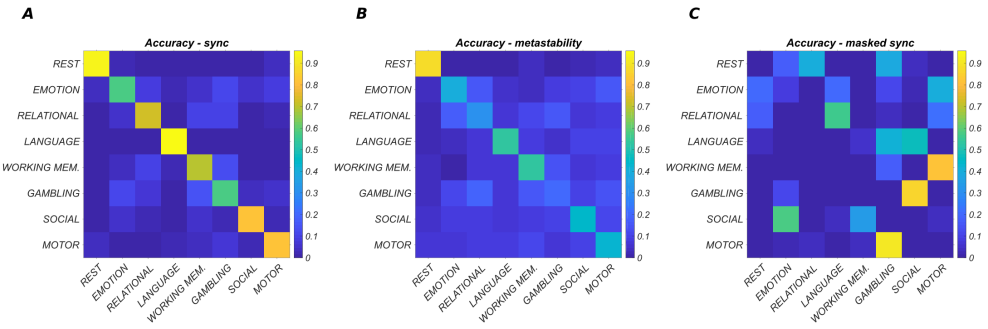


Figure 4.5: Convolutional neural network performance in terms of classification accuracy where each row represents the true class and each column represents the classification made by the neural network. Diagonal elements report the percentage of instances correctly classified. Off-diagonal elements report the percentage of instances that are incorrectly classified. Inputs were classified as belonging to one of eight different network states (seven tasks plus one resting state condition) where each row/column corresponded to the interaction of one network with 13 others (in terms of either synchrony or metastability). A, Classification accuracy in terms of the synchrony between networks (average accuracy = 76%; chance level 12.5%). B, Classification accuracy in terms of the metastability between networks (average accuracy = 46%). C, Classification accuracy in terms of occluded network synchrony (average accuracy = 2%). Here, classification accuracy was reduced by masking out (setting to zero) a small subset of network interactions (see Fig. 4.6).

## Each task is characterised by a small number of task-evoked changes in synchrony i.e. there is a task-specific network architecture

We sought to dissociate the highly correlated quantities of metastability and synchrony (see supplementary information) using a deep learning framework. Accordingly, task and rest network states captured by the 14×14 interaction matrices (of metastability and synchrony) were provided as input to a CNN for classification. The network correctly identified the 7 different tasks (plus rest) based on synchrony with high accuracy (with an average of 76%; compared to a chance level of 12.5%; Fig. 4.5A) but performed

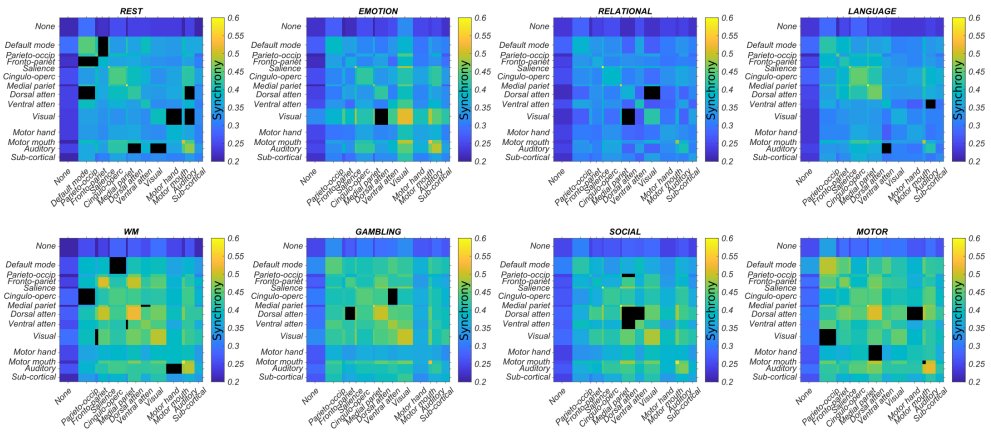


Figure 4.6: Each network state (one rest and seven tasks) is defined by a small number of task-evoked changes in synchrony between resting state networks. Here, network connectivity important for correct classification in more than 90% of individuals (as determined by guided backpropagation) is masked out (black). Such 'occluded' inputs are associated with exceptionally poor classification accuracy (Fig. 4.5C). The width of each column/row has been scaled to reflect the relative number of regions in each network.

less well when trained on metastability (with an average of only 46%; Fig. 4.5B). The high sensitivity (true positive rate) and specificity (true negative rate) exhibited by the classifier when trained on synchronous interactions between networks, suggested that each behavioural domain was characterised by a small number of task-specific network changes. We tested this hypothesis by identifying a small number of inputs (interactions between networks) important for correct classification in each task (Fig. 4.6) and masking them out. Based upon these 'occluded' inputs, the pre-trained classifier was no longer capable of discriminating between network configurations (the seven tasks and one rest state; Fig. 4.5C).

In detail, guided backpropagation was used to identify inputs (the interactions between networks) important for correctly classifying each task. Guided backpropagation provides a set of gradients relating input to output. High gradients at the input level have a large effect on the output and are therefore important for classification. Recall, that each row/column of the 14×14 input represented the interaction of a single network with 14

others. Thus, guided backpropagation produced a 14×14 matrix of gradients. The eight different network configurations (task plus rest interaction matrices) associated with each subject translated into a total of 4,528 gradient matrices. A consensus across all subjects for a particular task was obtained by setting each subject's top 10% of gradients (the most positive gradients) to one and the remaining entries to zero, summing the matrices, and dividing by the total number of subjects. Entries important for correct classification in more than 90% of individuals were set to zero in the input (the interaction matrix). The performance of the pre-trained classifier was then re-evaluated based on the occluded input data. In a separate experiment, retraining on the occluded inputs also produced extremely poor classification accuracy (not shown).

## Different behaviours recruit a similar set of metastable connections

So far, we have demonstrated that increases in metastability can be distinguished from increases in synchrony in two ways: (1) their overall network size–that is, increases in metastability encompass a wider network of cognitive systems than those based on synchrony and (2) their discriminatory utility–tasks can be identified with high accuracy based on a small subset of network changes in synchrony (but much less so in terms of metastability). Taking these findings as a whole, we hypothesised that commonalities between tasks may be centred around a metastable core of task-general network interactions.

To quantify the degree to which the seven task-based configurations shared features in common, we used a dimension-reduction tool – principal component analysis (PCA) – to reduce a larger set of variables (the seven task-based interaction matrices) to a smaller set (a single task-general network architecture). Accordingly, the seven task-based interaction matrices based on metastability were entered into a PCA to yield a single task-general architecture for each subject. On average, the first principal component accounted for 78% of the variance between the seven tasks.

The loadings (the ingredients making up the first principal component recipe) were positive and were distributed equally between the seven tasks suggesting that each task-based configuration contributed equally to the task-general structure. These included emotion perception=0.37, relational reasoning=0.37, language processing=0.36, working memory=0.36, gambling/reward learning=0.36, social cognition=0.37, and motor responses=0.38. This result likely speaks to the high similarity between task-based configurations engaged by different behaviours (see supplementary information). An exemplar task-general architecture was subsequently derived through simple averaging of subjects.

## Task general architecture is composed of high and low metastability subnetworks

We explicated this structure by performing another PCA analysis on the interaction matrices obtained by subtracting task from rest. In doing so, the task general architecture was decomposed into both high (Fig. 4.7; top) and low (Fig. 4.7; middle) metastability subnetworks. High metastability (Fig. 4.7; red) was found in networks associated with cognitive control. These included dorsal attention (selective attention in external visuospatial domains) and fronto-parietal networks (adaptive task control). Tertiary contributions from the thalamus were also apparent (category learning). In contrast, low metastability (Fig. 4.7; blue) was linked to unimodal (or modality specific) sensory processing architecture including motor, auditory, and visual networks. From one perspective, this result is quite surprising. One would expect motor cortex to shift from rest to task due to motor demands on task however primary sensory regions – including motor cortex – appear to prioritise dynamic stability.

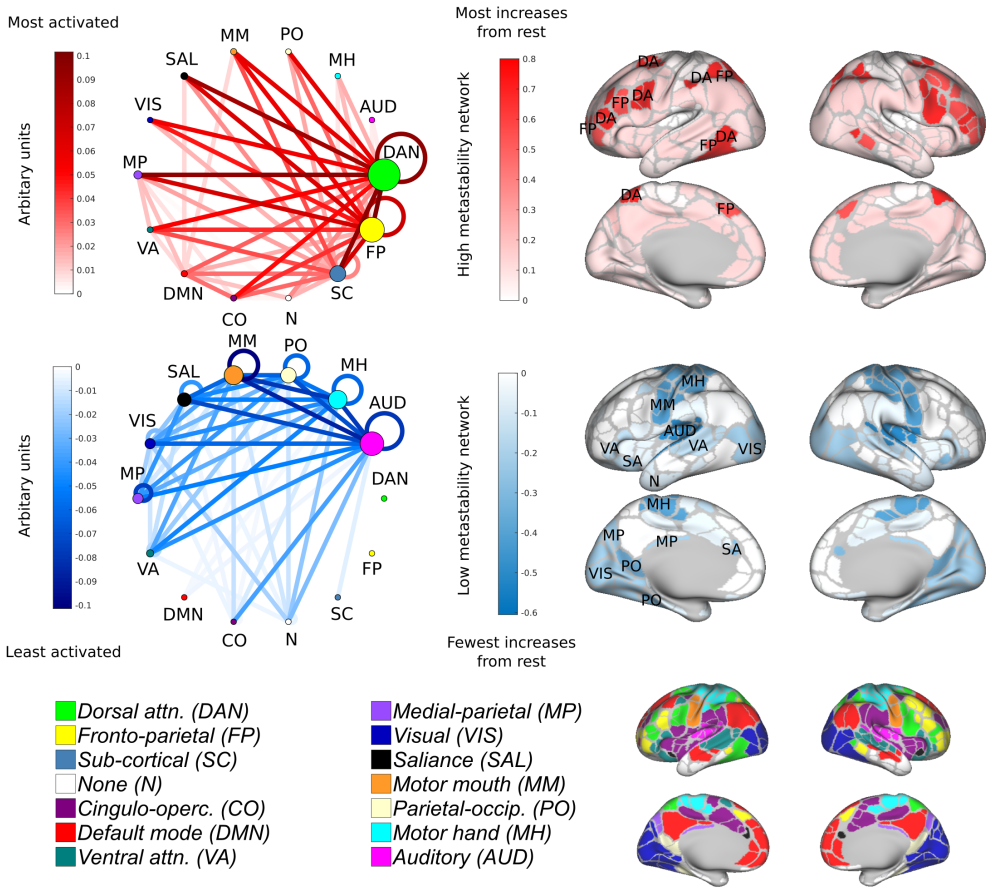


Figure 4.7: Principal component analysis reveals different behaviours are characterised by a similar set of metastable connections: a task-general network structure. Task-based reasoning recruited high metastability in regions associated with cognitive control (top; red) and low metastability in regions associated with sensory processing (blue; middle). On average the 1st principal component accounted for 78% of the variance with loadings distributed equally between the seven tasks. Regions associated with cognitive control including those in dorsal attention network (DA; selective attention in visuospatial domains), fronto-parietal network (FP; adaptive task control), and thalamus (category learning) constituted a high metastability subnetwork (top; red). Conversely, unimodal sensory networks (including MH, MM; motor, AUD; auditory, and VIS; visual) comprised a low metastability subnetwork (middle; blue). Regions are colour coded by the sum of their ingoing/outgoing connectivity. Nodes are colour coded according to the Gordon atlas (bottom). Node diameter is proportional to the sum of ingoing/outgoing connectivity. Recurrent connections correspond to activity within a network.

## High metastability of cognitive control systems at rest is predictive of task performance

The metastable interactions between large-scale networks during task engagement were then examined for behavioural relevance. Behavioural accuracy scores for each subject were entered into a linear regression analysis as the dependent variable with one of 196 (14×14) task-based network connections (estimated in terms of metastability) as predictors. Overall, metastable interactions between networks during task did not explain the variance in cognitive ability. Evidence for the counter case–that cognitive ability was informed by the brain's spontaneous network dynamics–was then sought. Accordingly, resting state metastability was entered as an additional independent factor into the linear regression analysis. Across the three in-scanner tasks, several network connections demonstrated a significant positive association between metastability and cognitive performance ($p < 0.01$; FDR corrected for multiple comparisons). The analysis was then expanded to include three additional cognitive measures acquired outside the scanner: fluid intelligence, crystallised intelligence, and executive function. Across the three tasks, several network connections demonstrated a significant positive association between metastability and cognitive performance ($p < 0.01$; FDR corrected for multiple comparisons). Finally, the addition of reaction time data across the six tasks did not increase the percentage of explained variance in cognitive performance.

Interactions between networks are presented as a circular graph where each edge represents a significant positive correlation between network metastability and cognition (Fig. 4.8). In the main, the metastability of large-scale networks related to cognitive control was strongly related to performance. These included dorsal attention, cingulo-opercular and fronto-parietal networks, and to a lesser extent the salience and ventral attention networks. In general, the metastability of networks related to primary sensory processing (including motor, auditory, and visual networks) was less relevant to task performance. These results are broadly consistent with the task-general network architecture previously discussed.

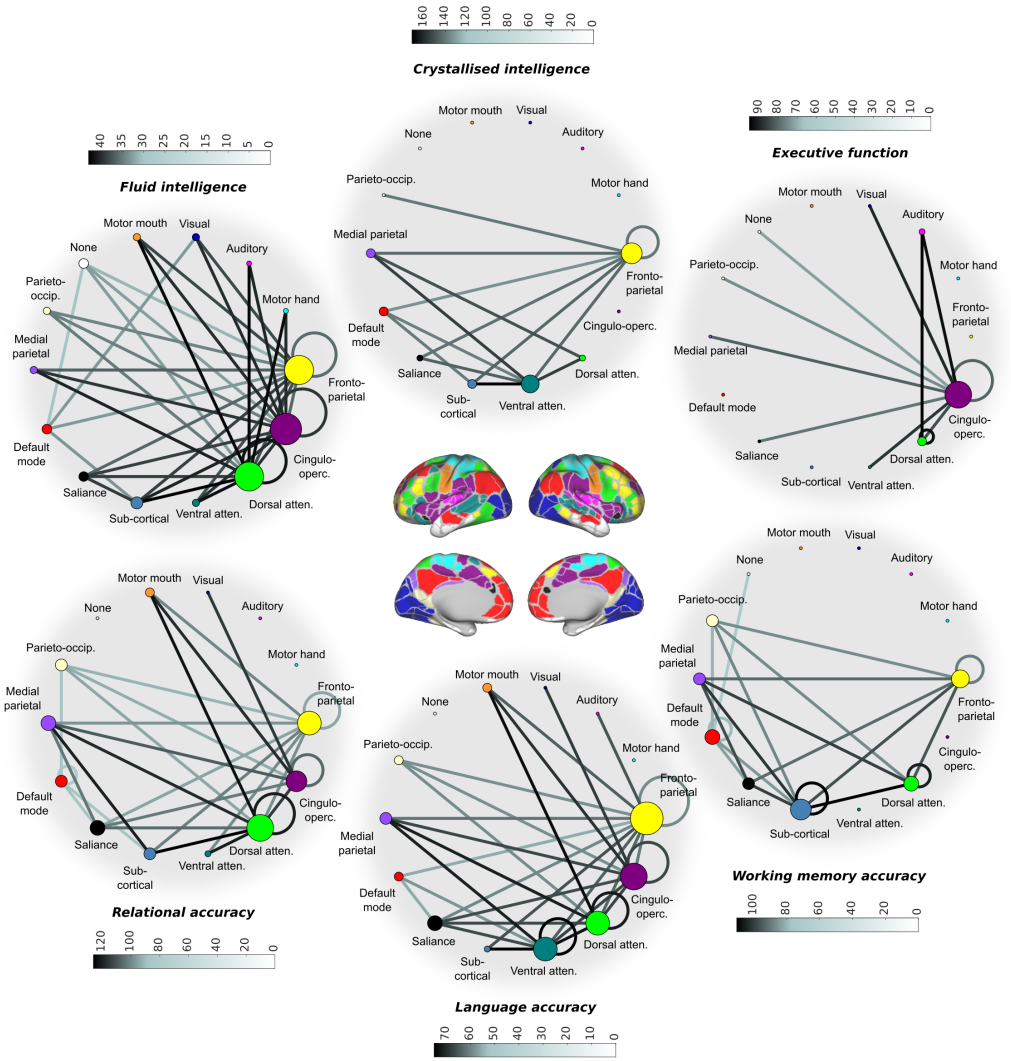


Figure 4.8: Resting state metastability of cognitive control networks is predictive of task performance. Each edge represents a statistically significant positive correlation between the intrinsic metastability of a connection and cognition ($p < 0.01$; FDR corrected). Measures of high order cognition were estimated out of scanner (top); measures of behavioural accuracy were conducted in-scanner (bottom). Edges are shaded to reflect standardised effect sizes (Pearson's r or correlation coefficients). Nodal diameter is scaled to reflect the sum of their ingoing/outgoing connectivity. Overall, metastability of connections associated with fronto-parietal (adaptive task control), cingulo-opercular (sustained tonic attention), and dorsal attention networks (attending to visuospatial stimuli) were most relevant to task performance. Note the very different network profiles induced by tests of fluid versus crystallised intelligence.

Concerning specific tasks, the metastability of connections associated with cognitive control networks was strongly related to fluid intelligence. These included dorsal attention, cingulo-opercular, and fronto-parietal networks. In contrast, the metastability of these networks was less important in the prosecution of crystallised intelligence, which can be observed as a more circumscribed network of significant positive correlations. Finally, cingulo-opercular network metastability was strongly associated with executive function/inhibitory control. Compared to the other in-scanner tasks (relational reasoning and language processing) the working memory task displayed a strong association between metastability and performance in the thalamus and default mode network. In addition, language processing was distinguished from relational reasoning and working memory by virtue of the association between metastability and cognition in the connectivity of the ventral attention network. Overall, all six behavioural domains, including relational reasoning, language processing, working memory, fluid intelligence, crystallised intelligence, and executive function/inhibitory control, demonstrated significant positive correlations between cognitive performance and metastability of task-positive control networks in the resting state. Principally, these included the dorsal attention, cingulo-opercular, and fronto-parietal networks.

## High metastability within (and between) cognitive control systems at rest promotes efficient switching into task

We next examined the link between cognitive performance and the efficiency of the transformation between rest and task-based neural architectures. One hypothesis is that subjects perform better when their intrinsic resting state architecture is already similar to the task-general configuration i.e. their resting state is 'pre-configured' for a variety of different tasks (Cole, Bassett, Power, Braver and Petersen, 2014; Schultz and Cole, 2016). Accordingly, subjects with highly correlated resting and task-general interaction matrices were assigned high update efficiency whilst subjects with highly dissimilar

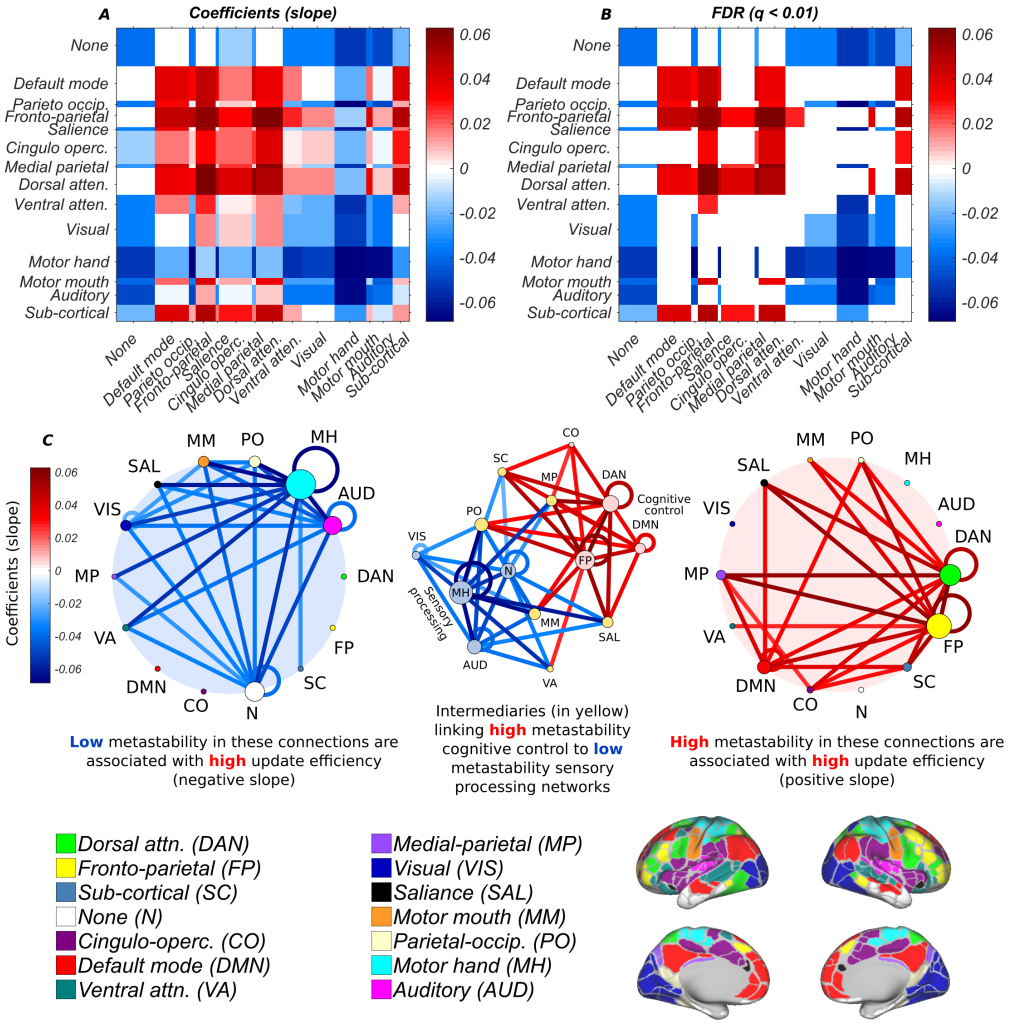


Figure 4.9: The efficiency of the transformation between resting and task-based network architecture is conditioned on high metastability in the couplings of cognitive control networks and low metastability in the couplings of sensory networks. A, Slope (coefficients) of the regression line (negative or positive) relating metastability of network connectivity to update efficiency. B, Statistically significant correlations between metastability of network connectivity and update efficiency ($p < 0.01$; FDR corrected). C, Statistically significant correlations between metastability and update efficiency in low (blue; left) and high (red; right) metastability subnetworks ($p < 0.01$; FDR corrected) where low metastability is associated with unimodal sensory networks (auditory, motor, and visual) and high metastability is related to cognitive control (dorsal attention, fronto-parietal, cingulo-opercular, and default-mode networks). Some networks such as the salience, medial parietal, parieto-occipital, and thalamus were sites of convergence for both high and low metastability connections (yellow; centre). Nodal diameter has bee scaled to reflect the sum of their ingoing/outgoing edges.

resting and task-general interaction matrices were assigned low update efficiency. Even though it is self-evident that for high update efficiency to be achieved a subject's resting and task-general architectures must be in agreement, that is, high metastability connections at rest must also be high during task and vice versa, not all of these relationships will necessarily hold statistically at the chosen significance level ($p < 0.01$; FDR). For this reason, we correlated the metastability of individual connections with update efficiency for all subjects and obtained the slope of the regression equation (Fig. 4.9.A) and its significance (Fig. 4.9.B).

A significant positive relationship between update efficiency and metastability was found in the fronto-parietal, dorsal attention, cingulo-opercular, and default mode networks (Fig. 4.9.C; right; red), and a significant negative relationship in the motor, auditory, and visual networks (Fig. 4.9.C; left; blue); ($p < 0.01$; FDR corrected for multiple comparisons). As expected, these results correspond to the structure of the task-general architecture (Fig. 4.7). Overall, high update efficiency was associated with dynamic flexibility in the connectivity of networks implicated in cognitive control and dynamic stability in primary sensory regions. Some networks such as the salience, ventral attention, medial parietal, parieto-occipital, and thalamus were sites of convergence for both high and low metastability connections (Fig. 4.9.C; centre; yellow nodes). Some caution is necessary when interpreting these results: even though it is tempting to claim that dorsal attention and fronto-parietal control networks are responsible for transitioning efficiently between rest and task-based configurations, the present findings are correlative rather than causative.

## Subjects with similar resting and task-general architectures demonstrate superior performance

We next asked if cognitive ability was informed by the efficiency of the transformation between rest and task-based configurations (Cole, Bassett, Power, Braver and Petersen, 2014; Schultz and Cole, 2016). To this end, behavioural accuracies and update efficiencies from the three in-scanner tasks

were entered into linear regression analyses. Statistically significant ($p < 0.05$; FDR corrected for multiple comparisons) relationships were identified suggesting that cognitive ability, is, to some extent, contingent on resting state architecture being 'pre-configured' to a task-general arrangement. These included: relational reasoning ($F(1,564) = 5.0$ $p < 0.026$, $r = 0.21$), language processing ($F(1,564) = 5.3$, $p < 0.021$, $r = 0.24$), and working memory ($F(1,564) = 4.9$, $p < 0.027$, $r = 0.20$).

## 4.5 Discussion

The present paper set out to answer a relatively simple question: is metastable neural dynamics higher at rest or during the performance of an explicit task? We sought to answer this question by comparing the metastability of the brain's large-scale networks when subjects were in an unconstrained resting state and when subjects were actively engaged in several cognitively demanding exercises. Current theory suggests that spontaneous neural dynamics represent a repository of functional states from which more stable global brain states emerge. Metastability between networks should therefore be maximal when subjects are at 'cognitive rest' and diminished during times of heightened cognitive load. Surprisingly, our findings support an alternative possibility: metastability (or dynamic flexibility) between neural networks is actively enhanced by the attendant demands of a task (Fig. 4.2). Cognitive engagement was characterised by two types of network architecture: (1) a task-general network structure based on widespread changes in metastability and (2) a task-specific network structure based on a small number of task-evoked changes in synchrony. Task-general architecture was principally characterised by high metastability in cognitive control networks and low metastability in sensory regions. Crucially, subjects with resting state architectures similar or 'pre-configured' to a task-general configuration displayed superior cognitive performance. Furthermore, although resting state networks were dynamically linked into context-dependent neurocognitive states by task engagement, cognitive performance was more closely linked to the intrinsic activity of large-scale networks. High metastability

in the intrinsic connectivity of cognitive control networks was associated with novel problem solving (or fluid intelligence) but was less important in tasks contingent on previous experience (or crystallised intelligence). Taken together, our findings suggest a key linkage between the intrinsic metastability of the brain's large-scale network connectivity and cognition.

The present study used one measure of connectivity–metastability–to assess the dynamic stability within and between large-scale networks of the brain. Increased stability of dynamic functional connectivity appears to be a general property of cognitive engagement across multiple behavioural paradigms irrespective of the type of dynamic functional connectivity method employed (Cohen, 2018). Consistent with the properties of a critical system, dynamic functional connectivity is especially stable during tasks requiring sustained attention (Haimovici et al., 2013; Meisel et al., 2013). Sub-critical dynamics and increased global synchrony (or increased average synchrony in our case) may be associated with a reduced ability to respond to different system inputs during task (Fagerholm et al., 2015). Such stability appears to be arise from increased integration across cognitive control networks and between cognitive control and other task-relevant networks (Elton and Gao, 2015; Hutchison and Morton, 2015; Chen, Xu, Zhou, Wang, Yang, Wang, Dong, Yang, Zang, Zuo and Weng, 2015). On the surface, increased stability between networks during task engagement appears at odds with the present finding of increased metastability. How can something be both flexible and stable at the same time? Fortunately, the paradox is resolved when we recognise that metastability and synchrony are correlated attributes of brain function (see supplementary information). Thus, even though metastability (or the variation in synchrony) is increasing, so too is the average synchrony (which can be viewed as a measure of stability in this context). It should be emphasised that purely synchronous episodes of spatio-temporal coordination between networks is not reflective of typical neurocognitive processing and in extreme cases may reflect chronic dysfunction e.g. epilepsy. Our measure of synchrony reflects this reality by reporting the average synchrony (or mean phase coherence) over a period of time corresponding to a series of concatenated task blocks. Using this

approach, we show that task blocks are characterised by on average higher levels of synchrony and higher levels of metastability at the same time. That is, synchrony (the mean phase coherence over time) and metastability (the variation in the mean phase coherence over time) increase together– a behaviour observed in cortical slice cultures excited pharmacologically (Yang et al., 2012). In light of this, synchrony and metastability should be considered as related rather than contrary methods of viewing brain activity. Two possibilities exist: (1) that metastability is the price paid for higher on average synchrony i.e. it is a form of noise or (2) metastability is an adaptive process reflecting the ongoing engagement and disengagement of neural systems relevant to cognitive and affective states. Our finding, that cognitive performance is linked to the intrinsic metastability of large-scale networks connectivity, strongly supports a functional view of metastability. Our results are consistent with theoretical and empirical findings suggesting that intrinsic neural architecture is organised to support a range of functional states which can be a posteriori selected via exogenous input (Cabral et al., 2014; Hansen et al., 2014; Kringelbach et al., 2015; Ponce-Alvarez et al., 2015; Deco and Kringelbach, 2016; Deco et al., 2017). One may argue that metastability is being driven by the variation in synchrony obtained by artificially concatenating a series of disjoint task blocks. However, in principle, metastability within a single task block should also be enhanced on the provision that synchrony also increases. Presently, the temporal limits imposed by fMRI and the relatively short task runs preclude a direct test of this hypothesis.

Task engagement was principally characterised by enhanced metastability in the connectivity of cognitive control networks (Fig. 4.3). These included dorsal attention, fronto-parietal, cingulo-opercular, default-mode, and ventral attention networks. The present finding is consistent with the notion that task-positive networks are areas of the brain that respond with activation increases to attention-demanding environments. The organisational state of the system may facilitate or inhibit the processing of incoming external stimuli by enacting a series of task-relevant synergies over the duration of the task (Kelso, 2009). Each of the networks presented similar but

not identical patterns of engagement across the seven tasks. Two of the four, the dorsal attention and fronto-parietal networks, demonstrated consistent activity across all seven of the in-scanner tasks and were associated with the greatest increases in metastability. This raises the question of why dorsal fronto-parietal regions are involved in such a puzzling variety of tasks? One proposal is that cognitive computations relying on dorsal fronto-parietal areas are concerned with a single core function, namely 'offline motor planning' or 'action emulation' (Ptak et al., 2017). Such findings are consistent with the observation that hubs of the fronto-parietal network alter their pattern of functional connectivity with nodes of other networks based on goal directed cognition in a highly adaptive domain-general manner (Cole et al., 2013; Cole, Repovš and Anticevic, 2014). Another possibility, is that increased metastability between dorsal fronto-parietal regions and task-relevant networks reflects the rhythmic perceptual sampling of the 'spotlight of attention' aliased into the low frequency components of the slow haemodynamic response (Fiebelkorn et al., 2018; Helfrich et al., 2018). Changes in metastability were not limited to interactions between cortical networks; they also involved subcortical, specifically, thalamo-cortical components. Thalamic input is known to wire the contextual associations upon which complex decisions depend into weakly connected cortical circuits (Halassa and Kastner, 2017; Schmitt et al., 2017). Greater metastability between thalamus and dorsal fronto-parietal areas during task may signal context-dependent modulation through cortico-thalamo-cortical feedback.

The seven in-scanner tasks showed remarkably similar patterns of increased metastability between large-scale networks (Fig. 4.3). Such findings resonate with prior studies showing similar patterns of static functional connectivity between different tasks (Cole, Bassett, Power, Braver and Petersen, 2014; Schultz and Cole, 2016). Similarities between functional network configurations evoked under different behavioural paradigms constitute what has been referred to as a 'task-general architecture' (Cole, Bassett, Power, Braver and Petersen, 2014; Schultz and Cole, 2016). Our findings suggest that different behaviours recruit a similar set of network connections through metastable coupling. We base this claim on three

observations: (1) increases in metastability were more widespread than increases in synchrony (Fig. 4.4); (2) increases in synchrony were highly specific to each task, whereas increases in metastability were more task-general (Fig. 4.5; Fig. 4.6); and (3) most of the variance (78%) between tasks was accounted for by a single principal component (Fig. 4.7). Our task-general configuration was organised into distinct regions of both high and low metastability (Fig. 4.7). Networks related to cognitive control exhibited dynamic flexibility whereas primary sensory networks displayed dynamic stability. These findings map onto our present understanding of cortical organisation and function. Primary sensory areas are responsible for processing a single modality whereas higher order association areas must integrate information into more complex representations e.g. language, executive function, attention, and memory. Thus, each step up the hierarchy entails integrating information from a greater diversity of sources, and this, in turn, is reflected in a region's dynamic flexibility. From another perspective, widespread increases in metastability are quite surprising. They appear to indicate that most of the brain is involved during task which appears to contradict findings from cognitive fMRI studies showing only limited activation. One possibility is that some of these changes in metastability are linked to suppression of a given network during task performance.

Even during periods of apparent 'rest' a subject's network connectivity continued to display strong integrative and segregative tendencies linked to cognitive performance. Remarkably, a subject's ability to answer questions correctly, both in and out of the scanner, related to their intrinsic neural dynamics (Fig. 4.8). Curiously, task-based changes in metastability were not related to cognitive performance, rather, subjects whose dynamics explored a greater range of network configurations at rest demonstrated the highest cognitive test scores and behavioural accuracy. Unlike crystallised intelligence, which relied on previously acquired skills and experience, the flexibility of network states afforded by metastable neural dynamics was especially advantageous in domains requiring fluid intelligence. Network organisation and dynamic flexibility may be related properties of the system. For instance, the flexible network transitions afforded by metastable neural

dynamics may be necessary to engage the 'difficult-to-reach' networks states associated with novel problem solving (or fluid intelligence) but be less important for accessing the 'easy-to-reach' network configurations associated with local knowledge and experience (or crystallised intelligence) (Barbey, 2018). The link between metastable neural dynamics and fluid intelligence was especially pronounced in systems involved in cognitive control. Our results resonate with prior observations linking cognitive control capacity to fluid intelligence (Conway et al., 2002; Cole and Schneider, 2007; Cole et al., 2012).

So why is metastability at rest predictive of behavioural and cognitive performance as opposed to metastability during the task itself? The idea that functional couplings between regions at rest contain information relevant to cognition, perception, and behaviour is supported by substantial empirical evidence (Sadaghiani et al., 2010; Sadaghiani and Kleinschmidt, 2013). Static resting state functional connectivity has been linked to a number of general cognitive abilities that include, amongst others, IQ, executive function, episodic memory and reading comprehension (for review, see Vaidya and Gordon, 2013). Thus, rather than simply reflecting invariant structural anatomy, historical co-activation patterns, or internal dynamics of local areas, intrinsic activity predicts subsequent perceptual processing (Hesselmann, Kell and Kleinschmidt, 2008; van Dijk et al., 2008; Busch et al., 2009; Mathewson et al., 2009; Sadaghiani et al., 2009; Lou et al., 2014; Van Den Berg et al., 2016). Our findings support the idea that metastability–the ability to transition between network configurations–appears to be a fixed property of a subject's neural architecture. Subjects exhibiting high metastability at rest also demonstrated high metastability during the execution of a task (see supplementary information). Individual differences in metastable neural dynamics likely stem from a combination of innate and experiential influences on the anatomical connectivity between regions; a view consistent with prior observations linking reduced metastability to altered network topology (Hellyer et al., 2015; Váša et al., 2015; Córdova-Palomera et al., 2017; Alderson et al., 2018). Cognitive performance was also linked to the efficiency of the transformation between

rest and task-based neural architectures. Specifically, subjects whose resting state was similar to the task-general architecture garnered the highest cognitive scores. From this standpoint, successful cognition is predicated on an adequate a priori dynamic configuration before the onset of task-relevant stimuli–as opposed to simple ad hoc adjustments after the fact (Bolt et al., 2018). Given that the resting state reflects previous experience and the anticipation of likely future events, a resting state network architecture pre-configured to task is more in line with future cognitive requirements (Bar, 2011). For this reason, resting state activity may reflect the brain's predictive engagement with the environment (Sadaghiani et al., 2010; Sadaghiani and Kleinschmidt, 2013; Clark, 2016). In the main, update efficiency, or the ability to switch from a rest- to a task-based configuration mapped onto our task-general architecture (Fig. 4.9). Accordingly, high update efficiency was associated with dynamic flexibility in dorsal attention and fronto-parietal control networks and dynamic stability in primary sensory networks. Such findings conform to our intuitive expectation that cortical networks require varying amounts of dynamic flexibility to fulfil their function. Presumably, sensory networks function even when subjects are cognitively at rest, hence, metastability increases less in these regions during times of heightened cognitive demand. Interestingly, several regions demonstrated high and low metastability components. These included the salience network of which the insula–a known site of multi-modal integration of sensory, motor, emotional, and cognitive information–is a part (**?**). Update efficiency based on a stationary measure of correlation between pairwise regions has been considered in previous research (Schultz and Cole, 2016). Our work differs from this approach in that we consider the update efficiency within the context of a dynamic measure of network connectivity in which both integrative and segregative tendencies coexist (Kelso and Haken, 1995; Kelso, 2012; Tognoli and Kelso, 2014*a*).

Potential limitations of the findings presented here should be noted. Firstly, it is worth emphasising that the division of neural activity into intrinsic and task-evoked activity may be an artificial distinction and not an actual division respected by neural properties (Bolt et al., 2018). Moreover,

the finding of increased metastability during task relative to rest may, to some extent, be dependent on factors related to experimental design including: (1) the time frame considered and (2) the temporal resolution of the imaging modality used. A major limitation of this approach is that the instantaneous synchrony of BOLD signal between regions is low frequency. Since metastability corresponds to the variation in instantaneous synchronisation, metastability can only be measured over extended scanning runs. Increased metastability was identified in a series of concatenated task blocks. A more desirable experimental setup would compensate for fMRI's lack of temporal precision by measuring metastability over an extended period within a single task block. Doing so would ameliorate the potential confound of introducing variations in synchrony (our definition of metastability) by including rest, cue, and fixation blocks. In the present paper, we mitigated this risk by estimating metastability with non-task block data removed. Due to restrictions on the length of the runs, metastability was estimated using the active and control components of the task, hence, participants were not exclusively performing the 'cognitive task' but the 'control task' designed to compensate for non-specific effects (e.g. the zero back condition in the working memory task). However, in most cases there was either no control condition (e.g. the motor task) or subjects still performed a meaningful exercise in the control task condition (e.g. the language task which comprised a story and math component). The current measure of metastability captures the overall variation in synchrony over time (a measure of the networks capacity for integration and segregation) or alternately, the overall dynamic stability of the system. In order to capture the explicit dwell time in each configuration an alternate approach, such as Hidden Markov Modelling, may be more appropriate (Vidaurre et al., 2017, 2018).

The results were robust in that metastability was not driven by bias associated with using time series of different lengths (we used the same number of data points for rest and task), nor by alternating periods of rest and task within a single run (we removed cue and fixation blocks). Despite attention to such factors, it remains of critical importance to establish the validity of

observed synchronisation dynamics in light of recent findings questioning the link between time varying functional connectivity and task-relevant neural information (Hindriks et al., 2016; Laumann et al., 2017; Liégeois et al., 2017). Rapid changes in synchronisation may not be directly tied to external task demands, but rather to internally driven factors that include attention, motivation, arousal, fatigue, goals, or levels of consciousness (Kucyi et al., 2017; Kucyi, 2017). For example, network integration during rest is linked with greater pupil diameter, a proxy for arousal, as well as better task performance (Shine, Bissett, Bell, Koyejo, Balsters, Gorgolewski, Moodie and Poldrack, 2016). Changes in pupil diameter are thought to coincide with the activity of neuromodulators including noradrenaline and acetylcholine (Larsen and Waters, 2018). Similarly, across repeated resting state scans of the same individual, higher levels of fatigue are related to more stable estimates of dynamic functional connectivity, whereas higher levels of attention are related to more variable measures of dynamic functional connectivity (Shine, Koyejo and Poldrack, 2016). Rapid dynamics likely include both meaningful neural information and physiological signals that relate to differences in rate or volume of blood flow, respiration, and heart rate. Untangling the relationship between rapid dynamics, internal mentation, cognitive performance, affective states, physiological noise, and general cognition will become increasingly important as we seek to understand the neural basis of human behaviour.

## 4.6 Conclusion

In this study, the theoretical framework of metastable coordination dynamics was used to explore how large-scale self-organising network interactions give rise to cognition. The dual nature of this coordination – a simultaneous integration and segregation over space and time – occurs in the absence of input, suggesting the brain is not primarily reflexive or stimulus driven but spontaneously metastable. A second type of order, imposed externally in response to environmental and stimulus contingencies, is associated with task engagement. During task execution, dynamic brain states enact variability-

reducing synergies whereby the brain experiences a phase transition to a more globally ordered cooperative state. Notably, this type of metastable transition was consistently higher than during equivalent periods of rest. Our analysis also revealed a critical linkage between key factors of general intelligence and dynamics, namely, high metastability in regions devoted to cognitive control during tests of fluid intelligence, and low metastability in the same regions during tests of crystallised intelligence.

The current study highlights the link between dynamic principles of network coordination and cognitive performance. The forthcoming chapter tests the essential proposition that coordination between local areas, as indexed by probabilistic effective connectivity, is disrupted by structural disconnection in an example of incipient neurodegeneration, MCI. This condition is characterised by memory performance significantly worse than healthy age matched controls but not serious enough to qualify for dementia. The following chapter seeks a structural basis for this dysfunction in the fibre pathways linking the thalamus – a critical structure for conscious awareness – to regions of the cortex associated with pathological activity in AD, the DMN.

# 5 Disrupted thalamus white matter anatomy and posterior default mode network effective connectivity in amnestic mild cognitive impairment

## 5.1 Overview

AD and its prodromal state amnestic mild cognitive impairment (aMCI) are characterised by widespread abnormalities in inter-areal white matter fibre pathways and parallel disruption of DMN resting state functional and effective connectivity. In healthy subjects, DMN and task positive network interaction are modulated by the thalamus suggesting that abnormal task-based DMN deactivation in aMCI may be a consequence of impaired thalamo-cortical white matter circuitry. Thus, this study uses a multimodal approach to assess white matter integrity between thalamus and DMN components and associated effective connectivity in HCs relative to aMCI patients. Twenty-six HC and 20 older adults with aMCI underwent structural, functional and diffusion MRI scanning using the high angular resolution diffusion-weighted acquisition protocol. The DMN of each subject was identified using ICA and resting state effective connectivity was calculated between thalamus and DMN nodes. White matter integrity changes between thalamus and DMN were investigated with constrained spherical deconvolution (CSD) tractography. Significant structural deficits in thalamic

white matter projection fibres to posterior DMN components posterior cingulate cortex (PCC) and lateral inferior parietal lobe (IPL) were identified together with significantly reduced effective connectivity from left thalamus to left IPL. Crucially, impaired thalamo-cortical white matter circuitry correlated with memory performance. Disrupted thalamo-cortical structure was accompanied by significant reductions in IPL and PCC cortico-cortical effective connectivity. No structural deficits were found between DMN nodes. Taken together, these findings suggest that abnormal posterior DMN activity may be driven by changes in thalamic white matter connectivity; a view supported by the close anatomical and functional association of thalamic nuclei effected by AD pathology and the posterior DMN nodes. Dysfunctional posterior DMN activity in aMCI is consistent with disrupted cortico-thalamo-cortical processing and thalamic-based dissemination of hippocampal disease agents to cortical hubs. Overall, these findings support a critical linkage between structural disconnection of the brain's intrinsic functional architecture and cognitive performance.[1]

## 5.2 Introduction

AD is a chronic neurodegenerative disorder affecting approximately 6% of people over the age of 65 and accounting for 60 to 70% of dementia cases (Burns and Iliffe, 2009). Typically, the AD-prodromal stage presents as mild cognitive impairment (MCI) (Stephan and Roebroeck, 2012) clinically defined as cognitive difficulties beyond those expected based on age and education, but insufficient to interfere with daily activities (Petersen et al., 1999). MCI can present with a variety of symptoms but is termed amnestic MCI (aMCI) in cases where memory loss is the predominant symptom. In AD, the first neurofibrillary tangles appear in the parahippocampal regions (stage I) followed later, and accompanied by cognitive symptoms, in the hippocampus formation (stage III) Braak and Braak (1991*c*,*a*, 1995). Understandably, this knowledge has reinforced focus on the hippocampus

[1] (Alderson et al., 2017)

in the context of memory loss in AD but much less well-known and less well-understood are the appearance of tangles and plaques in the thalamic nuclei in parallel with those in the hippocampus. Their appearance is often characterised as an event downstream of the hippocampus pathology transmitted by the projections of the mammillary bodies, but this view is challenged by metabolic studies indicating that the earliest consistent declines occur not in hippocampus but in posterior cingulate cortex (PCC) (Minoshima et al., 1994, 1997) where amyloid deposition is highest (Buckner et al., 2005; Mintun et al., 2006). The thalamus, with its dense network of reciprocal interconnections with both hippocampus and PCC, is therefore implicated by association (Vann et al., 2009; Aggleton et al., 2010).

Such a view is supported by detection of thalamic atrophy in presymptomatic familial AD on average 5.6 years prior to expected symptom onset (Ryan et al., 2013) together with increased amyloid burden (Knight et al., 2011) and substantial evidence suggesting that thalamic atrophy is present in MCI prior to AD (Chételat et al., 2005; Shiino et al., 2006; de Jong et al., 2008; Ferrarini et al., 2008; Cherubini et al., 2010; Roh et al., 2011; Pedro et al., 2012). Structural irregularities have a sufficient impact on thalamo-cortical circuits to allow healthy subjects to be differentiated from those with MCI through impaired functional integrity (Cantero et al., 2009). Conversely, carriers of the apolipoprotein  2 allele i.e. those showing a genetic predisposition against developing AD, demonstrate significantly enhanced functional (Patel et al., 2013) and structural (Chiang et al., 2012) integrity of the thalamus. Analysis of low frequency BOLD signal oscillations have revealed several resting state networks. Of these, the default mode network (DMN)(Raichle et al., 2001; Greicius et al., 2003; Damoiseaux et al., 2006) has consistently been identified as dysfunctional in both MCI and AD in the context of amyloid burden (Hedden et al., 2009; Drzezga et al., 2011; Sheline et al., 2011) and genetic risk (Roses, 1996; Sheline et al., 2010; Chhatwal et al., 2013). The DMN comprises medial prefrontal cortex (mPFC), middle temporal gyrus (MTG), lateral inferior parietal lobes (IPL), PCC, and hippocampus regions. These nodes have been identified as important hubs within the cortex (Buckner et al.,

2009) whose persistent background activity and dense, long range interconnectivity may facilitate the early deposition and prion-like transmission of amyloid plaques (Wermke et al., 2008; Raj et al., 2012) DMN topography is therefore recapitulated in the pattern of atrophy, hypometabolism and amyloid deposition within the cortex (Buckner et al., 2005, 2008).

Thalamus appears to play a role modulating distributed cortical networks (Di and Biswal, 2014*b*). It is therefore of note, that direct structural connections between the thalamus and DMN (or thalamo-DMN pathway) components have been described *in vivo* using diffusion tensor imaging (DTI) (Fernández-Espejo et al., 2012) and that these are sites of atrophy (Zarei et al., 2010). Crucially, lesions to the thalamus are known to cause DMN dysfunction (Jones et al., 2011). One suggestion is that abnormal task-induced deactivation of DMN response patterns in aMCI are a consequence of impaired thalamo-cortical signalling (Pihlajamäki and Sperling, 2009).

The thalamus sends widespread connections to its ipsilateral cortical hemisphere which are returned via cortico-thalamic feedback connections. Together these form a thalamo-cortico-thalamic feedback loop (Sherman and Guillery, 2006; Sherman, 2007; Zhang et al., 2008, 2010). Such an arrangement is critical for generating the ubiquitous oscillations of the cortex recorded by EEG and fMRI but its contribution (and other subcortical components) to regulating the DMN in health and disease is largely unexplored. On this basis, this study investigates the impact of impaired thalamo-cortical microscopic white matter anatomy on interactions in the DMN in aMCI patients. CSD-based probabilistic fibre tractography of the thalamo-DMN white matter pathways in a cohort of older adults with aMCI and healthy age-matched controls. The effective connectivity of the resting state thalamo-DMN interactions were also examined using a spatio-temporal formulation of GC. In contrast to simple statistical correlation (i.e. functional connectivity), effective connectivity is more ambitious and attempts to quantify the probabilistic causal influence one region exerts over another. Given that thalamo-cortical neural signals appear to coordinate distributed networks (Di and Biswal, 2014*b*), such an approach provides

greater scope for clarifying the interactions between thalamus and cortex during the transition between health and disease. It was predicted that abnormal DMN causal activity would be linked to structural deficits in the thalamo-DMN pathway.

## 5.3 Methods

### Participants

Twenty six HC participants and 20 older participants with aMCI took part in the study. The HCs were community-dwelling older adults recruited from the greater Dublin area (Ireland) via newspaper advertisements. They underwent a health screening questionnaire and a neuropsychological assessment, the Consortium to Establish a Registry for Alzheimer's Disease (CERAD)(Morris et al., 1989), in order to rule out possible cognitive impairment before inclusion in the study. The CERAD battery has been shown to be sensitive to the presence of age related cognitive decline (Welsh et al., 1991, 1992). All of the older participants included in the study scored no more than 1.5 SD below the standardized mean scores for subjects of a similar age and education level on any of the sub-tests. The aMCI participants were recruited from memory clinics in St. James Hospital and St. Patrick's Hospital in Dublin, Ireland, and were diagnosed by a clinician according to the Peterson criteria (Petersen et al., 1999) – i.e., abnormal memory scores for age and education level with no dementia. Hippocampal atrophy was not a factor in the diagnosis. Four were single amnestic aMCI, and 16 were multi-domain aMCI (Petersen, 2004). Neuropsychological measures were administered or supervised by an experienced neuropsychologist and included the mini-mental state examination (MMSE) (Folstein et al., 1975) and Cambridge cognitive examination (Huppert et al., 1995).

All of the participants were right-handed with no history of head trauma, neurological disease, stroke, transient ischemic attack, heart attack, or psychiatric illness. They completed the Geriatric Depression Scale (GSD) (Yesavage et al., 1983), the Eysenck Personality Questionnaire Revised Edi-

| | HC(n=26) | aMCI (n=20) | p* (df=44) |
|---|---|---|---|
| **Gender** | 15M,11F | 10M,10F | 1 |
| **Age** | 69.30 ± 6.35 | 69.05 ± 7.55 | 0.90 |
| **Ethnicity** | White (Irish) | White (Irish) | - |
| **Education** | 13.38 ± 3.73 | 14.32 ± 3.02 | 0.38 |
| **MMSE** | 28.65 ± 0.85 | 27.05 ± 2.17 | 0.0013 |
| **GDS** | 0.77 ± 1.07 | 2.58 ± 2.27 | 0.0008 |
| **EPQ E** | 8.04 ± 2.47 | 5.53 ± 3.37 | 0.0061 |
| **EPQ N** | 2.69 ± 2.43 | 3.78 ± 3.39 | 0.21 |
| **CR** | 16.65 ± 3.62 | 16.58 ± 4.97 | 0.95 |

Table 5.1: MMSE, mini-mental state exam; GDS, geriatric depression scale; EPQ E, Eysenck personality questionnaire extraversion scale; EPQ N, Eysenck personality questionnaire neuroticism scale; CR, cognitive reserve scale. Standard deviations are indicated. Results of independent samples t-tests, except for gender which was compared with a Fischer's exact test. Statistically significant differences are indicated in bold.

tion Short Scale (EPQ-R) (Eysenck and Eysenck, 1994), and a Cognitive Reserve Questionnaire (Rami et al., 2011) before the MRI scan (table 5.1). The groups did not differ in terms of age, gender, education level, or levels of cognitive reserve as assessed by the self-report Cognitive Reserve Questionnaire. The aMCI group had lower MMSE scores, higher GDS scores, and scored lower on the EPQ measure of extraversion than the HC group. The study had full ethical approval from the St. James Hospital and the Adelaide and Meath Hospital, incorporating the National Children's Hospital Research Ethics Committee and St Patrick's University Hospital Research Ethics Committee. All participants gave written informed consent before taking part in the study.

## 5.4 MRI data acquisition

Whole-brain high angular resolution diffusion imaging (HARDI) data were acquired on a 3.0 Tesla Philips Intera MR system (Best, The Netherlands) equipped with an eight channel head coil. A parallel sensitivity encoding (SENSE) approach (Pruessmann et al., 1999) with a reduction factor of two

was used during the DWI acquisition. Single-shot spin echo-planar imaging was used to acquire the DWI data with the following parameters: TE 79ms, TR 20,000ms, field of view (FOV) 248mm, matrix 112×112, isotropic voxel of 2.3mm×2.3mm×2.3mm, and 65 slices with 2.3mm thickness with no gap between the slices. Diffusion gradients were applied in 61 isotropically distributed orientations with b=3000s/mm2, and four images with b=0s/mm2 were also acquired. A high-resolution 3D T1-weighted anatomical image was acquired for each participant with the following parameters: TE=3.9ms, TR=8.5ms, FOV=230mm, slice thickness=0.9mm, voxel size=0.9mm×0.9mm×0.9mm. Resting-state fMRI data were also acquired during the scanning session. The scan lasted for 7 minutes during which time the participants were asked to keep their eyes open and fixate on a cross hairs in the centre of a screen behind the MR scanner, visible via a mirror. The BOLD signal changes were measured using a T2*-weighted echo-planar imaging sequence with TE=30ms and TR=2000ms. Each volume of data covered the entire brain with 39 slices, and the slices were acquired in interleaved sequence from inferior to superior direction. Two hundred ten volumes of data were acquired, with voxel dimensions of 3.5mm × 3.5mm × 3.85mm and a 0.35mm gap between the slices.

## Face-name encoding and recognition task protocol

Relationships between the participants structural/effective connectivity measures and memory were subsequently examined using data obtained from a face–name recognition task following the resting-state scan. The participants viewed a series of 27 emotional faces (Erwin et al., 1992) with a name presented underneath each one. This task was an implicit memory task, in that the participants later completed a surprise memory tasks to test their retention of both the faces and the face–name pairs, however, at the time of encoding, they were not explicitly asked to remember the face–name pairs. Rather, the participants were instructed to judge whether the names matched or suited the faces. It was explained that this was a subjective decision, with no right or wrong answer. The participants responded yes

or no by pressing a button on a MR-compatible response pad held in their right or left hand, respectively, using the index finger of either hand. Each face–name combination was presented for 4 sec and was shown twice during the run. The faces were positive, negative, or neutral in valence and there were equal numbers of valence types as well as gender. The presentation of the face–name pairs was grouped according to the emotional valence of the faces. In each instance, a group of either two, three, or four faces of one valence type was presented randomly using an event-related paradigm, subsequently, there was a delay during which a white cross hair was presented (control condition). The duration of the white cross was varied according to the duration of the face stimulus. For instance, if a single face was presented for 4 sec the subsequent white cross was also shown for 4 sec and then the next block of faces began. The stimuli were delivered using Presentation v.16.1 (Neurobehavioral Systems, Albany, CA). Approximately 15 min following the encoding phase, the participants performed a short computer-based recognition task. The emotional faces were presented one at a time on a black background with three names underneath. One of the names was the correct name; one name was a name that had been paired with a different face (distractor; incorrect name), while the third name was a new name (foil; incorrect name). The participants responded by pressing a button on the left, middle, or right side of a keyboard to correspond with the relative position of the name on the screen. The stimuli were presented for 5 sec and followed by an inter-trial interval of 5 sec. This longer trial length was to facilitate performance of this task as it was quite challenging. Before the task began, the participants completed a short practice run of five trials.

## 5.5 Resting state pre-processing

FMRI data processing was carried out using FEAT (FMRI Expert Analysis Tool) Version 6.00, part of FMRIB's Software Library (FSL; www.fmrib.ox.ac.uk/fsl). Registration to high resolution structural and/or standard space images was carried out using FNIRT (Andersson et al., 2007). The following

pre-statistics processing was applied; motion correction using MCFLIRT (Jenkinson et al., 2002), slice-timing correction using Fourier-space time-series phase-shifting, non-brain removal using BET (Smith, 2002), spatial smoothing using a Gaussian kernel of FWHM 3.0mm, grand-mean intensity normalisation of the entire 4D dataset by a single multiplicative factor, highpass temporal filtering (Gaussian-weighted least-squares straight line fitting, with sigma=50.0s).

## 5.6 Resting state effective connectivity

GC is a standard statistical tool for detecting the directional influence one system component exerts over another. The concept, originally introduced by Wiener (1956), and later incorporated into a data analysis framework by Granger (1969) is described as follows. If historical information from time series X significantly improves prediction accuracy of the future of time series Y in a multivariate autoregressive model (MVAR), GC is identified. This may be viewed of as a measure of model prediction error where GC quantifies the reduction in prediction error when past values of X are included in the explanatory variables of Y (Schelter et al., 2006).

Critically, the ability of GC to deal with indirect interactions depends on being able to measure all relevant variables in a system. Often, this is not possible, and both environmental (exogenous) inputs and unmeasured latent variables can confound accurate causal influences. Since only a fraction of the possible cortical and subcortical areas are considered latent variables are bound to exist. Hence controlling for exogenous inputs and latent variables is a critical issue when applying Granger causality to experimental data. In such cases where exogenous inputs are quantifiable partial GC may offer a more robust approach. However, it should also be noted that when the exogenous input is absent or small, both conditional and partial Granger causality can correctly infer the underlying causal relationships (Guo et al., 2008). Partial GC is not used in the present study, as the common exogenous input to thalamus and DMN regions is unclear.

By fitting a time invariant MVAR model to the experimental time series

the classic GC formulation ignores crucial time-varying properties of the system. Such an approach makes the tacit assumption that the longer the time series, the more reliable the GC estimates. While this may be correct in static circuit representations (Smith et al., 2011), under time-varying conditions this principle is no longer valid. A more robust method is to divide the time series into equal windows and consider them separately. Here, an optimal trade-off between the length of the time windows and the accuracy of the estimated coefficients for each window must be determined. Time windows that are too short prevent the accurate estimation of parameters, while time windows that are too long increase the probability of incorrect inferences of GC. Given a fixed number of change-points, the model can be fit into each time window and the variance of the residual errors estimated. The Granger prediction metric corresponds to the relative size of the errors from a univariate model in which current values of X are predicted from X, and a bivariate model in which current values of X are predicted both from past values of X and from past values of Y. If the model is a good fit to the data then the errors will be small and will have relatively little variability. Conversely, if the model is a poor fit to the data, the errors will be large and demonstrate high variability. Thus, the variance of the errors from the bivariate model is compared with the variance of the errors from the univariate model to provide an estimate of Granger causality. Accordingly, the current paper utilises a novel spatio-temporal GC formulation to quantify the effective connectivity changes between region of interest (Luo et al., 2013; Youssofzadeh et al., 2016). In this framework, finding the optimal time window length reduces to the solution of a constrained optimisation problem,

$$min_{l_0}(GC_{err}(l_0(m)) + \frac{1}{GC_{avg}(l_0(m))}$$

where we seek to simultaneously minimise model prediction error $GC_{err}$ (i.e. the weighted average of the variances of the residuals in each time window) and maximise detected causality information $GC_{avg}$ (i.e. the average GC over all time windows). This is performed for time windows of different

length $l_0(m) = t_1, ..., t_m$. The time window producing the lowest Bayesian information criterion is considered optimal. By considering optimal time windows, the spatio-temporal framework allows a more reliable and precise estimate of GC in experimental datasets with time varying properties. This approach has been shown to yield more accurate estimates of GC on resting state fMRI data than traditional GC metrics. In this case, the last 208 time points for each region under consideration were extracted from the functional image volume and divided into four windows with the first two time points removed to avoid start up transients. In terms of spatial resolution, GC is calculated between all pairs of voxels from the two regions of interest under consideration. The mean GC among all pairs of voxels was then used as the final estimate.

## CSD white matter tractography using MRtrix3

A method for controlling free water contamination of tissue and the resultant partial volume effects is especially important around the fornix where atrophy and CSF is prevalent. The free water elimination technique (Pasternak et al., 2009) has been successfully applied in previous tractography studies of ageing and aMCI (Metzler-Baddeley et al., 2012; Fletcher et al., 2014; Kehoe et al., 2015) however at higher b-values the Gaussian assumption underlying the bi-tensor model is no longer valid and a more simple heuristic is indicated. Accordingly, the standard free water elimination approach to identify and mask voxels with high free water content but fit the conventional DTI model to each voxel. The *dwipreproc* preprocessing script was to perform eddy current-induced distortion and motion correction using the FSL tool eddy (Andersson and Sotiropoulos, 2016). The standard MRtrix3 processing script *dwibiascorrect* was used to eliminate low frequency intensity inhomogeneities across the DWI series. The script uses bias field correction algorithms available in the FSL software package (Zhang et al., 2001).

Probabilistic white matter tractography was performed on the DWIs using the MRtrix3 software package (http://www.mrtrix.org/). Crossing

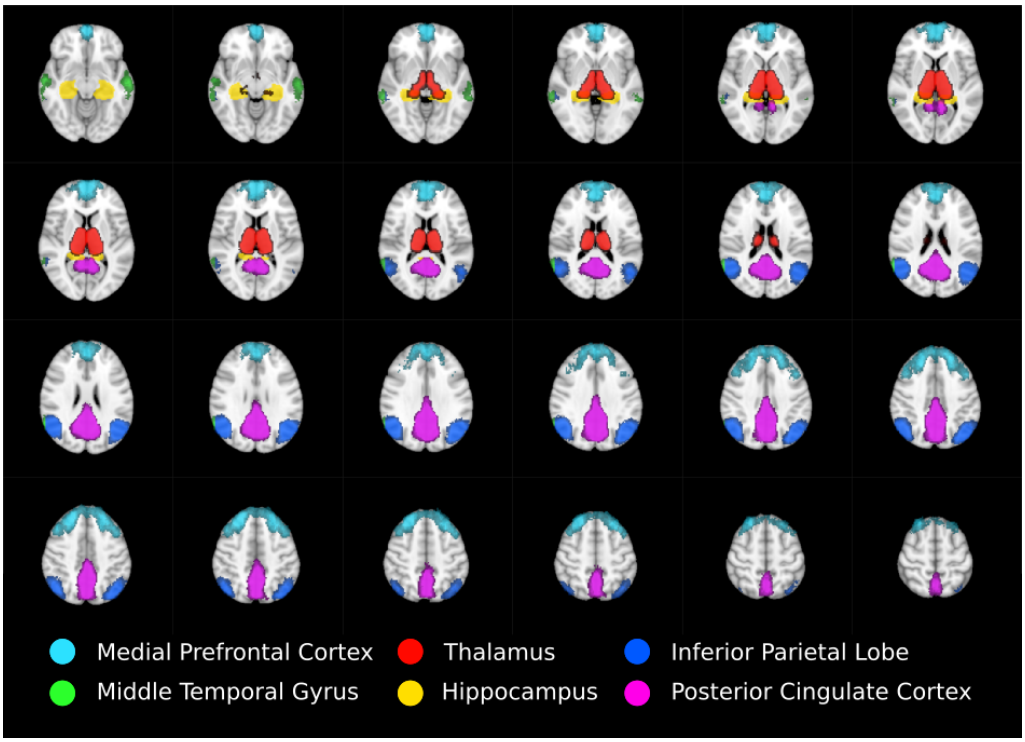


Figure 5.1: Regions of interest moving from inferior (top left) to superior (bottom right) defining thalamo-DMN white matter tractography masks. DMN components mPFC, MTG, IPL, and PCC were defined using probabilistic template (Wang, Kong, Chu, Tam, Lam, Wang, Northoff, Mok, Wang and Shi, 2014), while thalamus and hippocampus were defined using the Harvard-Oxford subcortical structural atlas.

fibres were resolved using the constrained spherical deconvolution algorithm (Tournier et al., 2004, 2012). MRtrix3 pre-processing included computing the diffusion tensors images (or diffusion ellipsoids) for each voxel from which the FA, DA, RD and MD images were subsequently generated. Whole-brain tractography was performed using every voxel as a seed point. The principle diffusion orientation at each point was estimated by the CSD tractography algorithm, which propagated in 0.1 mm steps along this direction. At each new location the fibre orientation(s) was estimated before the tracking moved a further 0.1 mm along the direction that subtended the smallest angle to the current trajectory. A trajectory was followed through the data until the scaled height of the fibre orientation density function

peak dropped below the default threshold, or the direction of the pathway changed through an angle of more than 90°.

Anatomical masks were used to divide the results into circumscribed regions. The DMN was defined by probabilistic template (Wang, Kong, Chu, Tam, Lam, Wang, Northoff, Mok, Wang and Shi, 2014) and the hippocampus and thalamus using the Harvard-Oxford subcortical structural atlas (Fig. 5.1). Streamlines beginning in one mask and terminating in another were considered in a pairwise fashion for all region of interest. In addition, the FSL tool FAST (FMRIB's Automated Segmentation Tool) was used to derive a white matter brain mask to constrain tractography. Any tracks tracts exiting the white matter were considered spurious and discarded. Tracts were prevented from propagating between hemispheres by a stop region placed down the midline corresponding to the corpus callosum. Statistically significant differences in the mean FA, DA, RD and MD of tracks in HC versus aMCI were tested by way of a two tailed two sample t-test at $p < 0.05$ corrected for multiple comparisons.

## Independent component analysis

The DMN was identified for each subject using ICA. Analysis was carried out using Probabilistic ICA (Beckmann and Smith, 2004) as implemented in MELODIC (Multivariate Exploratory Linear Decomposition into Independent Components) Version 3.14, part of FSL. The following data preprocessing was applied to the input data: masking of non-brain voxels, voxel-wise de-meaning of the data, normalisation of the voxel-wise variance. Pre-processed data were whitened and projected into a 62-dimensional subspace using probabilistic Principal Component Analysis where the number of dimensions was estimated using the Laplace approximation to the Bayesian evidence of the model order (Minka, 2001; Beckmann and Smith, 2004). The whitened observations were decomposed into sets of vectors which describe signal variation across the temporal domain (time-courses) and across the spatial domain (maps) by optimising for non-Gaussian spatial source distributions using a fixed-point iteration technique (Hyvärinen,

1999). Estimated component maps were divided by the standard deviation of the residual noise and thresholded by fitting a mixture model to the histogram of intensity values (Beckmann and Smith, 2004). The number of components was automatically estimated. The component corresponding to the DMN was selected by cross correlating all the components with a probabilistic DMN template (Wang, Dai, Gong, Zhou and He, 2014). The fMRI BOLD signal was extracted from DMN components mPFC, MTG, IPL, and PCC, combined with those extracted from hippocampus and thalamus masks, and analysed using the spatio-temporal GC method to determine the effective connectivity. A standard two tailed t-test was used to determine significant differences between the HC and aMCI patients at $p < 0.05$ corrected for multiple comparisons.

## 5.7 Results

### Comparison of resting state thalamo-DMN effective connectivity in HC versus aMCI subjects

The spatio-temporal GC effective connectivity analysis revealed significant differences in a circumscribed set of regions at the Bonferroni corrected threshold of $p < 0.0014$. In aMCI, several incoming connections to PCC and left IPL showed reduced casual connectivity. An especially pronounced decrease in causal interaction to left IPL from other DMN components, hippocampus, and thalamus was observed (Fig. 5.2A). Reduced connectivity to left IPL included incoming connections from left thalamus [$t(44) = 3.77$, $p < 0.001$], left [$t(44) = 4.3$, $p < 0.0001$] and right [$t(44) = 3.80$, $p < 0.001$] MTG and from right IPL [$t(44) = 3.83$ $p < 0.001$]. These changes correspond to a highly significant [$t(44) = 5.10$, $p < 0.00001$] decrease in average FA in the white matter between left thalamus and left IPL (Fig. 5.2B). Also in aMCI, significant reductions in connectivity to PCC from left MTG [$t(44) = 3.93$, $p < 0.001$] were found, together with significant reductions in connectivity to right IPL from PCC [$t(44) = 3.73$, $p < 0.001$] (Fig. 5.2A).

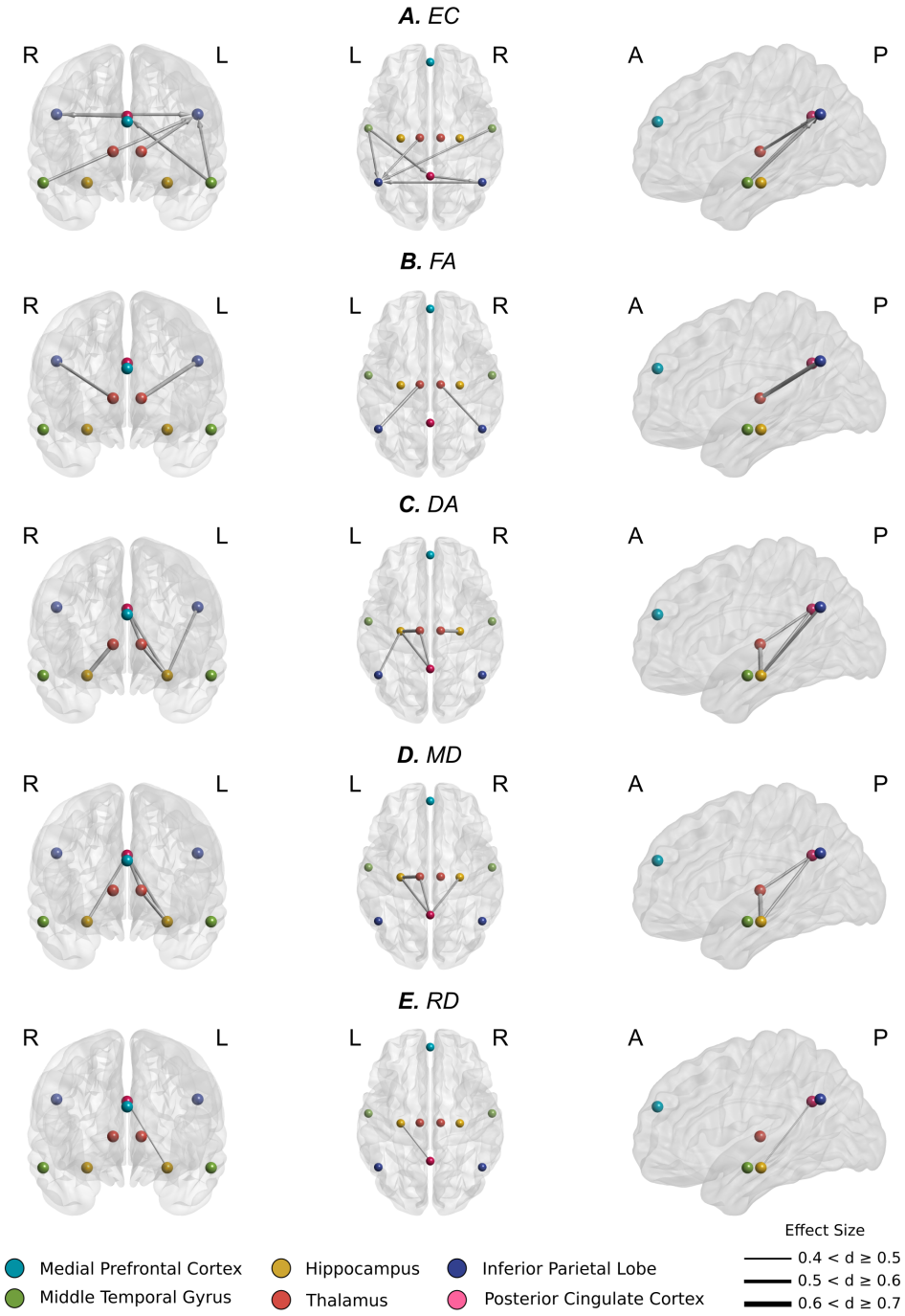


Figure 5.2: A, Significantly reduced incoming effective connectivity to left IPL from thalamus and posterior DMN nodes. B, Significantly reduced FA in thalamo-IPL tracts where the magnitude of reduction corresponded to the degree of effective connectivity disruption in A. C, Significantly reduced DA in the left Papez circuit including hippocampo-thalamus, thalamo-PCC, and PCC-hippocampal tracts. D, As in C, significantly reduced MD in the left Papez circuit. E, Significantly reduced RD in left hippocampo-PCC tracts.

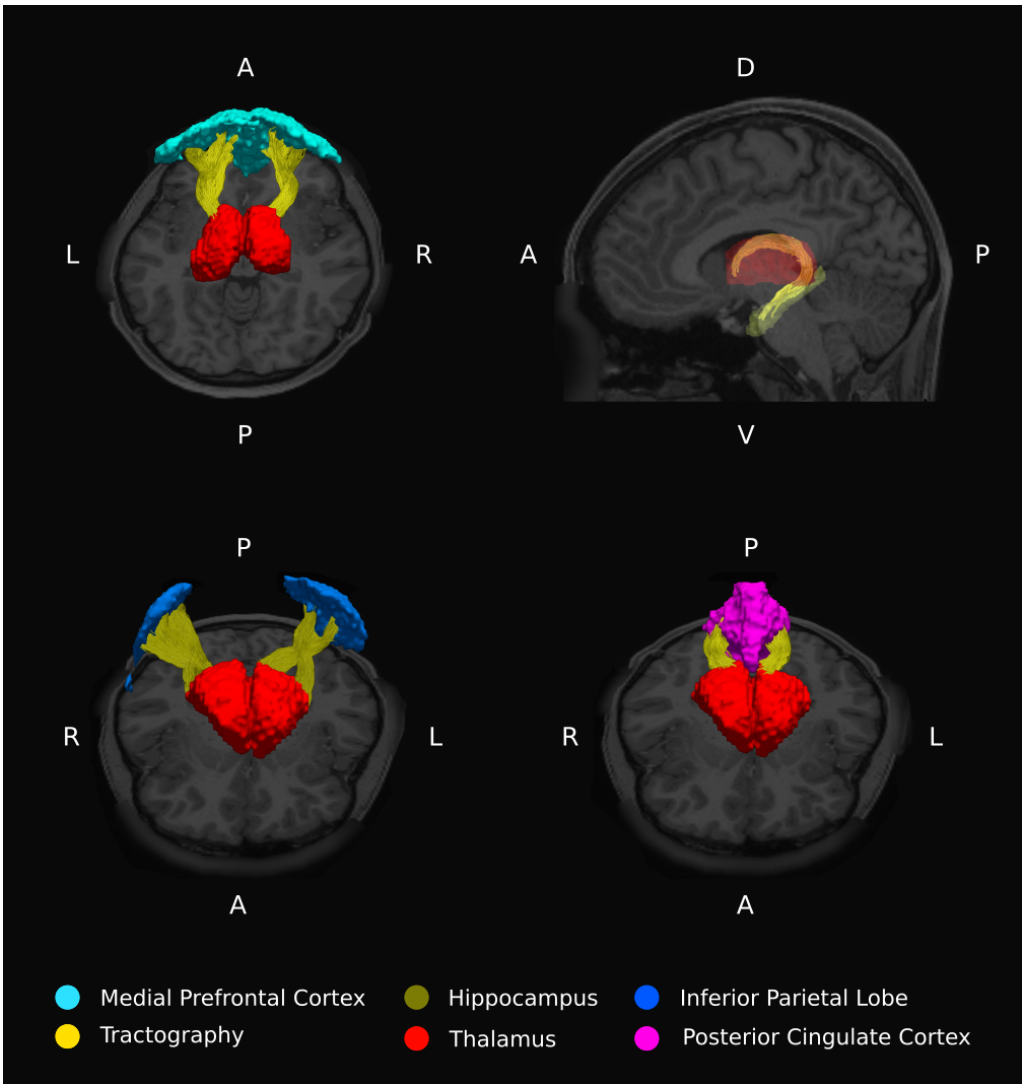


Figure 5.3: Example thalamo-DMN white matter tracts from a single representative healthy subject.

## Comparison of thalamo-DMN structural integrity in HC versus aMCI subjects

In aMCI, CSD white matter tractography identified statistically significant increases at the Bonferroni corrected threshold in average DA, RD, and MD in the white matter fibre pathways connecting thalamus to hippocampus, PCC, and IPL (Fig. 5.3). Significant decreases in average FA were also detected in the white matter between thalamus and IPL. These included:

- Significant decreases in FA (Fig. 5.2B) between right thalamus and right IPL [$t(44) = 3.81$, $p < 0.001$] and between left thalamus and left IPL [$t(44) = 5.24$, $p < 0.00001$].
- Significant increases in DA (Fig. 5.2C) between right thalamus and right hippocampus [$t(44) = -4.68$, $p < 0.0001$], right hippocampus and PCC [$t(44) = -4.02$, $p < 0.001$], left thalamus and left hippocampus [$t(44) = -5.33$, $p < 0.00001$], left thalamus and PCC [$t(44) = -3.91$, $p < 0.001$], left hippocampus and left IPL [$t(44) = -4.13$ $p < 0.001$], and left hippocampus and PCC [$t(44) = -3.91$, $p < 0.001$].
- These changes were recapitulated in the MD metric (Fig. 5.2D) with significant increases between right hippocampus and PCC [$t(44) = -3.69$, $p < 0.001$], left thalamus and left hippocampus [$t(44) = -4.34$, $p < 0.0001$], left thalamus and PCC [$t(44) < -3.63$, $p = 0.001$] and left hippocampus and PCC [$t(44) = -4.17$, $p < 0.001$].
- Finally, a significant increase in RD (Fig. 5.2E) between left hippocampus and PCC [$t(44) = -3.66$, $p < 0.001$] was also found.

## Empirical measures of effective and structural connectivity predict memory performance

To investigate whether empirical measures of effective and structural connectivity relate to memory, the diffusivity and GC metrics were separately regressed against the results from a face-name encoding and recognition task using gender, age, and motion parameter estimates as covariates of no

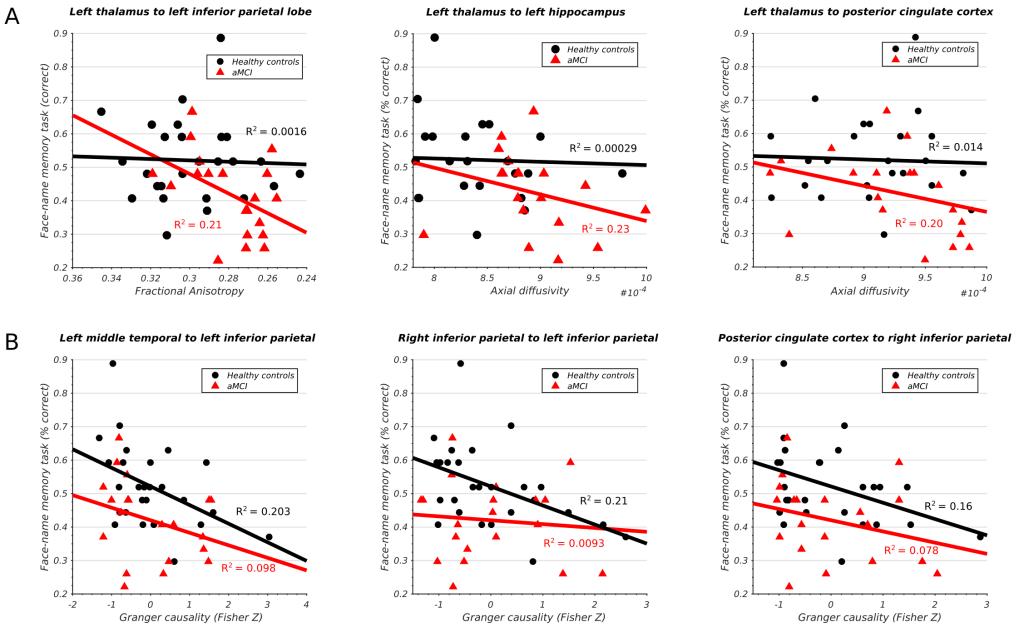


Figure 5.4: A, Significant association between structural integrity of thalamo-cortical white matter pathways and memory performance in aMCI subjects. B, Significant association between inferior parietal lobe effective connectivity and memory performance in HCs.

interest.

The aMCI cohort displayed a significant negative correlation between the integrity of the left thalamo-cortical white matter connectivity and memory in three DMN regions (Fig. 5.4A) including IPL [t(24) = -2.43, p $<$ 0.05], hippocampus [t(24) = -2.31, p $<$ 0.05], and PCC [t(24) = -2.21, p $<$ 0.05]. The healthy subjects displayed no such relationship. Conversely, the healthy cohort demonstrated a significant negative correlation between the effective connectivity of IPL and memory and three other DMN regions (Fig. 5.4B) including left MTG [t(24) = -2.47, p $<$ 0.05], right IPL [t(24) = -2.54, p $<$ 0.05], and PCC [t(24) = -2.21, p $<$ 0.05]. The same relationship was absent in the aMCI cohort. All results survived multiple-comparison correction with FDR (q $<$ 0.1).

## 5.8 Discussion

The appearance of atrophy, tangles, and plaques in thalamus is often characterised as a secondary process resulting from atrophy in the hippocampus and the prion-like transmission of pathology along the white matter topography (Raj et al., 2012). But such a view is inconsistent with evidence suggesting that the earliest metabolic changes occur not in hippocampus but in posterior DMN node PCC. Thus, structural deficits in thalamus may be driving early PCC hypometabolism and initiating the cascade of DMN functional anomalies typically associated with early AD. Accordingly, a multimodal approach was used to assess the impact of thalamo-cortico-thalamic feedback loop integrity on DMN functionality in aMCI.

Significant structural abnormalities were found in the thalamo-PCC and thalamo-IPL white matter fibre pathways in the aMCI cohort (Fig. 5.2B, C, D, E). A pronounced reduction in left thalamo-IPL effective connectivity (Fig. 5.2A) corresponded with significant thalamo-IPL structural impairment (Fig. 5.2B). Critically, the integrity of thalamic white matter and memory was correlated in the aMCI cohort but not in the HCs (Fig. 5.4A). In general, the gradient of structural impairment followed a hippocampo-thalamo-PCC axis consistent with a prion-like dissemination of pathology (Raj et al., 2012) along the major white matter fibre pathways of the Papez circuit (Papez, 1937). No structural abnormalities were identified between cortical DMN components MPFC, MTG, IPL, and PCC, however significant disruption to incoming IPL effective connectivity was observed, and this distinguished aMCI from HC memory performance (Fig. 5.4B) with GC accounting for, on average, 19.1% of the memory performance in HC at the $p < 0.05$ significance threshold (FDR corrected for multiple-comparisons).

Overall, our findings are broadly suggestive. One interpretation is that disrupted effective connectivity in posterior DMN nodes PCC and IPL is, to some extent, inspired by incipient thalamo-cortical deafferentation. If true, this finding may help explain abnormal task-induced DMN response patterns typically found in aMCI and AD subjects (Pihlajamäki and Sperling, 2009).

## Impaired hippocampo-thalamo-PCC white matter anatomy and abnormal PCC effective connectivity

The current paper identified significant structural impairment between fibre pathways connecting hippocampus and thalamus (Fig. 5.2C, D), thalamus and PCC (Fig. 5.2C, D), and PCC and hippocampus (Fig. 5.2C, D, E). Measures of left thalamo-cortical structural integrity (including tracts to hippocampus and PCC) correlated with memory performance in the aMCI cohort but not in the HCs (Fig. 5.4A). Impaired structural relations within the hippocampo-thalamo-PCC complex are likely mediated by their close anatomical association. Together these structures comprise a limbic-diencephalic memory network (Nestor et al., 2003) connected through the circuit of Papez (Papez, 1937). This structure runs from hippocampus through fornix to anterior thalamus via mammillary bodies and onto PCC before returning to hippocampus to complete the circuit. Interestingly, the current study identified a decreasing gradient of structural impairment between hippocampus, thalamus, and PCC, suggesting that structural deafferentation of PCC through impaired hippocampus and thalamus fibre pathways, likely stems from pathology and atrophy originating in the hippocampal complex. Such a view is consistent with postmortem studies indicating that thalamic nuclei connected to hippocampus are a site of primary degeneration in AD (Xuereb et al., 1991).

Previous work has highlighted a staged disconnection process occurring both along the cingulum bundle between hippocampus and PCC (i.e. the direct route) and within the memory circuit of Papez encompassing thalamic intermediaries (i.e. the indirect route) (Villain et al., 2008). Such findings are consistent with early PCC hypometabolism (Matsuda, 2001; Valla et al., 2001; Mosconi et al., 2008; Zhu et al., 2013; Mutlu et al., 2016) where it frequently presents before clinical diagnosis (Minoshima et al., 1997; Johnson et al., 1998) as part of a constellation of metabolic effects focused around medial temporal lobe and thalamus, when memory loss is still a relatively isolated feature (Nestor et al., 2003). Interestingly, PCC hypometabolism appears to correlate with remote hippocampus atrophy

early in MCI but transition to both remote and local effects over the course of progression to AD (Teipel and Grothe, 2016).

The current study identified a significant correlation between the structural integrity of hippocampo-thalamus and thalamo-PCC fibre pathways (i.e. the indirect route) and memory in the aMCI cohort which was absent in the HCs (Fig. 5.4A). A similar pattern was identified in the hippocampo-PCC fibre pathway (i.e. the direct route) however this did not survive correction for multiple comparisons. Dysfunction of structures along the hippocampal output pathways to PCC have been linked to episodic memory impairment (Yakushev et al., 2011). The PCC's hub status (Hagmann et al., 2008) may predispose to amyloid deposition, atrophy, and hypometabolism (Buckner et al., 2005, 2009) where remote often diffuse damage accumulates as altered PCC connectivity through a form of diaschisis (Meguro et al., 1999; Leech and Sharp, 2014). One suggestion is that direct thalamo-PCC (Fig. 5.2C, D) and distal thalamo-IPL (Fig. 5.2B) white matter structural deficits operate in tandem to initiate a cascade of aberrant effective connectivity in PCC (Fig. 5.2A). Taken together, these findings are consistent with a progressive disconnection of PCC from downstream cortical and subcortical sources with differential effects operating on the direct versus indirect hippocampo-PCC pathways.

## Impaired thalamo-IPL white matter anatomy and abnormal IPL effective connectivity

The current paper identified significant impairments in thalamic white matter circuitry serving bilateral IPL where the magnitude of diffusivity change (Fig. 5.2B) correlated with the intensity and extent of effective connectivity disruption in each hemisphere (Fig 5.2A). Marked structural deficits were observed in left thalamo-IPL white matter connectivity together with significantly reduced effective connectivity from left thalamus. In the aMCI cohort, measures of reduced thalamo-IPL structural integrity correlated with memory performance (Fig. 5.4A). Left thalamo-IPL structural abnormalities were accompanied by widespread decreases in effective connectiv-

ity from other DMN regions. Similarly, in right hemisphere, thalamo-IPL structural deficits coocurred with disrupted incoming and outgoing IPL effective connectivity. Crucially, the relationship between IPL effective connectivity and memory was disrupted in the aMCI subjects but not in the HCs (Fig. 5.4B). Several converging findings implicate the pulvinar nucleus of the thalamus in this dysfunction. The pulvinar nuclei appear to play a role in cortico-cortical communication where they receive driving input from IPL and relay signals back to cortex via ascending thalamo-cortical projections (Saalmann et al., 2012). Since direct cortico-cortical projections far outnumber projections to pulvinar nucleus from cortex, the pulvinar is unlikely to be the primary route for the transfer of cortico-cortical sensory signals, rather, it may act to coordinate interactions between distributed cortical networks as a function of attention ((Basso et al., 2005). Interestingly, entorhinal cortex connects directly to pulvinar nucleus via a non-fornical temporopulvinar tract (Saunders et al., 2005; Zarei et al., 2013) which may provide a conduit for the prion-like transsynaptic spread of disease agents originating in hippocampus (Raj et al., 2012). Consistent with this hypothesis, the present study identified significant structural impairment between thalamus and hippocampus (Fig. 4.2C, D). Taken together, these findings are consistent with the idea that disrupted posterior DMN node effective connectivity is, to some extent, mediated by impaired thalamo-cortical white matter circuitry.

## Methodological considerations

Some limitations should be noted. The major weakness of the paper is that each thalamic nucleus has specific cortical connections and functions, yet the present analysis uses a holo-thalamic approach. It would be more informative to determine whether sub-nuclei show differential causal interactions between specific regions of thalamus and crucial DMN nodes and likewise, whether these connections show varying degrees of structural impairment. Such an approach would reveal the specificity of AD pathology for individual thalamic nuclei. Analysing the entire thalamus may dilute

these results. Our findings should therefore be considered as preliminary evidence warranting further investigation. It should also be noted that the indirect relationship between fMRI BOLD signal and the underlying neural mechanism is especially problematic when applying GC and should be noted as a weakness in the present study. Firstly, the study's sampling rate (repetition time or TR) of two seconds is considerably slower than the millisecond temporal resolution of the neuronal activity we seek to qualify. Secondly, the temporal precedence assumptions of GC can be violated by regional differences in the latency of the hemodynamic response (Handwerker et al., 2004; Friston, 2011). Since neurovascular coupling can be altered in complex ways by disease, the likelihood of such an event is magnified in the aMCI patient cohort (Handwerker et al., 2012). One typical scenario, is that region X causally influences Y at the neuronal level but has a longer time-to-peak in its HRF due to pathology of the neurovasculature. Thus, GC analysis of BOLD signal may incorrectly suggest that Y is causally implicated in causing X. Simulations show that GC performs well when the HRF delay between regions is short (Deshpande et al., 2010; Schippers et al., 2011) however sufficiently fast sampling, on par with the neuronal delays themselves, is required to ensure GC is fully invariant to HRF latency (Seth et al., 2013). Other simulations suggest that the relationship between GC at the neuronal level and GC at the fMRI level is reasonably preserved over a range of sampling rates and convolution parameters (Wen et al., 2013). Whatever the case, sub-second temporal resolutions have been made available (Feinberg et al., 2010; Feinberg and Yacoub, 2012) and are standard as part of the Human Connectome Project (Van Essen et al., 2013). The most recent advances enable a temporal resolution as fast as 50 ms (Boyacioglu and Barth, 2013).

Critically, GC makes no claims regarding the underlying physical mechanisms responsible for the observed differences in causal relationships between regions. In contrast, the DCM approach (Di and Biswal, 2014*a*) explicitly specifies dynamic effective relationships at the neuronal level, allowing the most likely structural model for generating the observed data to be identified. Applying DCM in future studies will help clarify thalamic

involvement in posterior DMN dysfunction. The choice of CSD-based tractography reflects the growing recognition that assumptions underlying the DTI model may not always be met in practice (Wheeler-Kingshott and Cercignani, 2009; Jones and Cercignani, 2010; Jones, 2010). The DTI model can only capture a unitary fibre direction within a single voxel despite observations that ninety percent of the brain is composed of multiple crossing fibres (Jeurissen et al., 2013). For this reason CSD attempts to map several fibre directions per voxel by taking advantage of the high number of diffusion encoding directions and large b-values acquired using the HARDI acquisition protocol (Tournier et al., 2007, 2008; Mielke et al., 2012; Farquharson et al., 2013). Using large b-values has an additional advantage. By allowing a sufficiently long diffusion path to be measured water molecules are more likely to collide with their container. This may be relevant in patients with neurodegenerative disorders who have increased permeability of membranes, greater extracellular space due to axonal atrophy, demyelination and glial pathology (Acosta-Cabronero and Nestor, 2014). To date, only a handful of tractography studies have utilised HARDI data and large b-values (de Schotten et al., 2011; Meng et al., 2013; Yeatman et al., 2014; Xie et al., 2015) and only one specifically in clinical aMCI and AD (Kehoe et al., 2015). The absence of indirect biomarkers of AD pathology (CSF biomarkers and/or amyloid PET imaging) should also be acknowledged as a weakness in the present paper.

## 5.9 Conclusion

The dynamic nature of thalamo-cortical dialogue suggests that abnormalities in DMN operation may best be understood from the perspective of thalamic dysfunction. The present study employed diffusion imaging and effective connectivity to clarify the relationship between the physical integrity of thalamic white matter projections and the activity of the DMN. Significant changes in the diffusivity metrics of thalamic white matter projection tracts to hippocampus, PCC and IPL (Fig. 5.2B, C, D) were identified. Effective connectivity changes corresponding to the same regions were

also observed (Fig. 5.2A). Interestingly, no structural deficits were found between DMN nodes suggesting that early changes in DMN activity could be a result of impaired thalamo-cortical structural integrity. Such a conclusion is supported by previous resting state MEG (Garcés et al., 2014), EEG (Schreckenberger et al., 2004; Garcés et al., 2013; Moretti, 2015), and fMRI (Greicius et al., 2004; Sorg et al., 2007; Damoiseaux et al., 2012) studies citing disruption in posterior thalamo-cortical alpha sources. Significant evidence suggests that thalamo-cortical circuitry underlies the generation and modulation of alpha and theta rhythms and that average power is attenuated in these frequency bands for MCI and AD subjects (Jeong, 2004; Koenig et al., 2005; Jelles et al., 2008; Park et al., 2008). Several recent modelling studies have proposed a candidate mechanism citing impairment to thalamic reticular fibres in MCI and AD as the source of the dysfunction (Bhattacharya et al., 2011, 2013; Li et al., 2011; Abuhassan et al., 2012, 2014). A corollary of this discussion is the extent to which cortical activity is dependent on cortico-cortical verses thalamo-cortical connections. It has been suggested that thalamic nuclei have a role in coordinating distributed cortical regions through cortico-thalamo-cortical pathways. Abnormalities originating in thalamic to PCC and IPL white matter may therefore be sufficient to engender posterior DMN dysfunction without appealing to comparable deficits in cortico-cortical tracts between DMN nodes. Such a view is consistent with the anatomy and timeline of pathogenesis with thalamic nuclei demonstrating pathology at an earlier stage of the disease than the cortex. Cortical atrophy may therefore be in response to thalamic white matter disruption with commensurate causal abnormalities occurring in response to changes in thalamo-cortical signalling rather than being instigated by structural changes within the cortex. Importantly, the present study is unable to confirm this hypothesis. Other scenarios, in which cortical pathology is causing a degeneration of thalamo-cortical tracts is also possible or likewise, a parallel disruption in both thalamus and cortex.

Overall, these results provide a compelling and previously unexplored physical basis for posterior DMN dysfunction and abnormal fMRI task-induced deactivation response patterns in aMCI and AD patients and un-

derscore the need to consider neurodegenerative changes within a wider system context involving both cortical and subcortical thalamic components. The present work complements a growing body of evidence that suggests effective connectivity is disrupted in neurodegenerative disorders such as aMCI and AD and that these changes are underpinned by structural deficits. For these reasons, joint effective and structural studies will play an increasingly important role in the future as we seek to understand how pathological changes in structural connectivity are reflected in altered network effective connectivity.

The previous two chapters have demonstrated: (1) the importance of meta- stable neural dynamics in general cognition and (2) the link between structural disconnection and impaired cognitive ability. The next chapter productively builds upon these observations to explore how metastable dynamics emerges from the static connections of the structural connectome and how metastable dynamics is informed by the brain's structural topology. An important next step in our understanding is to mechanistically link metastability to the structural integrity of the anatomical connectome. To this end, the following chapter builds and validates theoretical computer models based on the brain's macroscopic pattern of structural connectivity.

# 6 Metastable neural dynamics in Alzheimer's disease are disrupted by lesions to the structural connectome

## 6.1 Overview

Current theory suggests that brain regions interact to reconcile the competing demands of integration and segregation by leveraging metastable dynamics. An emerging consensus recognises the importance of metastability in healthy neural dynamics where the transition between network states over time is dependent upon the structural connectivity between brain regions. In AD – the most common form of dementia – these couplings are progressively weakened, metastability of neural dynamics are reduced and cognitive ability is impaired. Accordingly, this chapter uses a joint empirical and computational approach to examine how behaviourally relevant changes in neural metastability are contingent on the structural integrity of the anatomical connectome. Crucially, the empirical metastability of fMRI BOLD signal was found to be predictive of cognitive performance across the three cohorts: HC, MCI, and AD. Moreover, the effects of structural disconnection on synchrony versus metastability were dissociable. Finally, using whole-brain computer modelling, empirical decreases in metastability were mechanistically linked to the topological integrity of the structural connectome. Overall, the results of the joint computational and empiri-

cal analysis suggest an important causal relationship between metastable neural dynamics, cognition, and the structural efficiency of the anatomical connectome[1].

## 6.2 Introduction

Duality lies at the origin of many branches of science and philosophy wherein seemingly opposite forces interact to form a dynamic system in which the whole is greater than the sum of its assembled parts (Kelso, 1995). Rather than viewing apparently contrary phenomena as irreconcilable features of the world, the 'philosophy of complementary pairs' recognises their mutually related nature while simultaneously honouring their differences (Kelso and Engstrom, 2006; Engstrøm and Kelso, 2008). One such 'complementary pair' may be found in the dialogue between synchrony and asynchrony in the brain – a reflection of the growing consensus that the complementary nature of integrating and segregating tendencies is an essential feature of how brains operate (Bressler and Kelso, 2001, 2016). Accordingly, several developmental, traumatic, and neurodegenerative conditions could be described as an imbalance in the optimal working point of synchrony and asynchrony (Uhlhaas and Singer, 2006; Uhlhaas, 2015). Epilepsy, for example, could be described in terms of excess neural order – synchrony has become a tyrant. Conversely, several neuropsychiatric conditions, in which the structure of the brain is abnormal e.g. schizophrenia, autism, and AD are defined by an excess of neural disorder or asynchrony.

Recently, these observations have been placed on firm empirical and theoretical ground by appealing to a dynamical regime known as metastability (Kelso, 1995; Tognoli and Kelso, 2009, 2014*b*,*a*; Kelso, 2012), in which the tendency for local regions to express their independence is balanced with the requirement to integrate and coordinate information globally (Deco et al., 2015). The advent of DTI has permitted these observations to be tested *in-silico* (Deco, Ponce-Alvarez, Hagmann, Romani, Mantini and Corbetta,

[1] (Alderson et al., 2018)

2014). Here, networks of oscillators interact on a backbone of inferred inter-regional white matter known as the structural connectome (Ghosh et al., 2008*b*; Deco et al., 2009; Deco, Jirsa and McIntosh, 2013; Deco, Ponce-Alvarez, Mantini, Romani, Hagmann and Corbetta, 2013; Honey et al., 2010; Deco and Jirsa, 2012; Cabral et al., 2014; Breakspear, 2017). In this way, connectomic-based computer modelling permits an analysis of the structural connectivity's role in shaping the brain's functional architecture. The relationship between the connectome's structural integrity and metastable neural dynamics has previously been investigated in a model of traumatic brain injury (Hellyer et al., 2015). In this work, Hellyer et al. (2015) observed that decreases in neural metastability were behaviourally relevant and linked to damage within the connectome. In other work, Váša et al. (2015) appraised the impact of removing individual nodes on metastability in a systematic manner.

The relationship between structure and function is also altered in AD. AD presents as a steadily worsening constellation of symptoms that mirror the gradual accumulation of misfolded amyloid protein and neurofibrillary tangles. Accordingly, patients are situated on a continuum of phenotypes related to cognitive status ranging from mild memory loss in MCI through to advanced cognitive and behavioural deficits in overt AD. The transition between diagnostic categories is marked by a reliable asymptotic decline in overall neural metastability that conforms to the pathophysiological staging of the disease (Córdova-Palomera et al., 2017; Demirtaş et al., 2017).

In light of the foregoing, the present paper utilises a dual empirical and computational approach to investigate the relationship between topological properties of the structural connectome, metastable neural dynamics, and cognitive performance in HC subjects and in patients from across the AD spectrum. For this reason, resting state functional and structural neuroimaging data were obtained from the Alzheimer's Disease Neuroimaging Initiative (ADNI) (Mueller et al., 2005) in three subject groups including HC, MCI, and AD. The inclusion of resting state or task-free fMRI into the functional imaging suite has been especially advantageous to dementia researchers where subject compliance can be an issue – here subjects are

simply required to lie down and stay awake. In the absence of an assigned task, the ultra-low frequency ($< 0.1$HZ) BOLD signal demonstrates several distinct patterns of covariance across the cortex known as resting state networks (Damoiseaux et al., 2006). Several neurodegenerative disorders including AD (Buckner et al., 2008) show dissociable patterns of abnormal structure and function in these networks consistent with a disconnection syndrome (Seeley et al., 2009). Converging lines of evidence from experimental neuropathology (Braak and Braak, 1991*b*), neuroimaging (Greicius et al., 2004; Buckner et al., 2005), and transgenic animal studies (Palop and Mucke, 2010) support the contention that AD, in part, represents a disconnection syndrome. Indeed, recent empirical findings emphasise the importance of early inter-areal white matter connectivity in AD pathogenesis (O'Dwyer et al., 2011*a*,*b*) and challenge the conventional view that AD solely represents a disease of the grey matter (Sachdev et al., 2013). Contemporary observations suggest that: (1) white matter abnormalities occur while grey matter is still relatively preserved (Brun and Englund, 1986; de la Monte, 1989; Heise et al., 2010; Zhuang et al., 2012); (2) that demyelination and axonal abnormalities occur before the formation of amyloid plaque and neurofibrillary tangles (Desai et al., 2009, 2010); and (3) that impaired axonal transport not only precedes the downstream production of grey matter amyloid but actively participates in its formation (Wirths et al., 2006, 2007; Smith et al., 2007).

The study is structured as follows. Firstly, the global neural metastability of fMRI BOLD signal is estimated in resting state networks across the three subject populations (HC/MCI/AD). Secondly, the impact of macroscopic structural disconnection on large-scale neural metastability is evaluated using whole-brain computer modelling. Thirdly, the relationship between local network topology in the healthy connectome and the distribution of damage between nodes of the computer model is explored. Fourthly, this study examines how damage to the large-scale structural topology of the connectome relates to the metastability of the simulated neural dynamic. Fifthly, differences in synchrony and metastability of fMRI BOLD signal in patients and controls are investigated using the network based statistic

(NBS). Finally, it is ascertained if the empirical estimates of brain-wide neural metastability are linked to cognitive ability.

By virtue of these steps, it was found that: (1) macroscopic damage to the structural connectome elicited comparable reductions in simulated metastability to that observed in the empirical data; (2) damage to the computer model's connectivity was centred around highly connected nodes; (3) reductions in simulated neural metastability were the product of abnormal network topology; (4) widespread decreases in metastability between empirical resting state networks in AD subjects contrasted sharply with more focal decreases in synchrony; and (5) reductions in large-scale metastability of fMRI BOLD signal correlated with cognitive test scores across the AD spectrum. Overall, the results of our joint computational modelling and empirical analysis suggest a key linkage between metastable neural dynamics, cognition and the structural integrity of the human brain.

## 6.3 Methods

### Data overview

Data were obtained from the ADNI database (http://adni.loni.usc.edu). In the present study, baseline visit data collected from HC, MCI, and AD subjects who were recruited for ADNI-2 is examined. All subjects and their study partners completed the informed consent process, and the study protocols were reviewed and approved by the Institutional Review Board at each ADNI data collection site. The ADNI was launched in 2003 by the National Institute on Aging, the National Institute of Biomedical Imaging and Bioengineering, the Food and Drug Administration, private pharmaceutical companies and non-profit organizations as a public-private partnership. The primary goal of ADNI has been to test whether neuroimaging, fluid and genetic biomarkers, and cognitive assessments can be combined to measure the progression of MCI and early AD. Additional information is available at www.adni-info.org.

## Subjects

All ADNI participants underwent a 'screening' visit, during which they completed the Mini-Mental State Examination (MMSE) (Folstein et al., 1975), Clinical Dementia Rating (CDR) (Hughes et al., 1982) scale, and the Wechsler Memory Scale-Revised (WMS-R) (Wechsler, 1987) Logical Memory II test. Three cohorts composed of 36 HC, 33 MCI, and 34 AD were included in the fMRI study and 30 in each group were included in the DTI study. Since ADNI currently does not collect multi-modal DTI/fMRI imaging data for the same subjects, the DTI and fMRI cohorts comprised different individuals. For this reason, this study is unable to directly compare structural and functional data at the subject-level and instead compares participants at the group-level. This is justifed by appealing to the stereotypical spatio-temporal staging of neuropathology (Braak and Braak, 1991*b*; Braak et al., 1999) and biomarkers (Jack et al., 2013) across individuals. The detailed criteria used to define the three groups (HC/MCI/AD) are provided as information in the appendices (see section 8.2) along with full participant demographics (also see sections 8.3 and 8.4).

## MRI data acquisition

Standard protocols were used to acquire functional, structural, and diffusion tensor image data. Whole-brain structural and functional data were acquired on a 3.0 Tesla Philips Intera MR system (Philips, Best, Netherlands) equipped with an eight channel head coil and sensitivity encoding (SENSE) with a reduction factor of one. A high-resolution anatomical T1-weighted sagittal 3D MP-RAGE image was acquired with the following parameters: 1 x 1 mm2 in-plane resolution, 1.2 mm slice thickness, TR = 6.8 ms, TE = 3.2 ms, flip angle = $9^{o}$, 256 x 240 mm FOV, and 256 x 240 matrix. Resting-state fMRI data were also acquired. Subjects were instructed to keep their eyes open during the scan and fixate on a cross hair in the centre of a screen located behind the MR scanner, visible via a mirror. Each volume of data covered the entire brain with 48 slices, and the slices were acquired in interleaved sequence from inferior to superior di-

rection. One hundred and forty volumes were acquired. The BOLD signal changes were measured using a T2*-weighted echo-planar imaging sequence with the following parameters: 3.3 x 3.3 mm2 in-plane resolution, 3.3 mm slice thickness, TR = 3000 ms, TE = 30 ms, flip angle = 80º, 212 x 198.75 mm2 FOV, and 64 x 59 matrix.

Likewise, whole-brain structural and diffusion tensor data were acquired on a 3.0 Tesla General Electric Signa HDxt MR system (General Electric Medical Systems, Milwaukee, WI, USA) equipped with an 8HRBRAIN head coil. A high-resolution anatomical T1-weighted sagittal 3D IR-SPGR image was acquired with the following parameters: 1 x 1 mm2 in-plane resolution, 1.2 mm slice thickness, TR = 7 ms, TE = 2.85 ms, flip angle = 11º, 256 x 240 mm FOV, and 256 x 240 matrix. Single-shot spin echo-planar imaging was used to acquire the diffusion weighted image data with following parameters: 2.7 x 2.7 mm2 in-plane resolution and 2.7 mm slice thickness, TR = 13000 ms, TE = 68.4 ms, flip angle = 90º, 350 mm FOV, and 129 x 129 matrix. Diffusion gradients were applied in 41 isotropically distributed orientations with b = 1000 s/mm2, and five images with b = 0 s/mm2.

## Overview of MRI data analysis

The processing steps approximated the procedures outlined in the automated personalised processing pipeline (Schirner et al., 2015) and comprised (1) pre-processing of anatomical T1-weighted images, cortical reconstruction, tessellation and parcellation into 148 3D volume masks; (2) transformation of anatomical masks to fMRI space; (3) processing of fMRI data and extraction of mean BOLD signal from each 3D volume mask for calculating pairwise phase relations; (4) transformation of anatomical masks to diffusion space; (5) processing of diffusion weighted data and tractography between pairwise 3D volume masks to derive structural connectivity and mean FA matrices. FA corresponds to the primary direction of water molecule diffusion within a tract. An overview of the steps are provided in Figure 6.1.

The above workflow was employed to: (1) estimate the average struc-

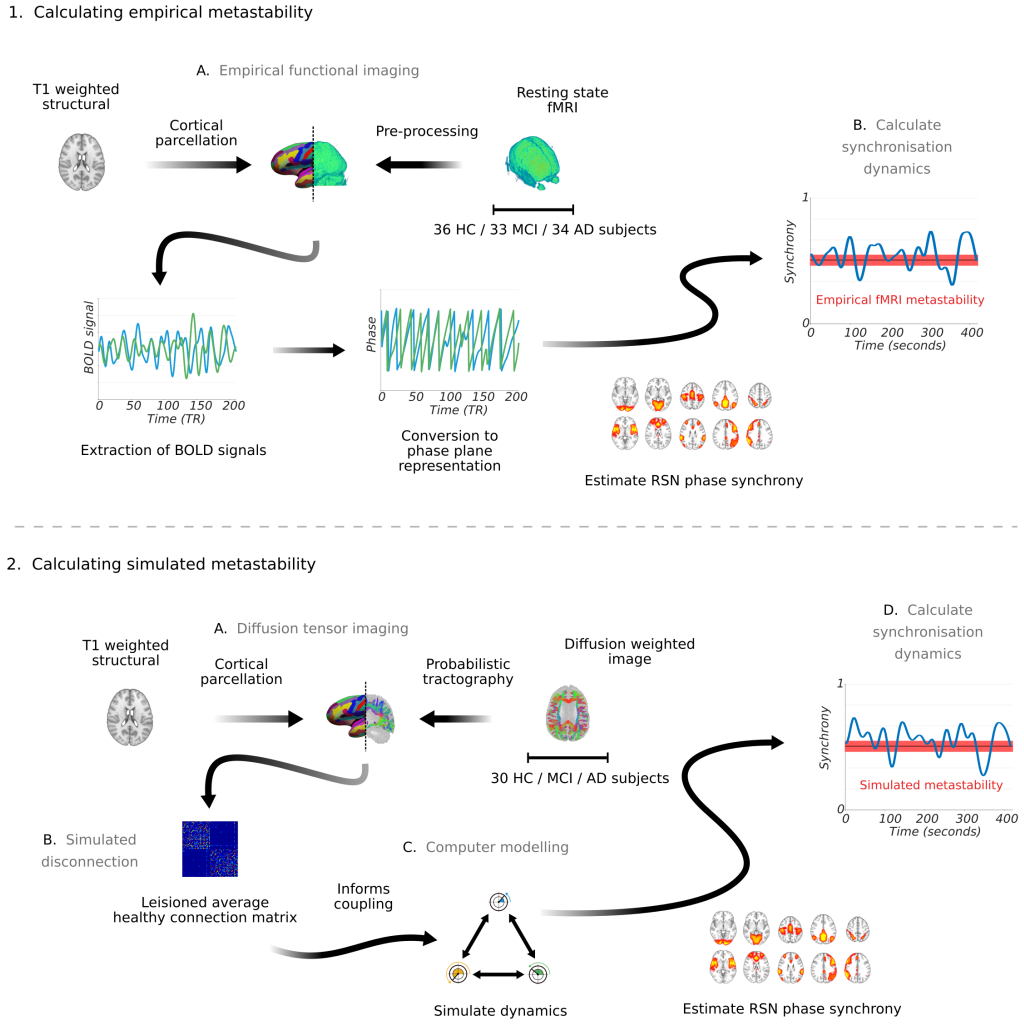


Figure 6.1: Overview of experimental design. Resting state fMRI BOLD signal was used to calculate empirical metastability across three groups including HC, MCI, and AD (top). 1.A, Each subject's T1-weighted structural image was parcellated into 148 regions from which average BOLD signal was extracted. Time series were then converted into complex phase plane representation using the Hilbert transform. 1.B, Estimates of resting state network metastability were then calculated. DTI data across the same three groups were used to inform the coupling strength between nodes in a simple oscillator model (bottom). 2.A, A subject's T1-weighted image was parcellated into 148 distinct regions which were subsequently used to constrain tractography. 2.B, Individual connectivity matrices were created for each clinical subject by lesioning the average control connectivity in tracts that significantly deviated from healthy control values. 2.C, Subject-level whole-brain computer models were constructed with coupling informed by the anatomical data. 2.D, Simulated phase output was subsequently used to estimate resting state network metastability.

tural connectivity of controls based on DTI track fibre density i.e. the healthy template and (2) estimate individual FA matrices for each MCI and AD subject. Subject-level connectomes were derived by lesioning the healthy template using each clinical subject's FA matrix (see: Generating subject-level structural connectivity). The resulting matrices then informed coupling strength between nodes in a simple oscillator model (see: Constructing the cortical network model).

## Anatomical MRI data analysis

The Freesurfer image analysis suite (http://surfer.nmr.mgh.harvard.edu) performed cortical reconstruction and volumetric segmentation based on the high resolution T1 weighted images. Briefly, these steps included motion correction (Reuter et al., 2010); intensity normalisation (Sled et al., 1998), skull stripping; removal of non-brain tissue, brain mask generation, cortical reconstruction, white matter and sub-cortical segmentation (Fischl et al., 2002; Fischl, Van Der Kouwe, Destrieux, Halgren, Ségonne, Salat, Busa, Seidman, Goldstein, Kennedy, Caviness, Makris, Rosen and Dale, 2004), cortical tessellation Fischl et al. (2001); Ségonne et al. (2007) generating grey-white matter interface surface-triangulations, and probabilistic atlas based cortical parcellation (Fischl, Salat, Van Der Kouwe, Makris, Ségonne, Quinn and Dale, 2004; Desikan et al., 2006) using the 2009 Destrieux atlas producing a cortical parcellation with 148 independent sulcal and gyral regions.

## Empirical DTI data analysis and tractography

Pre-processing of the diffusion MRI data included eddy current and motion correction with re-orientation of b-vectors. The b-zero image was linearly registered to the subject's anatomical T1-weighted image; the resulting transformation rule was stored for later use (see: Empirical fMRI data analysis).

Tractography was constrained by seed, target and stop masks. Masks were transformed from individual anatomical to individual diffusion space.

The grey-white matter interface surface triangulation was dilated into a 3D volume, labelled to match the adjacent cortical parcellation and split into 148 separate masks for use as seed and target regions. Tracks exiting the union of grey-white matter interface and cortical white matter were regarded as spurious and terminated. Registrations were performed using the FSL (FMRIB's Software Library, www.fmrib.ox.ac.uk/fsl) software package tool FLIRT (Jenkinson and Smith, 2001; Jenkinson et al., 2002; Greve and Fischl, 2009) and FNIRTs (Andersson et al., 2007).

Probabilistic white matter tractography was performed on the diffusion weighted images using the MRtrix3 software package (http://www.mrtrix.org). Crossing fibres were resolved using the CSD algorithm (Tournier et al., 2004, 2012). MRtrix3 pre-processing included computing the diffusion tensor images (or diffusion ellipsoids) for each voxel from which FA images were subsequently generated. To exclude noise, these were masked by the binary white matter parcellation created previously. Tracks were initiated from randomly distributed seed points within each voxel of the seed mask. Tracks successfully propagating from seed $i$ to target mask $j$ defined a connectivity matrix $C(i,j)$ of size $C_{148x148}$).

To mitigate bias associated with using seed and target masks of different sizes, tractography was performed in both directions; from seed to target mask $C(i,j)$ and from target to seed mask $C(j,i)$ with each set of tracks being consolidated into a single entry. The seed mask voxel and corresponding target mask voxel were identified and recorded for each track. To address the uncertainty surrounding the relationship between the number of tracks generated for a given pathway and the synaptic strength of that pathway, only distinct connections between seed and target voxels contributed toward overall track count. Track counts were subsequently converted into track density by dividing total track count between region $i$ and $j$ region by total seed and target mask volume and normalising between zero and one. Finally, the mean FA of each fibre bundle was recorded in matrix $FA(i,j)$ of size $FA_{148x148}$.

## Empirical fMRI data analysis

Excessive peaks in the resting state fMRI time series were first removed using AFNI's (https://afni.nimh.nih.gov/afni) *3dDespike* script. Functional connectivity matrices for each subject were then extracted using the FSL software package. Registration to high resolution structural and standard space images was performed using FLIRT and FNIRT respectively. FMRI data processing was carried out using FEAT (FMRI Expert Analysis Tool) Version 6.00. The following pre-statistics processing was applied: motion correction using MCFLIRT, slice-timing correction using Fourier-space time-series phase-shifting, non-brain removal using BET, spatial smoothing using a Gaussian kernel of FWHM 3.0mm, and grand-mean intensity normalisation of the entire 4D dataset by a single multiplicative factor. The first five image volumes were deleted to exclude possible T1-related saturation effects. The Freesurfer cortical parcellation was transformed to functional space by inverting the functional to T1 structural image transformation rule acquired earlier as part of the diffusion MRI preprocessing pipeline. To account for non-neural sources of physiological noise and head movement, the signals from white matter, cerebrospinal fluid and the six motion parameter time courses estimated by MCFLIRT were regressed out of the functional time series. The empirical BOLD signals were band-passed filtered in the functionally relevant 0.04–0.07Hz narrowband range to avoid including artefactual correlations and obtain meaningful signal phases (Glerean et al., 2012). Finally, the mean BOLD signal was extracted from each region in the T1-derived cortical parcellation. An overview of the steps are provided in Figure 6.1.

## Defining resting state networks from functional imaging data

ICA was used to separate the cortical resting state BOLD signals of the controls into independent components using FSL MELODIC. The optimal decomposition yielded fifteen components each representing a putative resting state network. The correlation of these components with the canonical

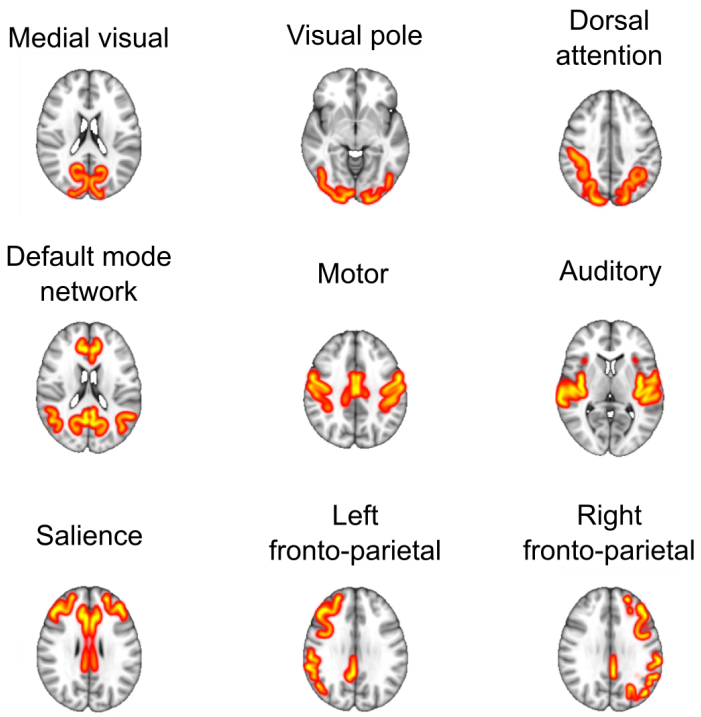


Figure 6.2: Nine canonical resting state networks reconstructed in MNI 152 space according to the 148 region's of the Destrieux atlas with a 3mm isotropic Gaussian blur. The resting state fMRI data of 36 control subjects was decomposed into fifteen independent components nine of which resembled canonical resting state networks (Smith and Nichols, 2009). These nine were subsequently projected into the same space as the Destrieux atlas. Regions exhibiting a mean z-score $> 2.3$ ($p < 0.01$) were entered into that network.

networks identified by Smith and Nichols (2009) yielded nine behaviourally relevant resting state networks. These included regions associated with medial visual, occipital pole, dorsal attention, default mode, motor, auditory, salience, and fronto-parietal areas.

The nine independent components were subsequently projected onto the 148 regions of interest from the Destrieux atlas (Hellyer et al., 2014). A region was classified as belonging to a particular resting state network if its mean z-score was greater than 2.3 ($p < 0.01$). In detail, the z-scores contained within a given region's voxels were summed and divided by the

total number of voxels in that region. If the mean z-score exceeded 2.3 ($p < 0.01$) that region was included in the resting state network. Figure 6.2 shows the nine canonical resting state networks reconstructed in MNI 152 space according to the 148 regions of the Destrieux atlas with a 3mm isotropic Gaussian blur.

## Calculating resting state network metastability

Mean BOLD signals were subsequently transformed into complex phase representation via Hilbert transform. The first and last ten time points were removed to minimise border effects (Ponce-Alvarez et al., 2015). Oscillator phases were similarly extracted from the cortical network model. The Kuramoto order parameter (a measure of instantaneous synchronisation) (Strogatz, 2000; Acebrón et al., 2005) was estimated for (1), the set of regions comprising single resting state network and (2), when evaluating their interactions, the set of regions comprising two resting state networks, as:

$$R_{RSN}(t) = \frac{1}{N} \sum_{k=1}^{N} e^{i\theta_k(t)}$$

where $k = 1,...,N$ is region number and $\theta_k(t)$ is the instantaneous phase of oscillator $k$ at time $t$. Under complete independence, all phases are uniformly distributed and $R_{RSN}$ approaches zero. Conversely, if all phases are equally distributed, $R_{RSN}$ approaches one and full synchrony. Global metastability was calculated using all 148 cortical regions. The maintenance of a particular communication channel through coherence implies a persistent phase relationship. The number or repertoire of such channels therefore corresponds to the variability of these phase relationships (i.e. the metastability) measured as the standard deviation of $R_{RSN}$ (Kringelbach et al., 2015; Deco and Kringelbach, 2016).

## Assessing connectivity changes between empirical resting state networks

Given that (1), the current formulation of metastability only permits calculation between a set of regions, and (2), that inter-connected subnetworks convey more behaviourally relevant information than single pairs of functional connectivity observed in isolation (Smith and Nichols, 2009), this study argues that an approach which exploits the clustering structure of connectivity alterations between functionally related networks may offer the optimal outcome in assessing connectivity changes between empirical resting state networks. Accordingly, the NBS is applied to measures of synchrony and metastability estimated from empirical fMRI data at the network rather than regional level.

The NBS is a non-parametric statistical test designed to deal with the multiple comparisons problem on a graph by identifying the largest connected sub-component (either increases or decreases) in topological space while controlling the family wise error rate (FWER). To date, several studies have used the method to identify pairwise regional connections that are associated with either an experimental effect or between-group difference in functional connectivity (Zalesky et al., 2010).

The present paper adopts a related but slightly different approach. Rather than applying the NBS to a matrix of pairwise regional correlations, the NBS is applied to measures of synchrony and metastability evaluated at the resting state network level. Accordingly, pairwise interactions between all nine resting state networks were evaluated using the approach described above. In the case of synchrony, the NBS is applied to 36 9x9 symmetric matrices derived from healthy controls and 34 9x9 symmetric matrices derived from subjects with AD. Of the matrices, each row/column represented an interaction between a resting state network and eight others. The same procedure is performed in the case of metastability. The mean synchrony and metastability of each group's interaction matrix is reported in the appendices (Figs. 8.2 and 8.3).

First mass univariate testing is used to test the hypothesis of interest

at every connection in the graph. Each connection is provided with a single test statistic capturing the evidence in favour of the null hypothesis, that is, there is no significant difference in the means of the two diagnostic groups (HC vs. MCI, HC vs. AD). Second, the test statistic is thresholded at an arbitrary value. The set of connections exceeding this threshold are admitted into a set of supra-threshold connections representing potential candidates for which the null hypothesis can be rejected. The third step is to identify topological clusters among the supra-threshold connections for which a connected path can be found between any two nodes. It is important to note that clustering is not in physical space, rather the NBS clusters in topological space where a cluster corresponds to a connected graph component. The null hypothesis is therefore rejected or confirmed at the level of the whole structure rather than at the level of individual connections. The final step is to compute a FWER-corrected p-value for each component using permutation testing. For each permutation, the above three steps are repeated to construct an empirical null distribution of the largest connected component size. The FWER-corrected p-value for a component of a given size is estimated as the proportion of permutations for which the largest component was of the same size or greater. The size of a component can be measured in two ways: (1) as the total number of connections or extent of that component or (2) as the sum of the test statistic values across all connections, namely, the intensity of that component. Extent is appropriate for detecting relatively weak effects that extend to encompass many connections while intensity is more suitable for detecting strong, focal effects confined to a limited number of connections. The minimal threshold revealing the largest disconnected sub-component in the network was selected.

## Generating subject-level structural connectivity

The derivation of structural connectivity relied on changes in FA which are more closely linked to axonal degeneration and demyelination (Aung et al., 2013; Teipel et al., 2014) than track count, which lacks a clear biological in-

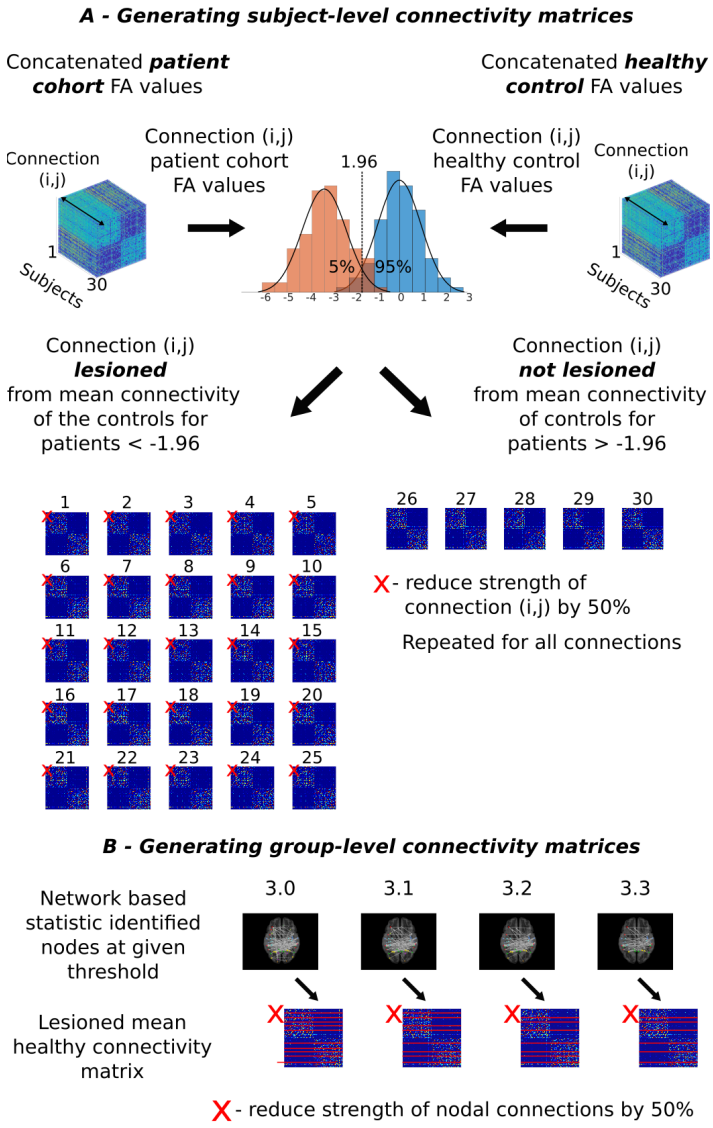


Figure 6.3: Estimation of subject-level structural disconnection in diagnostic groups (MCI/AD). A. Subject-level connectivity matrices were derived by lesioning the average control network or 'healthy template' in locations where tracts demonstrated unusually low FA. The FA value for a single tract was extracted from all 30 controls to form a normal distribution with characteristic mean and standard deviation (blue). The same procedure in the patient cohort yielded a second normal distribution with a mean offset from the first (orange). Patients with tracts displaying FA values less than -1.96 standard deviations from the mean of the controls ($p < 0.05$; uncorrected) were considered damaged and lesioned from the average structural network of the controls, the strength of these connections being weakened by 50%. Repeating the procedure for all tracts yielded 30 subject-level connectivity matrices per diagnostic group (MCI/AD). B, Group-level structural connectivity matrices (MCI/AD) were derived for different values of the network based statistic threshold. Nodes forming part of significantly disconnected FA sub-components were considered damaged and lesioned from the average control network or 'healthy template', the strength of these connections being weakened by 50

terpretation. Figure 6.3.A shows the procedure for generating subject-level connectivity matrices. Tracts demonstrating significantly lower FA than controls ($p < 0.05$; uncorrected) were lesioned from the healthy template i.e. the average structural connectivity of controls. This corresponded to a 5% probability that a control subject would exhibit an FA value this low. Since total denervation was unlikely, the strength of coupling was weakened by 50% with values ranging from 25-75% producing comparable results.

In detail, FA values $FA(i,j)$ of tracks running between pairwise regions $i$ and $j$ were concatenated for all 30 controls to form a 3D matrix $HC(i,j,k)$ of size $HC_{148x148x30}$. The same procedure was performed for the two patient cohorts to form $MCI(i,j,k)$ and $AD(i,j,k)$ . The mean and standard deviation of the resulting normal distribution for $HC(i,j,*)$ was then used to convert FA values in the corresponding pairwise regions $i$ and $j$ of $MCI(i,j,*)$, and $AD(i,j,*)$ into z-values.

Comparison between the normal distribution of FA values for the tract $(i,j)$ in the control population and the normal distribution of FA values for the tract $(i,j)$ in the patient population was then possible. Patients were assigned their own copy of the healthy template prior to lesioning. Patients whose FA value was less than -1.96 standard deviations from the mean of the control FA distribution (corresponding to $p < 0.05$; uncorrected) had their tracts lesioned from the healthy template. The process was repeated for all tracts to produce 30 subject-level connectivity matrices in each patient cohort (MCI/AD).

## Building a consensus distribution of structural lesions

The presence or absence of a lesioned tract was recorded in a binary matrix for each clinical subject. The summation of matrices within a diagnostic grouping yielded a single consensus distribution of lesioned tracts for all subjects where each index corresponded to the total number of subjects with a lesioned tract at that location. Summing each row provided a regional measure corresponding to the total number of lesions in the connectivity of that region. Figure 6.4 shows this metric normalised between zero and

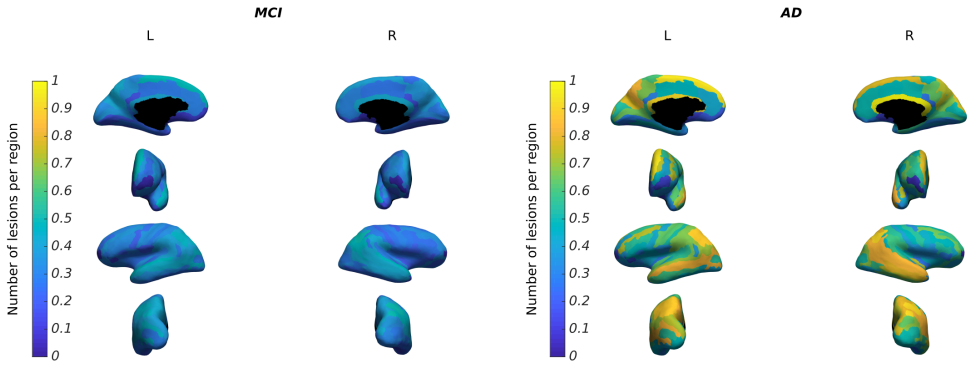


Figure 6.4: Total number of lesions pertaining to each region of the Destrieux cortical atlas in MCI (left) and AD cohorts (right), where blue indicates zero lesions and yellow the highest number recorded (normalised between zero and one). In both diagnostic groups, the majority of lesions concentrated in the default mode network. Notice however the relative difference in magnitude between the two groups.

one plotted on the inflated cortical surface of the Destrieux atlas where dark blue corresponds to zero lesions and yellow to the highest number recorded. The purpose of the consensus distribution was three-fold: (1) to demonstrate how lesions were distributed on the cortical surface; (2) to determine which features of nodal topology were most associated with damage; and (3) to evaluate the distribution of lesions within the rich-club i.e. a network of high degree nodes that are more connected to each other than expected by chance (van den Heuvel and Sporns, 2011).

## Generating group-level structural connectivity

Since networks grow or shrink in size depending on the choice of NBS threshold (note however the FWER is always controlled regardless of the choice of threshold) this study employs a model-based fitting approach to determine the most likely structural skeleton (and hence threshold) responsible for generating the observed dynamic. In this scenario, the NBS is used to guide the lesioning process. The resulting structure is used to inform coupling in the cortical network model. Firstly, the NBS identifies

the largest disconnected sub-component in the FA matrix of the diagnostic group at a particular threshold. Secondly, the identified nodes are lesioned from the healthy template by having the strength of their connections reduced by 50%. Finally, the simulated dynamic (measured as resting state network synchrony and metastability) is correlated with empirical estimates based on fMRI BOLD signal allowing the most probable structural skeleton and hence most appropriate choice of threshold to be inferred. A control was provided by lesioning the same number of random nodes from the healthy template. Figure 6.3.B shows the procedure for generating group-level (MCI/AD) structural connectivity information at different values of the NBS threshold.

## Constructing the cortical network model

The network model consisted of 148 nodes each described by a single Kuramoto phase oscillator (Kuramoto, 1984; Acebrón et al., 2005; Breakspear, 2017). Here, global synchronisation dynamics emerge through the reciprocal interaction of pairwise nodes coupled through the underlying anatomical structure. Despite its apparent simplicity, the Kuramoto model generates macroscopic dynamics comparable to significantly more complex spiking models at a significantly reduced computational cost (Messé et al., 2014). The phase $\theta(t)$ of each oscillator $i$ is governed by the equation:

$$\frac{d\theta_i}{dt} = \omega_i + \frac{1}{N}\sum_{j=1}^{N} K_{i,j}\sin(\theta_j - \theta_i - \rho) i = 1,...,N$$

where $\omega$ represents the oscillator's natural frequency i.e. the phase change of an uncoupled node per time step, $N$ the total number of connections made by the oscillator, $K_{i,j}$ the strength of coupling between oscillators $i$ and $j$, and $\rho$ a fixed phase lag. In this context, phase lag is used as a tuning parameter to match the simulated metastability to that of the empirical BOLD data while coupling $K_{i,j}$ is kept constant (see: Computational model validation and tuning). Collective synchronisation between a set of oscillators can be achieved by increasing the coupling strength

between the oscillating units, or by introducing a homogeneous distribution of frequencies between the oscillators. However, these strategies fail in the case where coupling between oscillators induces phase lags (Kundu et al., 2017). Such a scenario is common among many real-world systems (including the brain) where components take time to respond to their neighbouring oscillators. Under phase-frustration, the system indefinitely avoids synchronisation, even when frequencies are homogeneous and coupling is relatively strong. The phase lag parameter between oscillators can therefore be conceptualised as form of fixed time delay (Shanahan, 2010; Wildie and Shanahan, 2012). Metastable fluctuations in synchrony are only present for a critical range of the phase lag parameter. In this regime, integrative and segregative tendencies between oscillators are continually engaged but never fully reconciled.

The present paper simulates the BOLD signal directly using low frequency oscillators (Ponce-Alvarez et al., 2015). Such an approach should be distinguished from previous work where simulated electro-physiological signals (Hellyer et al., 2014, 2015; Váša et al., 2015) were transformed into BOLD signals using Balloon-Windkessel hemodynamics (Cabral et al., 2011; Cabral, Hugues, Kringelbach and Deco, 2012). Since the match between simulated and empirical functional connectivity is largely insensitive to the inclusion of hemodynamic effects (Messé et al., 2014), Balloon-Windkessel hemodynamics are not included here.

A noise term was not explicitly included in the model so as to emphasise the spontaneous metastable transitions between states and to preclude the possibility that noise driven fluctuations were driving the model between different stable attractors. The low variability in the simulated data (as compared to the empirical) reflects the lack of explicit noise in the model. Heterogeneity in the simulation arises from two sources (1) a heavy tail distribution of connections weights and (2) a distribution of intrinsic frequencies. The intrinsic frequencies are characterised as limit cycles randomly distributed in the low frequency 0.04–0.07 Hz range of empirical BOLD signal oscillation. The oscillator's intrinsic frequency $f_i$ and natural frequency $\omega_i$ are related through the equation $f_i = \frac{\omega_i}{2\pi}$. The model was

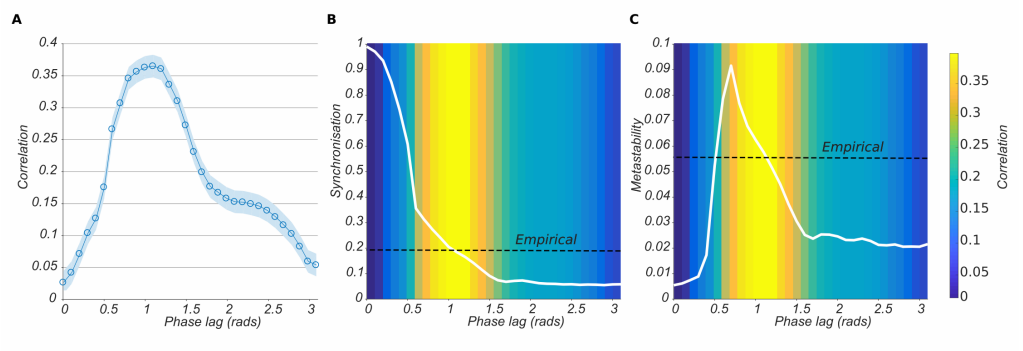


Figure 6.5: Model validation and tuning. A, Correlation between simulated and empirical functional connectivity for increasing value of phase lag parameter with 95% CI. B, Mean simulated global synchrony for increasing value of phase lag parameter with correlation overlaid for comparison. Correlation peaks where simulated synchronisation matches empirical synchronisation. C, Mean simulated global metastability for increasing value of phase lag parameter with correlation overlaid for comparison. Again, correlation peaks where simulated metastability matches empirical metastability.

numerically simulated in MATLAB 2016a (https://uk.mathworks.com) using the Runge-Kutta (RK4) integration scheme with a time step of 10 ms which has been shown to offer a good balance between accuracy and cost of computation. To ensure robust estimation of metastability and synchrony, the simulation is run for 1000 sec. with oscillator phase initialised randomly. The first 200 sec. of simulation time are discarded to remove initial transients.

## Tuning and validating the cortical network model

Since empirical metastability intersected the curve of simulated metastability at two points and was thus, mathematically speaking, not a well defined function i.e. there were multiple values of phase lag that produced the same value of metastability, it alone was insufficient to tune the model. Instead, model validation and tuning was performed by correlating the average functional connectivity of the empirical BOLD data of healthy subjects with the average functional connectivity of the simulated cortical model over several

runs at a given value of the phase lag parameter (Fig. 6.5.A). The value of phase lag producing the highest correlation ( 1.1 rads) between simulated and empirical functional connectivity corresponded to the regime where empirical and simulated data agreed with each other (Fig. 6.5.B, C) (Cabral et al., 2011; Cabral, Hugues, Kringelbach and Deco, 2012; Hellyer et al., 2014, 2015; Váša et al., 2015). Pearson's correlation coefficients were calculated on pairwise BOLD signals to yield a functional connectivity matrix for each control subject. The mean functional connectivity of all controls was then calculated through simple averaging. Oscillator phase was transformed into a smooth periodic function representing BOLD signal, and Pearson's correlation coefficients were calculated between pairwise nodes of the model. One-hundred runs were conducted for different values of the phase lag parameter (0 to $\pi$ ) with the functional connectivity of each phase lag obtained through simple averaging. Oscillator phases were randomly initialised prior to each run and coupling between nodes informed by the average structural connectivity of the controls.

## Evaluating the healthy structural connectome's local topology

The local topological organisation of each of the 148 nodes of the healthy template (i.e. the average structural network of the controls) was evaluated using the main graph theoretic measures (Bullmore and Sporns, 2009; Sporns, 2013*b*). This included a measure of connectivity centrality – the eigenvector centrality. Under this framework, nodes have high eigenvector centrality if they have many neighbours, if their neighbours are highly connected or both). In other words, a node is important if it is linked by other important nodes. Two local measures of segregation/integration are applied – the clustering coefficient, or fraction of all possible edges linking a node's neighbours, and the local efficiency – the inverse average shortest path length between a node's neighbours. Finally, a measure of modularity is applied that relied upon an *a priori* definition of network modules or network components demonstrating high intra-connectivity but

sparse inter-connectivity (see: Defining resting state networks from functional imaging data). These included the participation coefficient, which captures how evenly a node's connections are distributed between modules. Metrics were evaluated using the Brain Connectivity Toolbox (Rubinov and Sporns, 2010). Full definitions are provided in the appendices (see section 8.1).

### Evaluating the lesioned structural connectome's large-scale topological organisation at the subject-level

Four large-scale analogues of the previously described local measures are also applied, namely, the mean eigenvector centrality, the mean clustering coefficient, global efficiency, and mean participation coefficient on the subject-level connectivity matrices. Three of these measures were discussed previously, the fourth – global efficiency – is closely related to path length and captures the trade-off between minimising network costs and maximising topological efficiency. For this reason, high global efficiency is associated with reduced wiring and metabolic costs, and faster, less noisy information transmission (Bullmore and Sporns, 2012). Full definitions are provided in the appendices (see section 8.1).

## 6.4 Results

### Empirical estimates of large-scale neural metastability measured in fMRI BOLD signal are significantly reduced in AD

The metastability of the resting state fMRI BOLD signal was estimated for each cohort (Fig. 6.6; in grey). Global metastability of healthy subjects declined asymptotically over the course of disease progression. One-way ANOVA identified a statistically significant difference between groups

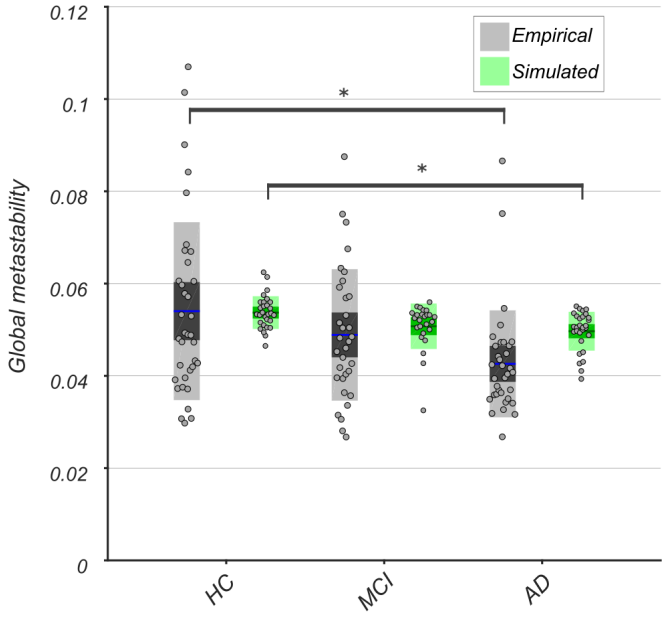


Figure 6.6: Empirical global metastability of fMRI BOLD signal (in grey) and simulated global metastability (in green). Simulated metastability was calculated from a computer model with anatomically informed coupling. Empirical metastability was estimated from fMRI BOLD signal. Bars display mean, 95% CI, and one standard deviation for the three cohorts (HC/MCI/AD) with individual subjects indicated. One-way ANOVA revealed significantly lower metastability of large-scale neural dynamics in AD compared to controls for both empirical and simulated data (*$p < 0.01$).

($F(2,101) = 4.77$, $p = 0.011$). Subsequent Tukey post hoc test revealed significantly lower neural metastability in AD patients compared to controls ($p = 0.0073$).

## Empirically defined macroscopic structural disconnection drives reduced metastability in large-scale simulations of neural dynamics

The impact of macroscopic structural disconnection on the large-scale neural dynamic was assessed by informing coupling between nodes in a simple

oscillator model with subject-level connectivity data. Figure 6.6 shows the simulated metastability of each subject group (in green) compared to empirical estimates of global metastability (in grey). Since the simulated results were contingent on the choice of starting parameters (the initial oscillator phases), the average global metastability produced from each subject's connectivity matrix over 100 runs (signified by a grey dot) is calculated. For each run, a different set of initial oscillator phases was supplied. Each group (set of 30 subjects) received the same set of randomly initialised phases. Statistical tests were then conducted on the average values (the grey dots).

In agreement with empirical observations, simulated global metastability declined according to diagnostic status. One-way ANOVA determined a statistically significant difference between groups ($F(59,88) = 7.83$, $p = 0.0007$). Subsequent Tukey post hoc test revealed significantly lower neural metastability in simulations informed by the subject-level connectivity matrices of AD patients as compared to controls ($p = 0.00065$). Importantly, this result was robust against changes in the initial starting parameters.

## Local topological measures predict damage to the computer model's connectivity

Existing studies typically report finding significant differences in graph theoretic measures in clinical groups as compared controls (Tijms et al., 2013). However, here the graph theoretic measure is related to the total number of lesions in the connectivity of each node. In doing so, the degree to which damage is correlated with specific features of the connectome's topology is quantified. Since strength of coupling between nodes is determined by subject-level connectome data, it should be emphasised that these results provide insight into how connectivity is damaged between nodes in the computer model. Accordingly, lesion count was entered into a linear regression analysis as dependent variable with one of four local graph metrics as predictors (Fig. 6.7).

Patients demonstrated a statistically significant relationship between the

number of lesions a node receives and key features of its structural topology, corrected for multiple comparisons at the Bonferroni p-level of $p < 0.001$. The relationship was more pronounced in the AD cohort. For the MCI group, these included eigenvector centrality ($F(1,146) = 89.2$, $p = 8.17e\text{-}17$), clustering coefficient ($F(1,146) = 75.7$, $p = 6.26e\text{-}15$), local efficiency ($F(1,146) = 93.3$, $p = 2.24e\text{-}17$) and participation coefficient ($F(1,146) = 33.7$, $p = 3.87e\text{-}08$). For AD patients, these included eigenvector centrality ($F(1,146) = 125$, $p = 2.58e\text{-}21$), clustering coefficient ($F(1,146) = 124$, $p = 3.12e\text{-}21$), local efficiency ($F(1,146) = 106$, $p = 5.3e\text{-}19$) and participation coefficient ($F(1,146) = 35.1$, $p = 2.19e\text{-}08$).

Figure 6.7 (A-D) shows the total number of lesions in a node's connections plotted against the four measures of local topology. Since the results for the MCI group were qualitatively no different from AD, only the latter are presented.

## High-degree hubs of the rich-club are selectively vulnerability to damage

The human connectome is organised into a densely interconnected core of high-degree hub nodes known as the rich-club (van den Heuvel and Sporns, 2011). The relationship between a nodes rich-club membership and the total number of lesions within its connections was investigated .

Figure 6.7.E shows all 148 nodes rank ordered by degree with each node's normalised lesion count indicated by colour (ranging from zero lesions, blue, to the highest number of lesions recorded, yellow) and dashed horizontal lines signalling the rich-club regime. Figure 6.7.F (left) shows all nodes drawn at the centre of mass of their respective cortical parcellations, with diameter proportional to degree and normalised lesion count indicated by colour. For visualisation purposes, the diameter of the corpus callosum has been scaled to correspond to $k = 70$. Figure 6.7.F (right) shows those nodes and their edges with degree $k > 60$ that qualify for rich-club membership. As in previous work, a densely inter-connected core spanning multiple cortices and resting state networks is identified (see Fig. 8.1 located in

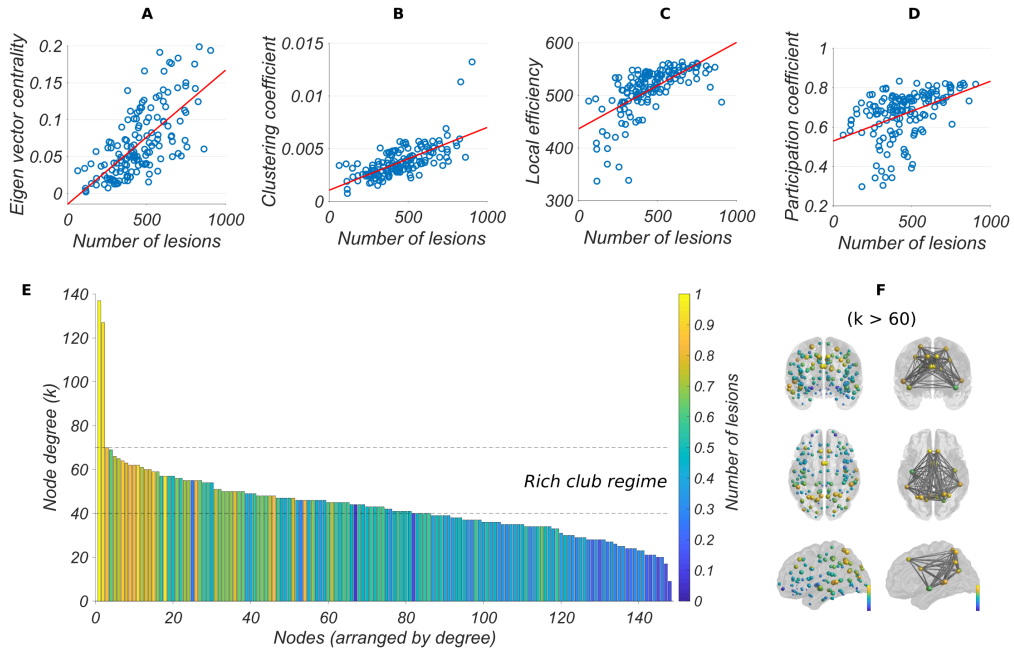


Figure 6.7: Local topological features of the average healthy connectome predict damage to nodal connectivity in the computer model (top) of AD subjects. This included A, eigenvector centrality, B, participation coefficient, C, clustering coefficient and D, local efficiency. All relationships were significant, corrected for multiple comparisons at the Bonferroni p-level of $p < 0.001$. Nodes of the rich club regime demonstrate the highest number of lesions (bottom). E, All 148 nodes of the Destrieux atlas rank ordered by degree with lesion count ranging from zero lesions, in blue, to the highest number recorded, in yellow, normalised to lie between zero and one. Dashed horizontal lines signal the rich-club regime between degrees $k = 40$ and $k = 70$. F, All 148 nodes of the Destrieux atlas plotted at the centre of mass of their respective cortical parcellations (left) with diameter proportional to degree and normalised lesion count indicated by colour. Nodes (and their edges) with degree $> 60$ qualifying for rich-club membership (right).

the appendices for the normalised unweighted rich-club coefficient curve). These regions (and their respective resting state networks; see Fig. 6.2) included parieto-occipital sulcus (medial visual), intra-parietal sulcus (dorsal attention), precuneus and superior temporal sulcus (default mode), superior parietal lobule (default mode adjacent), inferior segment of the circular sulcus of the insula (auditory), and pericallosal sulcus of the corpus callosum (salience).

## Macroscopic topological organisation predicts simulated neural metastability

Simulated global metastability was entered into a linear regression analysis as dependent variable with large-scale graph theoretic measures of structural connectivity as predictors. Since correlations could potentially be driven by a small number of extreme values, outliers in the data were removed prior to performing linear regression. An outlier was defined as a value that is more than three scaled median absolute deviations away from the median. Linear regression was performed for both the MCI and AD groups independently, as well as across all participants. Performing the regression with and without outliers did not qualitatively change the result.

Figure 6.8 shows the association between macroscopic topological organisation (after lesioning) and simulated global metastability. Both MCI and AD patients demonstrated a statistically significant relationship between simulated global metastability and the large-scale measures of structural topology, corrected for multiple comparisons at the Bonferroni p-level of $p < 0.0063$. These included mean eigenvector centrality ($F(1,43) = 18.7$, $p = 0.00009$), mean clustering coefficient ($F(1,46 = 16.2$, $p = 0.0002$), global efficiency ($F(1,38) = 14.1$, $p = 0.0006$), and mean participation coefficient ($F(1,45) = 13.9$, $p = 0.00005$).

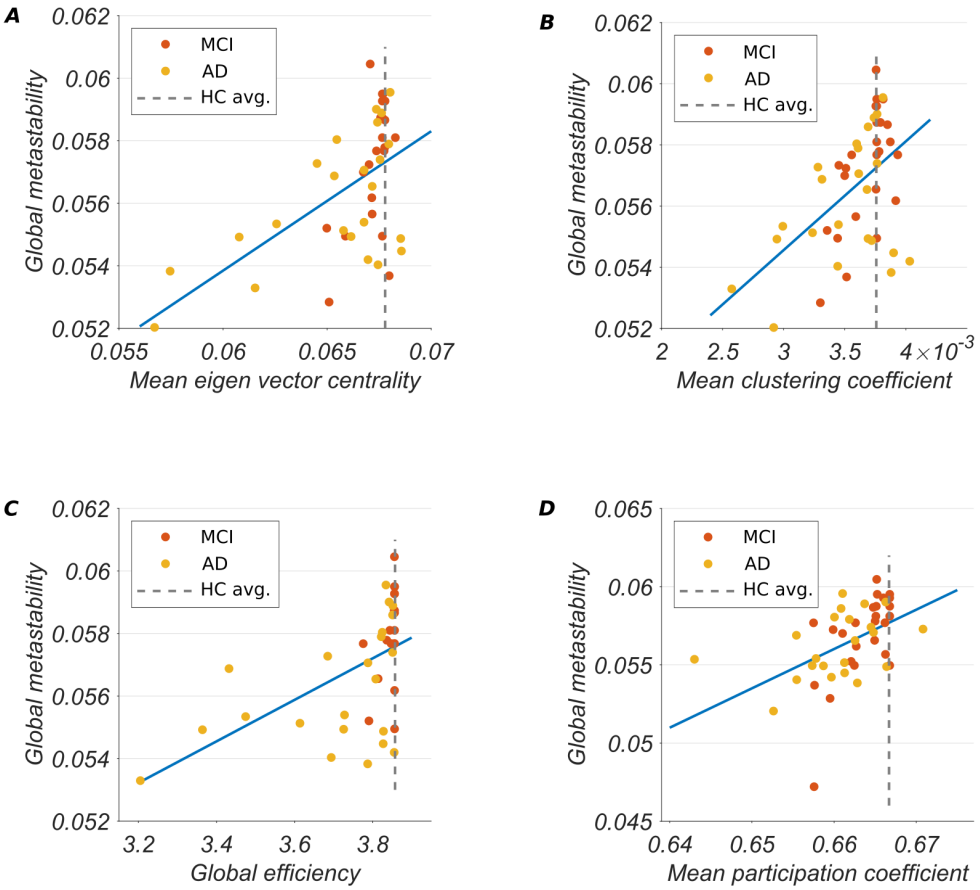


Figure 6.8: Relationship between macroscopic topological organisation including A, mean eigenvector centrality, B, mean clustering coefficient, C, global efficiency and D, mean participation coefficient after lesioning and simulated global metastability in MCI (in red) and AD cohorts (in yellow). A significant positive association was found between macroscopic measures of structural topology and simulated global metastability corrected for multiple comparisons at the Bonferroni p-level of $p < 0.0063$. For reference, vertical dashed line indicates the value obtained in the group-averaged control network.

## Widespread decreases in metastability between empirical resting state networks in AD

This study sought to identify network-level alterations in synchrony and metastability of resting state BOLD signal in the MCI and AD cohorts.

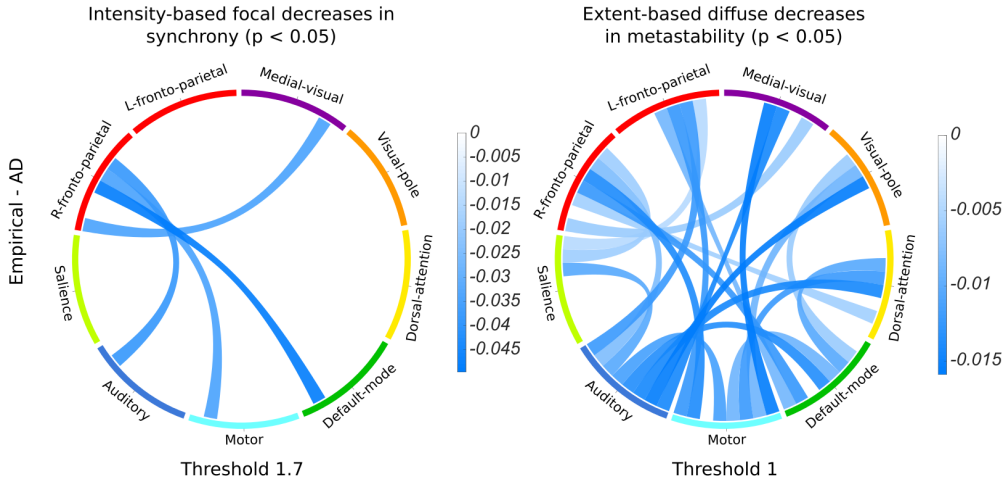


Figure 6.9: Statistically significant ($p < 0.05$; corrected) intensity-based decreases in focal synchrony between a circumscribed set of resting state networks identified using the network based statistic in fMRI data (left). Statistically significant ($p < 0.05$; corrected) extent-based decreases in metastability between a widespread set of resting state networks identified using the network based statistic in fMRI data (right). In both cases, the NBS was applied to matrices of synchrony and metastability calculated from empirical fMRI BOLD data at the resting state network level where thresholds were set to reveal the largest disconnected sub-graphs that were statistically significant.

Accordingly, the NBS was applied to the 9x9 matrices of synchrony and metastability estimated from empirical fMRI BOLD data for each subject, where each row/column represented the interaction of a single resting state network with eight others.

The NBS identified statistically significant ($p = 0.033$; corrected) intensity-based focal decreases in synchrony between large-scale networks in AD. These included decreases between right fronto-parietal and sensory-motor networks, and between right fronto-parietal and default mode network.

The NBS also identified statistically significant ($p = 0.043$; corrected) extent-based decreases in metastability that subsumed all nine resting state networks in AD. Recall that extent is indicative of a relatively weak effect spread over many connections while intensity is associated with stronger

effects confined to a small number of connections. No significant differences were identified in the MCI cohort for either synchrony ($p = 0.29$; corrected) or metastability ($p = 0.86$; corrected). Figure 6.9 shows the statistically significant sub-graphs ($p < 0.05$; corrected) of decreased synchrony (left) and metastability (right) identified by the NBS in the AD cohort. This is in contrast with hypersychronized connectivity found in other works. The lack of statistical power in the present study may be precluding these subtle changes in connectivity from being detected.

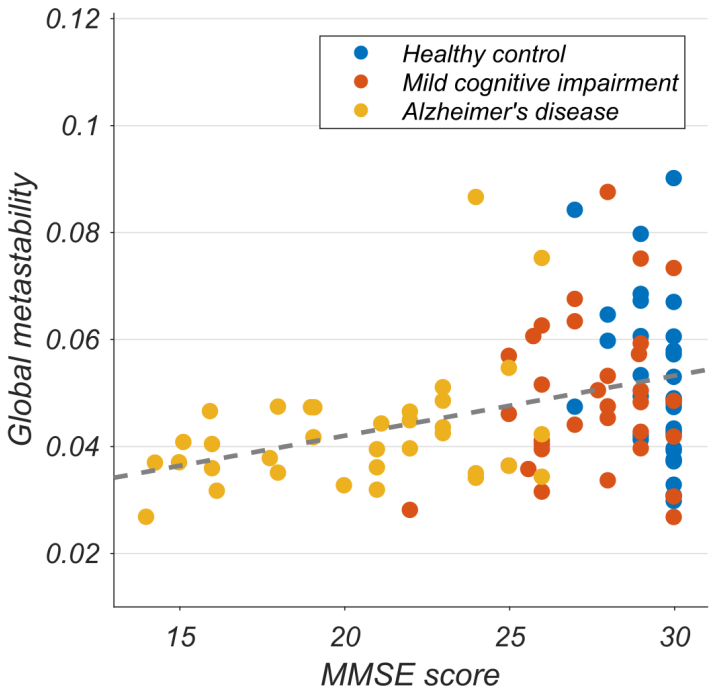


Figure 6.10: Relationship between global cognitive test scores and brain-wide metastability of fMRI BOLD signal. A significant association between global cognitive performance (MMSE) and empirical macroscopic neural metastability was found across all participants ($p < 0.01$). In this context, global metastability may be considered a summary measure of network flexibility.

## Empirical measures of metastability predict cognitive performance in AD

To understand how empirical measures of neural metastability relate to cognitive performance, a multiple linear regression was performed with MMSE test score as dependent variable, global metastability as predictor, and age, motion, and total volume of grey matter as covariates of no interest. Figure 6.10 shows MMSE test score plotted against brain-wide metastability of empirical fMRI BOLD signal where each dot represents a single subject. A statistically significant association ($t(98) = 11.6$, $p = 0.0009$) was found between empirical measures of macroscopic neural metastability and cognitive performance across all subjects.

## Dissociable networks of decreased FA identified in MCI and AD using dual NBS and model-based fitting approach

To identify the structural correlates underlying the observations of decreased synchrony between fronto-parietal and sensory-motor network in the AD cohort (Fig. 6.9), a joint model-based fitting and NBS procedure was invoked. In doing so, dissociable networks of decreased FA between diagnostic groups was identified. The AD cohort showed marked decreases in FA within portions of frontal and posterior cortex commensurate with fronto-parietal network. In contrast, the MCI cohort showed decreased FA in regions situated more centrally.

Figure 6.11.A shows the mean correlation between simulated synchrony (generated from the NBS identified structure) and mean empirical synchrony (measured using fMRI BOLD signal) in MCI patients drawn in blue with 95% CI. For comparison, the mean correlation between the simulated synchrony of a random control (generated by lesioning an equivalent number of random nodes) and mean empirical synchrony (measured using fMRI BOLD signal) is overlaid in red with 95% CI. Cohen's d effect size was used (indicated by black dashed line) to assess the standardised differ-

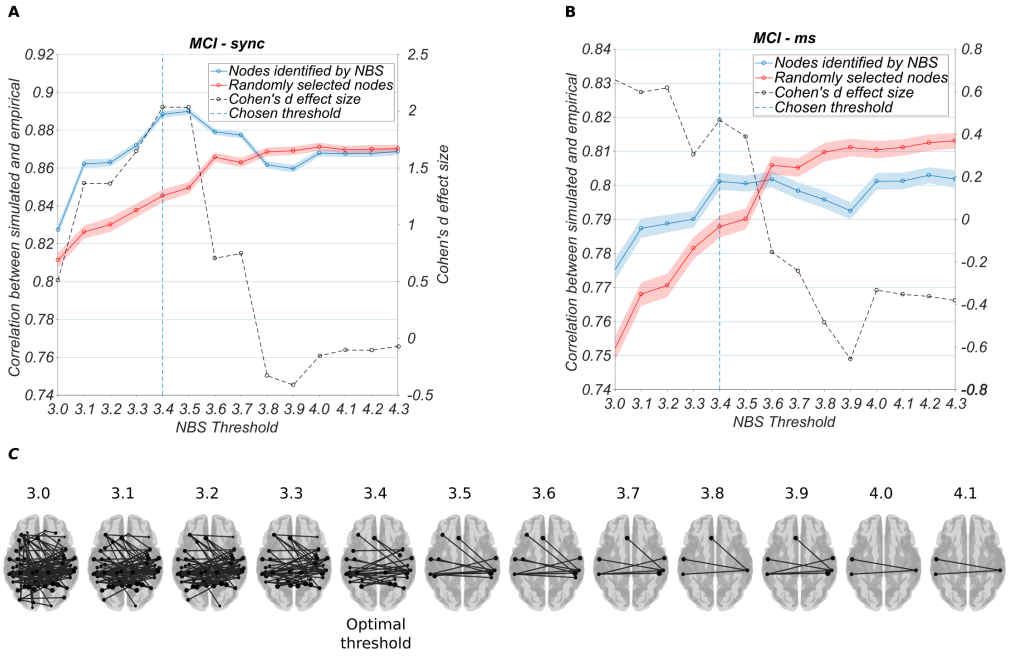


Figure 6.11: Identifying group-level structural connectivity in the MCI cohort. A, Mean correlation between simulated synchrony and empirical synchrony drawn in blue with 95% CI. Mean correlation between simulated synchrony of a random control and empirical synchrony is in red with 95% CI. Cohen's d effect size is indicated by black dashed line. Correlation between simulated and empirical synchrony peaked (r = 0.88) and Cohen effect size maximised (d = 2.1) at NBS threshold 3.4. B, Same as in A but for metastability. C, Disconnected FA sub-networks identified by the NBS in a group of 30 patients with MCI at different thresholds ($p < 0.05$; corrected). Nodes are positioned at the centre of mass of their respective cortical parcellation. At each threshold, identified nodes had their connectivity lesioned from the average control connectivity. The resulting structure informed coupling strength between nodes in a group-level simulation.

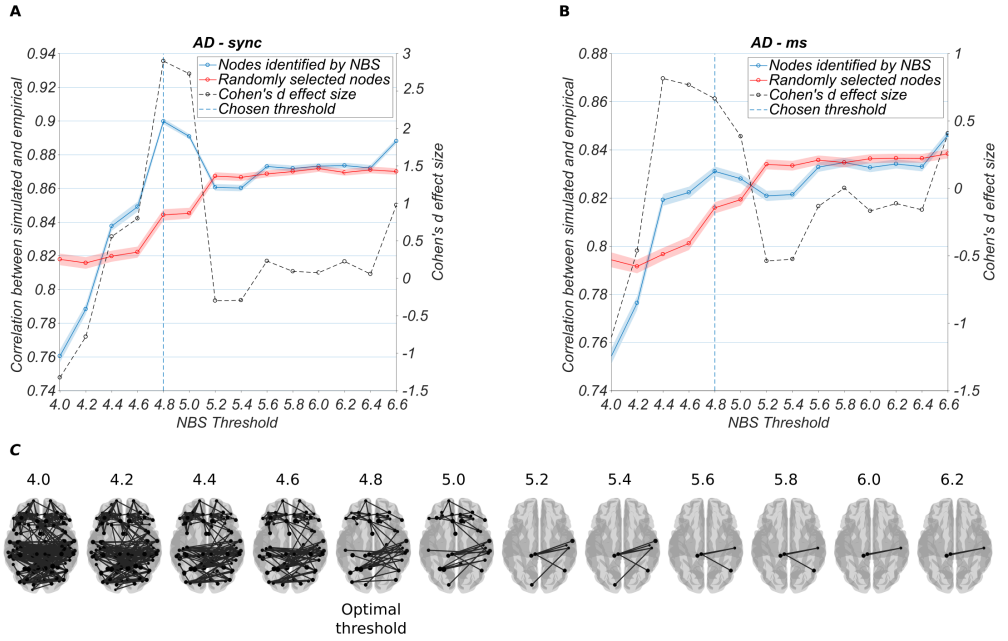


Figure 6.12: Identifying group-level structural connectivity in the AD cohort. A, See Fig. 6.11 for description. Correlation between simulated and empirical synchrony peaked (r = 0.9) and Cohen effect size maximised (d = 2.9) at NBS threshold 4.8. B, Same as in A but for metastability. C, Disconnected FA sub-networks identified by the NBS in a group of 30 patients with AD at different thresholds ($p < 0.05$; corrected). See Fig. 6.11 for description.

ence between the two means (blue and red) at different values of the NBS threshold.

The NBS threshold (3.4) at which correlation between simulated and empirical synchrony approximately peaked (r = 0.88; blue line) and the Cohen effect size was maximised (d = 2.10) is indicated by vertical dashed line. Two-sample t-test at the chosen threshold (3.4) revealed a statistically significant difference ($t(998) = 21.99$, $p < 0.01$; uncorrected) between 1) the mean correlations of the model informed by the group-level structure versus empirical fMRI data (blue), and 2) the mean correlations of the model informed by a randomly lesioned structure versus empirical fMRI data (red). Figures 8.2 and 8.3 located in the appendices show the correlation between

simulated and empirical data at the chosen threshold.

Figure 6.11.B shows the mean correlation between simulated metastability (generated from the NBS identified structure) and empirical metastability (measured using fMRI BOLD signal) drawn in blue with 95% CI. Again, random controls are highlighted in red. At the chosen NBS threshold of 3.4, correlations between simulated and empirical metastability peaked ($r = 0.8$) and the Cohen effect size was moderate ($d = 0.5$). Two-sample t-test at this threshold (3.4) revealed a statistically significant difference ($t(998) = 6.38$, $p < 0.01$; uncorrected) between (1) the mean correlations of the model informed by the group-level structure versus empirical fMRI data (blue) and (2) the mean correlations of the model informed by a randomly lesioned structure versus empirical fMRI data (red). Figure 6.11.C shows the disconnected FA sub-graph determined by the NBS ($p < 0.05$; corrected) for the MCI cohort at each threshold. The nodes identified at the chosen threshold are shown in figure 8.4 located in the appendices.

The same procedure was applied to the AD cohort. Figure 6.12.A shows the NBS threshold (4.8) at which correlation between simulated and empirical synchrony peaked ($r = 0.90$) and the Cohen effect size was maximised ($d = 2.9$) as vertical dashed line. Two-sample t-test at this threshold (4.8) revealed a statistically significant difference ($t(998) = 29.26$, $p < 0.01$; uncorrected) between (1) the mean correlations of the model informed by the NBS identified structure versus empirical fMRI data (blue), and (2) the mean correlations of the model informed by a randomly lesioned structure versus empirical fMRI data (red). Figures 8.2 and 8.3 located in the appendices show the correlation between simulated and empirical data at the chosen threshold.

Figure 6.12.B shows that at the chosen NBS threshold of 4.8, correlations between simulated and empirical metastability are close to their peak ($r = 0.83$; blue line) and the Cohen effect size is moderate ($d = 0.75$). Two-sample t-test at this threshold (4.8) revealed a statistically significant difference ($t(998) = 9.68$, $p < 0.01$; uncorrected) between (1) the mean correlations of the model informed by the NBS identified structure versus empirical fMRI data (blue) and (2) the mean correlations of the model in-

formed by a randomly lesioned structure versus empirical fMRI data (red). Figure 6.12.C shows the disconnected FA sub-graph determined by the NBS ($p < 0.05$; corrected) for the AD cohort at each threshold. The nodes identified at the chosen threshold are shown in figure 8.5 located in the appendices.

## 6.5 Discussion

Structure, function, and cognition, can be arranged into an ontological triad each influencing the other. Interference to one component destabilises the triad, leading to measurable changes in the activity of the remaining two. This paper asked two broadly interrelated questions. How do higher level cognitive processes emerge from the interactions of dynamical networks of anatomically based brain connectivity, and how do disruptions to the topology of this structure impact network dynamics and ultimately cognition? To answer these questions, the neural dynamics of MCI and AD subjects were interrogated for changes in metastability. In AD, macroscopic damage to the structural connectome produced reductions in simulated metastability comparable to that observed in empirical fMRI data (Fig. 6.6). Damage to the computer model's connectivity was focused around nodes scoring high in topological centrality, integration, and efficiency (Fig. 6.7). Reductions in simulated metastability were associated with damage to the connectome's global topology (Fig. 6.8). Brain-wide decreases in metastability contrasted sharply with more focal decreases in synchrony between resting state networks important for cognitive control (Fig. 6.9). Finally, the empirical decreases showed behavioural relevance, correlating with a subject's global cognitive ability (Fig. 6.10). Overall, the results of our dual computer modelling and empirical study suggest a causal relationship between metastability of neural dynamics, cognitive performance and the structural integrity of the human connectome.

Reduced metastability was found in the global neural dynamic of fMRI BOLD signal in AD patients compared to healthy controls (Fig. 6.6). In a computer model informed by subject-level connectivity data, macroscopic

structural disconnection was associated with reduced metastability of resting state neural dynamic in AD (Fig. 6.6) that matched similar declines in empirical data. Damage was selectively distributed according to the topological properties of each node in the healthy connectome (Fig. 6.7.A-D). Rich-club hubs (Fig. 6.7.E-F) and long distance, inter-modular tracts were especially vulnerable. Reductions in simulated metastability correlated with damage to the structural connectome's large-scale topology (Fig. 6.8). Decreases in metastability were evident between most of the brain's resting state networks (Fig. 6.9). This is especially important in AD, as resting state networks are known to display a high degree of behavioural relevance (Smith and Nichols, 2009). The level of neural metastability exhibited by a subject was related to the degree of behavioural impairment measured through cognitive testing (Fig. 6.10). These results lend further support to previous empirical observations of reduced cognitive flexibility and resting state neural metastability in conditions where network topology has been altered (Hellyer et al., 2015; Váša et al., 2015).

Eigenvector centrality correlated positively with damaged connectivity in the computer model (Fig. 6.7.A). Our findings are consistent with the selective vulnerability demonstrated by topologically important hub nodes in neurodegenerative disorders (Crossley et al., 2014). In AD, the elevated metabolism of default mode network hubs appears to convey a greater risk of pathology (Buckner et al., 2009) – a view consistent with transgenic animal studies linking cellular activity to amyloid deposition (Cirrito et al., 2005; Bero et al., 2011) and simulations of activity dependent degeneration in hub regions (de Haan et al., 2012). Other hypotheses concerning the nature of brain network organisation and distribution of neuropathology have been proposed (Zhou et al., 2012). Foremost among these is the contention that pathology spreads transsynaptically in a prion-like manner between structurally and functionally related networks (Jaunmuktane et al., 2015). In support of this view, patterns of circumscribed atrophy are not randomly distributed with respect to the modular architecture of the brain. Rather, they appear to be constrained within specific resting state networks depending on the identity of the neurodegenerative disorder

(Seeley et al., 2009). In keeping with this hypothesis, a relatively simple anatomically constrained diffusion process accurately predicted spatial patterns of neurodegeneration in AD (Raj et al., 2012). Our results indicate that pathological material is disseminated through the cortex by a network of nodes scoring high in eigenvector centrality.

Topologically integrated nodes with high clustering coefficient (Fig. 6.7.B) and local efficiency (Fig. 6.7.C) constituted a second locus of disruption in the computer model. Local network features providing tight integration between neighbouring nodes may facilitate the spread of pathological disease vectors within local communities (Raj et al., 2012). To date, disrupted clustering coefficient has been reported across imaging modalities in AD (Tijms et al., 2013).

Damage to the computer model's connectivity also correlated with a node's participation coefficient (Fig. 6.7.D). Nodes scoring high in participation coefficient bridge segregated communities by distributing their long range connections evenly between modules. Our results provide a physical basis for reports of reduced participation coefficient reported in functional connectivity networks in AD (Brier et al., 2014). Power et al. (2013) identified regions with high participation coefficient as convergence zones for different functional subsystems. Damage to these nodes produced much greater disruption in resting state organisation than lesions of equivalent magnitude in more circumscribed networks Gratton et al. (2012). In another study, (Warren et al., 2014) demonstrated that nodes with high participation played a distinct role from nodes of high degree. Crucially, lesions to nodes with high participation coefficient produced impairment across a range of cognitive domains, whereas lesions to high degree nodes displayed more circumscribed cognitive deficits. Such results are consistent with the finding of reduced integration between network modules in our study and the global cognitive decline associated with AD. Furthermore, our results suggest a causal link between damage in high participation nodes, reduced metastability of neural dynamics, and decline in global cognitive performance.

Nodes demonstrating both high eigenvector centrality and high partici-

pation coefficient are likely part of the putative rich-club – a densely interconnected core of network hubs (van den Heuvel and Sporns, 2011; Pedersen and Omidvarnia, 2016). The rich-club phenomenon occurs when hub nodes connect more densely among themselves than nodes of lower degree. Pathways linking these regions constitute an expensive high-performance backbone for global integration. Accordingly, the rich-club accounts for the majority of shortest paths between node pairs (van den Heuvel et al., 2012). Simulations show that targeted attack of rich-club hubs impair global efficiency three times more than randomly directed attacks (van den Heuvel et al., 2012). Our results show disrupted rich-club organisation across the AD spectrum with nodes of the rich-club regime demonstrating the greatest number of lesions in their connectivity (Fig. 6.7.E-F). In line with this view, reduced metastability may be a signature of disrupted rich-club organisation consistent with its role in boosting functional diversity (Senden et al., 2014).

The drive for rich-club architecture is associated with the tendency for hubs to connect regions over large physical distances (van den Heuvel et al., 2012). In a similar vein, cross modality sensory information is often integrated over long distances by hubs located in heteromodal association cortex. Damage to long distance association and commissural tracts may therefore provide an anatomical basis for reports of attenuated long range functional connectivity in AD (Liu et al., 2014).

Importantly, MMSE test scores correlated positively with empirical resting state global metastability in AD patients (Fig. 6.10). The MMSE measures the severity and progression of longitudinal cognitive impairment by testing abilities related to memory, attention, and language. All three domains involve the large-scale integration of information across distributed sensory, motor, and cognitive control regions. For this reason, metastability may represent an important dynamical mechanism underlying general cognitive function.

Our study found decreases in global metastability (Fig. 6.6) that correspond to an extended network of behaviourally relevant cognitive subsystems (Fig. 6.9). This is consistent with the understanding that higher

order processes involving memory and attention (such as those putatively captured by the MMSE) are unlikely to reside within discrete topological modules. Instead, traditional modular architecture is likely dissolved in favour of a highly integrated global neuronal workspace (Dehaene et al., 1998). Measures of network integration including clustering coefficient, global efficiency, and participation coefficient, may therefore be more closely linked to higher order task performance than measures of segregation such as modularity (Bassett et al., 2011). In line with this view, reduced path length, heightened topological efficiency, and disrupted modular topology has been reported in functional networks during more challenging cognitive operations (Kitzbichler et al., 2011).

Instead of assessing topological properties of functional connectivity networks directly, computer modelling was used to examine the link between a connectome's large-scale integrative structure and its ability to generate metastable neural dynamics. This was accomplished by using anatomically derived subject-level connectivity data to inform coupling strength between nodes. In the present approach, changes in metastable dynamic could be directly linked to topological changes taking place in the structural connectome. Since the subject-level connectomes were derived by lesioning the healthy template i.e. the average structural connectivity of the controls, the finding of reduced topological efficiency is perhaps unsurprising. Of note however, is the direct causal relationship between degraded topological structure and reduced metastability in the simulated neural dynamics. Crucially, in the present research, simulated and empirical data are in qualitative agreement (Fig. 6.6).

Overall, AD was defined by reduced connectivity between topologically important and well-connected nodes, fragmented local network structure, increased path length between nodes, and reduced diversity of intermodule links. Accordingly, the structural connectomes belonging to MCI and AD subjects demonstrated a positive association between their simulated metastable dynamics and global measures of topological centrality, integration, and efficiency (Fig. 6.8.A-D). Such patterns of large-scale structural reorganisation may signal a shift in cost-efficiency trade-off in

the direction of lowered metabolic costs at the price of reduced integrative capacity (Bullmore and Sporns, 2012).

Interestingly, time resolved fluctuations in resting state functional connectivity are characterised by two different states (Zalesky et al., 2014), one consistent with a long distance, highly efficient, integrated workspace configuration, and another, more segregated, less metabolically demanding configuration favouring local efficiency. The spontaneous switching of these configurations likely underlies the variation in synchrony registered here as metastability. On this basis, reduced metastability in AD may reflect a change in the transition rate or dwell time of each configuration (Jones et al., 2012). One hypothesis is that AD patients spend more time in segregated, locally efficient configurations and less time in metabolically demanding states of global integration. Thus, the indiscriminate decrease in brain-wide metastability observed in AD (Fig. 6.9) may signal a reduction in the brain's dynamic repertoire when subjects are at rest.

Diffuse decreases in metastability were accompanied by more circumscribed decreases in focal synchrony between fronto-parietal and sensory-motor network and between fronto-parietal and default mode network (Fig. 6.9). These decreases were consistent with structural damage in a comparable set of regions (Fig. 6.12.C, also Figs. 8.4, and 8.5 in the appendices). The present results accord with recent findings of disrupted fronto-parietal network functional connectivity in AD (Zhao et al., 2018) and a growing consensus that frontal-parietal regions constitute a domain general control system for orchestrating more specialised networks (Vincent et al., 2008; Cole et al., 2013; Crossley et al., 2013). Recently, Dixon et al. (2018) revealed a novel processing stream between fronto-parietal and default mode network involved in regulating introspective behaviour. Of note are the associations between functions ascribed to the DMN and symptoms of AD. These include recollection of autobiographical events in the past (Andreasen et al., 1995; Buckner and Carroll, 2007; Buckner et al., 2008); simulation of prospective events and self-projection in the future (Schacter et al., 2007, 2008); and theory of mind and social cognition (Schilbach et al., 2008; Spreng et al., 2009). Fronto-parietal and default mode network interac-

tions have also been identified in autobiographical (Spreng et al., 2010) and working memory (Piccoli et al., 2015) that overlap with the core dysfunction of AD – the ability to author and recall one's own history (Gil et al., 2001). In fact, DMN dysfunction is considered a hallmark of incipient AD (Greicius et al., 2004). Tellingly, hypometabolism in default mode network structures has been found to correlate with anosognosia score in MCI patients (Therriault et al., 2018). The fronto-parietal control system has been proposed to play a central role in regulating mental health (Cole, Repovš and Anticevic, 2014). It's flexible hubs may implement adaptive feedback control to regulate symptoms as they arise. Our results indicate a possible role for the fronto-parietal network in default mode network dysfunction in AD.

Finally, some limitations should be noted. Since there are many ways of defining a network both functionally and structurally, and at multiple scales, the current results may only be valid for the Destrieux atlas parcellation. Since the major sulci and gyri are unlikely to align well with functional activity, future modelling work may benefit from using atlas regions defined multi-modally, that is, based on more than one neurobiological property (Glasser et al., 2016). In addition, the use of model-based fitting to select the structural skeleton responsible for generating the observed dynamic does not consider likely degeneracies in the structural data, i.e., the method only considers a subset of the possible structural lesions responsible for changes in empirical metastability. Any lesions outside the largest detected component are explicitly ignored. A significant limitation of the current computer model is its lack of clear predictive power. The high-level model prediction, that changes in structural anatomy are responsible for observed decreases in empirical resting metastability in AD, is coarse grained (and we already know that AD is associated with decreased metastability). Future work would prioritise longitudinal analyses designed to identify sequences of structural change leading to empirically observed decreases in metastability between resting state networks. Such work would permit the possibility of using the anatomically informed computer model to make subject-level inferences regarding the conversion from MCI to AD

based on the interrelationship of structure and function. Moreover, the use of mean-field models incorporating cellular properties would permit more granular (and less abstract) hypotheses concerning the processes governing alterations in structural connectivity to be empirically tested. A further, crucial improvement, would address the current omission of sub-cortical structures in the computer model, in particular the thalamus. Understanding how individual thalamic nuclei contribute to regulating the metastable interactions between networks represents a critical step for understanding brain function in health and disease.

## 6.6 Conclusion

Metastability is consistent with other descriptions of the brain as a dynamical system including the principle of self-organised criticality (Hesse and Gross, 2014). The results of our empirical simulation (Figure 6.5) imply a phase transition from a highly disordered (sub-critical) to a highly ordered (super-critical) state. Numerical simulations show a phase transition or bifurcation in behaviour that corresponds to the divide between asynchrony and synchrony when coupling between networked Kuramoto oscillators is systematically increased. In the current contribution, the transition between no, partial, and full phase locking in the computational model is governed by the disruption term or phase lag parameter. In finite systems such as the connectome, phase transitions do not occur at a precise point but are smoothed out over a parameter range (Moretti and Muñoz, 2013). Thus, a small region between 0.5 and 1.5 rad is identified that is not technically critical, but likely retains properties of criticality. These hallmarks of criticality lend dynamical systems their optimal information processing and storage capabilities (Shew and Plenz, 2013). Resting state dynamics of human brains demonstrate properties consistent with critical dynamics (Tagliazucchi et al., 2012). In this regime, the brain is likely poised at an equilibrium point of balanced excitation and inhibition where synchrony is maximally variable and pathological states of low or high synchrony are avoided (Yang et al., 2012). The consequences of highly variable synchrony

on information processing is not well understood. Since the maintenance of a particular communication channel through coherence relies on a persistent phase relationship, the continuous variation in phase associated with metastability is potentially commensurate with a large number of independent communication channels (Deco and Kringelbach, 2016).

In summary, this chapter interrogated a neurodegenerative disorder, AD, and its prodromal stage MCI, to clarify the relationship between structural network topology and metastable neural dynamics. Overall, the results indicate a causal relationship between structure, dynamics, and cognition and support the contention that structure and cognition can be bridged through metastability (Shew and Plenz, 2013). In AD, metastability of fMRI BOLD signal was decreased and this correlated with cognitive performance. Using a theoretical computer model based on empirical connectivity this chapter showed a direct link between reductions in metastability and structural damage. These findings offer a distinct perspective on the network-level role of metastability in cognition, its relation to structure, and its inexorable decline in neurodegenerative disease.

# 7 Summary and concluding remarks

## 7.1 Summary

Francisco Varela put cognition on a dynamic footing when he said "[…] the emergence of a cognitive act is a matter of coordination of many different regions allowing for different capabilities […]. They must be bound together in specific grouping appropriate to the specifics of the current situation […] and are thus necessarily transient (Varela, 1995)." Varela (1995) advanced the idea of a "transient coherency-generating process" through which dispersed neural assemblies were unified through synchronous oscillations. In Varela's view, transiency was essential as it generated the dynamic flow associated with the continual emergence of cognition. The self-organisation of neural activity into transient state dynamics is crucial for simultaneously satisfying momentary task demands and integrating these exogenous signals with the brain's ongoing intrinsic activity. Such mechanisms may be a crucial aspect of the unity of mind and experience arising from the integrated activity of brain and body (Kelso, 1995). Accordingly, the essential motivating hypothesis of this thesis was that findings across several levels of description, including the important causal relationships between structure, function, and cognition in the human brain, are reconcilable within a

single theoretical framework, by appealing to a dynamical regime known as metastability (Kelso, 2012; Kelso and Tognoli, 2007; Kelso, 2009; Tognoli and Kelso, 2014*b*). These strands, captured in the principal aims of the thesis, were to explore:

- the modulation of complex metastable neural dynamics by cognitive state during different types of behaviour.
- how structural connectivity confers cognitive flexibility on a fixed network topology through metastable neural dynamics.
- how structural disconnection impacts metastable neural dynamics and how this relates to cognitive performance.

The thesis presented three studies, each concerned with the interaction of structure, function, and cognition in the human brain. Chapter 4 introduced the theoretical framework of metastable coordination dynamics to examine how the interactions of large-scale brain networks support cognition. Motivated by the observation that the probability of network switching is maximised when subjects are cognitively 'at rest', the research reported in this chapter tested the essential proposition that metastable neural dynamics are higher at rest than during a cognitively demanding exercise. Surprisingly, the results supported an alternate possibility: that metastable neural dynamics is actively enhanced by the performance of a task. Task-based network structure was principally characterised by low metastability in sensory regions and high metastability in regions devoted to cognitive control. Also, subjects whose networks transitioned efficiently between rest- and task-based configurations demonstrated greater dynamic flexibility in regions associated with cognitive control and greater dynamic stability in regions related to sensory processing. Importantly, this dynamic flexibility appeared to confer greater problem solving abilities in tasks requiring fluid intelligence.

Chapter 5, leveraged an example of incipient neurodegeneration, MCI, to test the proposition that structural disconnection of large-scale networks was related to cognition. This chapter revealed that white matter connectivity between thalamus and cortex, as defined by tractography, was an

important factor in cognitive ability. Resting state effective connectivity was used to show that patterns of causation were disrupted in a key component of the brain's intrinsic resting state architecture, the DMN. Chapter 4 provided proof-of-principle that large-scale ICN activity is disrupted by structural disconnection in early AD. This work extended previous studies showing abnormal DMN deactivation in AD and suggested that abnormal patterns of functional connectivity are, to some extent, linked to structural disconnection.

Chapter 6 developed and validated a theoretical computer model designed to simulate the spontaneous interactions between anatomically connected pairs of cortical regions in the resting brain. The model was based on a network of coupled Kuramoto phase oscillators with connectivity informed by anatomical estimates. Models of this form have previously been used to examine whole-brain functional connectivity. Importantly, by tuning a key parameter or disruption term (the phase lag) the model exhibited qualitatively different behaviour, from fully synchronous to fully random oscillations. Tuning the parameter to match empirical estimates of functional connectivity afforded the opportunity to observe a phase transition within the dynamics of the model, such that behaviour was poised at a critical state half way between order and disorder. In this 'critical regime', functional interactions imposed on neural dynamics by the anatomical connectivity produced structured correlations in space and time, resembling empirical resting state connectivity. Overall, this work demonstrates that relatively simple models exhibit key features of the brain's spontaneous neural dynamics when informed by realistic connectivity.

Chapter 6 also brought together different strands of research, relating structural disconnection, neural dynamics, and cognition, to explore how general cognitive ability was shaped by underlying anatomical connectivity. This joint empirical and computational approach revealed behaviourally relevant changes in spontaneous neural dynamics that were linked to the structural integrity of the anatomical connectome. Empirical measures of neural metastability were associated with cognitive performance across a spectrum of neurodegeneration. In addition, declines in metastability were

mechanistically linked to different features of the brain's topological connectivity. Taken together, these findings suggest that metastability is an integral component of general cognition and that metastable neural dynamics is contingent on the topological integrity of the anatomical connectome.

## 7.2 Concluding remarks

A range of studies employing disparate methodologies for recording and interpreting brain data has shown that AD and schizophrenia, as well as neurodevelopmental disorders such as autism exhibit abnormal topological organisation of structural and functional networks. Although these studies often rely upon the analysis of whole-brain or specific fibre pathways and the functional connectivity associated with task-evoked neural processing, an increasing number of studies is exploiting the resting state protocol to explore the impact of disease and damage on the brain's large-scale functional couplings. The unconstrained nature of the protocol is especially suited to subjects with dementia as they are simply required to lie down and stay awake. The utility of this approach is that the same large-scale networks of the brain present at rest also occur during task. This suggests that abnormalities in the brain's functional interactions at rest also map onto the brain's neural architecture and cognitive performance during task execution. Human cognition is founded on the structural arrangement of brain connectivity and the complex patterns of neural dynamics it engenders. Thus, it is perhaps unsurprising that cognitive disorders are associated with disorganised network configurations. Despite arising through different mechanisms, be it developmental, genetic, or environmental (encompassing historical, cultural, and evolutionary factors), any process that alters the natural pattern of brain connectivity will have its counterpart in the brain's cognitive architecture. Characterising these patterns of network failure will continue to provide a useful marker of clinical dysfunction in the damaged or diseased brain.

Complex networks like the brain are of interest precisely because of the dynamics they exhibit. Transient dynamics such as metastability are useful

to brain function because they simultaneously offer stability *and* flexibility. In simple terms, if environmental perturbations are varied, systems must have a matching repertoire of internal responses at their disposal. The ability of a system to engage in a variety of functions across multiple levels of organisational description is a measure of its complexity. Structural connections constrain but do not completely determine functional activity. This is especially true over short time scales of observation where functional connectivity takes on its most dynamic characteristics. At the millisecond-scale, functional couplings show significant variability. This behaviour occurs during task-orientated processing and when the brain is cognitively at rest. It is important to emphasise that this phenomenon occurs in spite of the fact that structural connectivity is approximately fixed over the same period. It should be noted, however, that changes in structure not currently detected by MRI may still be occurring at the microscale. These observations underpin the notion of a 'functional repertoire' of brain states from which cognition emerges, and bolster the idea that critical dynamics underlie cognition.

The classic conception of 'cognitive architecture' is founded on the understanding that human cognition is fundamentally computational in nature i.e. it arises through a series of operations performed on symbolic representations. Key to this view, is the idea that human cognition may be understood without considering its physical instantiation. Today, a renewed convergence of neurobiology and cognition is arising from the need to understand the structural and functional basis of cognitive architecture. To this end, the study of neurocognitive circuits in non-human primates has mechanistically advanced our understanding of cognition. Moreover, complementary studies of the human brain using non-invasive methods has revealed task-specific activations of local areas. A promising area of investigation is emerging in the overlap between systems-level cognitive neuroscience and the discipline of network science. Region of interest-based analyses are increasingly being supplanted by techniques designed to understand how cognitive operations emerge from the dynamics of extended cortical (and subcortical) networks. These large-scale networks largely overlap with the

brain's macroscopic connectivity and emerge as coherent patterns of neural activity when subjects are at rest. The onset of task necessarily requires some deviation from this configuration, hence, networks operate and interact according to dynamic principles. Conceptualising the brain as a system of interacting local areas is useful because: (1) it transcends the dichotomy of local and global information processing; (2) it provides a framework for unifying endogenously and exogenously driven neural activity; and (3) it can be used to link spatio-temporal scales (from neurons to large-scale regions).

The multi-scale character of nervous systems is an essential property of their organisation and network architecture. Brain networks span multiple spatial and temporal scales, from the microlevel of individuals neurons to the macro-scale of cognitive networks and ultimately embodied organisms operating in an environment. Each level of the hierarchy is characterised by distinct dynamics; from local to global scales, the brain exhibits multiple levels of integration and segregation. Multi-scale systems exist on several levels simultaneously, hence, despite being hierarchical no individual level takes precedence over any other. Rather, each pattern of activity at one level of description critically depends on and informs processes unfolding at higher and lower scales. For this reason, large-scale network behaviour should not be viewed as a poorly resolved account of underlying microscopic behaviour but as a window into the system-level interactions that constitute cognition. Mean-field approaches like the Kuramoto phase oscillator leverage this observation to bridge the interactions of neuronal populations to system dynamics underpinning cognition. Novel insights into the structural and functional antecedents of human cognition are likely to continue as future studies exploit the marriage of network theory and theoretical computer modelling.

In summary, this thesis has demonstrated a key functional linkage between metastable neural dynamics and cognitive performance in a set of large-scale networks responsible for cognitive control. Moreover, the approach taken has leveraged an example of structural disconnection, namely AD, and its prodrome MCI, to mechanistically link anatomical connectivity,

metastability, and cognitive function. Damage to the brain's macroscopic structural connectivity was linked to reduced metastability in both empirical and simulated data, suggesting that metastable neural dynamics is contingent on the topological integrity of the underlying anatomical connectome. These results provide a compelling link between brain structure and function, and suggest the framework of metastable dynamics, in conjunction with theoretical computer modelling, offers an account for understanding the brain in health and disease.

## 7.3 Main thesis contributions

This thesis advances our understanding of the dynamical principles underlying essential brain operations that support higher-level cognition. The present work also clarifies how structure and dynamics interact in the damaged or diseased brain to create sub-optimal cognitive function. Portions of the work presented here have been previously published as two peer reviewed journal articles (Alderson et al., 2017, 2018). An additional manuscript is currently under review at *NeuroImage* journal.

Chapter 2 provided a thorough review of the literature pertaining to the nature of the structure–function dyad in the human brain, its relation to dynamics and the use of computational modelling in conjunction with network theory to provide insight. This contribution highlights areas of potential future investigation beyond the current state-of-the-art.

Chapter 3 confirmed the essential hypothesis that cortical regions are functionally coupled through metastable coordination dynamics into large-scale neurocognitive networks. This work provides evidence that metastable coordination dynamics in regions of the brain associated with cognitive control are critical for enabling fluid intelligence. Moreover, it demonstrates that the efficiency of transformation between rest- and task-based architectures is both underpinned by metastable neural dynamics and predictive of cognitive ability. Taken together, these findings shed new light on the dynamical principles underlying the brain's resting and cognitive organisation, and, critically, how they relate to task performance. Overall, the

present findings contribute to a growing literature suggesting that dynamic principles of self-organisation are critical attributes of brain, mind, and behaviour.

Chapter 4 linked the structural integrity of the thalamo-cortical loop to patterns of abnormal effective connectivity in the DMN of subjects with incipient neurodegenerative, namely, MCI. This work is consistent with previous observations suggesting that AD is characterised by dysfunctional activity in regions of DMN. Accordingly, this study leveraged a multi-modal approach, utilising a sophisticated spatio-temporal GC formulation and a cutting-edge CSD probabilistic fibre tractography algorithm, to investigate the causal and structural basis for impaired memory recall in MCI subjects. These findings build on previous observations of abnormal task-induced response deactivation patterns in the DMN of patients with AD and contribute to the growing consensus that patterns of abnormal functional connectivity are the result of network disconnection. The principal contribution of this chapter was to provide a novel causal pathway in the DMN dysfunction commonly identified in subjects with AD, namely, the structural integrity of the thalamo-DMN loop. This phenomenon is consistent with the known distribution and time course of pathology, beginning in hippocampus, travelling through thalamic nuclei, and terminating in posterior portions of DMN. Overall, this work reflects the growing consensus that pathological material is spread via the structural linkages of the brain.

Chapter 5 exploited dynamical accounts of the brain to reconcile perspectives from across the three domains of structure, function, and cognition. The principal contribution of this chapter was to mechanically link structure and metastability in a clinical condition characterised by anatomical disconnection. This work used network theory and whole-brain computer modelling to link the asymptotic decline of metastability over the course of AD to damaged network topology. Critically, the simulated data matched that obtained empirically, suggesting that impaired cognitive performance is linked to altered network topology. This work builds on previous theoretical and empirical findings that link the topological integrity of the anatomical connectome to the dynamic diversity associated

with cognition.

In summary, the major contributions are as follows. Firstly, this thesis has demonstrated that the interactions of large-scale networks are relevant to cognition, are metastable, and that this form of dynamic interplay is critical for enabling cognitive control. Secondly, this thesis has implicated a novel causal pathway – the so-called 'thalamo-DMN' loop – in patterns of disrupted functional connectivity and impaired memory recall commonly observed in the DMN of patients with MCI and AD. Thirdly, this thesis has shown that decreased metastability and impaired cognitive function stem, in part, from abnormal network topology. Taken together, these findings suggest the metastable regime of dynamics offers considerable potential as a theoretical and conceptual framework for mechanistically linking structure, function, and cognition in the human brain. The following section is devoted to exploring areas of potential future research.

## 7.4 Future directions

*"There are no small problems. Problems that appear small are large problems that are not understood."*

— S. Ramon y Cajal*, Advice for a Young Investigator*

The contributions made within this thesis form the foundation for future studies in a variety of research areas. In regard to theoretical modelling of the brain, the computational approach can be extended in several ways. Firstly, models can be further elaborated to provide more comprehensive descriptions of the brain's structure and function. Secondly, models can be used to further advance our understanding of the meaning and mechanisms underling observations of dynamic functional connectivity at rest and, crucially, during the performance of a task. Finally, models can be employed to further our understanding of the mechanisms underlying the behavioural and cognitive deficits associated with network damage.

The notion of metastability is compatible with extant measures of time-varying or dynamic functional connectivity (Gonzalez-Castillo and Bandettini, 2017). Like metastability, several properties of dynamic functional

connectivity have been identified which systematically track alterations in human behaviour and cognition (Cohen, 2018). At present, features of dynamic functional connectivity can be estimated but the mechanisms underlying these phenomena as well as their neuronal origin are not well understood. It is critical for our understanding of neural dynamics that these explanatory accounts move beyond primarily descriptive measures and begin to probe the causal mechanisms underlying these phenomena. Accordingly, future studies are required to reveal the neuronal substrate of dynamic functional connectivity, isolate genuine neural dynamics from physiological and other sources of noise and develop new methods to validate and improve the accuracy of dynamic functional connectivity. A promising approach is to use state-of-the-art computer modelling techniques to reveal the casual pathways of dynamic connectivity. These computer models, based on biologically plausible connectivity, have confirmed that alternating states of integration and segregation are contingent on the structural connectivity of the connectome. A further area of improvement lies in utilising methods designed to explicitly model and test causal relationships in the brain. One such approach, DCM, aims at revealing the underlying causal processes by which cortical regions communicate by comparing specific instantiations of neuronal activity and connectivity to empirical data (Friston, 2003). These and other methods offer a stronger account of causality in the brain than the inference of 'probabilistic causality' obtained through simple time series analysis. DCM should be utilised in future analyses to clarify the role of individual thalamic nuclei in the posterior DMN dysregulation associated with MCI.

A critical next step in our understanding of time-varying dynamics and its relation to cognition, is to explore alterations in dynamic functional connectivity that occur in response to cognitive demand (Hellyer et al., 2014). The present generation of whole-brain computer models is unable to account for the evolution of task-dependent changes in dynamic functional connectivity on a network of static structural elements. Several modelling studies have proposed mechanisms for directing the complex dynamics generated by the interaction of cortical regions. These include the neural gain afforded by

ascending neuromodulatory nuclei (Shine, Aburn, Breakspear and Poldrack, 2018; Shine, van den Brink, Hernaus, Nieuwenhuis and Poldrack, 2018) and the tonic input arising from the brainstem to the thalamus (Stratton and Wiles, 2015). Additional factors, such as top-down attentional control (Hellyer et al., 2014) and reverberating activity in the thalamo-cortical loop (Izhikevich and Edelman, 2008) have also been identified. Other potential areas of research include modelling the transition between sleep and wakefulness/high attention/vigilance. It is worth emphasising that whole-brain computer models routinely exclude the thalamo-cortical loop — a critical element of network organisation from which complex brain dynamics is likely to arise (Izhikevich and Edelman, 2008). Moreover, depending on the aims of the investigation, it may be appropriate to model certain aspects of network organisations such as microscopic circuitry, tissue structure, cell structure, synaptic kinetics, synaptic plasticity, and neuromodulatory control using compartmental spiking (or conductance-based) models. Future work should extend the computational approach to provide more detailed descriptions of the brain and incorporate key subcortical structures such as the thalamus (Bhattacharya et al., 2011, 2013; Abuhassan et al., 2012, 2014). Computational modelling may also be used to aid clinical diagnosis, assess the distribution and impact of pathology in the brain's network structure and dynamics, and provide stratified treatment and rehabilitation strategies. In this context, the present thesis uses computational modelling in conjunction with dynamic systems theory to understand the causal interactions between pathology, neural activity, and cognition. The era of 'big data' makes it increasingly important to provide neuroscientists, neurologists, and psychiatrists with novel interpretative structures to inform decision making (Stephan and Mathys, 2014; Montague et al., 2012). In the future, increasingly sophisticated computer models and machine learning techniques will be required to deliver: (1) accurate and personalised predictions about the likely clinical impact of disease and damage in AD, and other disorders; (2) practical biomarkers for tracking disease pathology and of patient stratification in treatment trials; and (3) a framework for developing hypotheses regarding novel treatment strategies including be-

havioural, pharmacological, and electrophysiological interventions such as deep brain stimulation (Lyons, 2011). In this context, the development of accurate and validated *in-silico* computer simulations of the brain will provide efficient test beds for exploring intervention strategies and developing cost effective treatment options. One example, transcranial direct current stimulation, has the potential of enabling rehabilitation. However, determining the frequency and site of application to achieve optimal results is a significant challenge. This approach becomes tractable when informed by realistic computer simulations of the brain based on observational studies of structure and function. Determining the optimal treatment strategies for individuals on the basis of genetic and structural brain information is also becoming increasingly feasible. Sophisticated brain mapping approaches have related genetic influences on brain structure to the risk of developing AD (Peper et al., 2007; Thompson et al., 2001). Incorporating this structural data into a computer model would allow the dynamic network interactions underlying these genetic differences to be objectively assessed. Subjects at genetic risk often display metabolic and structural alterations prior to the appearance of overt cognitive symptoms, therefore, a joint genetic, imaging and computational modelling approach would provide greater power for identifying at risk individuals and for testing treatment strategies. To facilitate early detection and treatment, future investigations of brain disorders will increasingly leverage multi-modal imaging data in conjunction with computational modelling to map structural alterations onto network dynamics. Moreover, tools of graph theory will provide an objective marker for predicting the course of a disease and for monitoring network recovery following damage (Bassett and Bullmore, 2009). A fruitful endeavour would be to leverage this knowledge to guide our application of theoretical computer modelling in the future.

Finally, a burgeoning literature presents the brain as a self-organised system operating at or near criticality (Beggs and Timme, 2012). Whilst there is substantial evidence that critical dynamics are an important component of brain activity, particularly in the resting state, understanding how critical dynamics relate not only to structure but also to cognition is

an interesting open question. For example, dependent on cognitive state, focused attention appears to modulate signatures of criticality in the brain, driving the brain's activity toward sub-critical dynamics. Future studies, incorporating multiple temporal and spatial scales are required to synthesise these observations across a range of behavioural states and to pivot the field away from epiphenomenal observations of self-organised criticality in the resting brain, toward understanding how network organisation informs neural activity in higher order cognitive function.

# 8 Appendices

## 8.1 Graph theoretic measures of structural topology

In the following, the weight of an edge between nodes $i$ and $j$ of graph $G$ with $N$ nodes corresponds to $G_{ij}$.

The *degree* is defined as the number of edges incident to a node or vertex:

$$k_i = \sum_{j=1}^{N} bin(G_{ij})$$

where $bin(G_{ij})$ is the binarised version of $G_{ij}$ equal to one where $G_{ij} > 0$ and zero otherwise. The *strength* of a node is the weighted analogue of degree, or sum of weights of a node's edges:

$$s_i = \sum_{j=1}^{N} G_{ij}$$

The *eigenvector* centrality of a node is high when it is has many connections (it is topologically important) or when it has few connections but is directly connected to a topologically important node:

$$e_i = \frac{1}{\lambda} \sum_{j=1}^{N} G_{ij} e_j$$

where $\lambda$ signifies the largest eigenvalue of $G_{ij}$ and $e$ the corresponding principal eigenvector.

The *clustering coefficient* is a measure of local integration/segregation. It quantifies the weighted fraction of edges that exist between a node's direct neighbours:

$$clust_i = \frac{1}{k_i(k_i - 1)} \sum_{j,k \epsilon N} (G_{ij} G_{ik} G_{jk})^{1/3}$$

The *global efficiency* is defined as the average of the inverse shortest path length between all pairs of nodes within the network.

The *local efficiency* of a node is the local analogue of global efficiency computed over the node's local neighbourhood. Thus, it is the inverse average shortest path length between a node's neighbours. The local efficiency is related to the clustering coefficient and is a measure of integration/segregation:

$$E_{loci} = E_{glob}(g_i) = \frac{1}{n(n-1)} \sum_{j \neq k \epsilon g_i} \frac{1}{d_{jk}}$$

where $g_i$ is the sub-graph consisting of the total $n$ neighbours of node $i$, and $d_{jk}$ is the shortest topological distance between nodes $j$ and $k$ within sub-graph $gi$. In weighted graphs, the shortest distance is calculated using topological lengths acquired by inversely mapping connectivity weights. Thus, stronger weights $1/G_{ij}$correspond to shorter distances and vice versa.

The weighted *participation coefficient* of a node captures the diversity of inter-module links. The participation coefficient will tend toward one for a node that shares its connections evenly between all modules and zero otherwise:

$$p_i = 1 - \sum_{m \epsilon M} \frac{s_i(m)}{s_i}^2$$

where $M$ is the set of modules and $S_i(m)$ is the strength of connections between node $i$ and all nodes in module $M$.

## 8.2 Subject data

Enrolled subjects were 55 to 90 (inclusive) years old with a minimum 6th-grade level of education; had a study partner able to provide an independent evaluation of functioning; could speak either English or Spanish; had adequate visual and auditory acuity to allow neuropsychological testing; were willing and able to undergo all test procedures, including neuroimaging; and agreed to longitudinal follow-up investigations. All subjects were without significant neurologic disease, major depression, history of schizophrenia or bipolar disorder, recent history of alcohol or substance abuse, pacemakers or other objects deemed unsafe for MRI. Those prescribed specific psychoactive medications were also excluded. Diagnostic groups were defined as follows. Cognitively Normal Subjects: MMSE scores between 24-30 (inclusive), a CDR of 0, non-depressed, non-MCI, and non-demented, education adjusted scores on delayed recall of one paragraph from WMS-R ( 9 for 16 or more years of education, 5 for 8-15 years of education, 3 for 0-7 years of education). MCI Subjects: MMSE scores between 24-30 (inclusive), a subjective memory concern reported by subject, informant, or clinician, objective memory loss measured by education adjusted scores on delayed recall of one paragraph from WMS-R ( 16 years: 9-11; 8-15 years: 5-9; 0-7 years: 3-6), a CDR of 0.5, absence of significant levels of impairment in other cognitive domains, essentially preserved activities of daily living, and an absence of dementia. AD Subjects: MMSE scores between 20-26 (inclusive), a CDR of 0.5 or 1.0, and meets National Institute of Neurological and Communicative Disorders and Stroke and the Alzheimer's Disease and Related Disorders Association criteria for probable AD.

## 8.3 Demographics of fMRI subjects

| | HC(n=36) | aMCI (n=33) | AD (n=34) |
|---|---|---|---|
| **Gender** | 17M,19F | 10M,13F | 16M,18F |
| **Age** | 74.46 ± 5.51 | 73.61 ± 5.60 | 73.79 ± 6.14 |
| **MMSE** | 29.17 ± 1.52 | 26.86 ± 2.58 | 19.32 ± 4.37 |
| **GDS** | 0.72 ± 1.11 | 2.39 ± 2.79 | 2.06 ± 1.43 |
| **CDR** | 0.04 ± 0.14 | 0.5 ± 0.18 | 0.94 ± 0.27 |
| **FAQ** | 0.14 ± 0.68 | 4.48 ± 4.65 | 16.59 ± 5.91 |
| **NPI** | 0.58 ± 1.25 | 3.63 ± 3.81 | 5.29 ± 3.59 |

Table 8.1: Standard deviations are indicated. MMSE, Mini-Mental State Exam; GDS, Geriatric Depression Scale; CDR, Clinical Dementia Rating Scale; FAQ, Functional Assessment Questionnaire; NPI, Neuropsychiatric Inventory.

## 8.4 Demographics of DTI subjects

| | HC(n=30) | aMCI (n=30) | AD (n=30) |
|---|---|---|---|
| **Gender** | 15M,15F | 17M,13F | 18M,12F |
| **Age** | 73.69 ± 6.88 | 75.07 ± 7.14 | 77.13 ± 7.74 |
| **MMSE** | 28.95 ± 1.15 | 27.81 ± 1.69 | 22.31 ± 3.69 |
| **GDS** | 0.91 ± 1.12 | 1.68 ± 1.59 | 1.79 ± 1.68 |
| **CDR** | 0.03 ± 0.11 | 0.36 ± 0.27 | 0.93 ± 0.29 |
| **FAQ** | 0.43 ± 1.44 | 2.27 ± 3.32 | 16.66 ± 5.01 |
| **NPI** | 0.47 ± 1.37 | 3.11 ± 3.08 | 4.21 ± 4.16 |

Table 8.2: Standard deviations are indicated. MMSE, Mini-Mental State Exam; GDS, Geriatric Depression Scale; CDR, Clinical Dementia Rating Scale; FAQ, Functional Assessment Questionnaire; NPI, Neuropsychiatric Inventory.

## 8.5 High-degree hubs of the rich-club are selectively vulnerability to damage

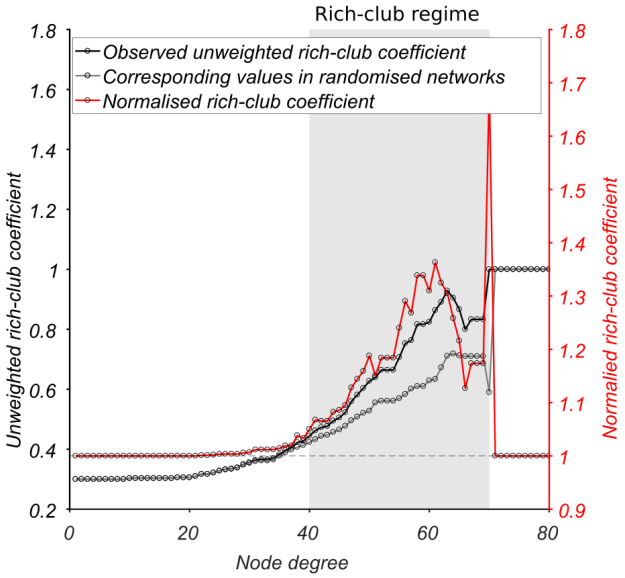


Figure 8.1: Normalised unweighted rich-club coefficient curve $\phi_{norm}(k)$ (in red) for the healthy group-averaged structural brain network over degrees $k$. Characteristic rich-club organisation with $\phi_{norm}(k) > 1$ is present between $k = 40$ and $k = 70$.

## 8.6 Fitting simulated synchronisation dynamics to empirical data

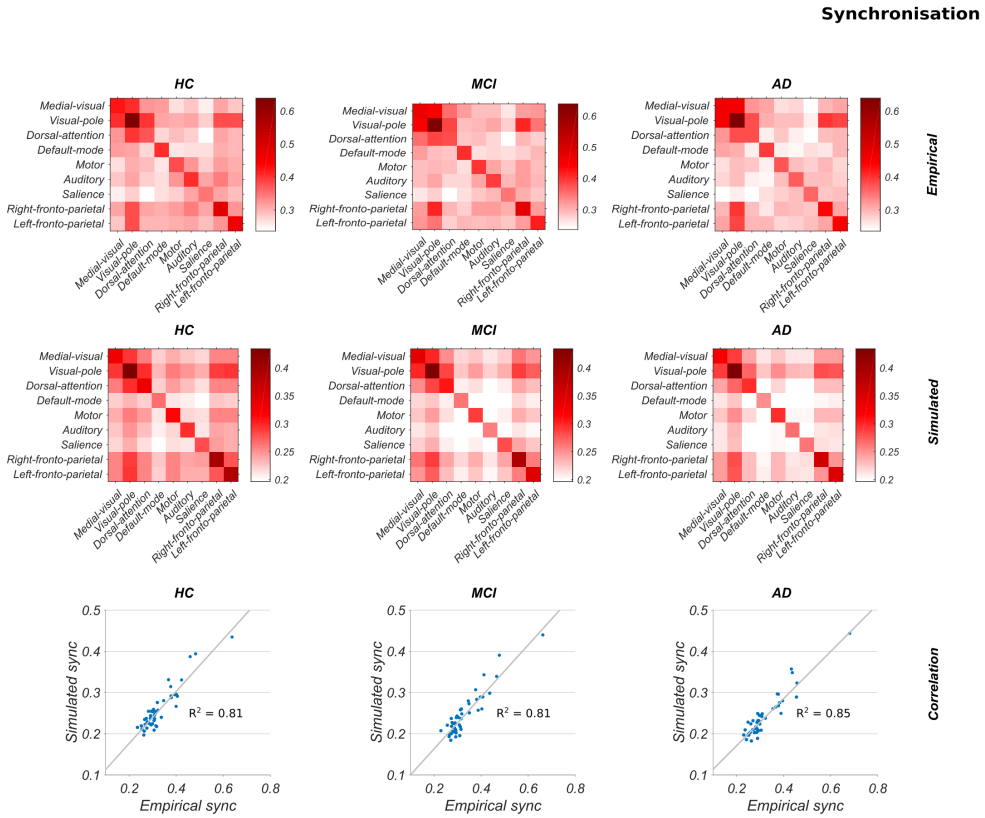


Figure 8.2: Empirical (top) and simulated (middle) synchrony between resting state networks at the chosen NBS threshold. Empirical data was estimated from fMRI BOLD signal and represents the mean for all subjects within a group. Simulated data are from a computer model with coupling between nodes informed at the group-level. The oscillators were provided with a random initial phase prior to each run of the model. The overall mean of several runs is reported. All subject groups showed a strong correlation between empirical and simulated synchrony (bottom).

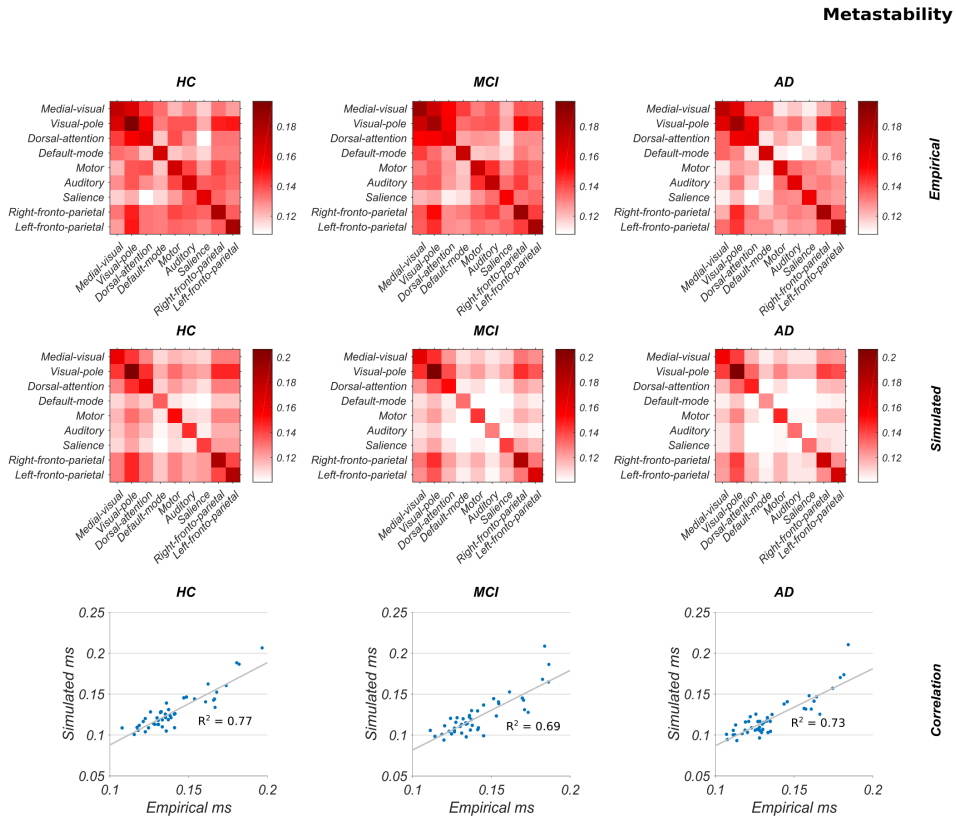


Figure 8.3: Empirical (top) and simulated (middle) metastability between resting state networks at the chosen NBS threshold. Empirical data was estimated from fMRI BOLD signal and represents the mean for all subjects within a group. Simulated data are from a computer model with coupling between nodes informed at the group-level. The oscillators were provided with a random initial phase prior to each run of the model. The overall mean of several runs is reported. All subject groups showed a strong correlation between empirical and simulated metastability (bottom).

## 8.7 Nodes identified by joint NBS and modelling approach

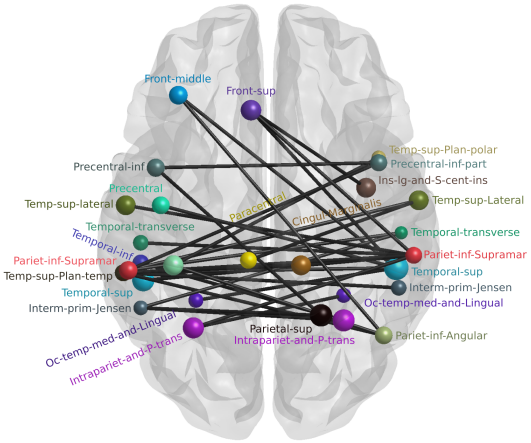


Figure 8.4: The disconnected FA sub-network (axial plane) identified by the NBS (p = 0.001; corrected) and model-fitting procedure in the MCI cohort corresponding to the t-statistic threshold of 3.4. Nodes of the Destrieux atlas drawn at the centre of mass of their respective cortical parcellation with diameter proportional to degree.

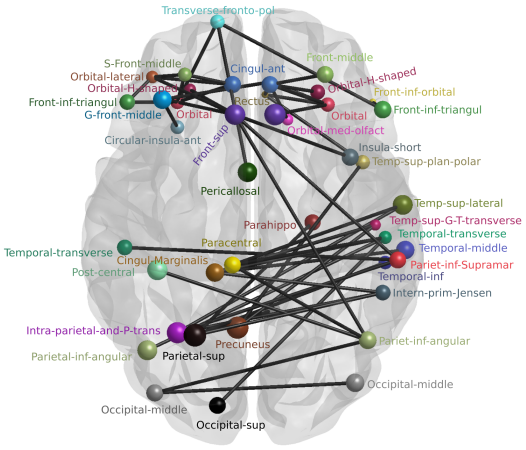


Figure 8.5: The disconnected FA sub-network (axial plane) identified by the NBS (p = 0.0001; corrected) and model-fitting procedure in the AD cohort corresponding to the t-statistic threshold of 4.8. Nodes of the Destrieux atlas drawn at the centre of mass of their respective cortical parcellation with diameter proportional to degree.

# Bibliography

Abuhassan, K., Coyle, D., Belatreche, A. and Maguire, L. (2014), 'Compensating for synaptic loss in Alzheimer's disease.', *Journal of computational neuroscience* **36**(1), 19–37.

Abuhassan, K., Coyle, D. and Maguire, L. P. (2012), 'Investigating the neural correlates of pathological cortical networks in Alzheimer's disease using heterogeneous neuronal models.', *IEEE transactions on bio-medical engineering* **59**(3), 890–6.

Acebrón, J. a., Bonilla, L. L., Vicente, C. J. P., Ritort, F. and Spigler, R. (2005), 'The Kuramoto model: A simple paradigm for synchronization phenomena', *Reviews of Modern Physics* **77**(1), 137–185.

Achard, S., Salvador, R., Whitcher, B., Suckling, J. and Bullmore, E. (2006), 'A resilient, low-frequency, small-world human brain functional network with highly connected association cortical hubs.', *The Journal of neuroscience : the official journal of the Society for Neuroscience* **26**(1), 63–72.

Acosta-Cabronero, J., Alley, S., Williams, G. B., Pengas, G. and Nestor, P. J. (2012), 'Diffusion Tensor Metrics as Biomarkers in Alzheimer's Disease', *PLoS ONE* **7**(11), e49072.

Acosta-Cabronero, J. and Nestor, P. J. (2014), 'Diffusion tensor imaging in Alzheimer's disease: insights into the limbic-diencephalic network and methodological considerations.', *Frontiers in aging neuroscience* **6**, 266.

Afraimovich, V. S., Rabinovich, M. I. and Varona, P. (2004), 'Heteroclinic contours in neural ensembles and the winnerless competition principle', *International Journal of Bifurcation and Chaos in Applied Sciences and Engineering* .

Aggleton, J. P., O'Mara, S. M., Vann, S. D., Wright, N. F., Tsanov, M., Erichsen, J. T., O'Mara, S. M., Vann, S. D., Wright, N. F., Tsanov, M. and Erichsen, J. T. (2010), 'Hippocampal-anterior thalamic pathways for memory: Uncovering a network of direct and indirect actions', *European Journal of Neuroscience* **31**(12), 2292–2307.

Alcaraz, F., Fresno, V., Marchand, A. R., Kremer, E. J., Coutureau, E. and Wolff, M. (2018), 'Thalamocortical and corticothalamic pathways differentially contribute to goal-directed behaviors in the rat', *eLife* .

Alderson, T. H., Bokde, A. L., Kelso, J., Maguire, L. and Coyle, D. (2018), 'Metastable neural dynamics in Alzheimer's disease are disrupted by lesions to the structural connectome', *NeuroImage* **183**, 438–455.

Alderson, T., Kehoe, E., Maguire, L., Farrell, D., Lawlor, B., Kenny, R., Lyons, D., Bokde, A. and Coyle, D. (2017), 'Disrupted thalamus white matter anatomy and posterior default mode network effective connectivity in amnestic mild cognitive impairment', *Frontiers in Aging Neuroscience* **9**(NOV).

Allen, E. A., Damaraju, E., Plis, S. M., Erhardt, E. B., Eichele, T. and Calhoun, V. D. (2014), 'Tracking whole-brain connectivity dynamics in the resting state', *Cerebral Cortex* **24**(3), 663–676.

Alstott, J., Breakspear, M., Hagmann, P., Cammoun, L. and Sporns, O. (2009), 'Modeling the impact of lesions in the human brain.', *PLoS computational biology* **5**(6), e1000408.

Alzheimer's Disease International (2008), 'The prevalence of dementia worldwide', *Alzheimer's Disease International* .

Amlien, I. K. and Fjell, A. M. (2014), 'Diffusion tensor imaging of white matter degeneration in Alzheimer's disease and mild cognitive impairment', *Neuroscience* **276**, 206–15.

Andersson, J. L. R., Jenkinson, M. and Smith, S. M. (2007), Non-linear registration aka Spatial normalisation FMRIB Technial Report TR07JA2, Technical report.

Andersson, J. L. and Sotiropoulos, S. N. (2016), 'An integrated approach to correction for off-resonance effects and subject movement in diffusion MR imaging', *NeuroImage* **125**, 1063–1078.

Andreasen, N. C., O'Leary, D. S., Cizadlo, T., Arndt, S., Rezai, K., Watkins, G. L., Ponto, L. L. B. and Hichwa, R. D. (1995), 'Remembering the past: Two facets of episodic memory explored with positron emission tomography', *American Journal of Psychiatry* **152**(11), 1576–1585.

Ashburner, J. (2012), 'SPM: A history', *NeuroImage* **62**(2), 791–800.

Ashwin, P. and Postlethwaite, C. (2013), 'On designing heteroclinic networks from graphs', *Physica D: Nonlinear Phenomena* .

Aung, W. Y., Mar, S. and Benzinger, T. L. (2013), 'Diffusion tensor MRI as a biomarker in axonal and myelin damage.', *Imaging in medicine* **5**(5), 427–440.

Badhwar, A., Tam, A., Dansereau, C., Orban, P., Hoffstaedter, F. and Bellec, P. (2017), 'Resting-state network dysfunction in Alzheimer's disease: A systematic review and meta-analysis', *Alzheimer's & Dementia: Diagnosis, Assessment & Disease Monitoring* **8**, 73–85.

Bak, P. and Chialvo, D. D. (2001), 'Adaptive learning by extremal dynamics and negative feedback', *Physical Review E - Statistical Physics, Plasmas, Fluids, and Related Interdisciplinary Topics* **63**(3).

Bak, P., Tang, C. and Wiesenfeld, K. (1987), 'Self-organized criticality: An explanation of the 1/f noise', *Physical Review Letters* **59**(4), 381–384.

Balaguer-Ballester, E., Moreno-Bote, R., Deco, G. and Durstewitz, D. (2018), 'Editorial: Metastable Dynamics of Neural Ensembles', *Frontiers in systems neuroscience* **11**.

Bandettini, P. A. (2012), 'Twenty years of functional MRI: The science and the stories'.

Barbey, A. K. (2018), 'Network Neuroscience Theory of Human Intelligence'.

Barch, D. M., Burgess, G. C., Harms, M. P., Petersen, S. E., Schlaggar, B. L., Corbetta, M., Glasser, M. F., Curtiss, S., Dixit, S., Feldt, C., Nolan, D., Bryant, E., Hartley, T., Footer, O., Bjork, J. M., Poldrack, R., Smith, S., Johansen-Berg, H., Snyder, A. Z. and Van Essen, D. C. (2013), 'Function in the Human Connectome: Task-fMRI and Individual Differences in Behavior', *NeuroImage* **80**, 169–189.

Basser, P. J., Pajevic, S., Pierpaoli, C., Duda, J. and Aldroubi, A. (2000), 'In vivo fiber tractography using DT-MRI data', *Magnetic Resonance in Medicine* .

Basser, P. J. and Pierpaoli, C. (1996), 'Microstructural and physiological features of tissues elucidated by quantitative-diffusion-tensor MRI', *Journal of Magnetic Resonance - Series B* .

Basser, P. J. and Pierpaoli, C. (1998), 'A simplified method to measure the diffusion tensor from seven MR images', *Magnetic Resonance in Medicine* .

Bassett, D. S., Brown, J. a., Deshpande, V., Carlson, J. M. and Grafton, S. T. (2011), 'Conserved and variable architecture of human white matter connectivity', *NeuroImage* **54**(2), 1262–1279.

Bassett, D. S. and Bullmore, E. (2006), 'Small-world brain networks.', *The Neuroscientist : a review journal bringing neurobiology, neurology and psychiatry* **12**(6), 512–23.

Bassett, D. S. and Bullmore, E. T. (2009), 'Human brain networks in health and disease.', *Current opinion in neurology* **22**(4), 340–7.

Bassett, D. S. and Bullmore, E. T. (2017), 'Small-World Brain Networks Revisited'.

Bassett, D. S., Khambhati, A. N. and Grafton, S. T. (2017), 'Emerging Frontiers of Neuroengineering: A Network Science of Brain Connectivity', *Annual Review of Biomedical Engineering* **19**(1), 327–352.

Bassett, D. S. and Sporns, O. (2017), 'Network neuroscience', *Nature Neuroscience* .

Bassett, D. S., Wymbs, N. F., Rombach, M. P., Porter, M. A., Mucha, P. J. and Grafton, S. T. (2013), 'Task-Based Core-Periphery Organization of Human Brain Dynamics', *PLoS Computational Biology* **9**(9).

Bassett, D. S., Yang, M., Wymbs, N. F. and Grafton, S. T. (2015), 'Learning-Induced Autonomy of Sensorimotor Systems', *Nature neuroscience* **18**(5), 744–751.

Bassett, D. S., Zurn, P. and Gold, J. I. (2018), 'On the nature and use of models in network neuroscience'.

Basso, M. A., Uhlrich, D. and Bickford, M. E. (2005), 'Cortical function: a view from the thalamus.', *Neuron* **45**(4), 485–8.

Beckmann, C. F. (2012), 'Modelling with independent components', *NeuroImage* **62**(2), 891–901.

Beckmann, C. F., DeLuca, M., Devlin, J. T. and Smith, S. M. (2005), 'Investigations into resting-state connectivity using independent component analysis', *Philosophical Transactions of the Royal Society B: Biological Sciences* **360**(1457), 1001–1013.

Beckmann, C. F. and Smith, S. M. (2004), 'Probabilistic Independent Component Analysis for Functional Magnetic Resonance Imaging', *IEEE Transactions on Medical Imaging* **23**, 137–152.

Beckmann, C., Mackay, C., Filippini, N. and Smith, S. M. (2009), 'Group comparison of resting-state FMRI data using multi-subject ICA and dual regression', *NeuroImage* **47**, S148.

Bedrosian, E. (1962), 'A Product Theorem for Hilbert Transforms', *Rand Corporation Memorandum (RM-3439-PR)* .

Beggs, J. M. and Plenz, D. (2003), 'Neuronal Avalanches in Neocortical Circuits', *The Journal of Neuroscience* **23**(35), 11167–11177.

Beggs, J. M. and Timme, N. (2012), 'Being critical of criticality in the brain', *Frontiers in Physiology* **3 JUN**.

Behrens, T. E. J., Johansen-Berg, H., Woolrich, M. W., Smith, S. M., Wheeler-Kingshott, C. a. M., Boulby, P. a., Barker, G. J., Sillery, E. L., Sheehan, K., Ciccarelli, O., Thompson, a. J., Brady, J. M. and Matthews, P. M. (2003), 'Non-invasive mapping of connections between human thalamus and cortex using diffusion imaging.', *Nature neuroscience* **6**(7), 750–7.

Behrens, T. E. J. and Sporns, O. (2012), 'Human connectomics.', *Current opinion in neurobiology* **22**(1), 144–53.

Berendse, H. W., Verbunt, J. P., Scheltens, P., Van Dijk, B. W. and Jonkman, E. J. (2000), 'Magnetoencephalographic analysis of cortical activity in Alzheimer's disease: A pilot study', *Clinical Neurophysiology* .

Bero, A. W., Yan, P., Roh, J. H., Cirrito, J. R., Stewart, F. R., Raichle, M. E., Lee, J. M. and Holtzman, D. M. (2011), 'Neuronal activity regulates the regional vulnerability to amyloid-beta deposition', *Nature Neuroscience* **14**(6), 750–756.

Bersini, H. and Sener, P. (2002), 'The connections between the frustrated chaos and the intermittency chaos in small Hopfield networks', *Neural Networks* .

Bhattacharya, B. S., Cakir, Y., Serap-Sengor, N., Maguire, L. and Coyle, D. (2013), 'Model-based bifurcation and power spectral analyses of thalamocortical alpha rhythm slowing in Alzheimer's Disease', *Neurocomputing* **115**, 11–22.

Bhattacharya, B. S., Coyle, D. and Maguire, L. P. (2011), 'Alpha and theta rhythm abnormality in Alzheimer's Disease: a study using a computational model.', *Advances in experimental medicine and biology* **718**, 57–73.

Binder, J. R. (2012), 'Task-induced deactivation and the resting state', *NeuroImage* **62**(2), 1086–1091.

Binder, J. R., Gross, W. L., Allendorfer, J. B., Bonilha, L., Chapin, J., Edwards, J. C., Grabowski, T. J., Langfitt, J. T., Loring, D. W., Lowe, M. J., Koenig, K., Morgan, P. S., Ojemann, J. G., Rorden, C., Szaflarski, J. P., Tivarus, M. E. and Weaver, K. E. (2011), 'Mapping Anterior Temporal Lobe Language Areas with fMRI: A Multicenter Normative Study', *NeuroImage* **54**(2), 1465–1475.

Biswal, B. B. (2012), 'Resting state fMRI: a personal history.', *NeuroImage* **62**(2), 938–44.

Blamire, A. M. (2012), 'The Yale experience in first advancing fMRI'.

Bloch, F. (1951), 'Nuclear induction', *Physica* .

Bloch, F. (1953), 'The principle of nuclear induction', *Science* .

Bloch, F., Hansen, W. W. and Packard, M. (1946), 'The nuclear induction experiment', *Physical Review* .

Boashash, B. (1992), 'Estimating and Interpreting The Instantaneous Frequency of a Signal—Part 1: Fundamentals', *Proceedings of the IEEE* .

Bolt, T., Anderson, M. L. and Uddin, L. Q. (2018), 'Beyond the Evoked/Intrinsic Neural Process Dichotomy.', *Network neuroscience (Cambridge, Mass.)* **2**(1), 1–22.

Boly, M., Balteau, E., Schnakers, C., Degueldre, C., Moonen, G., Luxen, A., Phillips, C., Peigneux, P., Maquet, P. and Laureys, S. (2007), 'Baseline brain activity fluctuations predict somatosensory perception in humans', *Proceedings of the National Academy of Sciences* **104**(29), 12187–12192.

Boly, M., Phillips, C., Tshibanda, L., Vanhaudenhuyse, A., Schabus, M., Dang-Vu, T. T., Moonen, G., Hustinx, R., Maquet, P. and Laureys, S. (2008), Intrinsic brain activity in altered states of consciousness: How conscious is the default mode of brain function?, *in* 'Annals of the New York Academy of Sciences', Vol. 1129, pp. 119–129.

Bonnelle, V., Ham, T. E., Leech, R., Kinnunen, K. M., Mehta, M. A., Greenwood, R. J. and Sharp, D. J. (2012), 'Salience network integrity predicts default mode network function after traumatic brain injury.', *Proceedings of the National Academy of Sciences of the United States of America* **109**(12), 4690–4695.

Bonnelle, V., Leech, R., Kinnunen, K. M., Ham, T. E., Beckmann, C. F., De Boissezon, X., Greenwood, R. J. and Sharp, D. J. (2011), 'Default Mode Network Connectivity Predicts Sustained Attention Deficits after Traumatic Brain Injury', *Journal of Neuroscience* **31**(38), 13442–13451.

Boyacioglu, R. and Barth, M. (2013), 'Generalized inverse imaging (GIN): Ultrafast fMRI with physiological noise correction', *Magnetic Resonance in Medicine* **70**(4), 962–971.

Braak, E., Griffing, K., Arai, K., Bohl, J., Bratzke, H. and Braak, H. (1999), 'Neuropathology of Alzheimer's disease: what is new since A. Alzheimer?', *European archives of psychiatry and clinical neuroscience* **249 Suppl**, 14–22.

Braak, H. and Braak, E. (1991*a*), 'Alzheimer's disease affects limbic nuclei of the thalamus.', *Acta neuropathologica* **81**, 261–268.

Braak, H. and Braak, E. (1991*b*), 'Demonstration of Amyloid Deposits and Neurofibrillary Changes in Whole Brain Sections', *Brain Pathology* **1**(3), 213–216.

Braak, H. and Braak, E. (1991*c*), 'Neuropathological stageing of Alzheimer-related changes.', *Acta neuropathologica* **82**, 239–259.

Braak, H. and Braak, E. (1995), 'Staging of Alzheimer's disease-related neurofibrillary changes', *Neurobiology of Aging* **16**(3), 271–278.

Braitenberg, V. and Schuz, A. (1991), *Anatomy of the Cortex*, Springer, Berlin.

Braun, J. and Mattia, M. (2010), 'Attractors and noise: Twin drivers of decisions and multistability'.

Braun, U., Schäfer, A., Walter, H., Erk, S., Romanczuk-Seiferth, N., Haddad, L., Schweiger, J. I., Grimm, O., Heinz, A., Tost, H., Meyer-Lindenberg, A. and Bassett, D. S. (2015), 'Dynamic reconfiguration of frontal brain networks during executive cognition in humans.', *Proceedings of the National Academy of Sciences of the United States of America* **112**(37), 11678–83.

Breakspear, M. (2017), 'Dynamic models of large-scale brain activity.', *Nature Neuroscience* **20**(3), 340–352.

Breakspear, M., Terry, J. R. and Friston, K. (2003), 'Modulation of excitatory synaptic coupling facilitates synchronization and complex dynamics in a biophysical model of neuronal dynamics.', *Network* **14**, 703–732.

Bressler, S. L. (1995), 'Large-scale cortical networks and cognition'.

Bressler, S. L. (2002), 'Understanding cognition through large-scale cortical networks', *Current Directions in Psychological Science* **11**(2), 58–61.

Bressler, S. L., Coppola, R. and Nakamura, R. (1993), 'Episodic multiregional cortical coherence at multiple frequencies during visual task performance', *Nature* .

Bressler, S. L. and Kelso, J. (2001), 'Cortical Coordination Dynamics and Cognition'.

Bressler, S. L. and Kelso, J. (2016), 'Coordination Dynamics in Cognitive Neuroscience', *Frontiers in Neuroscience* **10**, 397.

Bressler, S. L. and Mcintosh, A. R. (2007), 'The role of neural context in large-scale neurocognitive network operations', *Understanding Complex Systems* **2007**, 403–419.

Bressler, S. L. and Menon, V. (2010), 'Large scale brain networks in cognition', *Trends in cognitive Sciences* **14**(6), 278–291.

Bressler, S. L., Tang, W., Sylvester, C. M., Shulman, G. L. and Corbetta, M. (2008), 'Top-down control of human visual cortex by frontal and parietal cortex in anticipatory visual spatial attention.', *The Journal of neuroscience : the official journal of the Society for Neuroscience* **28**(40), 10056–61.

Bressler, S. L. and Tognoli, E. (2006), 'Operational principles of neurocognitive networks', *International Journal of Psychophysiology* **60**(2), 139–148.

Bridle, J. S. (1990), Probabilistic Interpretation of Feedforward Classification Network Outputs, with Relationships to Statistical Pattern Recognition, *in* 'Neurocomputing', pp. 227–236.

Brier, M. R., Thomas, J. B. and Ances, B. M. (2014), 'Network dysfunction in Alzheimer's disease: refining the disconnection hypothesis.', *Brain connectivity* **4**(5), 299–311.

Broca, P. (1861), 'Remarques sur le siége de la faculté du langage articulé, suivies d ' une observation d 'aphémie (perte de la parole)', *Bulletin de la Société Anatomique de Paris 6* pp. 330 – 357.

Brookmeyer, R., Johnson, E., Ziegler-Graham, K. and Arrighi, H. M. (2007), 'Forecasting the global burden of Alzheimer's disease', *Alzheimer's and Dementia* .

Brovelli, A., Ding, M., Ledberg, A., Chen, Y., Nakamura, R. and Bressler, S. L. (2004), 'Beta oscillations in a large-scale sensorimotor cortical network: Directional influences revealed by Granger causality', *Proceedings of the National Academy of Sciences of the United States of America* .

Brun, A. and Englund, E. (1986), 'A white matter disorder in dementia of the Alzheimer type: A pathoanatomical study', *Annals of Neurology* **19**(3), 253–262.

Buckner, R. L., Andrews-Hanna, J. R. and Schacter, D. L. (2008), 'The brain's default network: anatomy, function, and relevance to disease.', *Annals of the New York Academy of Sciences* **1124**, 1–38.

Buckner, R. L. and Carroll, D. C. (2007), 'Self-projection and the brain', *Trends in Cognitive Sciences* **11**(2), 49–57.

Buckner, R. L., Krienen, F. M., Castellanos, A., Diaz, J. C. and Yeo, B. T. T. (2011), 'The Organization of the Human Cerebellum Estimated by Intrinsic Functional Connectivity', *Journal of Neurophysiology* **106**(5), 2322–2345.

Buckner, R. L., Sepulcre, J., Talukdar, T., Krienen, F. M., Liu, H., Hedden, T., Andrews-Hanna, J. R., Sperling, R. a. and Johnson, K. a. (2009), 'Cortical hubs revealed by intrinsic functional connectivity: mapping, assessment of stability, and relation to Alzheimer's disease.', *The Journal of neuroscience : the official journal of the Society for Neuroscience* **29**(6), 1860–73.

Buckner, R. L., Snyder, A. Z., Shannon, B. J., LaRossa, G., Sachs, R., Fotenos, A. F., Sheline, Y. I., Klunk, W. E., Mathis, C. a., Morris, J. C. and Mintun, M. a. (2005), 'Molecular, structural, and functional characterization of Alzheimer's disease: evidence for a relationship between default activity, amyloid, and memory.', *The Journal of neuroscience : the official journal of the Society for Neuroscience* **25**(34), 7709–17.

Bullmore, E. (2012), 'The future of functional MRI in clinical medicine', *NeuroImage* **62**(2), 1267–1271.

Bullmore, E. and Sporns, O. (2009), 'Complex brain networks: Graph theoretical analysis of structural and functional systems', *Nature Reviews Neuroscience* **10**(3), 186–198.

Bullmore, E. and Sporns, O. (2012), 'The economy of brain network organization'.

Burgess, G. C., Kandala, S., Nolan, D., Laumann, T. O., Power, J. D., Adeyemo, B., Harms, M. P., Petersen, S. E. and Barch, D. M. (2016), 'Evaluation of Denoising Strategies to Address Motion-Correlated Artifacts in Resting-State Functional Magnetic Resonance Imaging Data from the Human Connectome Project', *Brain Connectivity* **6**(9), 669–680.

Burns, A. and Iliffe, S. (2009), 'Alzheimer's disease.', *BMJ (Clinical research ed.)* **338**, b158.

Busch, N. A., Dubois, J. and VanRullen, R. (2009), 'The Phase of Ongoing EEG Oscillations Predicts Visual Perception', *Journal of Neuroscience* **29**(24), 7869–7876.

Bush, P. C. and Sejnowski, T. J. (1994), 'Effects of inhibition and dendritic saturation in simulated neocortical pyramidal cells', *Journal of Neurophysiology* **71**, 2183–2193.

Buzsáki, G., Geisler, C., Henze, D. A. and Wang, X. J. (2004), 'Interneuron Diversity series: Circuit complexity and axon wiring economy of cortical interneurons'.

Cabral, J., Fernandes, H. M., Van Hartevelt, T. J., James, A. C., Kringelbach, M. L. and Deco, G. (2013), 'Structural connectivity in schizophrenia and its impact on the dynamics of spontaneous functional networks', *Chaos* **23**(4).

Cabral, J., Hugues, E., Kringelbach, M. L. and Deco, G. (2012), 'Modeling the outcome of structural disconnection on resting-state functional connectivity', *NeuroImage* **62**(3), 1342–1353.

Cabral, J., Hugues, E., Sporns, O. and Deco, G. (2011), 'Role of local network oscillations in resting-state functional connectivity.', *NeuroImage* **57**(1), 130–9.

Cabral, J., Kringelbach, M. L. and Deco, G. (2012), 'Functional graph alterations in schizophrenia: a result from a global anatomic decoupling?', *Pharmacopsychiatry* **45 Suppl 1**, 57–64.

Cabral, J., Kringelbach, M. L. and Deco, G. (2014), 'Exploring the Network Dynamics Underlying Brain Activity During Rest', *Progress in Neurobiology* **114**, 102–131.

Cabral, J., Kringelbach, M. L. and Deco, G. (2017), 'Functional connectivity dynamically evolves on multiple time-scales over a static structural connectome : Models and mechanisms', *NeuroImage* (March), 0–1.

Cammoun, L., Gigandet, X., Meskaldji, D., Thiran, J. P., Sporns, O., Do, K. Q., Maeder, P., Meuli, R. and Hagmann, P. (2012), 'Mapping the human connectome at multiple scales with diffusion spectrum MRI', *Journal of Neuroscience Methods* **203**(2), 386–397.

Cantero, J. L., Atienza, M., Gomez-Herrero, G., Cruz-Vadell, A., Gil-Neciga, E., Rodriguez-Romero, R. and Garcia-Solis, D. (2009), 'Functional integrity of thalamocortical circuits differentiates normal aging from mild cognitive impairment.', *Human brain mapping* **30**(12), 3944–57.

Caso, F., Agosta, F. and Filippi, M. (2016), 'Insights into White Matter Damage in Alzheimer's Disease: From Postmortem to in vivo Diffusion Tensor MRI Studies', *Neurodegenerative Diseases* **16**(1-2), 26–33.

Castelli, F., Happé, F., Frith, U. and Frith, C. (2013), Movement and mind: A Functional Imaging Study of Perception and Interpretation of Complex Intentional Movement Patterns, *in* 'Social Neuroscience: Key Readings', pp. 155–170.

Catani, M. (2006), 'Diffusion tensor magnetic resonance imaging tractography in cognitive disorders.', *Current opinion in neurology* **19**(6), 599–606.

Catani, M. and Ffytche, D. H. (2005), 'The rises and falls of disconnection syndromes.', *Brain : a journal of neurology* **128**(Pt 10), 2224–39.

Catani, M. and Mesulam, M. (2008), 'The arcuate fasciculus and the disconnection theme in language and aphasia: History and current state', *Cortex* **44**(8), 953–961.

Chen, B., Xu, T., Zhou, C., Wang, L., Yang, N., Wang, Z., Dong, H.-M., Yang, Z., Zang, Y.-F., Zuo, X.-N. and Weng, X.-C. (2015), 'Individual Variability and Test-Retest Reliability Revealed by Ten Repeated Resting-State Brain Scans over One Month.', *PloS one* **10**(12), e0144963.

Chen, J., Zhang, Z. and Li, S. (2015), 'Can multi-modal neuroimaging evidence from hippocampus provide biomarkers for the progression of amnestic mild cognitive impairment?', *Neuroscience Bulletin* **31**(1), 128–140.

Cherubini, A., Péran, P., Spoletini, I., Di Paola, M., Di Iulio, F., Hagberg, G. E., Sancesario, G., Gianni, W., Bossù, P., Caltagirone, C., Sabatini, U. and Spalletta, G. (2010), 'Combined volumetry and DTI in subcortical structures of mild cognitive impairment and Alzheimer's disease patients.', *Journal of Alzheimer's disease : JAD* **19**, 1273–1282.

Chételat, G., Landeau, B., Eustache, F., Mézenge, F., Viader, F., de la Sayette, V., Desgranges, B. and Baron, J.-C. (2005), 'Using voxel-based morphometry to map the structural changes associated with rapid conversion in MCI: a longitudinal MRI study.', *NeuroImage* **27**(4), 934–46.

Chhatwal, J. P., Schultz, A. P., Johnson, K., Benzinger, T. L. S., Jack, C., Ances, B. M., Sullivan, C. a., Salloway, S. P., Ringman, J. M., Koeppe, R. a., Marcus, D. S., Thompson, P., Saykin, A. J., Correia, S., Schofield, P. R., Rowe, C. C., Fox, N. C., Brickman, A. M., Mayeux, R., McDade, E., Bateman, R., Fagan, A. M., Goate, A. M., Xiong, C., Buckles, V. D., Morris, J. C. and Sperling, R. a. (2013), 'Impaired default network functional connectivity in autosomal dominant Alzheimer disease.', *Neurology* **81**(8), 736–44.

Chialvo, D. and Bak, P. (1999), 'Commentary: LEARNING FROM MISTAKES', *Neuroscience* **90**(4), 1137–1148.

Chiang, G. C., Zhan, W., Schuff, N. and Weiner, M. W. (2012), 'White matter alterations in cognitively normal apoE ??2 carriers: Insight into Alzheimer resistance?', *American Journal of Neuroradiology* **33**(7), 1392–1397.

Cirrito, J. R., Yamada, K. a., Finn, M. B., Sloviter, R. S., Bales, K. R., May, P. C., Schoepp, D. D., Paul, S. M., Mennerick, S. and Holtzman, D. M. (2005), 'Synaptic activity regulates interstitial fluid amyloid-beta levels in vivo', *Neuron* **48**(6), 913–922.

Clark, A. (2016), *Surfing Uncertainty: Prediction, Action, and the Embodied Mind*, Oxford University Press.

Cohen, J. R. (2018), 'The Behavioral and Cognitive Relevance of Time-varying, Dynamic Changes in Functional Connectivity', *NeuroImage* **180**(April 2017), 515–525.

Cole, M. W., Bassett, D. S., Power, J. D., Braver, T. S. and Petersen, S. E. (2014), 'Intrinsic and Task-evoked Network Architectures of the Human Brain', *Neuron* **83**(1), 238–251.

Cole, M. W., Repovš, G. and Anticevic, A. (2014), 'The Frontoparietal Control System: A Central Role in Mental Health.', *The Neuroscientist : a review journal bringing neurobiology, neurology and psychiatry* **20**(6), 652–64.

Cole, M. W., Reynolds, J. R., Power, J. D., Repovs, G., Anticevic, A. and Braver, T. S. (2013), 'Multi-task Connectivity Reveals Flexible Hubs for Adaptive Task Control', *Nature Neuroscience* **16**(9), 1348–1355.

Cole, M. W. and Schneider, W. (2007), 'The cognitive control network: Integrated cortical regions with dissociable functions', *NeuroImage* .

Cole, M. W., Yarkoni, T., Repovs, G., Anticevic, A. and Braver, T. S. (2012), 'Global Connectivity of Prefrontal Cortex Predicts Cognitive Control and Intelligence', *Journal of Neuroscience* **32**(26), 8988–8999.

Collin, G., Sporns, O., Mandl, R. C. W. and van den Heuvel, M. P. (2014), 'Structural and functional aspects relating to cost and benefit of rich club organization in the human cerebral cortex.', *Cerebral cortex (New York, N.Y. : 1991)* **24**(9), 2258–67.

Conway, A. R. A., Cowan, N., Bunting, M. F., Therriault, D. J. and Minkoff, S. R. B. (2002), 'A latent variable analysis of working memory capacity, short-term memory capacity, processing speed, and general fluid intelligence', *Intelligence* **30**(2), 163–183.

Córdova-Palomera, A., Kaufmann, T., Persson, K., Alnæs, D., Doan, N. T., Moberget, T., Lund, M. J., Barca, M. L., Engvig, A., Brækhus, A., Engedal, K., Andreassen, O. A., Selbæk, G. and Westlye, L. T. (2017), 'Disrupted global metastability and static and dynamic brain connectivity across individuals in the Alzheimer's disease continuum', *Scientific Reports* **7**, 40268.

Coste, C. P., Sadaghiani, S., Friston, K. and Kleinschmidt, A. (2011), 'Ongoing brain activity fluctuations directly account for intertrial and indirectly for intersubject variability in stroop task performance', *Cerebral Cortex* **21**(11), 2612–2619.

Cowan, J. D., Neuman, J. and van Drongelen, W. (2016), 'Wilson–Cowan Equations for Neocortical Dynamics', *Journal of Mathematical Neuroscience* .

Craddock, R. C., Jbabdi, S., Yan, C.-G., Vogelstein, J. T., Castellanos, F. X., Di Martino, A., Kelly, C., Heberlein, K., Colcombe, S. and Milham, M. P. (2013), 'Imaging human connectomes at the macroscale.', *Nature methods* **10**(6), 524–39.

Crossley, N. a., Mechelli, a., Scott, J., Carletti, F., Fox, P. T., McGuire, P. and Bullmore, E. T. (2014), 'The hubs of the human connectome are

generally implicated in the anatomy of brain disorders', *Brain* pp. 2117–2118.

Crossley, N. A., Mechelli, A., Vertes, P. E., Winton-Brown, T. T., Patel, A. X., Ginestet, C. E., McGuire, P. and Bullmore, E. T. (2013), 'Cognitive relevance of the community structure of the human brain functional coactivation network', *Proceedings of the National Academy of Sciences* **110**(28), 11583–11588.

Daianu, M., Dennis, E. L., Jahanshad, N., Nir, T. M., Toga, A. W., Jack, C. R., Weiner, M. W. and Thompson, P. M. (2013), 'Alzheimer's Disease Disrupts Rich Club Organization in Brain Connectivity Networks.', *Proceedings / IEEE International Symposium on Biomedical Imaging: from nano to macro. IEEE International Symposium on Biomedical Imaging* pp. 266–269.

Daianu, M., Jahanshad, N., Nir, T. M., Jack, C. R., Weiner, M. W., Bernstein, M. A. and Thompson, P. M. (2015), 'Rich club analysis in the Alzheimer's disease connectome reveals a relatively undisturbed structural core network.', *Human brain mapping* **36**(8), 3087–103.

Damasio, A. R. (1989), 'Time-locked multiregional retroactivation: A systems-level proposal for the neural substrates of recall and recognition', *Cognition* **33**(1-2), 25–62.

Damoiseaux, J. S. and Greicius, M. D. (2009), 'Greater than the sum of its parts: a review of studies combining structural connectivity and resting-state functional connectivity.', *Brain Structure and Function* **213**(6), 525–533.

Damoiseaux, J. S., Prater, K. E., Miller, B. L. and Greicius, M. D. (2012), 'Functional connectivity tracks clinical deterioration in Alzheimer's disease.', *Neurobiology of aging* **33**(4), 828.e19–30.

Damoiseaux, J. S., Rombouts, S. A. R. B., Barkhof, F., Scheltens, P., Stam, C. J., Smith, S. M. and Beckmann, C. F. (2006), 'Consistent resting-state

networks across healthy subjects', *Proceedings of the National Academy of Sciences* **103**(37), 13848–13853.

de Haan, W., Mott, K., van Straaten, E. C. W., Scheltens, P. and Stam, C. J. (2012), 'Activity dependent degeneration explains hub vulnerability in Alzheimer's disease.', *PLoS computational biology* **8**(8), e1002582.

de Jong, L. W., van der Hiele, K., Veer, I. M., Houwing, J. J., Westendorp, R. G. J., Bollen, E. L. E. M., de Bruin, P. W., Middelkoop, H. a. M., van Buchem, M. a. and van der Grond, J. (2008), 'Strongly reduced volumes of putamen and thalamus in Alzheimer's disease: an MRI study.', *Brain : a journal of neurology* **131**(Pt 12), 3277–85.

de la Monte, S. M. (1989), 'Quantitation of cerebral atrophy in preclinical and end-stage alzheimer's disease', *Annals of Neurology* **25**(5), 450–459.

De Luca, M., Beckmann, C. F., De Stefano, N., Matthews, P. M. and Smith, S. M. (2006), 'fMRI resting state networks define distinct modes of long-distance interactions in the human brain', *NeuroImage* **29**(4), 1359–1367.

de Reus, M. A. and van den Heuvel, M. P. (2013), 'The parcellation-based connectome: Limitations and extensions', *NeuroImage* .

de Schotten, M. T., Dell'Acqua, F., Forkel, S. J., Simmons, A., Vergani, F., Murphy, D. G. M. and Catani, M. (2011), 'A lateralized brain network for visuospatial attention', *Nature Neuroscience* **14**(10), 1245–1246.

Deco, G. and Corbetta, M. (2011), 'The Dynamical Balance of the Brain at Rest', *The Neuroscientist* **17**(1), 107–123.

Deco, G. and Jirsa, V. K. (2012), 'Ongoing Cortical Activity at Rest: Criticality, Multistability, and Ghost Attractors', *Journal of Neuroscience* **32**(10), 3366–3375.

Deco, G., Jirsa, V. K. and McIntosh, A. R. (2011), 'Emerging concepts for the dynamical organization of resting-state activity in the brain.', *Nature reviews. Neuroscience* **12**(1), 43–56.

Deco, G., Jirsa, V. K. and McIntosh, A. R. (2013), 'Resting brains never rest: Computational insights into potential cognitive architectures', *Trends in Neurosciences* **36**(5), 268–274.

Deco, G., Jirsa, V. K., Robinson, P. a., Breakspear, M. and Friston, K. (2008), 'The dynamic brain: from spiking neurons to neural masses and cortical fields.', *PLoS computational biology* **4**(8), e1000092.

Deco, G., Jirsa, V., McIntosh, A., Sporns, O. and Kötter, R. (2009), 'Key role of coupling, delay, and noise in resting brain fluctuations.', *Proceedings of the National Academy of Sciences of the United States of America* **106**(25), 10302–7.

Deco, G. and Kringelbach, M. L. (2014), 'Great expectations: Using whole-brain computational connectomics for understanding neuropsychiatric disorders'.

Deco, G. and Kringelbach, M. L. (2016), 'Metastability and Coherence: Extending the Communication through Coherence Hypothesis Using A Whole-Brain Computational Perspective'.

Deco, G., Kringelbach, M. L., Jirsa, V. K. and Ritter, P. (2017), 'The dynamics of resting fluctuations in the brain: Metastability and its dynamical cortical core', *Scientific Reports* **7**(1).

Deco, G., McIntosh, A. R., Shen, K., Hutchison, R. M., Menon, R. S., Everling, S., Hagmann, P. and Jirsa, V. K. (2014), 'Identification of optimal structural connectivity using functional connectivity and neural modeling.', *The Journal of neuroscience : the official journal of the Society for Neuroscience* **34**(23), 7910–7916.

Deco, G., Ponce-Alvarez, A., Hagmann, P., Romani, G. L., Mantini, D. and Corbetta, M. (2014), 'How local excitation-inhibition ratio impacts the whole brain dynamics.', *The Journal of neuroscience : the official journal of the Society for Neuroscience* **34**(23), 7886–98.

Deco, G., Ponce-Alvarez, A., Mantini, D., Romani, G. L., Hagmann, P. and Corbetta, M. (2013), 'Resting-State Functional Connectivity Emerges from Structurally and Dynamically Shaped Slow Linear Fluctuations', *Journal of Neuroscience* **33**(27), 11239–11252.

Deco, G., Senden, M. and Jirsa, V. (2012), 'How anatomy shapes dynamics: a semi-analytical study of the brain at rest by a simple spin model', *Frontiers in Computational Neuroscience* **6**(September), 1–7.

Deco, G., Tononi, G., Boly, M. and Kringelbach, M. L. (2015), 'Rethinking segregation and integration: contributions of whole-brain modelling.', *Nature reviews. Neuroscience* **16**(7), 430–9.

Dehaene, S., Kerszberg, M. and Changeux, J.-P. (1998), 'A neuronal model of a global workspace in effortful cognitive tasks', *Proceedings of the National Academy of Sciences* **95**(24), 14529–14534.

Delbeuck, X., Linden, M. V. D. and Collette, F. (2003), 'Alzheimer ' s Disease as a Disconnection Syndrome ?', **13**(2).

Delgado, M. R., Nystrom, L. E., Fissell, C., Noll, D. C. and Fiez, J. A. (2000), 'Tracking the Hemodynamic Responses to Reward and Punishment in the Striatum', *Journal of Neurophysiology* **84**(6), 3072–3077.

Demirtaş, M., Falcon, C., Tucholka, A., Gispert, J. D., Molinuevo, J. L. and Deco, G. (2017), 'A whole-brain computational modeling approach to explain the alterations in resting-state functional connectivity during progression of Alzheimer's disease', *NeuroImage: Clinical* **16**, 343–354.

Desai, M. K., Mastrangelo, M. A., Ryan, D. A., Sudol, K. L., Narrow, W. C. and Bowers, W. J. (2010), 'Early oligodendrocyte/myelin pathology in Alzheimer's disease mice constitutes a novel therapeutic target.', *The American journal of pathology* **177**(3), 1422–35.

Desai, M. K., Sudol, K. L., Janelsins, M. C., Mastrangelo, M. A., Frazer, M. E. and Bowers, W. J. (2009), 'Triple-transgenic Alzheimer's disease

mice exhibit region-specific abnormalities in brain myelination patterns prior to appearance of amyloid and tau pathology', *GLIA* **57**(1), 54–65.

Deshpande, G., Li, Z., Santhanam, P., Coles, C. D., Lynch, M. E., Hamann, S. and Hu, X. (2010), 'Recursive cluster elimination based support vector machine for disease state prediction using resting state functional and effective brain connectivity', *PLoS ONE* **5**.

Desikan, R. S., Ségonne, F., Fischl, B., Quinn, B. T., Dickerson, B. C., Blacker, D., Buckner, R. L., Dale, A. M., Maguire, R. P., Hyman, B. T., Albert, M. S. and Killiany, R. J. (2006), 'An automated labeling system for subdividing the human cerebral cortex on MRI scans into gyral based regions of interest', *NeuroImage* **31**, 968–980.

Desmond, J. E. and Glover, G. H. (2002), 'Estimating sample size in functional MRI (fMRI) neuroimaging studies: Statistical power analyses', *Journal of Neuroscience Methods* **118**(2), 115–128.

Di, X. and Biswal, B. B. (2014*a*), 'Identifying the default mode network structure using dynamic causal modeling on resting-state functional magnetic resonance imaging.', *NeuroImage* **86**, 53–9.

Di, X. and Biswal, B. B. (2014*b*), 'Modulatory interactions between the default mode network and task positive networks in resting-state.', *PeerJ* **2**, e367.

Diener, E. (2010), 'Neuroimaging: Voodoo, New Phrenology, or Scientific Breakthrough? Introduction to Special Section on fMRI', *Perspectives on Psychological Science* **5**(6), 714–715.

Dixon, M. L., De La Vega, A., Mills, C., Andrews-Hanna, J., Spreng, R. N., Cole, M. W. and Christoff, K. (2018), 'Heterogeneity within the frontoparietal control network and its relationship to the default and dorsal attention networks', *Proceedings of the National Academy of Sciences* **115**(7), E1598–E1607.

Doucet, G., Naveau, M., Petit, L., Delcroix, N., Zago, L., Crivello, F., Jobard, G., Tzourio-Mazoyer, N., Mazoyer, B., Mellet, E. and Joliot, M. (2011), 'Brain activity at rest: a multiscale hierarchical functional organization', *Journal of Neurophysiology* **105**(6), 2753–2763.

Douglas, R. J., Koch, C., Mahowald, M., Martin, K. A. and Suarez, H. H. (1995), 'Recurrent excitation in neocortical circuits', *Science (New York, N.Y.)* **269**(5226), 981–985.

Douglas, R. J. and Martin, K. A. C. (2004), 'Neuronal circuits of the neocortex.', *Annual review of neuroscience* **27**, 419–451.

Douw, L., van Dellen, E., Baayen, J. C., Klein, M., Velis, D. N., Alpherts, W. C. J., Heimans, J. J., Reijneveld, J. C. and Stam, C. J. (2010), 'The Lesioned Brain: Still a Small-World?', *Frontiers in Human Neuroscience* **4**, 174.

Drzezga, A., Becker, J. A., Van Dijk, K. R. a., Sreenivasan, A., Talukdar, T., Sullivan, C., Schultz, A. P., Sepulcre, J., Putcha, D., Greve, D., Johnson, K. a. and Sperling, R. a. (2011), 'Neuronal dysfunction and disconnection of cortical hubs in non-demented subjects with elevated amyloid burden.', *Brain : a journal of neurology* **134**(Pt 6), 1635–46.

Elton, A. and Gao, W. (2015), 'Task-related modulation of functional connectivity variability and its behavioral correlations', *Human Brain Mapping* **36**(8), 3260–3272.

Engstrøm, D. A. and Kelso, J. (2008), 'Coordination Dynamics of the Complementary Nature.', *Gestalt theory* **30**, 121–134.

Erwin, R. J., Gur, R. C., Gur, R. E., Skolnick, B., Mawhinney-Hee, M. and Smailis, J. (1992), 'Facial emotion discrimination: I. Task construction and behavioral findings in normal subjects', *Psychiatry Research* **42**(3), 231–240.

Evans, A. C., Janke, A. L., Collins, D. L. and Baillet, S. (2012), 'Brain templates and atlases'.

Eysenck, H. J. and Eysenck, S. B. G. (1994), 'Manual for the Eysenck Personality Questionnaire'.

Fagerholm, E. D., Hellyer, P. J., Scott, G., Leech, R. and Sharp, D. J. (2015), 'Disconnection of network hubs and cognitive impairment after traumatic brain injury.', *Brain* **138**(Pt 6), 1696–1709.

Fair, D. A., Cohen, A. L., Power, J. D., Dosenbach, N. U., Church, J. A., Miezin, F. M., Schlaggar, B. L. and Petersen, S. E. (2009), 'Functional brain networks develop from a "local to distributed" organization', *PLoS Computational Biology* **5**(5).

Faisal, A. A., Selen, L. P. and Wolpert, D. M. (2008), 'Noise in the nervous system'.

Farquharson, S., Tournier, J.-D., Calamante, F., Fabinyi, G., Schneider-Kolsky, M., Jackson, G. D. and Connelly, A. (2013), 'White matter fiber tractography: why we need to move beyond DTI.', *Journal of neurosurgery* **118**(June), 1367–77.

Feinberg, D. A., Moeller, S., Smith, S. M., Auerbach, E., Ramanna, S., Glasser, M. F., Miller, K. L., Ugurbil, K. and Yacoub, E. (2010), 'Multiplexed echo planar imaging for sub-second whole brain fmri and fast diffusion imaging', *PLoS ONE* **5**(12).

Feinberg, D. A. and Yacoub, E. (2012), 'The rapid development of high speed, resolution and precision in fMRI'.

Fernández-Espejo, D., Soddu, A., Cruse, D., Palacios, E. M., Junque, C., Vanhaudenhuyse, A., Rivas, E., Newcombe, V., Menon, D. K., Pickard, J. D., Laureys, S. and Owen, A. M. (2012), 'A role for the default mode network in the bases of disorders of consciousness.', *Annals of neurology* **72**(3), 335–43.

Ferrarini, L., Palm, W. M., Olofsen, H., van der Landen, R., Jan Blauw, G., Westendorp, R. G. J., Bollen, E. L. E. M., Middelkoop, H. A. M., Reiber, J. H. C., van Buchem, M. A. and Admiraal-Behloul, F. (2008), 'MMSE

scores correlate with local ventricular enlargement in the spectrum from cognitively normal to Alzheimer disease.', *NeuroImage* **39**(4), 1832–8.

Fiebelkorn, I. C., Pinsk, M. A. and Kastner, S. (2018), 'A Dynamic Interplay within the Frontoparietal Network Underlies Rhythmic Spatial Attention', *Neuron* **99**(4), 842–853.e8.

Fischl, B. (2012), 'FreeSurfer'.

Fischl, B., Liu, A. and Dale, A. M. (2001), 'Automated manifold surgery: Constructing geometrically accurate and topologically correct models of the human cerebral cortex', *IEEE Transactions on Medical Imaging* **20**(1), 70–80.

Fischl, B., Salat, D. H., Busa, E., Albert, M., Dieterich, M., Haselgrove, C., Van Der Kouwe, A., Killiany, R., Kennedy, D., Klaveness, S., Montillo, A., Makris, N., Rosen, B. and Dale, A. M. (2002), 'Whole brain segmentation: Automated labeling of neuroanatomical structures in the human brain', *Neuron* **33**, 341–355.

Fischl, B., Salat, D. H., Van Der Kouwe, A. J. W., Makris, N., Ségonne, F., Quinn, B. T. and Dale, A. M. (2004), Sequence-independent segmentation of magnetic resonance images, *in* 'NeuroImage', Vol. 23.

Fischl, B., Van Der Kouwe, A., Destrieux, C., Halgren, E., Ségonne, F., Salat, D. H., Busa, E., Seidman, L. J., Goldstein, J., Kennedy, D., Caviness, V., Makris, N., Rosen, B. and Dale, A. M. (2004), 'Automatically Parcellating the Human Cerebral Cortex', *Cerebral Cortex* **14**(January), 11–22.

FitzHugh, R. (1961), 'Impulses and Physiological States in Theoretical Models of Nerve Membrane', *Biophysical Journal* **1**(6), 445–466.

Fletcher, E., Carmichael, O., Pasternak, O., Maier-Hein, K. H. and DeCarli, C. (2014), 'Early brain loss in circuits affected by Alzheimer's disease is predicted by fornix microstructure but may be independent of gray matter', *Frontiers in Aging Neuroscience* **6**(MAY).

Folstein, M. F., Folstein, S. E. and McHugh, P. R. (1975), '"Mini-mental state"', *Journal of Psychiatric Research* **12**(3), 189–198.

Fornito, A., Zalesky, A. and Breakspear, M. (2015), 'The connectomics of brain disorders', *Nature Reviews Neuroscience* **16**(3), 159–172.

Fornito, A., Zalesky, A. and Bullmore, E. T. (2016), *Fundamentals of brain network analysis*, Academic Press.

Fornito, A., Zalesky, A., Pantelis, C. and Bullmore, E. T. (2012), 'Schizophrenia, neuroimaging and connectomics'.

Fourcaud, N. and Brunel, N. (2002), 'Dynamics of the firing probability of noisy integrate-and-fire neurons', *Neural Computation* .

Fox, M. D. and Raichle, M. E. (2007), 'Spontaneous fluctuations in brain activity observed with functional magnetic resonance imaging', *Nature Reviews Neuroscience* **8**(9), 700–711.

Fox, M. D., Snyder, A. Z., Vincent, J. L., Corbetta, M., Van Essen, D. C. and Raichle, M. E. (2005), 'The human brain is intrinsically organized into dynamic, anticorrelated functional networks.', *Proceedings of the National Academy of Sciences of the United States of America* **102**, 9673–9678.

Fox, M. D., Snyder, A. Z., Zacks, J. M. and Raichle, M. E. (2006), 'Coherent spontaneous activity accounts for trial-to-trial variability in human evoked brain responses', *Nature Neuroscience* **9**(1), 23–25.

Fox, M. D., Zhang, D., Snyder, A. Z. and Raichle, M. E. (2009), 'The global signal and observed anticorrelated resting state brain networks.', *Journal of neurophysiology* **101**(6), 3270–83.

Fox, P. T. (2012), 'The coupling controversy'.

Fraiman, D., Balenzuela, P., Foss, J. and Chialvo, D. R. (2009), 'Ising-like dynamics in large-scale functional brain networks', *Physical Review E - Statistical, Nonlinear, and Soft Matter Physics* **79**(6).

Freeman, W. J. (1979), 'Nonlinear gain mediating cortical stimulus-response relations', *Biological Cybernetics* .

Freeman, W. J. (1987), 'Simulation of chaotic EEG patterns with a dynamic model of the olfactory system', *Biological Cybernetics* .

Freeman, W. J. (2003), 'Evidence from human scalp electroencephalograms of global chaotic itinerancy', *Chaos* **13**(3), 1067–1077.

Freyer, F., Aquino, K., Robinson, P. A., Ritter, P. and Breakspear, M. (2009), 'Bistability and non-Gaussian fluctuations in spontaneous cortical activity', *Journal of Neuroscience* .

Freyer, F., Roberts, J. A., Becker, R., Robinson, P. A., Ritter, P. and Breakspear, M. (2011), 'Biophysical mechanisms of multistability in resting-state cortical rhythms', *Journal of Neuroscience* .

Fries, P. (2005), 'A mechanism for cognitive dynamics: Neuronal communication through neuronal coherence'.

Fries, P. (2009), 'Neuronal Gamma-Band Synchronization as a Fundamental Process in Cortical Computation', *Annual Review of Neuroscience* **32**(1), 209–224.

Fries, P. (2015), 'Rhythms for Cognition: Communication through Coherence'.

Friston, K. (1994), 'Functional and effective connectivity in neuroimaging: A synthesis', *Human Brain Mapping* **2**(1-2), 56–78.

Friston, K. (1997), 'Transients, metastability, and neuronal dynamics.', *NeuroImage* **5**(2), 164–71.

Friston, K. (2003), Dynamic Causal Modelling, *in* 'Human Brain Function: Second Edition', pp. 1063–1090.

Friston, K. (2009*a*), 'Causal modelling and brain connectivity in functional magnetic resonance imaging.', *PLoS biology* **7**(2), e33.

Friston, K. (2009*b*), 'Modalities, modes, and models in functional neuroimaging'.

Friston, K. (2011), 'Functional and effective connectivity: a review.', *Brain connectivity* **1**(1), 13–36.

Friston, K., Moran, R. and Seth, A. K. (2012), 'Analysing connectivity with Granger causality and dynamic causal modelling', pp. 1–7.

Friston, K., Preller K.H., C., M., C., H., J., H., A., R. and P., Z. (2017), 'Dynamic causal modelling revisited', *NeuroImage* **19**(February), 1273–1302.

Friston, K., Price, C. J., Fletcher, P., Moore, C., Frackowiak, R. S. and Dolan, R. J. (1996), 'The trouble with cognitive subtraction.', *NeuroImage* **4**, 97–104.

Gabor, D. (1947), 'Theory of communication', *Journal of the Institution of Electrical Engineers - Part I: General* .

Gallos, L. K., Makse, H. A. and Sigman, M. (2012), 'A small world of weak ties provides optimal global integration of self-similar modules in functional brain networks.', *Proceedings of the National Academy of Sciences of the United States of America* **109**(8), 2825–30.

Garcés, P., Angel Pineda-Pardo, J., Canuet, L., Aurtenetxe, S., López, M. E., Marcos, A., Yus, M., Llanero-Luque, M., Del-Pozo, F., Sancho, M. and Maestú, F. (2014), 'The Default Mode Network is functionally and structurally disrupted in amnestic mild cognitive impairment - a bimodal MEG-DTI study.', *NeuroImage. Clinical* **6**, 214–21.

Garcés, P., Vicente, R., Wibral, M., Pineda-Pardo, J. Á., López, M. E., Aurtenetxe, S., Marcos, A., de Andrés, M. E., Yus, M., Sancho, M., Maestú, F. and Fernández, A. (2013), 'Brain-wide slowing of spontaneous alpha rhythms in mild cognitive impairment.', *Frontiers in aging neuroscience* **5**, 100.

Gershon, R. C., Wagster, M. V., Hendrie, H. C., Fox, N. A., Cook, K. F. and Nowinski, C. J. (2013), 'NIH Toolbox for Assessment of Neurological and Behavioral Function', *Neurology* **80**(Issue 11, Supplement 3), S2–S6.

Geschwind, N. (1965), 'Disconnexion syndroms in animals and man', *Brain* **88**(2), 237–237.

Ghosh, A., Rho, Y., McIntosh, A. R., Kötter, R. and Jirsa, V. K. (2008*a*), 'Cortical network dynamics with time delays reveals functional connectivity in the resting brain.', *Cognitive neurodynamics* **2**(2), 115–20.

Ghosh, A., Rho, Y., McIntosh, A. R., Kötter, R. and Jirsa, V. K. (2008*b*), 'Noise during rest enables the exploration of the brain's dynamic repertoire', *PLoS Computational Biology* **4**(10).

Gil, R., Arroyo-Anllo, E. M., Ingrand, P., Gil, M., Neau, J. P., Ornon, C. and Bonnaud, V. (2001), 'Self-consciousness and Alzheimer's disease', *Acta Neurologica Scandinavica* **104**(5), 296–300.

Glahn, D. C., Winkler, A. M., Kochunov, P., Almasy, L., Duggirala, R., Carless, M. A., Curran, J. C., Olvera, R. L., Laird, A. R., Smith, S. M., Beckmann, C. F., Fox, P. T. and Blangero, J. (2010), 'Genetic control over the resting brain', *Proceedings of the National Academy of Sciences* **107**(3), 1223–1228.

Glasser, M. F., Smith, S. M., Marcus, D. S., Andersson, J. L. R., Auerbach, E. J., Behrens, T. E. J., Coalson, T. S., Harms, M. P., Jenkinson, M., Moeller, S., Robinson, E. C., Sotiropoulos, S. N., Xu, J., Yacoub, E., Ugurbil, K. and Van Essen, D. C. (2016), 'The Human Connectome Project's neuroimaging approach.', *Nature neuroscience* **19**(9), 1175–87.

Glasser, M. F., Sotiropoulos, S. N., Wilson, J. A., Coalson, T. S., Fischl, B., Andersson, J. L., Xu, J., Jbabdi, S., Webster, M., Polimeni, J. R., Van Essen, D. C. and Jenkinson, M. (2013), 'The minimal preprocessing pipelines for the Human Connectome Project', *NeuroImage* **80**, 105–124.

Glerean, E., Salmi, J., Lahnakoski, J. M., Jaaskelainen, I. P. and Sams, M. (2012), 'Functional magnetic resonance imaging phase synchronization as a measure of dynamic functional connectivity', *Brain Connect* **2**(2), 91–101.

Goebel, R., Roebroeck, A., Kim, D.-S. S. and Formisano, E. (2003), 'Investigating directed cortical interactions in time-resolved fMRI data using vector autoregressive modeling and Granger causality mapping', *Magnetic Resonance Imaging* **21**(10), 1251–1261.

Goedert, M. and Spillantini, M. G. (2006), 'A century of Alzheimer's disease'.

Gómez-Gardeñes, J., Moreno, Y. and Arenas, A. (2007*a*), Paths to synchronization on complex networks, *in* 'Physical Review Letters', Vol. 98.

Gómez-Gardeñes, J., Moreno, Y. and Arenas, A. (2007*b*), 'Synchronizability determined by coupling strengths and topology on complex networks', *Physical Review E - Statistical, Nonlinear, and Soft Matter Physics* **75**(6).

Gomez-Ramirez, J. and Wu, J. (2014), 'Network-Based Biomarkers in Alzheimer's Disease: Review and Future Directions', *Frontiers in Aging Neuroscience* **6**, 12.

Gong, P., Nikolaev, A. R. and Van Leeuwen, C. (2003), 'Scale-invariant fluctuations of the dynamical synchronization in human brain electrical activity', *Neuroscience Letters* **336**(1), 33–36.

Goñi, J., van den Heuvel, M. P., Avena-Koenigsberger, A., Velez de Mendizabal, N., Betzel, R. F., Griffa, A., Hagmann, P., Corominas-Murtra, B., Thiran, J.-P. and Sporns, O. (2014), 'Resting-brain functional connectivity predicted by analytic measures of network communication.', *Proceedings of the National Academy of Sciences of the United States of America* **111**(2), 833–8.

Gonzalez-Castillo, J. and Bandettini, P. A. (2017), 'Task-based dynamic functional connectivity: Recent findings and open questions', *NeuroImage* **180**(August 2017), 526–533.

Gordon, E. M., Laumann, T. O., Adeyemo, B., Huckins, J. F., Kelley, W. M. and Petersen, S. E. (2016), 'Generation and Evaluation of a Cortical Area Parcellation from Resting-State Correlations', *Cerebral Cortex* **26**(1), 288–303.

Grabner, G., Janke, A. L., Budge, M. M., Smith, D., Pruessner, J. and Collins, D. L. (2006), Symmetric atlasing and model based segmentation: an application to the hippocampus in older adults, *in* 'Med Image Comput Comput Assist Interv', Vol. 9, pp. 58–66.

Granger, C. W. J. (1969), 'Investigating Causal Relations by Econometric Models and Cross-spectral Methods', *Econometrica* **37**(3), 424.

Grassberger, P. and Procaccia, I. (1983), 'Characterization of strange attractors', *Physical Review Letters* .

Gratton, C., Nomura, E. M., Pérez, F. and D'Esposito, M. (2012), 'Focal Brain Lesions to Critical Locations Cause Widespread Disruption of the Modular Organization of the Brain', *Journal of Cognitive Neuroscience* **24**(6), 1275–1285.

Gray, C. M. and Singer, W. (1989), 'Stimulus-specific neuronal oscillations in orientation columns of cat visual cortex.', *Proceedings of the National Academy of Sciences* **86**(5), 1698–1702.

Greicius, M. D., Krasnow, B., Reiss, A. L. and Menon, V. (2003), 'Functional connectivity in the resting brain: A network analysis of the default mode hypothesis', *Proceedings of the National Academy of Sciences of the United States of America* **100**(1), 253–258.

Greicius, M. D., Srivastava, G., Reiss, A. L. and Menon, V. (2004), 'Default-mode network activity distinguishes Alzheimer's disease from healthy ag-

ing: evidence from functional MRI.', *Proceedings of the National Academy of Sciences of the United States of America* **101**(13), 4637–42.

Greve, D. N. and Fischl, B. (2009), 'Accurate and robust brain image alignment using boundary-based registration', *NeuroImage* **48**(1), 63–72.

Griffa, A. and Van den Heuvel, M. P. (2018), 'Rich-club neurocircuitry: function, evolution, and vulnerability.', *Dialogues in clinical neuroscience* .

Gros, C. (2009), 'Cognitive computation with autonomously active neural networks: An emerging field', *Cognitive Computation* .

Guckenheimer, J. and Holmes, P. (1988), 'Structurally stable heteroclinic cycles', *Mathematical Proceedings of the Cambridge Philosophical Society* .

Guo, S., Seth, A. K., Kendrick, K. M., Zhou, C. and Feng, J. (2008), 'Partial Granger causality–eliminating exogenous inputs and latent variables.', *Journal of neuroscience methods* **172**(1), 79–93.

Hagmann, P., Cammoun, L., Gigandet, X., Gerhard, S., Grant, P. E., Wedeen, V., Meuli, R., Thiran, J.-P., Honey, C. J. and Sporns, O. (2010), 'MR connectomics: Principles and challenges.', *Journal of neuroscience methods* **194**(1), 34–45.

Hagmann, P., Cammoun, L., Gigandet, X., Meuli, R., Honey, C. J., Wedeen, V. J. and Sporns, O. (2008), 'Mapping the structural core of human cerebral cortex.', *PLoS biology* **6**(7), e159.

Hagmann, P., Kurant, M., Gigandet, X., Thiran, P., Wedeen, V. J., Meuli, R. and Thiran, J.-P. (2007), 'Mapping human whole-brain structural networks with diffusion MRI.', *PloS one* **2**(7), e597.

Haimovici, A., Tagliazucchi, E., Balenzuela, P. and Chialvo, D. R. (2013), 'Brain organization into resting state networks emerges at criticality on a model of the human connectome', *Physical Review Letters* **110**(17), 1–4.

Haken, H. (1996), *Principles of Brain Functioning A Synergetic Approach to Brain Activity, Behavior and Cognition*, Springer.

Halassa, M. M. and Kastner, S. (2017), 'Thalamic functions in distributed cognitive control', *Nature Neuroscience* **20**(12), 1669–1679.

Haldeman, C. and Beggs, J. M. (2005), 'Critical branching captures activity in living neural networks and maximizes the number of metastable states', *Physical Review Letters* **94**(5), 058101.

Handwerker, D. A., Gonzalez-Castillo, J., D'Esposito, M. and Bandettini, P. A. (2012), 'The continuing challenge of understanding and modeling hemodynamic variation in fMRI'.

Handwerker, D. A., Ollinger, J. M. and D'Esposito, M. (2004), 'Variation of BOLD hemodynamic responses across subjects and brain regions and their effects on statistical analyses', *NeuroImage* **21**(4), 1639–1651.

Hansen, E. C. A., Battaglia, D., Spiegler, A., Deco, G. and Jirsa, V. K. (2014), 'Functional Connectivity Dynamics: Modeling the switching behavior of the resting state', *NeuroImage* **105**, 525–535.

Hariri, A. R., Tessitore, A., Mattay, V. S., Fera, F. and Weinberger, D. R. (2002), 'The amygdala response to emotional stimuli: A comparison of faces and scenes', *NeuroImage* **17**(1), 317–323.

Harriger, L., van den Heuvel, M. P. and Sporns, O. (2012), 'Rich club organization of macaque cerebral cortex and its role in network communication.', *PloS one* **7**(9), e46497.

Hasson, U. and Honey, C. J. (2012), 'Future trends in Neuroimaging: Neural processes as expressed within real-life contexts'.

He, Y., Chen, Z. J. and Evans, A. C. (2007), 'Small-world anatomical networks in the human brain revealed by cortical thickness from MRI', *Cerebral Cortex* .

He, Y., Dagher, A., Chen, Z., Charil, A., Zijdenbos, A., Worsley, K. and Evans, A. (2009), 'Impaired small-world efficiency in structural cortical networks in multiple sclerosis associated with white matter lesion load', *Brain* .

Hedden, T., Van Dijk, K. R. A., Becker, J. A., Mehta, A., Sperling, R. A., Johnson, K. A. and Buckner, R. L. (2009), 'Disruption of functional connectivity in clinically normal older adults harboring amyloid burden.', *The Journal of neuroscience : the official journal of the Society for Neuroscience* **29**(40), 12686–94.

Heise, V., Filippini, N., Ebmeier, K. P. and Mackay, C. E. (2010), 'The APOE varepsilon4 allele modulates brain white matter integrity in healthy adults.', *Molecular psychiatry* pp. 1–9.

Helfrich, R. F., Fiebelkorn, I. C., Szczepanski, S. M., Lin, J. J., Parvizi, J., Knight, R. T. and Kastner, S. (2018), 'Neural Mechanisms of Sustained Attention Are Rhythmic', *Neuron* **99**(4), 854–865.e5.

Hellyer, P. J., Scott, G., Shanahan, M., Sharp, D. J. and Leech, R. (2015), 'Cognitive Flexibility through Metastable Neural Dynamics Is Disrupted by Damage to the Structural Connectome', *Journal of Neuroscience* **35**(24), 9050–9063.

Hellyer, P. J., Shanahan, M., Scott, G., Wise, R. J. S., Sharp, D. J. and Leech, R. (2014), 'The control of global brain dynamics: opposing actions of frontoparietal control and default mode networks on attention.', *The Journal of neuroscience : the official journal of the Society for Neuroscience* **34**(2), 451–61.

Hermundstad, A. M., Bassett, D. S., Brown, K. S., Aminoff, E. M., Clewett, D., Freeman, S., Frithsen, A., Johnson, A., Tipper, C. M., Miller, M. B., Grafton, S. T. and Carlson, J. M. (2013), 'Structural foundations of resting-state and task-based functional connectivity in the human brain.', *Proceedings of the National Academy of Sciences of the United States of America* **110**(15), 6169–74.

Hesse, J. and Gross, T. (2014), 'Self-organized criticality as a fundamental property of neural systems', *Frontiers in Systems Neuroscience* **8**.

Hesselmann, G., Kell, C. A., Eger, E. and Kleinschmidt, A. (2008), 'Spontaneous local variations in ongoing neural activity bias perceptual decisions', *Proceedings of the National Academy of Sciences* **105**(31), 10984–10989.

Hesselmann, G., Kell, C. A. and Kleinschmidt, A. (2008), 'Ongoing Activity Fluctuations in hMT+ Bias the Perception of Coherent Visual Motion', *Journal of Neuroscience* **28**(53), 14481–14485.

Hilgetag, C. C. and Goulas, A. (2015), 'Is the brain really a small-world network?', *Brain Structure and Function* **221**(4), 2361–2366.

Hilgetag, C. C. and Kaiser, M. (2004), 'Clustered organization of cortical connectivity'.

Hindriks, R., Adhikari, M. H., Murayama, Y., Ganzetti, M., Mantini, D., Logothetis, N. K. and Deco, G. (2016), 'Can sliding-window correlations reveal dynamic functional connectivity in resting-state fMRI?', *NeuroImage* **127**, 242–256.

Hodge, M. R., Horton, W., Brown, T., Herrick, R., Olsen, T., Hileman, M. E., McKay, M., Archie, K. A., Cler, E., Harms, M. P., Burgess, G. C., Glasser, M. F., Elam, J. S., Curtiss, S. W., Barch, D. M., Oostenveld, R., Larson-Prior, L. J., Ugurbil, K., Van Essen, D. C. and Marcus, D. S. (2015), 'ConnectomeDB - Sharing Human Brain Connectivity Data.', *NeuroImage* **124**, 1102–1107.

Hodgkin, A. L. and Huxley, A. F. (1990), 'A quantitative description of membrane current and its application to conduction and excitation in nerve', *Bulletin of Mathematical Biology* .

Honey, C. J. and Kötter, R. (2007), 'Network structure of cerebral cortex shapes functional connectivity on multiple time scales', *Proceedings of the …* .

Honey, C. J. and Sporns, O. (2008), 'Dynamical consequences of lesions in cortical networks.', *Human brain mapping* **29**(7), 802–9.

Honey, C. J., Sporns, O., Cammoun, L., Gigandet, X., Thiran, J. P., Meuli, R. and Hagmann, P. (2009), 'Predicting human resting-state functional connectivity from structural connectivity.', *Proceedings of the National Academy of Sciences of the United States of America* **106**(6), 2035–40.

Honey, C. J., Thivierge, J.-P. and Sporns, O. (2010), 'Can structure predict function in the human brain?', *NeuroImage* **52**(3), 766–76.

Horwitz, B. (2003), 'The elusive concept of brain connectivity'.

Hudson, A. E., Calderon, D. P., Pfaff, D. W. and Proekt, A. (2014), 'Recovery of consciousness is mediated by a network of discrete metastable activity states', *Proceedings of the National Academy of Sciences of the United States of America* .

Huettel, S. A. (2009), *Functional Magnetic Resonance Imaging*, 2nd edn, Sinauer Associates.

Huettel, S. and Song, A. (2014), *Functional Magnetic Resonance Imaging*, 3rd edn, Sinaeur.

Hughes, C. P., Berg, L., Danziger, W. L., Coben, L. A. and Martin, R. L. (1982), 'A new clinical scale for the staging of dementia', *British Journal of Psychiatry* **140**(6), 566–572.

Huppert, F. A., Brayne, C., Gill, C., Paykel, E. S. and Beardsall, L. (1995), 'CAMCOG–a concise neuropsychological test to assist dementia diagnosis: socio-demographic determinants in an elderly population sample.', *The British journal of clinical psychology / the British Psychological Society* **34 ( Pt 4)**, 529–41.

Hurtado-Puerto, A. M., Russo, C. and Fregni, F. (2018), Alzheimer's disease, *in* 'Neuromethods'.

Hutchison, R. M. and Morton, J. B. (2015), 'Tracking the Brain's Functional Coupling Dynamics over Development', *Journal of Neuroscience* **35**(17), 6849–6859.

Hutchison, R. M., Womelsdorf, T., Allen, E. A., Bandettini, P. A., Calhoun, V. D., Corbetta, M., Della Penna, S., Duyn, J. H., Glover, G. H., Gonzalez-Castillo, J., Handwerker, D. A., Keilholz, S., Kiviniemi, V., Leopold, D. A., de Pasquale, F., Sporns, O., Walter, M. and Chang, C. (2013), 'Dynamic functional connectivity: Promise, issues, and interpretations', *NeuroImage* **80**, 360–378.

Hutchison, R. M., Womelsdorf, T., Gati, J. S., Everling, S. and Menon, R. S. (2013), 'Resting-state networks show dynamic functional connectivity in awake humans and anesthetized macaques', *Human Brain Mapping* **34**(9), 2154–2177.

Hutt, A. and beim Graben, P. (2017), 'Sequences by Metastable Attractors: Interweaving Dynamical Systems and Experimental Data', *Frontiers in Applied Mathematics and Statistics* .

Hwang, K., Bertolero, M. A., Liu, W. B. and D'Esposito, M. (2017), 'The human thalamus is an integrative hub for functional brain networks', *Journal of Neuroscience* .

Hyvärinen, A. (1999), 'Fast and robust fixed-point algorithms for independent component analysis', *IEEE Transactions on Neural Networks* **10**, 626–634.

Ito, J., Nikolaev, A. R. and Van Leeuwen, C. (2007), 'Dynamics of spontaneous transitions between global brain states', *Human Brain Mapping* .

Iturria-Medina, Y., Canales-Rodríguez, E. J., Melie-García, L., Valdés-Hernández, P. a., Martínez-Montes, E., Alemán-Gómez, Y. and Sánchez-Bornot, J. M. (2007), 'Characterizing brain anatomical connections using diffusion weighted MRI and graph theory.', *NeuroImage* **36**(3), 645–60.

Iturria-Medina, Y., Sotero, R. C., Canales-Rodríguez, E. J., Alemán-Gómez, Y. and Melie-García, L. (2008), 'Studying the human brain anatomical network via diffusion-weighted MRI and Graph Theory.', *NeuroImage* **40**(3), 1064–76.

Izhikevich, E. M. and Edelman, G. M. (2008), 'Large-scale model of mammalian thalamocortical systems', *Proceedings of the National Academy of Sciences* .

Jack, C. R., Knopman, D. S., Jagust, W. J., Petersen, R. C., Weiner, M. W., Aisen, P. S., Shaw, L. M., Vemuri, P., Wiste, H. J., Weigand, S. D., Lesnick, T. G., Pankratz, V. S., Donohue, M. C. and Trojanowski, J. Q. (2013), 'Tracking pathophysiological processes in Alzheimer's disease: An updated hypothetical model of dynamic biomarkers'.

Jacobs, H. I. L., Radua, J., Lückmann, H. C. and Sack, A. T. (2013), 'Meta-analysis of functional network alterations in Alzheimer's disease: Toward a network biomarker', *Neuroscience and Biobehavioral Reviews* **37**(5), 753–765.

Jansen, B. H. and Rit, V. G. (1995), 'Biological Cybernetics in a mathematical model of coupled cortical columns', **366**, 357–366.

Jaunmuktane, Z., Mead, S., Ellis, M., Wadsworth, J. D. F., Nicoll, A. J., Kenny, J., Launchbury, F., Linehan, J., Richard-Loendt, A., Walker, A. S., Rudge, P., Collinge, J. and Brandner, S. (2015), 'Evidence for human transmission of amyloid-$\beta$ pathology and cerebral amyloid angiopathy', *Nature* **525**(7568), 247–250.

Jbabdi, S., Behrens, T. E. and Smith, S. M. (2010), 'Crossing fibres in tract-based spatial statistics', *NeuroImage* **49**(1), 249–256.

Jelles, B., Scheltens, P., van der Flier, W. M., Jonkman, E. J., da Silva, F. H. L. and Stam, C. J. (2008), 'Global dynamical analysis of the EEG in Alzheimer's disease: frequency-specific changes of functional interactions.', *Clinical neurophysiology : official journal of the International Federation of Clinical Neurophysiology* **119**(4), 837–41.

Jenkinson, M., Bannister, P., Brady, M. and Smith, S. M. (2002), 'Improved optimization for the robust and accurate linear registration and motion correction of brain images', *NeuroImage* **17**, 825–841.

Jenkinson, M. and Smith, S. (2001), 'A global optimization method for robust affine registration of brain images.', *Med Image Anal* **5**, 143–156.

Jensen, A. R. and Cattell, R. B. (2006), 'Abilities: Their Structure, Growth, and Action', *The American Journal of Psychology* .

Jeong, J. (2004), 'EEG dynamics in patients with Alzheimer's disease.', *Clinical neurophysiology : official journal of the International Federation of Clinical Neurophysiology* **115**(7), 1490–505.

Jeurissen, B., Leemans, A., Tournier, J.-D., Jones, D. K. and Sijbers, J. (2013), 'Investigating the prevalence of complex fiber configurations in white matter tissue with diffusion magnetic resonance imaging.', *Human brain mapping* **34**(11), 2747–66.

Jirsa, V. K., Sporns, O., Breakspear, M., Deco, G. and Mcintosh, A. R. (2010), 'Towards the virtual brain: Network modeling of the intact and the damaged brain', *Archives Italiennes de Biologie* **148**(3), 189–205.

Jirsa, V. K. V. K. and McIntosh, A. R. A. R. (2007), *Handbook of brain connectivity*, Springer.

Johnson, K. A., Jones, K., Holman, B. L., Becker, J. A., Spiers, P. A., Satlin, A. and Albert, M. S. (1998), 'Preclinical prediction of Alzheimer's disease using SPECT.', *Neurology* **50**, 1563–1571.

Jones, D. K. (2010), 'Challenges and limitations of quantifying brain connectivity in vivo with diffusion MRI', *Imaging in Medicine* **2**(3), 341–355.

Jones, D. K. and Cercignani, M. (2010), 'Twenty-five pitfalls in the analysis of diffusion MRI data'.

Jones, D. K., Knösche, T. R. and Turner, R. (2013), 'White matter integrity, fiber count, and other fallacies: The do's and don'ts of diffusion MRI', *NeuroImage* **73**, 239–254.

Jones, D. T., Machulda, M., Vemuri, P., McDade, E., Zeng, G., Senjem, M., Gunter, J., Przybelski, S., Avula, R., Knopman, D., Boeve, B., Petersen, R. and Jack, C. (2011), 'Age-related changes in the default mode network are more advanced in Alzheimer's disease', *Alzheimer's & Dementia* **7**(4), S74–S75.

Jones, D. T., Vemuri, P., Murphy, M. C., Gunter, J. L., Senjem, M. L., Machulda, M. M., Przybelski, S. a., Gregg, B. E., Kantarci, K., Knopman, D. S., Boeve, B. F., Petersen, R. C. and Jack, C. R. (2012), 'Non-stationarity in the "resting brain's" modular architecture', *PLoS ONE* **7**(6), e39731.

Kaiser, M. (2011), 'A tutorial in connectome analysis: topological and spatial features of brain networks.', *NeuroImage* **57**(3), 892–907.

Kaiser, M. (2013), 'The potential of the human connectome as a biomarker of brain disease.', *Frontiers in human neuroscience* **7**(August), 484.

Kalia, M. (2003), 'Dysphagia and aspiration pneumonia in patients with Alzheimer's disease', *Metabolism: Clinical and Experimental* .

Kaneko, K. and Tsuda, I. (2003), 'Chaotic itinerancy', *Chaos* .

Kauffman, S. A. (1993), *The origins of order : self-organization and selection in evolution*, Oxford University Press.

Kawahara, J., Brown, C. J., Miller, S. P., Booth, B. G., Chau, V., Grunau, R. E., Zwicker, J. G. and Hamarneh, G. (2017), 'BrainNetCNN: Convolutional neural networks for brain networks; towards predicting neurodevelopment', *NeuroImage* **146**, 1038–1049.

Kehoe, E. G., Farrell, D., Metzler-Baddeley, C., Lawlor, B. A., Kenny, R. A., Lyons, D., McNulty, J. P., Mullins, P. G., Coyle, D. and Bokde,

A. L. (2015), 'Fornix white matter is correlated with resting-state functional connectivity of the thalamus and hippocampus in healthy aging but not in mild cognitive impairment - A preliminary study', *Frontiers in Aging Neuroscience* **7**(FEB), 10.

Kello, C. T., Anderson, G. G., Holden, J. G. and Van Orden, G. C. (2008), 'The pervasiveness of 1/f scaling in speech reflects the metastable basis of cognition', *Cognitive Science* **32**(7), 1217–1231.

Kello, C. T., Beltz, B. C., Holden, J. G. and Van Orden, G. C. (2007), 'The Emergent Coordination of Cognitive Function', *Journal of Experimental Psychology: General* **136**(4), 551–568.

Kelso, J. (1994), 'The informational character of self-organized coordination dynamics', *Human Movement Science* **13**(3-4), 393–413.

Kelso, J. (1995), *Dynamic Patterns: The Self-Organization of Brain and Behavior*, MIT Press, Cambridge, MA.

Kelso, J. (2009), Synergies: Atoms of Brain and Behavior, *in* D. Sternad, ed., 'Progress in motor control', New York, NY: Springer, pp. 83–91.

Kelso, J. (2012), 'Multistability and metastability: understanding dynamic coordination in the brain.', *Philosophical transactions of the Royal Society of London. Series B, Biological sciences* **367**(1591), 906–18.

Kelso, J. A. (2008), 'An essay on understanding the mind'.

Kelso, J. A. S. (1992), Coordination Dynamics of Human Brain and Behavior, *in* 'Evolution of Dynamical Structures in Complex Systems', Springer, Berlin, Heidelberg, pp. 223–234.

Kelso, J., Dumas, G. and Tognoli, E. (2013), 'Outline of a general theory of behavior and brain coordination', *Neural Networks* **37**, 120–131.

Kelso, J. and Engstrom, D. (2006), *The Complementary Nature*, MIT Press, Cambridge, MA.

Kelso, J. and Haken, H. (1995), New laws to be expected in the organism: Synergetics of brain and behavior. In What is Life?, *in* M. Murphy and L. O'Neill, eds, 'What is life? The next 50 years.', Cambridge: Cambridge University Press, pp. 137–160.

Kelso, J. and Tognoli, E. (2007), 'Toward a complementary neuroscience: Metastable coordination dynamics of the brain', *Understanding Complex Systems* **2007**, 39–59.

Kingma, D. P. and Ba, J. L. (2015), 'Adam: a Method for Stochastic Optimization', *International Conference on Learning Representations 2015* pp. 1–15.

Kingsley, P. B. (2006), 'Introduction to diffusion tensor imaging mathematics: Series Part I-III', *Concepts in Magnetic Resonance Part A: Bridging Education and Research* **28**(2), 101–179.

Kinnunen, K. M., Greenwood, R., Powell, J. H., Leech, R., Hawkins, P. C., Bonnelle, V., Patel, M. C., Counsell, S. J. and Sharp, D. J. (2010), 'White matter damage and cognitive impairment after traumatic brain injury', *Brain* pp. —-.

Kinouchi, O. and Copelli, M. (2006), 'Optimal dynamical range of excitable networks at criticality', *Nature Physics* **2**(5), 348–351.

Kitzbichler, M. G., Henson, R. N. A., Smith, M. L., Nathan, P. J. and Bullmore, E. T. (2011), 'Cognitive Effort Drives Workspace Configuration of Human Brain Functional Networks', *Journal of Neuroscience* **31**(22), 8259–8270.

Kitzbichler, M. G., Smith, M. L., Christensen, S. R. and Bullmore, E. (2009), 'Broadband criticality of human brain network synchronization.', *PLoS Computational Biology* **5**(3), e1000314.

Kiviniemi, V., Kantola, J. H., Jauhiainen, J., Hyvärinen, A. and Tervonen, O. (2003), 'Independent component analysis of nondeterministic fMRI signal sources', *NeuroImage* **19**(2), 253–260.

Knight, W. D., Kim, L. G., Douiri, A., Frost, C., Rossor, M. N. and Fox, N. C. (2011), 'Acceleration of cortical thinning in familial Alzheimer's disease', *Neurobiology of Aging* **32**, 1765–1773.

Koch, C. and Laurent, G. (1999), 'Complexity and the nervous system'.

Koenig, T., Prichep, L., Dierks, T., Hubl, D., Wahlund, L. O., John, E. R. and Jelic, V. (2005), 'Decreased EEG synchronization in Alzheimer's disease and mild cognitive impairment.', *Neurobiology of aging* **26**(2), 165–71.

Kringelbach, M. L., McIntosh, A. R., Ritter, P., Jirsa, V. K. and Deco, G. (2015), 'The Rediscovery of Slowness: Exploring the Timing of Cognition', *Trends in Cognitive Sciences* **19**(10), 616–628.

Kucyi, A. (2017), 'Just a thought: How mind-wandering is represented in dynamic brain connectivity', *NeuroImage* **180**(June 2017), 505–514.

Kucyi, A., Hove, M. J., Esterman, M., Hutchison, R. M. and Valera, E. M. (2017), 'Dynamic Brain Network Correlates of Spontaneous Fluctuations in Attention', *Cerebral cortex (New York, N.Y. : 1991)* **27**(3), 1831–1840.

Kumar, A., Singh, A. and Ekavali (2015), 'A review on Alzheimer's disease pathophysiology and its management: an update', *Pharmacological Reports* **67**(2), 195–203.

Kundu, P., Hens, C., Barzel, B. and Pal, P. (2017), 'Perfect synchronization in networks of phase-frustrated oscillators', *EPL* **120**(4).

Kuramoto, Y. (1984), *Chemical Oscillations, Waves, and Turbulence*, Vol. 19 of *Springer Series in Synergetics*, Springer Berlin Heidelberg, Berlin, Heidelberg.

Kwong, K. K. (2012), 'Record of a single fMRI experiment in May of 1991'.

Laird, A. R., Fox, P. M., Eickhoff, S. B., Turner, J. A., Ray, K. L., McKay, D. R., Glahn, D. C., Beckmann, C. F., Smith, S. M. and Fox, P. T. (2011), 'Behavioral Interpretations of Intrinsic Connectivity Networks', *Journal of Cognitive Neuroscience* **23**(12), 4022–4037.

Landeiro, F., Wace, H., Ghinai, I., Nye, E., Mughal, S., Walsh, K., Roberts, N., Lecomte, P., Wittenberg, R., Wolstenholme, J., Handels, R., Roncancio-Diaz, E., Potashman, M. H., Tockhorn-Heidenreich, A. and Gray, A. M. (2018), 'Resource utilisation and costs in predementia and dementia: A systematic review protocol', *BMJ Open* .

Langton, C. G. (1990), 'Computation at the edge of chaos', *Physica D: Nonlinear Phenomena* **42**, 12–37.

Larsen, R. S. and Waters, J. (2018), 'Neuromodulatory correlates of pupil dilation'.

Larter, R., Speelman, B. and Worth, R. M. (1999), 'A coupled ordinary differential equation lattice model for the simulation of epileptic seizures', *Chaos* .

Laughlin, R. B. and Pines, D. (2013), The Theory of Everything, *in* 'Emergence'.

Laumann, T. O., Snyder, A. Z., Mitra, A., Gordon, E. M., Gratton, C., Adeyemo, B., Gilmore, A. W., Nelson, S. M., Berg, J. J., Greene, D. J., McCarthy, J. E., Tagliazucchi, E., Laufs, H., Schlaggar, B. L., Dosenbach, N. U. and Petersen, S. E. (2017), 'On the Stability of BOLD fMRI Correlations', *Cerebral Cortex* **27**(10), 4719–4732.

Le Bihan, D. (2011), 'Diffusion, confusion and functional MRI.', *NeuroImage* .

Le Bihan, D., Mangin, J. F., Poupon, C., Clark, C. A., Pappata, S., Molko, N. and Chabriat, H. (2001), 'Diffusion tensor imaging: Concepts and applications', *Journal of Magnetic Resonance Imaging* .

Lee, L., Harrison, L. M. and Mechelli, A. (2003), A report of the functional connectivity workshop, Dusseldorf 2002, *in* 'NeuroImage', Vol. 19, pp. 457–465.

Lee, W. H., Doucet, G. E., Leibu, E. and Frangou, S. (2018), 'Resting-state network connectivity and metastability predict clinical symptoms in schizophrenia', *Schizophrenia Research* **201**, 208–216.

Leech, R. and Sharp, D. J. (2014), 'The role of the posterior cingulate cortex in cognition and disease.', *Brain : a journal of neurology* **137**(Pt 1), 12–32.

Lewis, C. M., Baldassarre, A., Committeri, G., Romani, G. L. and Corbetta, M. (2009), 'Learning sculpts the spontaneous activity of the resting human brain.', *Proceedings of the National Academy of Sciences of the United States of America* **106**(41), 17558–63.

Li, H.-J., Hou, X.-H., Liu, H.-H., Yue, C.-L., He, Y. and Zuo, X.-N. (2015), 'Toward systems neuroscience in mild cognitive impairment and Alzheimer's disease: A meta-analysis of 75 fMRI studies', *Human Brain Mapping* **36**(3), 1217–1232.

Li, X., Coyle, D., Maguire, L., Watson, D. R. and McGinnity, T. M. (2011), 'Gray matter concentration and effective connectivity changes in Alzheimer's disease: a longitudinal structural MRI study.', *Neuroradiology* **53**(10), 733–48.

Liégeois, R., Laumann, T. O., Snyder, A. Z., Zhou, J. and Yeo, B. T. (2017), 'Interpreting temporal fluctuations in resting-state functional connectivity MRI', *NeuroImage* **163**(August), 437–455.

Linkenkaer-Hansen, K., Nikouline, V. V., Palva, J. M. and Ilmoniemi, R. J. (2001), 'Long-Range Temporal Correlations and Scaling Behavior in Human Brain Oscillations', *The Journal of Neuroscience* **21**(4), 1370–1377.

Liu, Y., Yu, C., Zhang, X., Liu, J., Duan, Y., Alexander-Bloch, A. F., Liu, B., Jiang, T. and Bullmore, E. (2014), 'Impaired long distance functional connectivity and weighted network architecture in alzheimer's disease', *Cerebral Cortex* **24**(6), 1422–1435.

Lopes da Silva, F. H., Hoeks, A., Smits, H. and Zetterberg, L. H. (1974), 'Model of brain rhythmic activity - The alpha-rhythm of the thalamus', *Kybernetik* .

López, M. E., Bruña, R., Aurtenetxe, S., Pineda-Pardo, J. Á., Marcos, A., Arrazola, J., Reinoso, A. I., Montejo, P., Bajo, R. and Maestú, F. (2014), 'Alpha-band hypersynchronization in progressive mild cognitive impairment: A magnetoencephalography study', *Journal of Neuroscience* .

Lou, B., Li, Y., Philiastides, M. G. and Sajda, P. (2014), 'Prestimulus alpha power predicts fidelity of sensory encoding in perceptual decision making', *NeuroImage* **87**, 242–251.

Lowe, M. J. (2012), 'The emergence of doing "nothing" as a viable paradigm design.', *NeuroImage* **62**(2), 1146–51.

Lowe, M. J., Sakaie, K. E., Beall, E. B., Calhoun, V. D., Bridwell, D. A., Rubinov, M. and Rao, S. M. (2016), 'Modern methods for interrogating the human connectome', *Journal of the International Neuropsychological Society* .

Luo, Q., Lu, W., Cheng, W., Valdes-Sosa, P. A., Wen, X., Ding, M. and Feng, J. (2013), 'Spatio-temporal Granger causality: a new framework.', *NeuroImage* **79**, 241–63.

Lyons, M. K. (2011), 'Deep brain stimulation: Current and future clinical applications'.

Maass, W., Natschläger, T. and Markram, H. (2002), 'Real-time computing without stable states: A new framework for neural computation based on perturbations', *Neural Computation* .

Mac Donald, C. L., Dikranian, K., Bayly, P., Holtzman, D. and Brody, D. (2007), 'Diffusion Tensor Imaging Reliably Detects Experimental Traumatic Axonal Injury and Indicates Approximate Time of Injury', *Journal of Neuroscience* **27**(44), 11869–11876.

Mac Donald, C. L., Dikranian, K., Song, S. K., Bayly, P. V., Holtzman, D. M. and Brody, D. L. (2007), 'Detection of traumatic axonal injury with diffusion tensor imaging in a mouse model of traumatic brain injury', *Experimental Neurology* **205**(1), 116–131.

Mason, M. F., Norton, M. I., Van Horn, J. D., Wegner, D. M., Grafton, S. T. and Macrae, C. N. (2007), 'Wandering minds: The default network and stimulus-independent thought', *Science* **315**(5810), 393–395.

Masters, C. L., Bateman, R., Blennow, K., Rowe, C. C., Sperling, R. A. and Cummings, J. L. (2015), 'Alzheimer's disease', *Nature Reviews Disease Primers* **1**, 15056.

Masuda, N. and Aihara, K. (2004), 'Global and local synchrony of coupled neurons in small-world networks', *Biological Cybernetics* **90**(4), 302–309.

Mathewson, K. E., Gratton, G., Fabiani, M., Beck, D. M. and Ro, T. (2009), 'To See or Not to See: Prestimulus Phase Predicts Visual Awareness', *Journal of Neuroscience* **29**(9), 2725–2732.

Matsuda, H. (2001), 'Cerebral blood flow and metabolic abnormalities in Alzheimer's disease.', *Annals of nuclear medicine* **15**(2), 85–92.

Mattson, M. P. (2004), 'Pathways towards and away from Alzheimer's disease'.

Mazor, O. and Laurent, G. (2005), 'Transient dynamics versus fixed points in odor representations by locust antennal lobe projection neurons', *Neuron* .

McIntosh, A. R. (1999), 'Mapping Cognition to the Brain Through Neural Interactions', *Memory* **7**(5-6), 523–548.

McIntosh, A. R. (2000), 'Towards a network theory of cognition'.

McIntosh, A. R. (2004), 'Contexts and catalysts', *Neuroinformatics* **2**(2), 175–181.

McIntosh, A. R. (2007), Large-scale network dynamics in neurocognitive function, *in* 'Representation and Brain', pp. 337–358.

McKeown, M. J. (2000), 'Detection of consistently task-related activations in fMRI data with hybrid independent component analysis', *NeuroImage* .

Meguro, K., Blaizot, X., Kondoh, Y., Le Mestric, C., Baron, J. C. and Chavoix, C. (1999), 'Neocortical and hippocampal glucose hypometabolism following neurotoxic lesions of the entorhinal and perirhinal cortices in the non-human primate as shown by PET. Implications for Alzheimer's disease', *Brain* **122**, 1519–1531.

Meisel, C., Olbrich, E., Shriki, O. and Achermann, P. (2013), 'Fading Signatures of Critical Brain Dynamics during Sustained Wakefulness in Humans', *Journal of Neuroscience* **33**(44), 17363–17372.

Meng, X., Jun, C., Wang, Q., Zhang, X., Li, Z., Li, Q., Hou, J., Zeng, Q. and Ma, X. (2013), 'High b-value diffusion tensor imaging of the remote white matter and white matter of obstructive unilateral cerebral arterial regions.', *Clinical radiology* **68**(8), 815–22.

Menon, V. (2011), 'Large-scale brain networks and psychopathology: a unifying triple network model.', *Trends in cognitive sciences* **15**(10), 483–506.

Messé, A., Rudrauf, D., Benali, H. and Marrelec, G. (2014), 'Relating Structure and Function in the Human Brain: Relative Contributions of Anatomy, Stationary Dynamics, and Non-stationarities', *PLoS Computational Biology* **10**(3).

Mesulam, M. (2009), 'Defining Neurocognitive Networks in the BOLD New World of Computed Connectivity', *Neuron* **62**(1), 1–3.

Mesulam, M. M. (1998), 'From sensation to cognition'.

Mesulam, M.-M. (2000), *Principles of behavioral and cognitive neurology*, Oxford University Press.

Meszlényi, R. J., Buza, K. and Vidnyánszky, Z. (2017), 'Resting State fMRI Functional Connectivity-Based Classification Using a Convolutional Neural Network Architecture', *Frontiers in Neuroinformatics* **11**.

Metzler-Baddeley, C., Jones, D. K., Steventon, J., Westacott, L., Aggleton, J. P. and O'Sullivan, M. J. (2012), 'Cingulum microstructure predicts cognitive control in older age and mild cognitive impairment', *J Neurosci* **32**(49), 17612–17619.

Mielke, M. M., Okonkwo, O. C., Oishi, K., Mori, S., Tighe, S., Miller, M. I., Ceritoglu, C., Brown, T., Albert, M. and Lyketsos, C. G. (2012), 'Fornix integrity and hippocampal volume predict memory decline and progression to Alzheimer's disease.', *Alzheimer's & dementia : the journal of the Alzheimer's Association* **8**(2), 105–13.

Miller, B. L. (2010), 'A commentary on "disconnexion syndromes in animals and man".', *Neuropsychology review* **20**(2), 126–7.

Minka, T. P. (2001), 'Automatic choice of dimensionality for PCA', *Advances in neural information processing systems* pp. 598–604.

Minoshima, S., Foster, N. L. and Kuhl, D. E. (1994), 'Posterior cingulate cortex in Alzheimer's disease.', *Lancet* **344**(8926), 895.

Minoshima, S., Giordani, B., Berent, S., Frey, K. A., Foster, N. L. and Kuhl, D. E. (1997), 'Metabolic reduction in the posterior cingulate cortex in very early Alzheimer's disease.', *Annals of neurology* **42**(1), 85–94.

Mintun, M. A., Larossa, G. N., Sheline, Y. I., Dence, C. S., Lee, S. Y., MacH, R. H., Klunk, W. E., Mathis, C. A., Dekosky, S. T. and Morris, J. C. (2006), '[11C]PIB in a nondemented population: Potential antecedent marker of Alzheimer disease', *Neurology* **67**, 446–452.

Montague, P. R., Dolan, R. J., Friston, K. and Dayan, P. (2012), 'Computational psychiatry', *Trends in Cognitive Sciences* **16**(1), 72–80.

Moretti, D. V. (2015), 'Theta and alpha EEG frequency interplay in subjects with mild cognitive impairment: evidence from EEG, MRI, and SPECT brain modifications.', *Frontiers in aging neuroscience* **7**, 31.

Moretti, P. and Muñoz, M. A. (2013), 'Griffiths phases and the stretching of criticality in brain networks', *Nature Communications* **4**.

Morgan, R. J. and Soltesz, I. (2008), 'Nonrandom connectivity of the epileptic dentate gyrus predicts a major role for neuronal hubs in seizures', *Proceedings of the National Academy of Sciences* **105**(16), 6179–6184.

Morris, J. C., Heyman, A., Mohs, R. C., Hughes, J. P., van Belle, G., Fillenbaum, G., Mellits, E. D. and Clark, C. (1989), 'The Consortium to Establish a Registry for Alzheimer's Disease (CERAD). Part I. Clinical and neuropsychological assessment of Alzheimer's disease.', *Neurology* **39**, 1159–1165.

Mosconi, L., Tsui, W. H., Herholz, K., Pupi, A., Drzezga, A., Lucignani, G., Reiman, E. M., Holthoff, V., Kalbe, E., Sorbi, S., Diehl-Schmid, J., Perneczky, R., Clerici, F., Caselli, R., Beuthien-Baumann, B., Kurz, A., Minoshima, S. and de Leon, M. J. (2008), 'Multicenter standardized 18F-FDG PET diagnosis of mild cognitive impairment, Alzheimer's disease, and other dementias.', *Journal of nuclear medicine : official publication, Society of Nuclear Medicine* **49**(3), 390–398.

Mountcastle, V. B. (1997), 'The columnar organization of the neocortex'.

Mueller, S. G., Weiner, M. W., Thal, L. J., Petersen, R. C., Jack, C., Jagust, W., Trojanowski, J. Q., Toga, A. W. and Beckett, L. (2005), 'The Alzheimer's Disease Neuroimaging Initiative', *Neuroimaging Clinics of North America* **15**(4), 869–877.

Musso, F., Brinkmeyer, J., Mobascher, A., Warbrick, T. and Winterer, G. (2010), 'Spontaneous brain activity and EEG microstates. A novel EEG/fMRI analysis approach to explore resting-state networks'.

Mutlu, J., Landeau, B., Tomadesso, C., de Flores, R., Mézenge, F., de La Sayette, V., Eustache, F. and Chételat, G. (2016), 'Connectivity disruption, atrophy, and hypometabolism within posterior cingulate networks in Alzheimer's disease', *Frontiers in Neuroscience* **10**(DEC).

Nagumo, J., Arimoto, S. and Yoshizawa, S. (1962), 'An Active Pulse Transmission Line Simulating Nerve Axon*', *Proceedings of the IRE* **50**(10), 2061–2070.

Nair, V. and Hinton, G. E. (2010), 'Rectified Linear Units Improve Restricted Boltzmann Machines', *Proceedings of the 27th International Conference on Machine Learning* (3), 807–814.

Nestor, P. J., Fryer, T. D., Smielewski, P. and Hodges, J. R. (2003), 'Limbic hypometabolism in Alzheimer's disease and mild cognitive impairment', *Annals of Neurology* **54**(3), 343–351.

Netoff, T. I. (2004), 'Epilepsy in Small-World Networks', *Journal of Neuroscience* **24**(37), 8075–8083.

Norris, D. G. (2012), 'Spin-echo fMRI: The poor relation?', *NeuroImage* **62**(2), 1109–1115.

Ódor, G. (2016), 'Critical dynamics on a large human Open Connectome network', *Physical Review E* **94**(6), 062411.

O'Dwyer, L., Lamberton, F., Bokde, A. L. W., Ewers, M., Faluyi, Y. O., Tanner, C., Mazoyer, B., O'Neill, D., Bartley, M., Collins, D. R., Coughlan, T., Prvulovic, D. and Hampel, H. (2011*a*), 'Multiple indices of diffusion identifies white matter damage in mild cognitive impairment and Alzheimer's disease.', *PloS one* **6**(6), e21745.

O'Dwyer, L., Lamberton, F., Bokde, A. L. W., Ewers, M., Faluyi, Y. O., Tanner, C., Mazoyer, B., O'Neill, D., Bartley, M., Collins, D. R., Coughlan, T., Prvulovic, D. and Hampel, H. (2011*b*), 'Using diffusion tensor imaging and mixed-effects models to investigate primary and secondary

white matter degeneration in Alzheimer's disease and mild cognitive impairment.', *Journal of Alzheimer's disease : JAD* **26**(4), 667–82.

Ogawa, S. (2012), 'Finding the BOLD effect in brain images'.

Ogawa, S., Lee, T. M., Kay, A. R. and Tank, D. W. (1990), 'Brain magnetic resonance imaging with contrast dependent on blood oxygenation.', *Proceedings of the National Academy of Sciences of the United States of America* **87**(24), 9868–72.

Omurtag, A., Knight, B. W. and Sirovich, L. (2000), 'On the simulation of large populations of neurons', *Journal of Computational Neuroscience* .

Pajevic, S. and Plenz, D. (2009), 'Efficient network reconstruction from dynamical cascades identifies small-world topology of neuronal avalanches', *PLoS Computational Biology* **5**(1).

Palop, J. and Mucke, L. (2010), 'Amyloid-beta Induced Neuronal Disease : From Synapses toward Neural Networks', *Nature neuroscience* **13**(7), 812–818.

Papadopoulos, L., Kim, J. Z., Kurths, J. and Bassett, D. S. (2017), 'Development of structural correlations and synchronization from adaptive rewiring in networks of Kuramoto oscillators', *Chaos* .

Papez, J. (1937), 'A proposed mechanism of emotion', *Archives of Neurology & Psychiatry* **38**(4), 725–743.

Park, H. J. and Friston, K. (2013), 'Structural and functional brain networks: From connections to cognition'.

Park, Y.-M., Che, H.-J., Im, C.-H., Jung, H.-T., Bae, S.-M. and Lee, S.-H. (2008), 'Decreased EEG synchronization and its correlation with symptom severity in Alzheimer's disease.', *Neuroscience research* **62**(2), 112–7.

Pasternak, O., Sochen, N., Gur, Y., Intrator, N. and Assaf, Y. (2009), 'Free water elimination and mapping from diffusion MRI', *Magnetic Resonance in Medicine* **62**(3), 717–730.

Paszke, A., Chanan, G., Lin, Z., Gross, S., Yang, E., Antiga, L. and Devito, Z. (2017), 'Automatic differentiation in PyTorch', *Advances in Neural Information Processing Systems 30* (Nips), 1–4.

Patel, K. T., Stevens, M. C., Pearlson, G. D., Winkler, A. M., Hawkins, K. A., Skudlarski, P. and Bauer, L. O. (2013), 'Default mode network activity and white matter integrity in healthy middle-aged ApoE4 carriers', *Brain Imaging and Behavior* **7**(1), 60–67.

Pedersen, M. and Omidvarnia, A. (2016), 'Further Insight into the Brain's Rich-Club Architecture', *Journal of Neuroscience* **36**(21), 5675–5676.

Pedro, T., Weiler, M., Yasuda, C. L., D'Abreu, A., Damasceno, B. P., Cendes, F. and Balthazar, M. L. F. (2012), 'Volumetric brain changes in thalamus, corpus callosum and medial temporal structures: Mild alzheimer's disease compared with amnestic mild cognitive impairment', *Dementia and Geriatric Cognitive Disorders* **34**(3-4), 149–155.

Pennanen, C., Kivipelto, M., Tuomainen, S., Hartikainen, P., Hänninen, T., Laakso, M. P., Hallikainen, M., Vanhanen, M., Nissinen, A., Helkala, E.-L. L., Vainio, P., Vanninen, R., Partanen, K. and Soininen, H. (2004), 'Hippocampus and entorhinal cortex in mild cognitive impairment and early AD.', *Neurobiology of Aging* **25**(3), 303–10.

Peper, J. S., Brouwer, R. M., Boomsma, D. I., Kahn, R. S. and Hulshoff Pol, H. E. (2007), 'Genetic influences on human brain structure: A review of brain imaging studies in twins'.

Pereda, E., Quiroga, R. Q. and Bhattacharya, J. (2005), 'Nonlinear multivariate analysis of neurophysiological signals'.

Perl, D. P. (2010), 'Neuropathology of Alzheimer's disease'.

Petersen, R. C. (2004), 'Mild cognitive impairment as a diagnostic entity.', *Journal of internal medicine* **256**(3), 183–94.

Petersen, R. C., Smith, G. E., Waring, S. C., Ivnik, R. J., Tangalos, E. G. and Kokmen, E. (1999), 'Mild cognitive impairment: clinical characterization and outcome.', *Archives of neurology* **56**(3), 303–8.

Petersen, S. E. and Sporns, O. (2015), 'Brain Networks and Cognitive Architectures'.

Piccoli, T., Valente, G., Linden, D. E. J., Re, M., Esposito, F., Sack, A. T. and Salle, F. D. (2015), 'The Default Mode Network and the Working Memory Network Are Not Anti-Correlated during All Phases of a Working Memory Task', *PLOS ONE* **10**(4), e0123354.

Pihlajamäki, M. and Sperling, R. A. (2009), 'Functional MRI assessment of task-induced deactivation of the default mode network in Alzheimer's disease and at-risk older individuals.', *Behavioural neurology* **21**(1), 77–91.

Plenz, D. and Thiagarajan, T. C. (2007), 'The organizing principles of neuronal avalanches: cell assemblies in the cortex?'.

Poil, S. S., Van Ooyen, A. and Linkenkaer-Hansen, K. (2008), 'Avalanche dynamics of human brain oscillations: Relation to critical branching processes and temporal correlations', *Human Brain Mapping* **29**(7), 770–777.

Poldrack, R. A. (2012), 'The future of fMRI in cognitive neuroscience', *NeuroImage* **62**(2), 1216–1220.

Poldrack, R. A. and Farah, M. J. (2015), 'Progress and challenges in probing the human brain', *Nature* **526**(7573), 371–379.

Poline, J.-B. B. and Brett, M. (2012), 'The general linear model and fMRI: Does love last forever?', *NeuroImage* **62**(2), 871–880.

Ponce-Alvarez, A., Deco, G., Hagmann, P., Romani, G. L., Mantini, D. and Corbetta, M. (2015), 'Resting-State Temporal Synchronization Networks Emerge from Connectivity Topology and Heterogeneity', *PLoS Computational Biology* **11**(2).

Power, J. D., Barnes, K. A., Snyder, A. Z., Schlaggar, B. L. and Petersen, S. E. (2012), 'Spurious but systematic correlations in functional connectivity MRI networks arise from subject motion', *NeuroImage* **59**(3), 2142–2154.

Power, J. D., Cohen, A. L., Nelson, S. M., Wig, G. S., Barnes, K. A., Church, J. A., Vogel, A. C., Laumann, T. O., Miezin, F. M., Schlaggar, B. L. and Petersen, S. E. (2011), 'Functional Network Organization of the Human Brain', *Neuron* **72**(4), 665–678.

Power, J. D., Mitra, A., Laumann, T. O., Snyder, A. Z., Schlaggar, B. L. and Petersen, S. E. (2014), 'Methods to detect, characterize, and remove motion artifact in resting state fMRI', *NeuroImage* **84**, 320–341.

Power, J. D., Schlaggar, B. L., Lessov-Schlaggar, C. N. and Petersen, S. E. (2013), 'Evidence for hubs in human functional brain networks', *Neuron* **79**(4), 798–813.

Power, J. D., Schlaggar, B. L. and Petersen, S. E. (2015), 'Recent progress and outstanding issues in motion correction in resting state fMRI', *NeuroImage* **105**, 536–551.

Prichard, D. and Theiler, J. (1994), 'Generating surrogate data for time series with several simultaneously measured variables', *Physical Review Letters* .

Pruessmann, K. P., Weiger, M., Scheidegger, M. B. and Boesiger, P. (1999), 'SENSE: Sensitivity encoding for fast MRI', *Magnetic Resonance in Medicine* **42**, 952–962.

Ptak, R., Schnider, A. and Fellrath, J. (2017), 'The Dorsal Frontoparietal Network: A Core System for Emulated Action'.

Purcell, E. M. (1953), 'Research in Nuclear Magnetism', *Science* .

Purcell, E. M., Torrey, H. C. and Pound, R. V. (1946), 'Resonance absorption by nuclear magnetic moments in a solid [7]'.

Quiroga, R. Q., Reddy, L., Kreiman, G., Koch, C. and Fried, I. (2005), 'Invariant visual representation by single neurons in the human brain', *Nature* **435**(7045), 1102–1107.

Rabinovich, M., Huerta, R. and Laurent, G. (2008), 'Transient Dynamics for Neural Processing', *Source: Science, New Series* .

Rabinovich, M. I., Huerta, R., Varona, P. and Afraimovich, V. S. (2008), 'Transient cognitive dynamics, metastability, and decision making.', *PLoS computational biology* **4**(5), e1000072.

Rabinovich, M. I., Varona, P., Selverston, A. I. and Abarbanel, H. D. (2006), 'Dynamical principles in neuroscience', *Reviews of Modern Physics* .

Radanovic, M., Pereira, F. R. S., Stella, F., Aprahamian, I., Ferreira, L. K., Forlenza, O. V., Busatto, G. F. and Radanovic (2013), 'White matter abnormalities associated with Alzheimer's disease and mild cognitive impairment: a critical review of MRI studies.', *Expert review of neurotherapeutics* **13**(5), 483–93.

Raichle, M. E. (2009), 'A paradigm shift in functional brain imaging.', *The Journal of neuroscience : the official journal of the Society for Neuroscience* **29**(41), 12729–34.

Raichle, M. E. (2010), 'Two views of brain function.', *Trends in cognitive sciences* **14**(4), 180–90.

Raichle, M. E. (2011), 'The restless brain.', *Brain connectivity* **1**(1), 3–12.

Raichle, M. E. (2015), 'The Brain's Default Mode Network', *Annual Review of Neuroscience* .

Raichle, M. E., MacLeod, A. M., Snyder, A. Z., Powers, W. J., Gusnard, D. A. and Shulman, G. L. (2001), 'A default mode of brain function.', *Proceedings of the National Academy of Sciences of the United States of America* **98**(2), 676–82.

Raichle, M. E. and Mintun, M. A. (2006), 'Brain work and brain imaging', *Annual Review of Neuroscience* **29**(1), 449–476.

Raj, A., Kuceyeski, A. and Weiner, M. (2012), 'A network diffusion model of disease progression in dementia.', *Neuron* **73**(6), 1204–15.

Rami, L., Valls-Pedret, C., Bartrés-Faz, D., Caprile, C., Solé-Padullés, C., Castellvi, M., Olives, J., Bosch, B. and Molinuevo, J. L. (2011), 'Cognitive reserve questionnaire. Scores obtained in a healthy elderly population and in one with Alzheimer's disease', *Revista de neurologia* **52**, 195–201.

Reuter, M., Rosas, H. D. and Fischl, B. (2010), 'Highly accurate inverse consistent registration: A robust approach', *NeuroImage* **53**(4), 1181–1196.

Roebroeck, A., Formisano, E. and Goebel, R. (2005), 'Mapping directed influence over the brain using Granger causality and fMRI', *NeuroImage* **25**(1), 230–42.

Roh, J. H., Qiu, A., Seo, S. W., Soon, H. W., Kim, J. H., Kim, G. H., Kim, M.-J., Lee, J.-M. and Na, D. L. (2011), 'Volume reduction in subcortical regions according to severity of Alzheimer's disease.', *Journal of neurology* **258**(6), 1013–20.

Rosen, B. R. and Savoy, R. L. (2012), 'fMRI at 20: Has it changed the world?', *NeuroImage* **62**(2), 1316–1324.

Rosenblum, M. G., Pikovsky, A. S. and Kurths, J. (1996), 'Phase synchronization of chaotic oscillators', *Physical Review Letters* .

Roses, A. D. (1996), 'Apolipoprotein E alleles as risk factors in Alzheimer's disease.', *Annual review of medicine* **47**, 387–400.

Rubinov, M. and Bullmore, E. (2013), 'Fledgling pathoconnectomics of psychiatric disorders.', *Trends in cognitive sciences* **17**(12), 641–7.

Rubinov, M. and Sporns, O. (2010), 'Complex network measures of brain connectivity: Uses and interpretations', *NeuroImage* **52**(3), 1059–1069.

Rubinov, M., Sporns, O., van Leeuwen, C. and Breakspear, M. (2009), 'Symbiotic relationship between brain structure and dynamics.', *BMC neuroscience* **10**, 55.

Ryan, N. S., Keihaninejad, S., Shakespeare, T. J., Lehmann, M., Crutch, S. J., Malone, I. B., Thornton, J. S., Mancini, L., Hyare, H., Yousry, T., Ridgway, G. R., Zhang, H., Modat, M., Alexander, D. C., Rossor, M. N., Ourselin, S. and Fox, N. C. (2013), 'Magnetic resonance imaging evidence for presymptomatic change in thalamus and caudate in familial Alzheimer's disease', *Brain* **136**, 1399–1414.

Saalmann, Y. B., Pinsk, M. A., Wang, L., Li, X. and Kastner, S. (2012), 'The pulvinar regulates information transmission between cortical areas based on attention demands.', *Science (New York, N.Y.)* **337**(6095), 753–6.

Sachdev, P. S., Zhuang, L., Braidy, N. and Wen, W. (2013), 'Is Alzheimer's a disease of the white matter?', *Current Opinion in Psychiatry* **26**(3), 244–251.

Sadaghiani, S. and D'Esposito, M. (2015), 'Functional characterization of the cingulo-opercular network in the maintenance of tonic alertness', *Cerebral Cortex* **25**(9), 2763–2773.

Sadaghiani, S., Hesselmann, G., Friston, K. J. and Kleinschmidt, A. (2010), 'The relation of ongoing brain activity, evoked neural responses, and cognition', *Frontiers in Systems Neuroscience* .

Sadaghiani, S., Hesselmann, G. and Kleinschmidt, A. (2009), 'Distributed and Antagonistic Contributions of Ongoing Activity Fluctuations to Auditory Stimulus Detection', *Journal of Neuroscience* **29**(42), 13410–13417.

Sadaghiani, S. and Kleinschmidt, A. (2013), 'Functional interactions between intrinsic brain activity and behavior', *NeuroImage* **80**, 379–386.

Sanz-Leon, P., Knock, S. A., Spiegler, A. and Jirsa, V. K. (2015), 'Mathematical framework for large-scale brain network modeling in The Virtual Brain.', *NeuroImage* **111**, 385–430.

Saunders, R. C., Mishkin, M. and Aggleton, J. P. (2005), 'Projections from the entorhinal cortex, perirhinal cortex, presubiculum, and parasubiculum to the medial thalamus in macaque monkeys: identifying different pathways using disconnection techniques.', *Experimental brain research* **167**(1), 1–16.

Savoy, R. L. (2001), 'History and future directions of human brain mapping and functional neuroimaging', *Acta Psychologica* **107**(1-3), 9–42.

Schacter, D. L., Addis, D. R. and Buckner, R. L. (2007), 'Remembering the past to imagine the future: The prospective brain'.

Schacter, D. L., Addis, D. R. and Buckner, R. L. (2008), 'Episodic simulation of future events: Concepts, data, and applications'.

Schelter, B., Winterhalder, M. and Timmer, J. (2006), 'Handbook of Time Series Analysis'.

Schilbach, L., Eickhoff, S. B., Rotarska-Jagiela, A., Fink, G. R. and Vogeley, K. (2008), 'Minds at rest? Social cognition as the default mode of cognizing and its putative relationship to the "default system" of the brain', *Consciousness and Cognition* **17**(2), 457–467.

Schippers, M. B., Renken, R. and Keysers, C. (2011), 'The effect of intra- and inter-subject variability of hemodynamic responses on group level Granger causality analyses', *NeuroImage* **57**(1), 22–36.

Schirner, M., Rothmeier, S., Jirsa, V. K., McIntosh, A. R. and Ritter, P. (2015), 'An automated pipeline for constructing personalised virtual brains from multimodal neuroimaging data', *NeuroImage* **117**, 343–357.

Schmidt, R., LaFleur, K. J. R., de Reus, M. A., van den Berg, L. H. and van den Heuvel, M. P. (2015), 'Kuramoto model simulation of neural

hubs and dynamic synchrony in the human cerebral connectome.', *BMC neuroscience* **16**, 54.

Schmitt, L. I., Wimmer, R. D., Nakajima, M., Happ, M., Mofakham, S. and Halassa, M. M. (2017), 'Thalamic amplification of cortical connectivity sustains attentional control', *Nature* **545**(7653), 219–223.

Schreckenberger, M., Lange-Asschenfeldt, C., Lange-Asschenfeld, C., Lochmann, M., Mann, K., Siessmeier, T., Buchholz, H.-G., Bartenstein, P. and Gründer, G. (2004), 'The thalamus as the generator and modulator of EEG alpha rhythm: a combined PET/EEG study with lorazepam challenge in humans.', *NeuroImage* **22**(2), 637–44.

Schultz, D. H. and Cole, M. W. (2016), 'Higher Intelligence Is Associated with Less Task-Related Brain Network Reconfiguration', *The Journal of Neuroscience* **36**(33), 8551–8561.

Seeley, W. W., Crawford, R. K., Zhou, J., Miller, B. L. and Greicius, M. D. (2009), 'Neurodegenerative Diseases Target Large-Scale Human Brain Networks', *Neuron* **62**(1), 42–52.

Ségonne, F., Pacheco, J. and Fischl, B. (2007), 'Geometrically accurate topology-correction of cortical surfaces using nonseparating loops', *IEEE Transactions on Medical Imaging* **26**(4), 518–529.

Senden, M., Deco, G., De Reus, M. A., Goebel, R. and Van Den Heuvel, M. P. (2014), 'Rich club organization supports a diverse set of functional network configurations', *NeuroImage* **96**, 174–182.

Senden, M., Reuter, N., van den Heuvel, M. P., Goebel, R. and Deco, G. (2017), 'Cortical rich club regions can organize state-dependent functional network formation by engaging in oscillatory behavior', *NeuroImage* **146**, 561–574.

Seth, A. K., Chorley, P. and Barnett, L. C. (2013), 'Granger causality analysis of fMRI BOLD signals is invariant to hemodynamic convolution but not downsampling', *NeuroImage* **65**, 540–55.

Shanahan, M. (2006), 'A cognitive architecture that combines internal simulation with a global workspace', *Consciousness and Cognition* **15**(2), 433–449.

Shanahan, M. (2010), 'Metastable chimera states in community-structured oscillator networks.', *Chaos (Woodbury, N.Y.)* **20**(1), 013108.

Shanahan, M. (2012), 'The brain's connective core and its role in animal cognition', *Philosophical Transactions of the Royal Society B: Biological Sciences* **367**(1603), 2704–2714.

Shehzad, Z., Kelly, A. M. C., Reiss, P. T., Gee, D. G., Gotimer, K., Uddin, L. Q., Lee, S. H., Margulies, D. S., Roy, A. K., Biswal, B. B., Petkova, E., Castellanos, F. X. and Milham, M. P. (2009), 'The resting brain: Unconstrained yet reliable', *Cerebral Cortex* **19**(10), 2209–2229.

Sheline, Y. I., Morris, J. C., Snyder, A. Z., Price, J. L., Yan, Z., D'Angelo, G., Liu, C., Dixit, S., Benzinger, T., Fagan, A., Goate, A. and Mintun, M. A. (2010), 'APOE4 allele disrupts resting state fMRI connectivity in the absence of amyloid plaques or decreased CSF A$\beta$42.', *The Journal of neuroscience : the official journal of the Society for Neuroscience* **30**, 17035–17040.

Sheline, Y. I., Raichle, M. E., Snyder, A. Z., Morris, J. C., Head, D., Wang, S. and Mintun, M. a. (2011), 'Amyloid Plaques Disrupt Resting State Default Mode Network Connectivity in Cognitively Normal Elderly', *Biological psychiatry* **67**(6), 584–587.

Sherman, S. M. (2007), 'The thalamus is more than just a relay.', *Current opinion in neurobiology* **17**(4), 417–422.

Sherman, S. M. and Guillery, R. W. (2006), *Exploring the thalamus*.

Shew, W. L. and Plenz, D. (2013), 'The Functional Benefits of Criticality in the Cortex', *The Neuroscientist* **19**(1), 88–100.

Shiino, A., Watanabe, T., Maeda, K., Kotani, E., Akiguchi, I. and Matsuda, M. (2006), 'Four subgroups of Alzheimer's disease based on patterns of

atrophy using VBM and a unique pattern for early onset disease.', *NeuroImage* **33**(1), 17–26.

Shine, J. M., Aburn, M. J., Breakspear, M. and Poldrack, R. A. (2018), 'The modulation of neural gain facilitates a transition between functional segregation and integration in the brain', *eLife* **7**.

Shine, J. M., Bissett, P. G., Bell, P. T., Koyejo, O., Balsters, J. H., Gorgolewski, K. J., Moodie, C. A. and Poldrack, R. A. (2016), 'The Dynamics of Functional Brain Networks: Integrated Network States during Cognitive Task Performance', *Neuron* **92**(2), 544–554.

Shine, J. M., Koyejo, O. and Poldrack, R. A. (2016), 'Temporal metastates are associated with differential patterns of time-resolved connectivity, network topology, and attention', *Proceedings of the National Academy of Sciences of the United States of America* .

Shine, J. M., van den Brink, R. L., Hernaus, D., Nieuwenhuis, S. and Poldrack, R. A. (2018), 'Catecholaminergic manipulation alters dynamic network topology across cognitive states.', *Network neuroscience (Cambridge, Mass.)* **2**(3), 381–396.

Skudlarski, P., Jagannathan, K., Calhoun, V. D., Hampson, M., Skudlarska, B. A. and Pearlson, G. (2008), 'Measuring brain connectivity: Diffusion tensor imaging validates resting state temporal correlations', *NeuroImage* .

Sled, J. G., Zijdenbos, a. P. and Evans, a. C. (1998), 'A nonparametric method for automatic correction of intensity nonuniformity in MRI data.', *IEEE transactions on medical imaging* **17**(1), 87–97.

Smith, R. E., Tournier, J.-D. D., Calamante, F. and Connelly, A. (2013), 'SIFT: Spherical-deconvolution informed filtering of tractograms', *NeuroImage* **67**, 298–312.

Smith, R., Keramatian, K. and Christoff, K. (2007), 'Localizing the rostrolateral prefrontal cortex at the individual level', *NeuroImage* **36**(4), 1387–1396.

Smith, S. M. (2002), 'Fast robust automated brain extraction', *Human Brain Mapping* **17**, 143–155.

Smith, S. M. (2012), 'The future of FMRI connectivity.', *NeuroImage* **62**(2), 1257–66.

Smith, S. M., Fox, P. T., Miller, K. L., Glahn, D. C., Fox, P. M., Mackay, C. E., Filippini, N., Watkins, K. E., Toro, R., Laird, A. R. and Beckmann, C. F. (2009), 'Correspondence of the brain' s functional architecture during activation and rest', *Proceedings of the National Academy of Sciences of the United States of America* **106**, 13040–13045.

Smith, S. M., Jenkinson, M., Woolrich, M. W., Beckmann, C. F., Behrens, T. E., Johansen-Berg, H., Bannister, P. R., De Luca, M., Drobnjak, I., Flitney, D. E., Niazy, R. K., Saunders, J., Vickers, J., Zhang, Y., De Stefano, N., Brady, J. M. and Matthews, P. M. (2004), Advances in functional and structural MR image analysis and implementation as FSL, *in* 'NeuroImage', Vol. 23.

Smith, S. M., Miller, K. L., Salimi-Khorshidi, G., Webster, M., Beckmann, C. F., Nichols, T. E., Ramsey, J. D. and Woolrich, M. W. (2011), 'Network modelling methods for FMRI.', *NeuroImage* **54**(2), 875–91.

Smith, S. M. and Nichols, T. E. (2009), 'Threshold-free cluster enhancement: addressing problems of smoothing, threshold dependence and localisation in cluster inference.', *NeuroImage* **44**(1), 83–98.

Snyder, A. Z. and Raichle, M. E. (2012), 'A brief history of the resting state: the Washington University perspective.', *NeuroImage* **62**(2), 902–10.

Soares, J. M., Marques, P., Alves, V. and Sousa, N. (2013), 'A hitchhiker's guide to diffusion tensor imaging.', *Frontiers in neuroscience* **7**(March), 31.

Sompolinsky, H., Crisanti, A. and Sommers, H. J. (1988), 'Chaos in random neural networks', *Physical Review Letters* .

Sorg, C., Calhoun, V. D., Eichele, T., La, L., Riedl, V., Mu, M., Kurz, A., Zimmer, C., Wohlschla, A. M., Drzezga, A. and Fo, H. (2007), 'Selective changes of resting-state networks in individuals at risk for Alzheimer ' s disease', *PNAS* **104**(47).

Sormaz, M., Murphy, C., Wang, H.-t., Hymers, M., Karapanagiotidis, T., Poerio, G., Margulies, D. S., Jefferies, E. and Smallwood, J. (2018), 'Default mode network can support the level of detail in experience during active task states', *Proceedings of the National Academy of Sciences* **115**(37), 9318–9323.

Spadone, S., Della Penna, S., Sestieri, C., Betti, V., Tosoni, A., Perrucci, M. G., Romani, G. L. and Corbetta, M. (2015), 'Dynamic reorganization of human resting-state networks during visuospatial attention.', *Proceedings of the National Academy of Sciences of the United States of America* **112**(26), 8112–7.

Sporns, O. (2000), 'Theoretical Neuroanatomy: Relating Anatomical and Functional Connectivity in Graphs and Cortical Connection Matrices', *Cerebral Cortex* **10**(2), 127–141.

Sporns, O. (2006), 'Small-world connectivity, motif composition, and complexity of fractal neuronal connections', *BioSystems* **85**(1), 55–64.

Sporns, O. (2010), *Networks of the Brain*, The MIT Press.

Sporns, O. (2011*a*), *Networks of the brain*, MIT Press.

Sporns, O. (2011*b*), 'The human connectome: a complex network.', *Annals of the New York Academy of Sciences* **1224**, 109–25.

Sporns, O. (2011*c*), 'The non-random brain: efficiency, economy, and complex dynamics.', *Frontiers in computational neuroscience* **5**(February), 5.

Sporns, O. (2012), 'From simple graphs to the connectome: networks in neuroimaging.', *NeuroImage* **62**(2), 881–6.

Sporns, O. (2013*a*), 'Making sense of brain network data.', *Nature methods* **10**(6), 491–3.

Sporns, O. (2013*b*), 'Network attributes for segregation and integration in the human brain.', *Current opinion in neurobiology* **23**(2), 162–171.

Sporns, O. (2013*c*), 'The human connectome: origins and challenges.', *NeuroImage* **80**, 53–61.

Sporns, O. (2014), 'Contributions and challenges for network models in cognitive neuroscience.', *Nature neuroscience* **17**(5), 652–60.

Sporns, O. and Honey, C. J. (2006), 'Small worlds inside big brains.', *Proceedings of the National Academy of Sciences of the United States of America* **103**(51), 19219–20.

Sporns, O. and Tononi, G. (2001), 'Classes of network connectivity and dynamics', *Complexity* **7**(1), 28–38.

Sporns, O., Tononi, G. and Edelman, G. M. (2000), 'Connectivity and complexity: The relationship between neuroanatomy and brain dynamics'.

Spreng, N. R. (2012), 'The fallacy of a "task-negative" network', *Frontiers in Psychology* **3**(MAY), 1–5.

Spreng, R. N., Mar, R. A. and Kim, A. S. N. (2009), 'The Common Neural Basis of Autobiographical Memory, Prospection, Navigation, Theory of Mind, and the Default Mode: A Quantitative Meta-analysis', *Journal of Cognitive Neuroscience* **21**(3), 489–510.

Spreng, R. N., Stevens, W. D., Chamberlain, J. P., Gilmore, A. W. and Schacter, D. L. (2010), 'Default network activity, coupled with the frontoparietal control network, supports goal-directed cognition', *NeuroImage* **53**(1), 303–317.

Srivastava, N., Hinton, G., Krizhevsky, A., Sutskever, I. and Salakhutdinov, R. (2014), 'Dropout: A Simple Way to Prevent Neural Networks from Overfitting', *Journal of Machine Learning Research* **15**, 1929–1958.

Stam, C. J. (2004), 'Functional connectivity patterns of human magnetoencephalographic recordings: A 'small-world' network?', *Neuroscience Letters* **355**(1-2), 25–28.

Stam, C. J., de Haan, W., Daffertshofer, a., Jones, B. F., Manshanden, I., van Cappellen van Walsum, a. M., Montez, T., Verbunt, J. P. a., de Munck, J. C., van Dijk, B. W., Berendse, H. W. and Scheltens, P. (2009), 'Graph theoretical analysis of magnetoencephalographic functional connectivity in Alzheimer's disease.', *Brain : a journal of neurology* **132**(Pt 1), 213–24.

Stam, C. J., Jones, B. F., Nolte, G., Breakspear, M. and Scheltens, P. (2007), 'Small-world networks and functional connectivity in Alzheimer's disease.', *Cerebral cortex (New York, N.Y. : 1991)* **17**(1), 92–9.

Stam, C. J., Nolte, G. and Daffertshofer, A. (2007), 'Phase lag index: Assessment of functional connectivity from multi channel EEG and MEG with diminished bias from common sources', *Human Brain Mapping* .

Stam, C. and van Straaten, E. (2012), 'The organization of physiological brain networks', *Clinical Neurophysiology* **123**(6), 1067–1087.

Stefanescu, R. A. and Jirsa, V. K. (2011), 'Reduced representations of heterogeneous mixed neural networks with synaptic coupling', *Physical Review E - Statistical, Nonlinear, and Soft Matter Physics* .

Stephan, K. E. and Friston, K. (2007), 'Models of effective connectivity in neural systems'.

Stephan, K. E. and Friston, K. (2010), 'Analyzing effective connectivity with fMRI.', *Wiley interdisciplinary reviews. Cognitive science* **1**(3), 446–459.

Stephan, K. E. and Mathys, C. (2014), 'Computational approaches to psychiatry', *Current Opinion in Neurobiology* **25**, 85–92.

Stephan, K. E. and Roebroeck, A. (2012), 'A short history of causal modeling of fMRI data.', *NeuroImage* **62**(2), 856–63.

Stratton, P. and Wiles, J. (2015), 'Global segregation of cortical activity and metastable dynamics.', *Frontiers in systems neuroscience* **9**, 119.

Strogatz, S. H. (2000), 'From Kuramoto to Crawford: exploring the onset of synchronization in populations of coupled oscillators', *Physica D: Nonlinear Phenomena* **143**(1), 1–20.

Sun, F. T., Miller, L. M. and D'Esposito, M. (2004), 'Measuring interregional functional connectivity using coherence and partial coherence analyses of fMRI data', *NeuroImage* **21**(2), 647–658.

Supekar, K., Menon, V., Rubin, D., Musen, M. and Greicius, M. D. (2008), 'Network analysis of intrinsic functional brain connectivity in Alzheimer's disease.', *PLoS computational biology* **4**(6), e1000100.

Tagliazucchi, E., Balenzuela, P., Fraiman, D. and Chialvo, D. R. (2012), 'Criticality in large-scale brain fmri dynamics unveiled by a novel point process analysis', *Frontiers in Physiology* **3 FEB**.

Teipel, S. and Grothe, M. J. (2016), 'Does posterior cingulate hypometabolism result from disconnection or local pathology across preclinical and clinical stages of Alzheimer's disease?', *European Journal of Nuclear Medicine and Molecular Imaging* **43**(3), 526–536.

Teipel, S. J., Grothe, M. J., Filippi, M., Fellgiebel, A., Dyrba, M., Frisoni, G. B., Meindl, T., Bokde, A. L. W., Hampel, H., Kl??ppel, S. and Hauenstein, K. (2014), 'Fractional anisotropy changes in Alzheimer's disease depend on the underlying fiber tract architecture: A multiparametric DTI study using joint independent component analysis', *Journal of Alzheimer's Disease* **41**(1), 69–83.

Theiler, J., Eubank, S., Longtin, A., Galdrikian, B. and Doyne Farmer, J. (1992), 'Testing for nonlinearity in time series: the method of surrogate data', *Physica D: Nonlinear Phenomena* .

Therriault, J., Ng, K. P., Pascoal, T. A., Mathotaarachchi, S., Kang, M. S., Struyfs, H., Shin, M., Benedet, A. L., Walpola, I. C., Nair, V., Gauthier, S., Rosa-Neto, P. and Alzheimer's Disease Neuroimaging Initiative, F. t. A. D. N. (2018), 'Anosognosia predicts default mode network hypometabolism and clinical progression to dementia.', *Neurology* **90**(11), e932–e939.

Thompson, P. M., Cannon, T. D., Narr, K. L., Van Erp, T., Poutanen, V. P., Huttunen, M., Lönnqvist, J., Standertskjöld-Nordenstam, C. G., Kaprio, J., Khaledy, M., Dail, R., Zoumalan, C. I. and Toga, A. W. (2001), 'Genetic influences on brain structure', *Nature Neuroscience* .

Tijms, B. M., Wink, A. M., de Haan, W., van der Flier, W. M., Stam, C. J., Scheltens, P. and Barkhof, F. (2013), 'Alzheimer's disease: connecting findings from graph theoretical studies of brain networks', *Neurobiology of Aging* **34**(8), 2023–2036.

Todd, S., Barr, S., Roberts, M. and Passmore, A. P. (2013), 'Survival in dementia and predictors of mortality: a review', *International Journal of Geriatric Psychiatry* **28**(11), n/a–n/a.

Tognoli, E. and Kelso, J. (2009), 'Brain coordination dynamics: True and false faces of phase synchrony and metastability', *Progress in Neurobiology* **87**(1), 31–40.

Tognoli, E. and Kelso, J. (2014*a*), 'Enlarging the scope: grasping brain complexity.', *Frontiers in systems neuroscience* **8**, 122.

Tognoli, E. and Kelso, J. (2014*b*), 'The Metastable Brain', *Neuron* **81**(1), 35–48.

Tomescu, M. I., Rihs, T. A., Becker, R., Britz, J., Custo, A., Grouiller, F., Schneider, M., Debbané, M., Eliez, S. and Michel, C. M. (2014), 'De-

viant dynamics of EEG resting state pattern in 22q11.2 deletion syndrome adolescents: A vulnerability marker of schizophrenia?', *Schizophrenia Research* .

Tononi, G., Edelman, G. M. and Sporns, O. (1998), 'Complexity and coherency: Integrating information in the brain'.

Tononi, G., Sporns, O. and Edelman, G. M. (1994), 'A measure for brain complexity: relating functional segregation and integration in the nervous system.', *Proceedings of the National Academy of Sciences of the United States of America* **91**(11), 5033–7.

Tournier, J. D., Calamante, F. and Connelly, A. (2007), 'Robust determination of the fibre orientation distribution in diffusion MRI: Non-negativity constrained super-resolved spherical deconvolution', *NeuroImage* **35**, 1459–1472.

Tournier, J.-D., Calamante, F. and Connelly, A. (2012), 'MRtrix: Diffusion tractography in crossing fiber regions', *International Journal of Imaging Systems and Technology* **22**(1), 53–66.

Tournier, J.-D., Calamante, F., Gadian, D. G. and Connelly, A. (2004), 'Direct estimation of the fiber orientation density function from diffusion-weighted MRI data using spherical deconvolution.', *NeuroImage* **23**(3), 1176–85.

Tournier, J.-D., Yeh, C.-H., Calamante, F., Cho, K.-H., Connelly, A. and Lin, C.-P. (2008), 'Resolving crossing fibres using constrained spherical deconvolution: validation using diffusion-weighted imaging phantom data.', *NeuroImage* **42**(2), 617–25.

Tsuda, I. (2001), 'Toward an interpretation of dynamic neural activity in terms of chaotic dynamical systems', *Behavioral and Brain Sciences* .

Turner, R. (2012), 'The NIH experience in first advancing fMRI'.

Uhlhaas, P. (2015), 'Neural dynamics in mental disorders.', *World psychiatry : official journal of the World Psychiatric Association (WPA)* **14**(2), 116–8.

Uhlhaas, P. J. and Singer, W. (2006), 'Neural Synchrony in Brain Disorders: Relevance for Cognitive Dysfunctions and Pathophysiology'.

Uurbil, K. (2012), 'Development of functional imaging in the human brain (fMRI); the University of Minnesota experience'.

Valdes, P. A., Jimenez, J. C., Riera, J., Biscay, R. and Ozaki, T. (1999), 'Nonlinear EEG analysis based on a neural mass model', *Biological Cybernetics* .

Valdes-Sosa, P. a., Roebroeck, A., Daunizeau, J. and Friston, K. (2011), 'Effective connectivity: influence, causality and biophysical modeling.', *NeuroImage* **58**(2), 339–61.

Valla, J., Berndt, J. D. and Gonzalez-Lima, F. (2001), 'Energy hypometabolism in posterior cingulate cortex of Alzheimer's patients: superficial laminar cytochrome oxidase associated with disease duration.', *The Journal of neuroscience : the official journal of the Society for Neuroscience* **21**, 4923–4930.

Van De Ven, V. G., Formisano, E., Prvulovic, D., Roeder, C. H. and Linden, D. E. J. (2004), 'Functional connectivity as revealed by spatial independent component analysis of fMRI measurements during rest', *Human Brain Mapping* **22**(3), 165–178.

Van De Ville, D., Britz, J. and Michel, C. M. (2010), 'EEG microstate sequences in healthy humans at rest reveal scale-free dynamics', *Proceedings of the National Academy of Sciences of the United States of America* .

Van Den Berg, B., Appelbaum, L. G., Clark, K., Lorist, M. M. and Woldorff, M. G. (2016), 'Visual search performance is predicted by both prestimulus and poststimulus electrical brain activity', *Scientific Reports* **6**.

van den Heuvel, M., Mandl, R. C. W., van den Heuvel, M. P. and Mandl, R. C. W. (2009), 'Functionally linked resting-state networks reflect the underlying structural connectivity architecture of the human brain', *Human brain mapping* .

van den Heuvel, M. P. and Fornito, A. (2014), 'Brain networks in schizophrenia'.

van den Heuvel, M. P., Kahn, R. S., Goni, J. and Sporns, O. (2012), 'High-cost, high-capacity backbone for global brain communication', *Proceedings of the National Academy of Sciences* **109**(28), 11372–11377.

van den Heuvel, M. P., Mandl, R. C. W., Stam, C. J., Kahn, R. S. and Hulshoff Pol, H. E. (2010), 'Aberrant Frontal and Temporal Complex Network Structure in Schizophrenia: A Graph Theoretical Analysis', *Journal of Neuroscience* **30**(47), 15915–15926.

van den Heuvel, M. P. and Sporns, O. (2011), 'Rich-club organization of the human connectome.', *The Journal of neuroscience : the official journal of the Society for Neuroscience* **31**(44), 15775–86.

van den Heuvel, M. P. and Sporns, O. (2013), 'Network hubs in the human brain.', *Trends in cognitive sciences* **17**(12), 683–96.

van den Heuvel, M. P., Sporns, O., Collin, G., Scheewe, T., Mandl, R. C. W., Cahn, W., Goñi, J., Hulshoff Pol, H. E., Kahn, R. S., Goni, J., Pol, H. E. and Kahn, R. S. (2013), 'Abnormal rich club organization and functional brain dynamics in schizophrenia', *JAMA psychiatry* **70**(8), 783–92.

van Dijk, H., Schoffelen, J.-M., Oostenveld, R. and Jensen, O. (2008), 'Prestimulus Oscillatory Activity in the Alpha Band Predicts Visual Discrimination Ability', *Journal of Neuroscience* **28**(8), 1816–1823.

Van Essen, D. C., Anderson, C. H. and Felleman, D. J. (1992), 'Information processing in the primate visual system: An integrated systems perspective'.

Van Essen, D. C., Smith, J., Glasser, M. F., Elam, J., Donahue, C. J., Dierker, D. L., Reid, E. K., Coalson, T. and Harwell, J. (2017), 'The Brain Analysis Library of Spatial maps and Atlases (BALSA) database', *NeuroImage* **144**(Pt B), 270–274.

Van Essen, D. C., Smith, S. M., Barch, D. M., Behrens, T. E., Yacoub, E. and Ugurbil, K. (2013), 'The WU-Minn Human Connectome Project: An overview', *NeuroImage* **80**, 62–79.

van Zijl, P. C., Hua, J. and Lu, H. (2012), 'The BOLD post-stimulus undershoot, one of the most debated issues in fMRI'.

Vann, S. D., Aggleton, J. P. and Maguire, E. A. (2009), 'What does the retrosplenial cortex do?', *Nature reviews. Neuroscience* **10**, 792–802.

Varela, F. J. (1995), Resonant cell assemblies: A new approach to cognitive functions and neuronal synchrony, *in* 'Biological Research', Vol. 28, pp. 81–95.

Varela, F., Lachaux, J. P., Rodriguez, E. and Martinerie, J. (2001), 'The brainweb: phase synchronization and large-scale integration.', *Nature reviews. Neuroscience* **2**(4), 229–39.

Váša, F., Shanahan, M., Hellyer, P. J., Scott, G., Cabral, J. and Leech, R. (2015), 'Effects of lesions on synchrony and metastability in cortical networks.', *NeuroImage* **118**, 456–67.

Vidaurre, D., Abeysuriya, R., Becker, R., Quinn, A. J., Alfaro-Almagro, F., Smith, S. M. and Woolrich, M. W. (2018), 'Discovering dynamic brain networks from big data in rest and task'.

Vidaurre, D., Smith, S. M. and Woolrich, M. W. (2017), 'Brain network dynamics are hierarchically organized in time', *Proceedings of the National Academy of Sciences of the United States of America* .

Villain, N., Desgranges, B., Viader, F., de la Sayette, V., Mézenge, F., Landeau, B., Baron, J.-C., Eustache, F. and Chételat, G. (2008), 'Relationships between hippocampal atrophy, white matter disruption, and gray

matter hypometabolism in Alzheimer's disease.', *The Journal of neuroscience : the official journal of the Society for Neuroscience* **28**(24), 6174–6181.

Vincent, J. L., Kahn, I., Snyder, A. Z., Raichle, M. E. and Buckner, R. L. (2008), 'Evidence for a Frontoparietal Control System Revealed by Intrinsic Functional Connectivity', *Journal of Neurophysiology* **100**(6), 3328–3342.

Vogels, T. P., Rajan, K. and Abbott, L. F. (2005), 'Neural Network Dynamics', *Annual Review of Neuroscience* **28**(1), 357–376.

Wager, S., Wang, S. and Liang, P. (2013), 'Dropout Training as Adaptive Regularization arXiv : 1307 . 1493v2 [ stat . ML ] 1 Nov 2013', *Nips* pp. 1–11.

Wang, D., Kong, Y., Chu, W. C. W., Tam, C. W. C., Lam, L. C. W., Wang, Y., Northoff, G., Mok, V. C. T., Wang, Y. and Shi, L. (2014), 'Generation of the probabilistic template of default mode network derived from resting-state fMRI.', *IEEE transactions on bio-medical engineering* **61**(10), 2550–5.

Wang, J., Gu, B. J., Masters, C. L. and Wang, Y.-J. (2017), 'A systemic view of Alzheimer disease — insights from amyloid-$\beta$ metabolism beyond the brain', *Nature Reviews Neurology* **13**(10), 612–623.

Wang, Z., Dai, Z., Gong, G., Zhou, C. and He, Y. (2014), 'Understanding Structural-Functional Relationships in the Human Brain: A Large-Scale Network Perspective.', *The Neuroscientist : a review journal bringing neurobiology, neurology and psychiatry* .

Warren, D. E., Power, J. D., Bruss, J., Denburg, N. L., Waldron, E. J., Sun, H., Petersen, S. E. and Tranel, D. (2014), 'Network measures predict neuropsychological outcome after brain injury', *Proceedings of the National Academy of Sciences* **111**(39), 14247–14252.

Watts, D. J. and Strogatz, S. H. (1998), 'Collective dynamics of 'small-world' networks', *Nature* **393**(6684), 440–442.

Wechsler, D. (1987), *Manual for Wechsler Memory Scale - Revised*.

Welsh, K. A., Butters, N., Hughes, J. P., Mohs, R. C. and Heyman, A. (1992), 'Detection and staging of dementia in Alzheimer's disease. Use of the neuropsychological measures developed for the Consortium to Establish a Registry for Alzheimer's Disease.', *Archives of neurology* **49**, 448–452.

Welsh, K., Butters, N., Hughes, J., Mohs, R. and Heyman, A. (1991), 'Detection of abnormal memory decline in mild cases of Alzheimer's disease using CERAD neuropsychological measures.', *Archives of neurology* **48**, 278–281.

Wen, X., Rangarajan, G. and Ding, M. (2013), 'Is Granger Causality a Viable Technique for Analyzing fMRI Data?', *PLoS ONE* **8**(7).

Wermke, M., Sorg, C., Wohlschläger, A. M. and Drzezga, A. (2008), 'A new integrative model of cerebral activation, deactivation and default mode function in Alzheimer's disease.', *European journal of nuclear medicine and molecular imaging* **35 Suppl 1**, S12–24.

Wernicke, C. (1876), 'Das Urwindungssystem des menschlichen Gehirns', *Archiv f??r Psychiatrie und Nervenkrankheiten* **6**(1), 298–326.

Wheatley, T., Milleville, S. C. and Martin, A. (2007), 'Understanding animate agents: Distinct roles for the social network and mirror system: Research report', *Psychological Science* **18**(6), 469–474.

Wheeler-Kingshott, C. A. M. and Cercignani, M. (2009), 'About "axial" and "radial" diffusivities.', *Magnetic resonance in medicine* **61**(5), 1255–60.

Wiener, N. (1948), *Cybernetics: or the control and communication in the animal and the machine*.

Wiener, N. (1956), The Theory of Prediction, *in* 'Modern Mathematics for Engineers', Vol. 58, pp. 323–329.

Wildie, M. and Shanahan, M. (2012), 'Metastability and chimera states in modular delay and pulse-coupled oscillator networks', *Chaos* **22**(4), 043131.

Wilson, H. R. and Cowan, J. D. (1972), 'Excitatory and Inhibitory Interactions in Localized Populations of Model Neurons', *Biophysical Journal* .

Wirths, O., Weis, J., Kayed, R., Saido, T. C. and Bayer, T. A. (2007), 'Age-dependent axonal degeneration in an Alzheimer mouse model', *Neurobiology of Aging* **28**(11), 1689–1699.

Wirths, O., Weis, J., Szczygielski, J., Multhaup, G. and Bayer, T. A. (2006), 'Axonopathy in an APP/PS1 transgenic mouse model of Alzheimer's disease', *Acta Neuropathologica* **111**(4), 312–319.

Wojtuń, K., Kadzioļka, W., Kobak, G. and Kadziolłka, J. (2010), 'Ropień śródpiersia przedniego jako cieżkie powiklłanie urazu komunikacyjnego', *Kardiochirurgia i Torakochirurgia Polska* **7**(4), 436–438.

Wolf, A., Swift, J. B., Swinney, H. L. and Vastano, J. A. (1985), 'Determining Lyapunov exponents from a time series', *Physica D: Nonlinear Phenomena* .

Wolff, M. and Vann, S. D. (2019), 'The cognitive thalamus as a gateway to mental representations', *Journal of Neuroscience* .

Woolrich, M. W., Jbabdi, S., Patenaude, B., Chappell, M., Makni, S., Behrens, T., Beckmann, C., Jenkinson, M. and Smith, S. M. (2009), 'Bayesian analysis of neuroimaging data in FSL.', *NeuroImage* **45**(1 Suppl).

Xie, S., Zuo, N., Shang, L., Song, M., Fan, L. and Jiang, T. (2015), 'How does B-value affect HARDI reconstruction using clinical diffusion MRI data?', *PloS one* **10**(3), e0120773.

Xuereb, J. H., Perry, R. H., Candy, J. M., Perry, E. K., Marshall, E. and Bonham, J. R. (1991), 'Nerve cell loss in the thalamus in Alzheimer's disease and Parkinson's disease.', *Brain : a journal of neurology* **114 ( Pt 3**, 1363–79.

Yakushev, I., Schreckenberger, M., Müller, M. J., Schermuly, I., Cumming, P., Stoeter, P., Gerhard, A. and Fellgiebel, A. (2011), 'Functional implications of hippocampal degeneration in early Alzheimer's disease: A combined DTI and PET study', *European Journal of Nuclear Medicine and Molecular Imaging* **38**(12), 2219–2227.

Yang, H., Shew, W. L., Roy, R. and Plenz, D. (2012), 'Maximal Variability of Phase Synchrony in Cortical Networks with Neuronal Avalanches', *The Journal of Neuroscience* **32**(3), 1061 –1072.

Yeatman, J. D., Weiner, K. S., Pestilli, F., Rokem, A., Mezer, A. and Wandell, B. a. (2014), 'The vertical occipital fasciculus: A century of controversy resolved by in vivo measurements', *Proceedings of the National Academy of Sciences* **111**(48), E5214–E5223.

Yeo, B. T. T., Krienen, F. M., Sepulcre, J., Sabuncu, M. R., Lashkari, D., Hollinshead, M., Roffman, J. L., Smoller, J. W., Zöllei, L., Polimeni, J. R., Fischl, B., Liu, H. and Buckner, R. L. (2011), 'The organization of the human cerebral cortex estimated by intrinsic functional connectivity', *Journal of Neurophysiology* **106**(3), 1125–1165.

Yesavage, J. A., Brink, T. L., Rose, T. L., Lum, O., Huang, V., Adey, M. and Leirer, V. O. (1983), 'Development and validation of a geriatric depression screening scale: a preliminary report.', *Journal of psychiatric research* **17**(1), 37–49.

Yildiz, I. B. and Kiebel, S. J. (2011), 'A hierarchical neuronal model for generation and online recognition of birdsongs', *PLoS Computational Biology* .

Youssofzadeh, V., Prasad, G., Naeem, M. and Wong-Lin, K. F. (2016), 'Temporal Information of Directed Causal Connectivity in Multi-Trial ERP Data using Partial Granger Causality', *Neuroinformatics* .

Zalesky, A., Fornito, A., Cocchi, L., Gollo, L. L. and Breakspear, M. (2014), 'Time-resolved resting-state brain networks.', *Proceedings of the National Academy of Sciences of the United States of America* **111**(28), 10341–6.

Zalesky, A., Fornito, A., Harding, I. H., Cocchi, L., Yücel, M., Pantelis, C. and Bullmore, E. T. (2010), 'Whole-brain anatomical networks: does the choice of nodes matter?', *NeuroImage* **50**(3), 970–83.

Zarei, M., Beckmann, C. F., Binnewijzend, M. A. A., Schoonheim, M. M., Oghabian, M. A., Sanz-Arigita, E. J., Scheltens, P., Matthews, P. M. and Barkhof, F. (2013), 'Functional segmentation of the hippocampus in the healthy human brain and in Alzheimer's disease', *NeuroImage* **66**, 28–35.

Zarei, M., Patenaude, B., Damoiseaux, J. S., Morgese, C., Smith, S., Matthews, P. M., Barkhof, F., Rombouts, S. a. R. B., Sanz-Arigita, E. and Jenkinson, M. (2010), 'Combining shape and connectivity analysis: an MRI study of thalamic degeneration in Alzheimer's disease.', *NeuroImage* **49**(1), 1–8.

Zeki, S. (1993), *A Vision of the Brain*, London : Blackwell.

Zhang, D. and Raichle, M. E. (2010), 'Disease and the brain's dark energy'.

Zhang, D., Snyder, A. Z., Fox, M. D., Sansbury, M. W., Shimony, J. S. and Raichle, M. E. (2008), 'Intrinsic functional relations between human cerebral cortex and thalamus.', *Journal of neurophysiology* **100**(4), 1740–1748.

Zhang, H., Wang, S., Liu, B., Ma, Z. and Yang, M. (2010), 'Resting Brain Connectivity: Changes during the Progress of Alzheimer Disease.', *Radiology* **256**(2).

Zhang, Y., Brady, M. and Smith, S. (2001), 'Segmentation of brain MR images through a hidden Markov random field model and the

expectation-maximization algorithm', *IEEE Transactions on Medical Imaging* **20**(1), 45–57.

Zhao, Q., Lu, H., Metmer, H., Li, W. X. and Lu, J. (2018), 'Evaluating functional connectivity of executive control network and frontoparietal network in Alzheimer's disease', *Brain Research* **1678**, 262–272.

Zhou, C. and Kurths, J. (2006), 'Hierarchical synchronization in complex networks with heterogeneous degrees', *Chaos* **16**(1).

Zhou, C., Zemanová, L., Zamora, G., Hilgetag, C. C. and Kurths, J. (2006), 'Hierarchical organization unveiled by functional connectivity in complex brain networks', *Physical Review Letters* **97**(23).

Zhou, C., Zemanová, L., Zamora-López, G., Hilgetag, C. C. and Kurths, J. (2007), 'Structure–function relationship in complex brain networks expressed by hierarchical synchronization', *New Journal of Physics* **9**(6), 178–178.

Zhou, J., Gennatas, E. D., Kramer, J. H., Miller, B. L. and Seeley, W. W. (2012), 'Predicting regional neurodegeneration from the healthy brain functional connectome.', *Neuron* **73**(6), 1216–27.

Zhou, Y., Dougherty, J. H., Hubner, K. F., Bai, B., Cannon, R. L. and Hutson, R. K. (2008), 'Abnormal connectivity in the posterior cingulate and hippocampus in early Alzheimer's disease and mild cognitive impairment.', *Alzheimer's & dementia : the journal of the Alzheimer's Association* **4**(4), 265–70.

Zhu, D. C., Majumdar, S., Korolev, I. O., Berger, K. L. and Bozoki, A. C. (2013), 'Alzheimer's disease and amnestic mild cognitive impairment weaken connections within the default-mode network: a multimodal imaging study.', *Journal of Alzheimer's disease : JAD* **34**(4), 969–84.

Zhuang, L., Sachdev, P. S., Trollor, J. N., Kochan, N. A., Reppermund, S., Brodaty, H. and Wen, W. (2012), 'Microstructural white matter changes

in cognitively normal individuals at risk of amnestic MCI', *Neurology* **79**(8), 748–754.